

1957 - July

NEW YORK UNIVERSITY
COLLEGE OF ENGINEERING
RESEARCH DIVISION

Department of Meteorology and Oceanography
and
Engineering Statistics Group

The
DIRECTIONAL SPECTRUM
of a
WIND GENERATED SEA

As determined from data obtained by the
STEREO WAVE OBSERVATION PROJECT

by

Joseph Chase
Louis J. Cote
Wilbur Marks
Emanuel Mehr
Willard J. Pierson, Jr.
F. Claude Rönne
George Stephenson
Richard C. Vetter
Robert G. Walden



with the assistance of personnel from the following organizations:

David Taylor Model Basin
George Washington University Logistics Research Project
Naval Air Development Unit, N.A.S. South Weymouth, Mass.
Office of Naval Research
U. S. Navy Hydrographic Office
U. S. Naval Photographic Interpretation Center
Woods Hole Oceanographic Institution

GC
211
.N4
1957

Prepared for
THE OFFICE OF NAVAL RESEARCH
UNDER CONTRACT NONR 285(03)

Abstract of a Wind generated
and from data obtained
Observation Project
e, etc.
Eng.

A standard linear barcode is positioned vertically on the right side of the page. It consists of vertical black bars of varying widths on a white background.

NEW YORK UNIVERSITY
COLLEGE OF ENGINEERING
RESEARCH DIVISION
Department of Meteorology and Oceanography
and
Engineering Statistics Group

The
DIRECTIONAL SPECTRUM
of a
WIND GENERATED SEA

As determined from data obtained by the

STEREO
WAVE
OBSERVATION
PROJECT

by

Joseph Chase
Louis J. Cote
Wilbur Marks
Emanuel Mehr
Willard J. Pierson, Jr.
F. Claude Rönne
George Stephenson
Richard C. Vetter
Robert G. Walden

with the assistance of personnel from the following organizations:

David Taylor Model Basin
George Washington University Logistics Research Project
Naval Air Development Unit, N. A. S., South Weymouth, Mass.
Office of Naval Research
U. S. Navy Hydrographic Office
U. S. Naval Photographic Interpretation Center
Woods Hole Oceanographic Institution

Prepared for
The Office of Naval Research
under Contract Nonr 285(03)

THE DIRECTIONAL SPECTRUM OF A WIND GENERATED SEA
AS DETERMINED FROM DATA OBTAINED BY THE
STEREO WAVE OBSERVATION PROJECT

By

Joseph Chase Woods Hole Oceanographic Institution
Louis J. Cote. Department of Meteorology and Oceanography, College
of Engineering, New York University (now at
Syracuse University, Dept. of Mathematics)
Wilbur Marks Woods Hole Oceanographic Institution (now at
David Taylor Model Basin)
Emanuel Mehr Engineering Statistics Group, Research Division,
College of Engineering, New York University
Willard J. Pierson, Jr. . Dept. of Meteorology and Oceanography, College
of Engineering, New York University
F. Claud Ronne Woods Hole Oceanographic Institution
George Stephenson . . . The George Washington University, Logistics
Research Project, Washington, D. C. (now at Com-
putation Laboratory, Research Division, Math. Dept.,
New York University, College of Engineering)
Richard C. Vetter. . . . Geophysics Branch, Office of Naval Research
Robert G. Walden . . . Woods Hole Oceanographic Institution

and members of the staff of the U. S. Navy Hydrographic Office.

JULY 1957

This report is a technical report prepared for limited
distribution for the Office of Naval Research under contract
Nonr 285(03) at the Research Division of the College of
Engineering of New York University. Reproduction in whole
or in part for any purpose of the United States Government
is permitted.

Table of Contents

Page

Part 1. INTRODUCTION	1
Willard J. Pierson, Jr.	
Part 2. COOPERATING AGENCIES AND ORGANIZATION	3
Richard C. Vetter	
Part 3. HISTORY	18
Wilbur Marks	
Part 4. OPERATIONAL PROCEDURE	26
Wilbur Marks and F. Claude Ronne	
Part 5. WAVE FORECASTS.	31
U. S. Navy Hydrographic Office	
Part 6. PHOTOGRAMMETRIC EVALUATION OF PROJECT SWOP . .	40
U. S. Navy Hydrographic Office	
Part 7. PRELIMINARY ANALYSIS, CHOICE OF GRID SPACING, AND DISCUSSION OF ALIASING	49
Willard J. Pierson, Jr., Wilbur Marks, and Joseph Chase	
Part 8. EQUATIONS FOR LEVELING THE DATA, ESTIMATING THE SPECTRA, AND CORRECTING THE WAVE POLE RECORDS .	58
Louis J. Cote and Willard J. Pierson, Jr.	
Part 9. THE LEVELED DATA, THE NUMERICAL ANALYSIS, AND THE NUMERICAL RESULTS.	82
Emanuel Mehr and George Stephenson	
Part 10. ANALYSIS OF WAVE POLE DATA	134
Willard J. Pierson, Jr.	
Part 11. THE STEREO PAIRS, AND THE INTERPRETATION AND ANALYSIS OF THE DIRECTIONAL SPECTRUM IN TERMS OF WAVE THEORY	148
Willard J. Pierson, Jr.	
Part 12. CONCLUSIONS AND RECOMMENDATIONS	253
Willard J. Pierson, Jr.	
Appendix: THE DIMENSIONAL STABILITY OF PHOTOGRAPHIC FILMS.	257
Simeon Braunstein	

LIST OF ABBREVIATIONS

Bu Aer	Bureau of Aeronautics, Washington, D. C.
DTMB	David Taylor Model Basin, Washington, D. C.
HYDRO	U. S. Navy Hydrographic Office, Washington, D. C.
NADC	Naval Air Development Center, Johnsville, Pa.
NADU	Naval Air Development Unit, South Weymouth, Mass.
NPC	Naval Photographic Center, Washington, D. C.
NYU	New York University, New York
ONR	Office of Naval Research, Washington, D. C-
SIO	Scripps Institute of Oceanography, La Jolla, Calif.
WHOI	Woods Hole Oceanographic Institution, Woods Hole, Mass.

ERRATA

Page 33, line 11: For 74¹¹ read 74°.

Page 104, Table heading: For Data Set 2 read Data Set 3.

Page 180, line 16: Following and 11.3 should be a parenthetical
remark: (as drawn for the full set of data)

Part 1.

INTRODUCTION

On November 25, 1954, two aircraft rendezvoused with the R. V. ATLANTIS at a point in the North Atlantic. The aircraft made a sequence of passes over the ATLANTIS and flew back to base. Months of preparation went into the flight, months of thought went into the problem of what to do with the data obtained on the flight and by the ATLANTIS, and months of work went into the numerical processing of the data.

The results of the flight were stereo pairs of photographs of the sea surface. The ATLANTIS provided base line calibration and wave pole and visual observations. Two of the best pairs of photos were reduced to 5400 numbers on a rectangular grid. The wave pole records were reduced to a time series of discrete points of about 1,800 numbers each. The purpose was to take the two sets of 5400 numbers, estimate the directional spectrum of the waves on the sea surface and compare it with the frequency spectrum as estimated for the three sets of 1800 points read from the wave pole records as a check.

To go from the 10,800 stereo numbers and the 5,400 wave pole numbers to the desired spectra required a total of about 9,000,000 multiplications and an equal number of additions. After the directional spectra were computed, the results obtained were inconsistent with the theoretical models, and the stereo data had to be carefully re-analyzed with the result that part of the data had to be discarded. The 5400 numbers were reduced to about 3500 numbers, and the computations were done over again.

This task has just been accomplished, and the purpose of this report is to tell how the operation was planned, how the data were obtained, and how the computations were made. Finally, the results obtained will be analyzed and interpreted. The original data, the reduced data, and the results of all computations are included in both pictorial and tabular form.

As this report is studied by its readers, it will become apparent that it would never have been written were it not for the combined efforts of a very large number of people with diverse talents and abilities. They represent a wide variety of U. S. Navy organizations and civilian research organizations. As many as possible have been mentioned and thanked in this report, but some who have helped immensely in this work remain anonymous because it is not possible to list them all. Our thanks are extended to all individuals who helped in this work and to all cooperating groups, and the hope is expressed that the final analysis of the results will prove of sufficient value to justify the tremendous effort expended on this task.

Part 2

COOPERATING AGENCIES AND ORGANIZATION

This part concerns the arrangements, meetings, official letters, discussions and exchanges of ideas that went into bringing together the many diverse people and agencies who contributed to SWOP and without whose assistance SWOP would not have succeeded.

The problem as first presented in the fall of 1953 was to obtain an accurate representation of the directional properties of real ocean waves. The first job was to try to find out whether or not the proposed plan was feasible and to get and review the critical opinion of others as to whether or not it needed doing. Marks had been studying waves by stereo techniques, but on a much reduced scale. By taking photographs from a bridge, he was able to get useful data on the two-dimensional wave spectrum for a rather limited fetch. This, however, was quite a different thing from taking stereo-photos from airplanes far out in the open ocean. Letters were written to people doing wave research asking their opinion. In the replies there was general agreement that a good statistical treatment of a whole area of the sea surface was necessary before the art of understanding waves could be much advanced. In a letter to the author in February 1954, Walter Munk, of the SIO, stated that ".... the two-dimensional analysis is certainly the essential problem now. In fact, I have some serious doubts as to whether further extensive work on frequency analysis of records taken at a single point is even worthwhile. If one uses a spectral presentation of waves, one should really go all the way or not at all."

Assured that the study was needed, the first of a long series of letters, official and otherwise, which helped bring together all the necessary people and components which were needed to make the plan succeed were written. In addition to the actual task of taking the photos under suitable wave conditions the data had to be analyzed on a stereo planigraph or similar instrument and facilities for the immense task of computing the required quantities with high speed digital computers had to be obtained.

The first piece of official correspondence on SWOP in the files is dated November 9, 1953. It was a formal letter from the Chief of Naval Research to the Chief of Naval Operations outlining the reasons for the SWOP project and asking for certain services. Cameras, airplanes and a radio link for firing the cameras were requested. The letter went via the Bureau of Aeronautics for comment. It picked up a favorable endorsement recommending that the project be assigned to the Photographic Squadron VJ-62 in Sanford, Florida. To the practiced eye of our friends in CNO it was obvious that the proposed job was much more complicated than the letter indicated.

The Naval Photo Interpretation Center was asked by CNO to study the proposal and comment. As a result of the review, a number of critical points were raised. There were problems of control of aircraft height, of control of distance between aircraft, of tilt and of simultaneous firing of the cameras. Establishing a pattern that was to become a routine method of solving the problems which arose, a conference of all concerned was called to discuss each point in detail. This conference which was held at the Naval Photo-

graphic Interpretation Center, Anacostia, Maryland, on March 2, 1954 is described by Marks in Part 4 of this report.

It would have been useless, however, to proceed with plans and the construction of equipment for SWOP without some assurance that a vessel could be made available. The vessel would have to go to the target area some place in the North Atlantic and wait, no one knew exactly how long, for favorable meteorological conditions to occur. This assurance was given by WHOI. The ATLANTIS could be put at the disposal of SWOP given sufficient advance notice. Getting an oceanographic research vessel with a very heavy schedule of other "equally important" projects under such circumstances would have been extremely difficult without the enthusiastic and understanding co-operation of Dr. Columbus Iselin of WHOI.

The next item on our critical list was the weather. The Division of Oceanography, U. S. Navy Hydrographic Office was asked for advice concerning the best time and place for finding the desired wave conditions. A report on this aspect of the work is given in Part 6 of this report.

The errors which could be anticipated in the data had been estimated and it had been shown that significant results could be obtained in spite of these errors. By May of 1954 enough arguments had been mustered to permit another try through official channels to get the airplanes and cameras we had to have.

During a conversation with Cdr. James* about the possibility of using blimps to do the job, he suggested that NADU was the place to go for help.

*ONR Air Branch

Fortunately, Cdr. Robert H. Woods, Commanding Officer of the Naval Air Development Unit, and Cdr. Hoel, also of NADU, were in Washington on some other business and the problem was discussed with them. They were both interested, even enthusiastic about our project. We talked about using two of NADU's blimps to do the job. Their stability, slow motion and freedom from vibration were particularly appealing. At last, operational people were interested in helping us. In the next few months the officers and men at NADU accepted each problem in the series of many to be overcome in our job as a challenge and made it a point to find the best answer in each case. It is impossible to give NADU too much credit for the magnificent job they did for us.

On 16 July 1954, an interoffice memorandum was written explaining the necessity of assigning a priority of "B" to our project with NADU. The stringent weather requirements we had to meet and the necessity of being able to plan well in advance in order to have the WHOI R/V ATLANTIS, the NADU airships, and the weather all be at the right place at the same time were outlined. The priority was granted and on 19 July a letter was sent from ONR to NADU setting up a project directive for the accomplishment of SWOP. An abstract of the project contained in this letter will provide some idea of the plans at this point:

"The Naval Air Development Unit will make one flight consisting of two aircraft (equipped with trimetrogon cameras and an FM radio link for the purpose of triggering the two cameras simultaneously) to a target area approximately 300 to 400 miles out over the North Atlantic. The Woods Hole Oceanographic Institution research vessel "Atlantis" will be

in the center of the target area making numerous and continuous wave observations and providing a "ground control" for the aerial photography by determining accurate distances between the "Atlantis" and a buoy. Personnel from the Woods Hole Oceanographic Institution will assist in installation of the cameras and construct the FM radio link."

The stabilization of the airships in the rough weather they were apt to encounter while flying our mission was a problem. We expected to lick this by gyrostabilizing the camera mounts.

On 19 July, arrangements were made through our Property Branch for the loan of the following equipment from the Photographic Division in the Bureau of Aeronautics:

4 CA-8 aerial reconnaissance cameras
2 Gyrostabilizing mounts
8 rolls of Topographic Base, Panchromatic film
9 1/2" x 200'

BuAer was most cooperative and helpful in loaning us this much needed equipment.

On 21 July another letter was sent to NADU from ONR designating Wilbur Marks of WHOI as ONR field representative for the SWOP project. Two weeks later a conference was held at South Weymouth to set up detailed specifications and plans for SWOP. Lt. jg. Chandler was assigned to organize NADU's participation in SWOP. He, LCdr Champlin, Cdr Hoel and Marks were able to clarify ideas about some of the equipment requirements. The author went to work trying to get some of the items not available at Woods Hole or NADU which they thought they would need. The results of the conference are described by Marks in Part 4. A most important

result was the decision to change over from blimps to P2V's.

A meeting on the 19th of August marked another milestone in the step by step progress we were making. Marks, Ronne, Whitney and Walden from Woods Hole, Cdr. Leffen, LCdrs. Finlayson, Docktor, and Price from NADC, two representatives from Hydro, Pierson from NYU, and myself from ONR attended, and Cdr. Wood, Cdr. Hoel, LCdr. Champlin, LCdr. Hollingshead and Lt. jg Chandler acted as hosts at NADU. Thanks mainly to the staff at NADU, a detailed program for the accomplishment of the operation was worked out. The participants were assigned various tasks and dates were set up for tentative completion of various phases of the project.

As a result of the conference my tasks were to arrange for the development of the film at Bermuda and Anacostia, to get official authorization through BuAer for the installation of the cameras on the P2V's by the NADC and to get the necessary films and magazines (also through BuAer) sent to WHOI.

A date was set for the test flight, 27 September, and a target date for the actual photographs at sea, 1 October. Considering the many things that still needed doing and the arrangements that had to be made, this was pushing things just a bit. But to delay longer would have put us into the winter months with less chance of getting just the right meteorological conditions.

On 25 October a letter was written to the Naval Photographic Center, NAS Anacostia, asking them to develop our black and white and color film

obtained both during the test flights for SWOP and the actual project flights. We wanted immediate development of the test flight film in order to be able to check out the photographic system. The P2V's were to land at Anacostia immediately after flying the test hop so that the films could be developed at the NPC and inspected by someone from the Photogrammetry Division of the U. S. Navy Hydrographic Office for accuracy with a minimum of delay. The test flight was planned for the third week in September. The results of the analysis of the test data and of the data finally obtained are described by members of the staff of the Photogrammetry Division of the U. S. Navy Hydrographic Office in Part 6.

The flight check showed that one of the two cameras sent to Johnsville for installation was defective. Luckily we had originally asked for four cameras so we had spares to fall back on. The Photogrammetry Division at Hydro checked these cameras for us and were able to find two good cameras for us out of the four BuAer had originally sent.

On September 16th a letter was sent from ONR to Hydro asking for their assistance in providing the required wave forecast. This request was made supplementary to the request for services from the Photogrammetry Branch and was intended to be part of the same project. Hydro, of course, agreed to provide these additional services. This aspect of the work is also discussed in Part 5.

On the 29th the test flight was made. I was waiting at the field at Anacostia for the P2V's to arrive. It was slightly after the desk workers quit-

ting time when both planes touched down. The magazines were removed from both cameras and taken to the Navy Photo Center for development. Later that night the films had been inspected. Everything was fine except that the corners of the pictures taken from both cameras were blurred. The cameras had been mounted too high up in the fuselage of the aircraft so that part of the field of view was being cut off. Some minor surgery on the mounts was all that was required. By the 12th of October everything was ready to roll and Marks issued detailed instructions to all parties outlining exactly what and how each was to do his part.

On the 15th the Woods Hole Port Captain issued letter instructions to the ATLANTIS Captain to depart Woods Hole on or about the 17th for latitude 39N, longitude 63.5W to the rendezvous with the waves, the weather and the P2V's. It was hoped that SWOP would be over and done with by the 25th so that the ATLANTIS could be back at Woods Hole on the 27th as early in the day as possible.

When the right weather and cloud conditions finally occurred, the ATLANTIS was there after waiting for one week; the planes were there; the cameras were functioning; and on the 25th of October the pictures were taken.

There remained the unexciting task of cleaning up after the operation. All the various items of borrowed equipment had to be returned. There was more correspondence back and forth piecing together some of the loose ends. Marks sent down a data sheet for the distance between the raft and the ATLANTIS in each pair of photographs. Prints of the best stereo pair according to the judgment of Hydro's Photogrammetrists were sent to him.

Details of the grid arrangement were worked out. BuAer was notified that the operational part of SWOP was over and all concerned were thanked for their help and cooperation. A similar letter was sent to NADU via their boss, the Commander, U. S. Navy Air Bases, 1st Naval District.

The films exposed over the North Atlantic were developed and sent to the Hydrographic Office. The low light intensity available during the SWOP flight threatened to produce negatives of marginal value, but careful development by the NPC at Anacostia saved the day.

Hydro looked over the stereo pairs, picked one of the best and began contouring.

Further work came to a temporary halt while Hydro's presentation of the contours were sent to Pierson and Marks for study. As was expected there was some tilt in the contouring. The Photogrammetry people at Hydro did their best to level the stereo-pair before contouring, but we all realized that with no established reference plane from which to work, perfect leveling would be impossible. The contours showed a range of heights from one foot to 24 feet while actual wave pole measurements taken on the spot from the ATLANTIS gave a significant wave height of about 7 feet. In addition to this tilt a somewhat closer look showed a ridge running almost exactly down the center of the 2,000' x 4,000' rectangle caused by the stereo-photos paralleled by a trough about 500' away. In order for this feature to be real, a wave with a height of at least 9 feet and a period of about 14 seconds would have been in the area photographed. No such wave

could have been generated by any known meteorological disturbance in the Atlantic area. We were forced to conclude that the contoured surface was not only tilted but warped in some sort of "barrel" shape with axis parallel to the long sides of the contoured rectangle. Fortunately, this barrel type of distortion was not present in other stereo pairs and the only real problem turned out to be that of removing tilt from the analysis and determining a zero reference plane.

The tilt was not too serious. Mathematical analysis could take most of the tilt out of the data. After a discussion with Hydro, it was suggested by me that we have Hydro give us the data in the form of discrete elevations on a grid system. They felt that such data would be more accurate and take less time than contouring. It looked as if it were about time for another small conference to see where we stood and determine just what should be done.

Dr. Pierson came down from NYU on the first of March and we had a very profitable discussion with the people at Hydro's Photogrammetry Branch. He was finally able to decide on a simple 30 x 30 foot grid system with sides parallel to the photographs. Unfortunately, the sides of the photographs did not line up with the direction of the surface waves as expected. The preliminary analysis of the data is described in Part 7 of this report.

The important thing, however, was to have the grid system point in the same geometrical direction in each of the three pairs of photographs

which were to be processed for spot heights. By careful selection from the available prints, Hydro was able to come up with two good pairs with identical orientation and another which was only 5° different in direction from the other two. They set up the grid system in the third so that it was aligned in the same direction as in the first two. A grid system of 60×90 points was finally settled upon, and Hydro began the laborious task of grinding out 5,400 spot heights for each of three pairs of stereo photographs of the sea surface.

With the data soon to be pouring out of Hydro, the next important problem was to get it analyzed. We turned again to the DTMB UNIVAC. By this time the demands for time on their computer had grown tremendously. They would, however, be willing to run the analysis if it were first programmed. Dr. Pierson investigated the possibility of having the programming done at NYU. The Engineering Statistics group of the NYU Research Division, under the direction of Mr. Leo Tick undertook to do the task in about two months. So, while Hydro was amassing the tables of numbers that were so important, Mr. Emanuel Mehr was working out the problems of telling a mass of vacuum tubes and wires (the UNIVAC) what to do with the numbers we intended to feed it. By the first of April, Hydro was beginning to grind out the data and I went out to see how they were doing and talk with them about the project. I was very much impressed with the careful and accurate job they were doing. They felt that their observations were accurate to plus or minus one foot and reproducibility to about $2/5$ ths of a foot. As a check, I

picked out two spot heights which they had already determined and asked for a check. In both cases the operator came within 1/5 foot of the previously recorded reading. By the 21st of April the first set of 5,400 spot heights had been completed and Hydro was proofreading the typed tables. These were forwarded to ONR on May 6, 1955. The second set of 5,400 SWOP numbers came into my office from Hydro. By this time they were turning out work at a good rate and doing an even more accurate job. Their estimate was that the second batch of data was accurate to within plus or minus .5 feet.

By the first of July Hydro had forwarded the last set of the three sets of data. This also was accurate to within plus or minus .5 feet. Thus one phase of the SWOP operation came to a close. The extraction of the raw data from the stereo photographs had been completed.

The question of whether or not we should have Hydro contour another set of photos in order to show up some of the fine structure which would be eliminated from data taken from spot heights alone arose at this time. It was agreed that this should be done but at a later date when SWOP was farther along.

It remained to analyze this data carefully to eliminate the tilt which was known to be present in each model and finally to subject the data to analysis on an electronic computer. Our attentions were now focused to the problem of getting a firm commitment from DTMB concerning use of their UNIVAC. It looked as if our original estimate of the time required for the

analysis had been an order of magnitude too small. The workers at NYU worked out a method for leveling the data that would take about one and one-half hours of UNIVAC time. We hoped to get this done on the DTMB UNIVAC. Later the job was done commercially at New York. While working out the details of the programming of the data Mehr upped the estimate of total UNIVAC time to over 20 hours.* This made things look a little dark for us as far as getting the job done at DTMB was concerned.

On 26th August our letter to DTMB asking them for UNIVAC time was answered. The Model Basin wanted to program the analysis instead of having it done at NYU and wanted to examine the data to see whether or not it would be practical to do the work on their UNIVAC. Their desire to do their own programming was understandable since an improperly programmed operation could run up the total time used by the UNIVAC considerably. However, Mehr had already done most of the programming at NYU. Another conference appeared to be in order, so on 19 September Dr. Polachek and Mr. Shapiro and Mr. St. Denis of DTMB and Mr. Mehr of NYU and myself met at DTMB to discuss the problem. Mr. Mehr had finished programming the analysis. All that remained to be done was to "de-bug" his programming setup and then run the analysis. He estimated that about 20 good UNIVAC hours would be required for each of the three sets of data. Considering their other high priority commitments for the UNIVAC this was way out of line with what we hoped to get. I agreed to try to find funds to de-bug and run the first set of data commercially, the plan being then to

*For each set of data.

turn the rest of the data over to DTMB to have it run in bits and pieces as time became available. Additional funds were made available to NYU by ONR to perform the first part of this analysis, and I wrote an official letter to DTMB outlining our plan. We would have the analysis on the first set of data done commercially to provide an absolute check on the programming and then turn the remaining work over to DTMB.

From the beginning it had been our expectation that we would be able to use the UNIVAC computer at DTMB to perform the analysis of the SWOP data. That things did not turn out this way should not be taken as a reflection against DTMB or any of the people on its staff. Without the encouragement from DTMB, in particular, from Manley St. Denis, early in our planning stage concerning possible use of their computer, we might not have gone ahead.

Arrangements were finally made to have the work done on the "Logistics Computer", ONR Logistics Branch. Thanks are due to Dr. Max Woodbury and Dr. Fred D. Rigby of the ONR Logistics Branch for assistance in making the Logistics Computer available and to Dr. William Marlow, Principal Investigator of the Logistics Research Project, and Mr. George Stephenson, Head of the LRP Computation Laboratory in Washington, D.C. Fortunately the Logistics Computer was able to make use of some of the programming already worked out for the UNIVAC. The theory for leveling the data, and determining the spectrum is described in Part 8 of this report and the numerical procedures and the actual data obtained are given

in Part 9.

As one last check on the quality of our SWOP data we had one more contouring job done by Hydro. This time the reference level was determined by selecting points that had been leveled statistically. This leveled contoured model was forwarded in May 1956 along with an evaluation of the photogrammetric work. As mentioned before, the work done by the Photogrammetry Division of the U. S. Navy Hydrographic Office is described in Part 6 of this report.

And so, after 33 months and a correspondence file at ONR two and one-half inches thick, as of June 1956 SWOP has been completed except for the task of interpreting results, drawing conclusions from them, and preparing this report.

Part 3

HISTORY

For some years now the desirability of obtaining the two-dimensional sea spectrum has been explained in the literature (Pierson [1952] and St. Denis and Pierson [1953]). When most of the methods considered were found lacking, the technique of stereo-photography of the sea surface seemed most amenable to possible methods of analysis (Marks [1954a]).

Representatives of the Woods Hole Oceanographic Institution initiated the first steps necessary to convert the idea of aerial stereo-photography of ocean waves into fact. At a meeting in Washington, the requirements for such an undertaking were established, and, equally important, the Photogrammetry Division of the U. S. Navy Hydrographic Office expressed an interest in the job of reducing the photos to numerical data form. As a result of this discussion, the first formal plan for obtaining the stereo-pairs was set down (Von Arx [1952]). The basic requirements were as follows:

1. Two aircraft to fly parallel, 600 feet apart, at 1000 feet;
2. Each to have a CA-8 metrogon camera aimed vertically down and one long focus 35 mm camera aimed at companion aircraft to determine the length of the stereo-base line;
3. Cameras to be triggered within 10 milliseconds of each other by an FM pulse;
4. Smoke bomb pattern to provide ground control;
5. Upwind flight of planes with flaps down to reduce plane speed and

give better results;

6. Preliminary flight to determine best height and baseline suggested.

The stereo-photos were made three years after the date of this first meeting. Much thought, discussion, planning and revision took place in that interval, and yet the final operational plan differed little in essence from that set forth in the Von Arx note which is outlined above.

At this point, work on the problem ceased, and almost a year passed before interest was revived. Wave theory was advancing at a rapid rate, and W. J. Pierson, convinced that basic theoretical conclusions should be substantiated by experimental work, persuaded the Office of Naval Research to begin a project of aerial stereo-photography. Shortly afterward, the Woods Hole Oceanographic Institution agreed to help on the problem. Dr. Iselin, Senior Oceanographer, offered the services of the R V ATLANTIS to provide a horizontal scale factor and to obtain with a capacitance wave pole recorder a record of the sea surface as a function of time at a fixed point in order to determine the sea surface spectrum as a function of frequency. Since this frequency spectrum is the integral (with respect to direction) of a transformation of the two-dimensional spectrum to be obtained by stereo-photography, it is the only method of testing the validity of the directional spectrum.

As the mechanics of the project began to crystallize, the multitude of "minor problems" associated with an air-sea venture of this sort became evident, and a meeting was scheduled to coordinate the facilities available

at the moment and to provide general cognizance of the problems of the various groups involved. The U. S. Navy Photographic Interpretation Center (NPIC) was the host of a meeting at Washington, D. C. which was attended by representatives of New York University (NYU), Woods Hole Oceanographic Institution (WHOI), the Office of Naval Research (ONR), David Taylor Model Basin (DTMB) and the U. S. Navy Hydrographic Office (HYDRO).

The discussion was presided over by Mr. Richard C. Vetter (ONR). The results and conclusions of this conference provided the first link in the chain of events which ended in the successful aerial stereo-photography of the sea surface on October 25, 1954. The highlights of this meeting are listed:

1. A justification for the mission was given by Professor Pierson through a description of the basic theory of sea spectra and a step-by-step elimination of other possible techniques.
2. HYDRO expressed ability and willingness to contour the stereo-photos if they met certain photogrammetric specifications.
3. The stereo-baseline (distance between planes) is a vital factor in the contouring of the photos and will have to be resolved. Photography of one plane from the other was ruled out on grounds of measuring inaccuracy.
4. The necessity for a horizontal unit of measurement four or five times the length of the ATLANTIS provided another unanswered question.

5. Mr. Vetter (ONR) agreed to act as administrator for the project and to try to initiate the next link in the chain, which was to obtain permission for the use of two suitable aircraft.

As a result of this meeting the first operational plan was put on paper (Pierson [1954]), and the project achieved an air of respectability enhanced by the eagerness exhibited by the participants. Altitudes and baselines were defined. Sources of stereo-analysis error were given, and error magnitudes were estimated. A flying procedure was suggested. The number of pairs of photos which would be needed was estimated, and the functions of the ATLANTIS were established.

As soon as definite plans had been set down the project went into high gear. A visit by WHOI to Dr. Claus Aschenbrenner of the Optical Research Laboratory, Boston University was productive in two ways. His assurance as an expert photogrammetrist, that chances for success were high fell on welcome ears. Of more immediate importance, his disclosure that the French had achieved success with an FM triggering device was extremely heartening because this was a critical point in the scheme. A paper by Cruset*[1951] describing the activities in France along these lines, was studied carefully by R. G. Walden, head of the WHOI Electronic Division, and it was concluded that his staff could match and perhaps improve the French instrument with respect to differences in triggering time between cameras.

The ground control problem was solved at WHOI with the discovery

*See also Cruset [1954], in the references which follow.

of an additional use of the sonobuoy*. The sonobuoy would be placed on a raft payed out from the ATLANTIS about 1000 ft. downwind. A sound pulse would be released by a transducer on the ATLANTIS. The sonobuoy hydrophone would pick up the signal, which travels through water, convert it to an electromagnetic signal and retransmit it through air, at a given frequency, to be picked up by a receiver on the ship. The echo-sounder would record the time of one round trip. The trip through water takes about 0.2 seconds (for 1000 ft), and the return through air takes 1.08×10^{-6} seconds. The time of the return trip is considered negligible, and if the rate or propagation of sound in water is known as a function of temperature and salinity, then the distance traveled by the signal can be computed.

In July, ONR enlisted the interest of the Naval Air Development Unit at the Naval Air Station, South Weymouth, Mass. where a pair of blimps were available for the job. A request originated from ONR for the utilization of the NADU resources. At the same time, ONR ordered four cameras, two gyrostabilizing mounts and an abundance of film. WHOI was directed to set up and install the FM link. W. Marks (WHOI) was appointed field supervisor of the project.

As the pieces began to fall into place, certain difficulties became increasingly apparent.

1. The measurement of stereo-baseline had not been resolved.
2. Since weather plays a prominant role in determining the desired

*Sonobuoy Instruction Manual AN-SS Q2.

stationary sea state free from swell, it was decided that an expert wave-weather forecasting group should be asked to advise on the operation. The Division of Oceanography of the U. S. Navy Hydrographic Office was the logical group.

3. The pilots at NADU would have to be made a part of the operation as soon as possible.

The last item was perhaps the most urgent because the key to the feasibility of the entire undertaking was in the hands of the pilots at NADU. A meeting was arranged for August, 1954 at NADU, and WHOI and HYDRO presented the plan of operation. A day long discussion produced the following results:

1. The blimps were eliminated by mutual agreement of WHOI and NADU because the camera installations were inaccessible, there would be excessive vibrations, formation flying would be difficult and their radius of operation is restricted by short range and low flying speed.
2. A pair of P2V's was offered as an alternative. The advantages were that they could fly in most winds up to gale force with a speed in excess of 150 kts, that photographic facilities were available, that they had much greater range with 14 hrs flying time, that formation flight was not difficult and that the necessary radio and power equipment was available.
3. NADU was able to determine stereo-baseline by a gunsight technique. When the planes are spaced a measured distance on the ground, the

- lead plane fills a certain portion of the following plane's gunsight. If this condition is maintained in flight, then the baseline is known.
4. The Photogrammetry Division of HYDRO asked for a practice run over a specified course to provide an evaluation of the photography.
 5. Two weeks was set as the maximum operating time once the field work started.
 6. The cameras were to be sent to WHOI to facilitate preparation of the FM link.
 7. The aircraft are committed to the use of an A-priority group and will not be forthcoming without the consent of this group.
 8. A tentative meeting was scheduled at NADU for a final evaluation of plans after the planes were fully instrumented.

During the month of August, a U.S. Navy photographer first class was assigned to the project, ONR secured all the equipment asked for, and the Hydrographer committed the Photogrammetry Division to the stereo analysis job. The FM link was satisfactorily completed and installed, and a ground check was made. It was found that the FM link could trigger the cameras within one millisecond of each other (Walden [1955]). This was an improvement over the similar French instrument.

The final coordinating meeting was held at NADU on 19 August 1954. All of the mechanics were ironed out, and assignments were given to the various cooperating groups to be completed by the test date, tentatively set for 24 September. All groups received copies of the procedure for the test run and the actual exercise (Marks [1954b]).

References to Part 3

- Cruset, J., [1951]: Annales Francaises de Chronometrie. Institut Geographic National, 2nd series, Volume XVII, pp. 105-115.
- Cruset, J., [1954]: Evolution of French photogrammetric equipment from 1949 to 1954. Photogrammetric Engineering, September.
- Marks, W., [1954a]: The use of a filter to sort out directions in a short-crested Gaussian sea surface. Transactions A.G.U., v. 35, no. 5, pp. 758-766, October.
- Marks, W., [1954b]: Operational procedure for stereo-photography of ocean waves. Woods Hole Oceanographic Institution, unpublished manuscript, September.
- Pierson, W. J., Jr., [1952]: A unified mathematical theory for the analysis, propagation and refraction of storm generated ocean surface waves. Parts I and II. Research Division, College of Engineering, New York University, Department of Meteorology and Oceanography. Prepared for Beach Erosion Board, Department of the Army, and Office of Naval Research, Department of the Navy.
- Pierson, W. J., Jr., [1954]: Operational specifications for a program for stereo-photography of waves. Unpublished manuscript.
- St. Denis, M., and W. J. Pierson, Jr., [1953]: On the motions of ships in confused seas. Transactions of the Society of Naval Architects and Marine Engineers, vol. 61, pp. 280-357.
- Von Arx, S. S., [1952]: A program of stereo-photography of waves. Woods Hole Oceanographic Institution, unpublished manuscript, October.
- Walden, R. G. : A multiple activating electronic synchronizer. Reference no. 55-15 Woods Hole Oceanographic Institution, unpublished manuscript.

Part 4

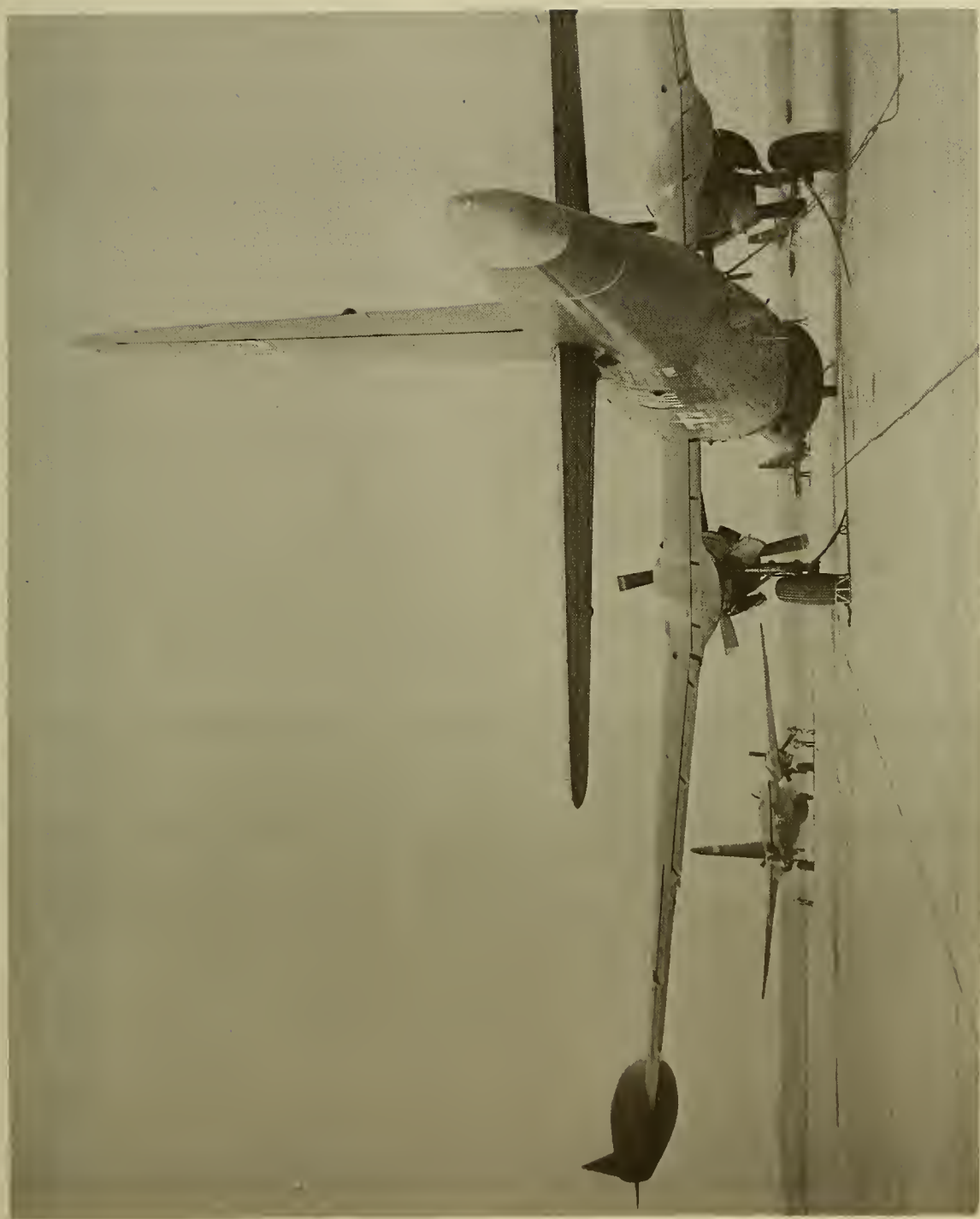
OPERATIONAL PROCEDURE

It is worthwhile to explain briefly the technique used for making the aerial stereo-photographs.

It is first desired to have a stationary sea free from swell traveling at an angle to the sea so that the data collected could be most easily interpreted. To this end, the Wave Forecasting Branch of the Division of Oceanography, U. S. Navy Hydrographic Office (HYDRO) was consulted. The area around 40N, 65W was chosen as the most likely place to achieve such results and the ATLANTIS was designated to take this position and advise periodically on weather.

HYDRO kept watch on the sea conditions, and at the appropriate time, some 24 hours in advance of the anticipated working time, notified WHOI which served as the coordinating center of field activity. NADU and the ATLANTIS were alerted, and when the wave situation persisted the planes were dispatched. As soon as possible, contact was made between the planes and the ATLANTIS. The wave pole and sonobuoy equipment were launched, and when the planes arrived on the scene preparation for the exercise was complete. Figure 4.1 shows the planes used in the operation. The planes took up positions in tandem and flew at 3000 ft (there was a layer of cumulus clouds directly above) upwind in a path such that the ATLANTIS would appear in some of the stereo pairs. When the run began, the cameras were "simultaneously" triggered by the FM link (figure 4.2), and a series of ten

FIGURE 4.1 THE P2V's USED ON PROJECT SWOP



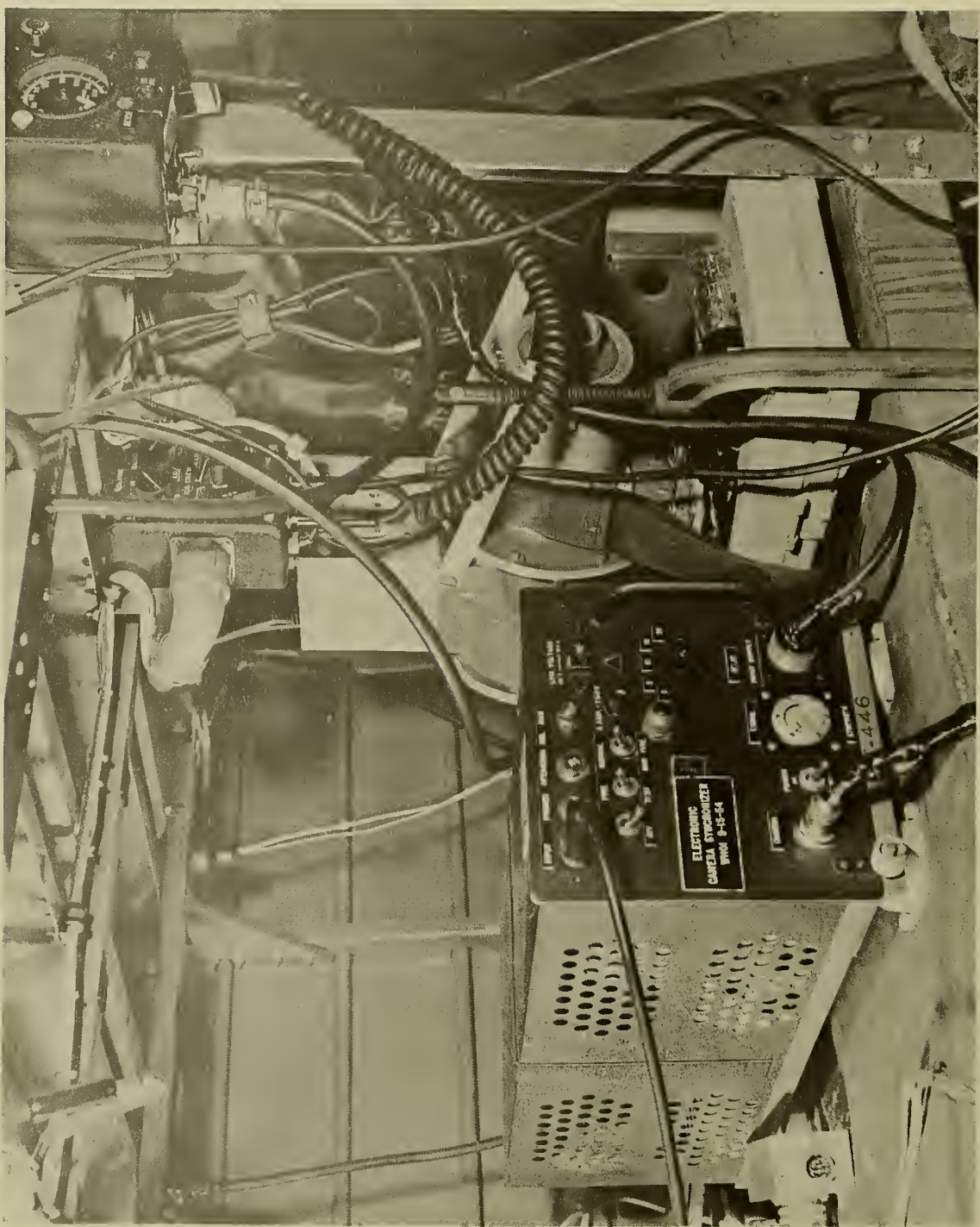
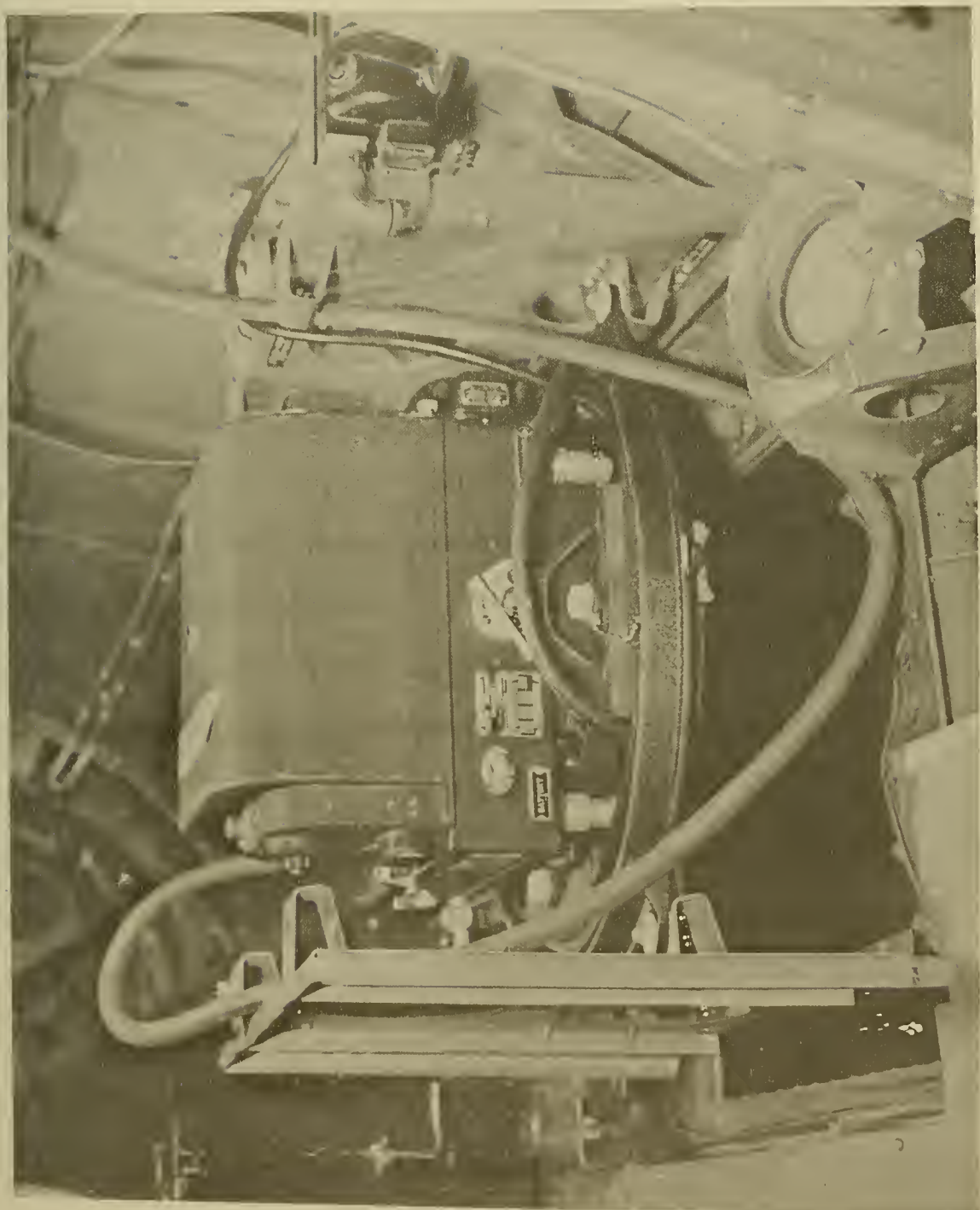


FIGURE 4.2
THE FM LINK

ONE OF THE MOUNTED CAMERAS

FIGURE 4.3



exposures were made at a recycling rate of 4 seconds. Ten such runs were made, and the end result was that each camera (figure 4.3) had taken 100 pictures. At the same time, the ATLANTIS was recording waves, and the variable distances between the sonobuoy and the ship.

At the conclusion of the program, the ship was secured, and the planes headed for NAS Anacostia where the film was processed at the U. S. Naval Photographic Center. The stereo-photographs were then turned over to HYDRO for preliminary analysis.

The success of the venture of 25 October 1954 is in no small part due to a practice test made some weeks earlier. The numerous "bugs" which were exposed and corrected could each have meant certain failure if they had gone undetected. Photography of a jeep traveling at 40 mph on the NADU runway established the recycling rate of the cameras and the efficiency of the FM link. The photo hatch, in one plane, obscured the fiducial marks on the photographs and the camera mount had to be modified. A run over a prescribed route indicated that altitude and station keeping of the planes required more attention. The following week, a second test was made and the results indicated that all gear was in good operating order. A detailed account of the operational technique appears in the literature, Marks and Rönne [1955] and Marks [1955].

References to Part 4

Marks, W., [1955]: Contouring the Sea Surface. Research Review, pp. 12-16, March.

Marks, W. and F. C. Rönne, [1955]: Aerial Stereo-Photography and Ocean Waves. Photog. Eng. v. 21, no. 1, 107-110, March.

Part 5

WAVE FORECASTS

Introduction

Operation SWOP came into being as a result of the establishment by ONR of a research project to be organized for the purpose of determining the two dimensional energy spectrum of a fully developed sea. One of the unsolved problems in present wave theory is that of the directional spectrum for a given sea condition. Since a vital part of the Pierson, Neumann, and James forecasting method [1955], now being published by the Hydrographic Office, is based on accurate knowledge of the directional spectrum, the project is one of considerable importance and interest. The presently assumed distribution of energy moving in the various directions in a fetch area is only approximated and the subject of considerable controversy. It is hoped that the successful conclusion of Operation SWOP will provide the desired information and result in improving the accuracy of our present wave forecasting techniques.

The Division of Oceanography of the U. S. Navy Hydrographic Office has participated in the project, both in selecting the site at which the operation was accomplished and in providing the wave forecasting service which made possible the aerial-photography under the required conditions.

Preliminary Planning

The following conditions were specified as necessary for successful execution of operation SWOP: (1) fully developed sea with significant height of 12 feet or greater, (2) ceiling in excess of 3000 feet, (3) excellent visibility, and (4) proper illumination level for aerial photography.

The request for selection of a site for SWOP, and prediction of occurrence of situations where the specifications could be met, were made early in September 1954. The planes necessary to carry out the stereo-photography were made available to the SWOP project for a ten day period in October 1954. The original plans were to carry out the operation in the Bermuda area. An analysis of historical wind and wave data at the Hydrographic Office indicated that there was an extremely low probability that the required conditions could be met in October in the Bermuda area. It was recommended that the operation be carried out off the east coast of the United States in the general area of 40N-65W. The statistics indicated that there was a high probability that at least one meteorological condition would occur during the ten day period in October with the potential of generating a 12 foot sea.

New plans for carrying our operation SWOP were formulated in accordance with the above recommendations. The photographic planes were now to be based at the NAS, South Weymouth, Mass. The WHOI ship ATLANTIS went to the area around 40N-65W to perform its functions in connection with the stereo-photographic project and to take wave obser-

vations for transmission to the U. S. Navy Hydrographic Office. The plan was that with the advent of predicted acceptable wave conditions, the ATLANTIS would steam toward the forecast point in order to arrive when wave conditions were favorable.

In order to make SWOP a successful operation, it was necessary that all four specifications be met. A note of pessimism was injected into the selection of 40N-65W as a site because of the type of meteorological conditions expected to prevail at the time wave conditions would be favorable. During the month of October in the area 40N-65W, wave generation would be accomplished by low systems moving up the east coast, accompanied by precipitation and low ceilings. Such conditions would preclude the execution of operation SWOP even though acceptable wave conditions were present. The realization that favorable wave conditions would exist in conjunction with unfavorable meteorological conditions made additional planning necessary. It was decided to carry out the photography when the low system was moving out of the operational area and the ceiling began to rise, but before the wind waves began to subside. This required accurate timing and a high degree of coordination between the Project Coordinator W. Marks of WHOI, the Photographic Planes, the R. V. ATLANTIS, and wave forecasting personnel at the U. S. Navy Hydrographic Office. The general plan for communication between the cooperating agencies, as submitted by Mr. Marks, indicated that the necessary timing could be accomplished. The wave forecasters at the Hydrographic Office were

reasonably confident that required sea conditions would be met and that they would be predicted with acceptable accuracy. In addition, it was felt that acceptable ceiling and visibility could be predicted.

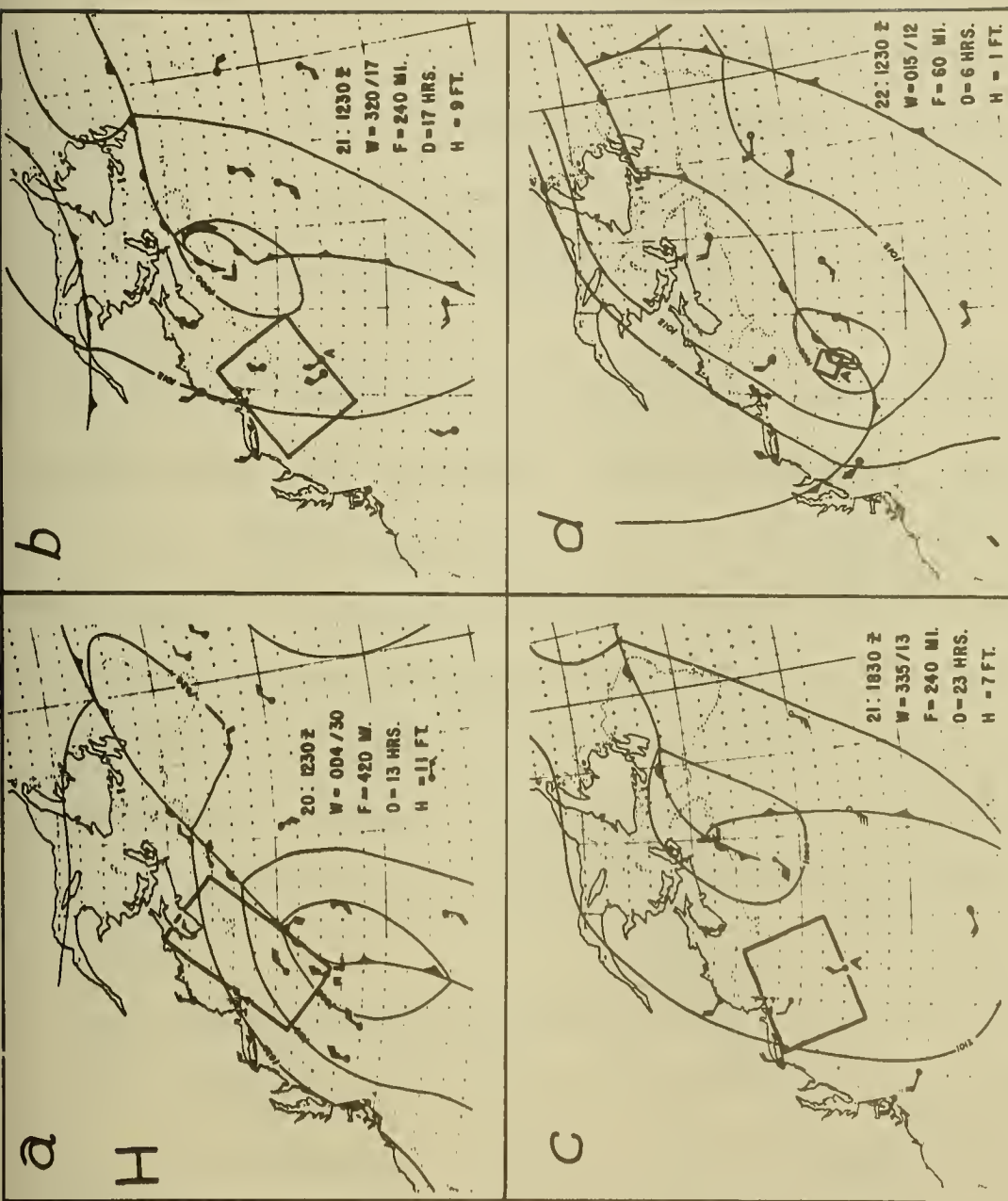
There remained only one problem with which the forecasting personnel could not cope; this was concerned with the requirement that the illumination level be sufficiently high to carry out the aerial photography. This requirement limits the operation to a daylight period of approximately six hours; and the sequence of increasing visibility, rising ceiling, with little or no decrease in wave height must necessarily occur during that time. Fortunately, these conditions did occur during daylight hours, with a decrease in wave height very shortly after the photography was accomplished. The careful preliminary planning, with consequent accurate timing, made possible the accomplishment of Operation SWOP.

Analysis of Meteorological Conditions*

The first significant wave height of over 5 1/2 feet was observed on October 20th at 1100Z, at which time the R. V. ATLANTIS was on station near 38°N 68°W. On the synoptic surface chart of 1230Z of October 18th, there was a quasi-stationary front oriented NNE-SSW and extending from Labrador to the Bahamas. A wave developed on this front during the 19th. By the 20th at 1230Z (fig. 5.1a) this wave was centered near 37°N 67.5°W

*Extracted from "Observations of the Growth and Decay of a Wave Spectrum" by Wilbur Marks and Joseph Chase, Woods Hole Oceanographic Institution, Woods Hole, Mass.

FIGURE 5.1 ESTIMATED FETCH AREAS FOR WEATHER SITUATION OF OCT. 2, 1954



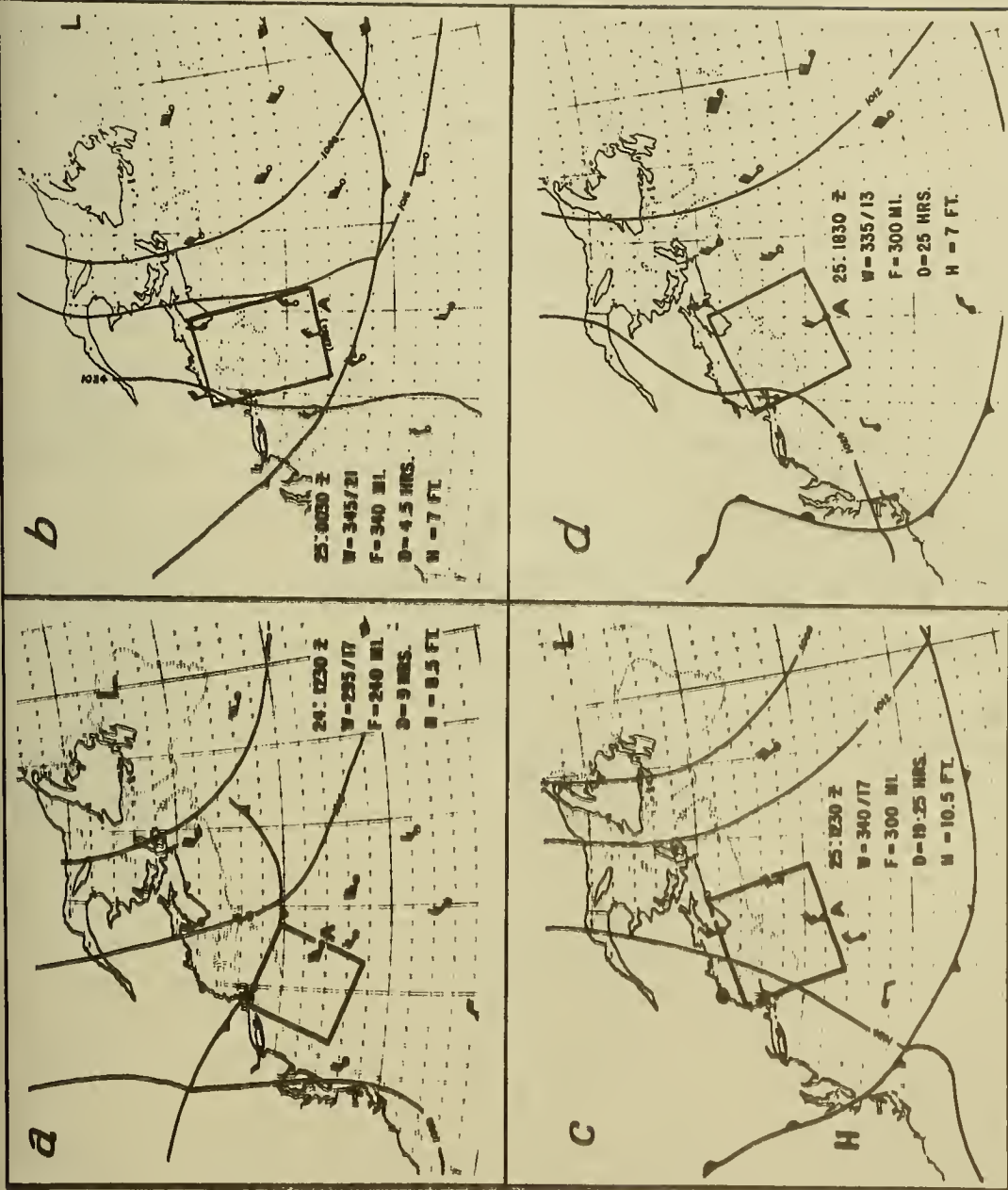
and had grown large enough to determine the wind pattern off the United States east coast. The position of the R. V. ATLANTIS is indicated by an A, and that portion of the wind field which generated waves that affected the R. V. ATLANTIS is outlined by the rectangle. The wind at the ship was nearly north while over the major part of the generating area it was north-easterly. The area of northerlies spread northward with the movement of the low.

By October 21st (figs. 5.1b and 5.1c) the frontal wave was well to the northeast leaving the ship in a northwest flow with the fetch length limited to the distance to the coast. A cold front oriented E-W is seen in eastern Canada (fig. 5.1b). This front moved southward passing the R. V. ATLANTIS during the morning of the 22nd. A small low which developed on this front is seen near the ship at 1230Z of the 22nd (fig. 5.1d). Later as this low moved northeastward a band of winds from the west-northwest moved southward to the ship. The flow was almost at right angles to the isobars and would have been difficult to forecast.

By 1230Z of the following day, the frontal system of the twenty-first had moved well to the east leaving the ship in a northwesterly flow for the 12 hours preceding the observation of 1200Z.

At 0030Z of October 24th the flow was westerly in the area ahead of the cold front moving south from New England. As the front got closer and assumed a WNW-ESE orientation, the flow became west-northwesterly as seen in the chart for 1230Z (fig. 5.2a). The front passed the R. V. ATLANTIS

FIGURE 5.2 ESTIMATED FETCH AREAS FOR WEATHER SITUATION OF OCT. 25, 1954



at about 1730 Z and the wind at the ship shifted to north-northwesterly (fig. 5.2b).

The principal low of the area at this time was centered east of Newfoundland and was moving eastward. The R. V. ATLANTIS was moved eastward to 39°N 65°W during the 24th and 25th to retain moderate to fresh breezes.

On the 25th, the day the aerial stereo-photographs were taken, the wind was north-northwest, Beaufort force 5 at 1230 Z (fig. 5.2c) diminishing to force 4 by 1830 (fig. 5.2d). The duration of wind up to the time of the wave observations was from 17 1/2 to 26 hours, making the test period the longest period of consistent force and direction for the cruise.

For the entire period from October 20th to the 25th there appears to have been little or no possibility of a contribution to the waves at the ship by wind fields in other parts of the North Atlantic. Therefore, the ship was essentially in the generating area at all times and no swell should be recorded.

Discussion of Predicted and Observed Wave Conditions

The first system with the potential of generating the required wave height appeared during 20 and 21 October. The prediction was for the development of waves 12 feet in height. The R. V. ATLANTIS reported 12 feet significant height at 201300 Z and was the maximum reported for this storm; wave heights ranged from 9.5 to 12 feet during the day. Although sea conditions were ideal, low ceilings with rain and accompanying poor

visibility prevailed throughout the day. This condition was expected to continue into the 21st with increasing ceiling and visibility but with slowly decreasing wave height. At 1300Z on the 21st, the R. V. ATLANTIS reported nine feet with gradual decrease in height becoming a reported seven feet at 1700Z. It was decided to take the stereo photographs on the morning of the 21st with the expected improved ceiling and visibility, and while the wave heights would still be acceptable, although not the originally desired 12 feet. The photographic planes took off, but one of the planes developed mechanical difficulties and was forced to return. No further opportunity was available to take advantage of this wave situation.

The second situation was expected to develop during the 23rd of October and carry into the 24th, but it was not expected to be quite of the intensity experienced on the 20th. Wave heights of 8.5 feet were reported by the R. V. ATLANTIS on the 23rd and 24th; the planes, however, were not available until the 25th. It was expected that the acceptable wave conditions would degenerate sometime during the 25th. On the 24th it appears that waves at least 7 feet in height would prevail during the night and early morning of the 25th, with gradual decrease during the morning. There was, however a good possibility that waves of at least seven feet significant height would continue into the early afternoon. On the basis of this possibility, it was planned that the stereo-photography be accomplished on the 25th. Fortunately acceptable wave heights continued into the early afternoon, and died down thereafter. Wave heights of seven to nine feet were reported by the R. V. ATLANTIS during the time the photography was accomplished.

Part 6

PHOTOGRAMMETRIC EVALUATION OF PROJECT SWOP

Introduction

Aerial photogrammetry is the science of obtaining reliable horizontal and vertical measurements of all unobscured natural and man-made features appearing in aerial photographs. Since the aerial photograph is a detailed and permanent record of a given section of the earth's surface, it furnishes more completely than any other means the information required in the preparation of maps and charts. Geometrically, all photographs are perspective views and all maps are orthographic views of the earth's surface. The science of aerial photogrammetry is used to convert the perspective views of the aerial photographs into the orthographic view of a map, and also to record properly all the photographed information into a true map presentation.

For regular photogrammetric mapping purposes, aerial photography obtained with the camera optical axis vertical, is accomplished in such a manner that there is approximately 60 percent overlap between photographs in line-of-flight, and approximately 30 percent sidelap between adjacent strips of photographs. The 60 percent overlap provides at least two different views of all features photographed, and is necessary to achieve the stereoscopic effect by which interpretation and measurements may be accomplished.

There are several types of photogrammetric instruments capable of utilizing aerial photography to plot topographic map manuscripts. All the first-order photogrammetric instruments are precision mechanical-optical stereoscopic devices which re-create the three-dimensional view of the photographed area and permit the plotting of horizontal and vertical information of the terrain onto a map manuscript. The accuracy of this information is basically a function of the flying height of the photographic aircraft and the type of plotting instrument.

Application to Project SWOP

Photogrammetric techniques lend themselves to the solution of many non-mapping problems. Thus, the ocean wave data required for the complete fulfillment of Project SWOP are readily obtained by photogrammetric techniques. Because of the nature of the project, however, several unusual problems were introduced. Ordinarily, over the stable terrain, stereoscopic photo coverage is obtained by the proper exposure interval of the aerial camera during flight of a single aircraft. Since the sea surface is in constant motion, two photographic aircraft with synchronized cameras were required to "stabilize" the images in the stereoscopic photo coverage. Also, some known ground control is a requisite for accurate photogrammetric mapping. No such control exists on the sea surface; therefore, for SWOP, a vessel towing a raft at a known distance was necessary to establish the "ground control". If all other factors are equal, greater final accuracy is obtained with lower flying height, and greater area coverage is obtained

with higher altitude. In order to conform with both the desired final accuracy and area coverage for the project, the optimum photographic conditions were determined and are shown in figure 6.1.

Test Flight

Of primary importance to the successful photographic accomplishment, was the ability to assure simultaneous exposure of the two aerial cameras. It was therefore necessary to build and check an electronic link to fire the two cameras. Oscillograph measurements made on the ground with the engines turned up, indicated that the cameras could be fired within one millisecond of each other, or better. To further substantiate this ability, a test flight was made over an airfield runway. Traveling in tandem at 160 mph, the two aircraft continuously photographed a truck traveling in the opposite direction at 40 mph (the fastest wave speed anticipated). The photographs were made with various delays installed in the cameras. That is, one camera was purposely fired 5 milliseconds after the other one. Then the delay was reversed. The result was that in no pair of photographs could it be visually ascertained that there was any change in position of the truck. Furthermore, the photos were enlarged 25 times and no difference could be measured that was greater than the measuring error itself.

Operation Procedure

The sea surface presents a relief pattern which is always moving and changing its shape, and it offers no fixed marks which can be used as control. However, as in the case of the rough sea required for this project,

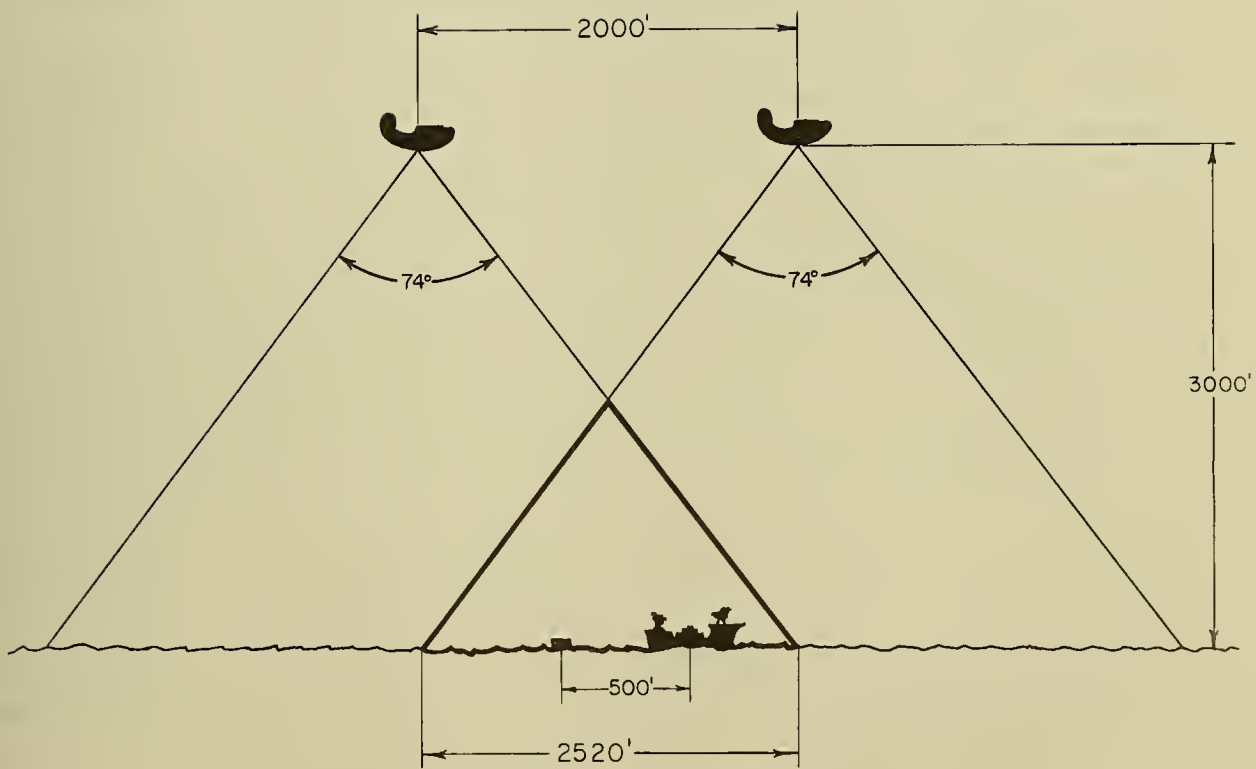


FIG. 6.1 SCHEMATIC REPRESENTATION OF OPERATIONAL PROCEDURE

there was a great deal of contrast between the foam and the water, and this contrast was utilized for the separation of tonal values in the photographs. The serious problem of reflection glare was overcome by taking the pictures when the solar altitude was below 40°. This, however, reduced the light intensity and caused a reduction in image definition.

The operational procedure involved the use of two aircraft flying in tandem 2,000 feet apart and at an altitude of 3,000 feet. Each plane was equipped with a standard mapping camera (Navy CA-8) and the cameras were triggered simultaneously from the forward (master) plane by an FM radio link. The square 9" x 9" format of the aerial photography represents 74" side-to-side coverage from the camera lens. The planes flew directly into the wind, thereby eliminating crab and reducing the air speed.

To help establish the ground control, the research vessel ATLANTIS was stationed in the operational area. The vessel towed a target raft 500 feet behind it. The distance between the raft and the ship was continuously monitored by a sonar buoy on the raft which received a radio impulse through the air from the vessel, and retransmitted the signal to the vessel through water. The distance was recorded every two seconds.

The planes adjusted their altimeters to the barometer on the ship at the time the pictures were taken. The distance between the two planes was maintained at about 2,000 feet by means of a range finder located in the slave plane, and utilizing the wing span of the master plane as base line.

The ATLANTIS was instructed by radio at the moment each photographic run started and a side-mark was made on the record of the distance monitoring device. Ten pairs of photographs were taken on each run which required about 36 seconds. A total of 100 stereo pairs was accomplished for the project.

Stereo Analysis

The stereophotogrammetric graphic results were prepared by the Photogrammetry Branch of the U.S. Navy Hydrographic Office. A total of four stereo pairs of aerial photographs was selected for detailed analysis. They were chosen on the basis of photographic quality and also because they showed the ATLANTIS-raft combination. The instrument used was the Zeiss Stereoplanigraph, considered to be among the most accurate of the first-order photogrammetric plotting instruments. The direct reading ability of this instrument is 0.01 mm.

The first model (a model is the rectangular overlapping portion of two aerial photographs which can be viewed stereoscopically) was contoured by establishing an assumed vertical datum. That is, in each corner of the model the low point of a trough was assumed zero elevation and the contour data throughout the model was based on that datum. Each model represented a ground rectangle with sides of approximately 2700 feet and 1800 feet, or nearly 5 million square feet of ocean surface, at a scale of 1:3,000. This model was used to determine the spacing to be used on the spot height grid, but it is not reproduced herein.

In order to determine the energy spectrum of the sea surface a grid of spot heights must be made. Accordingly, the next three models to be analyzed presented this spot height data. A total of 5612 spot heights per model were determined at 30 feet ground distances in a square grid pattern.

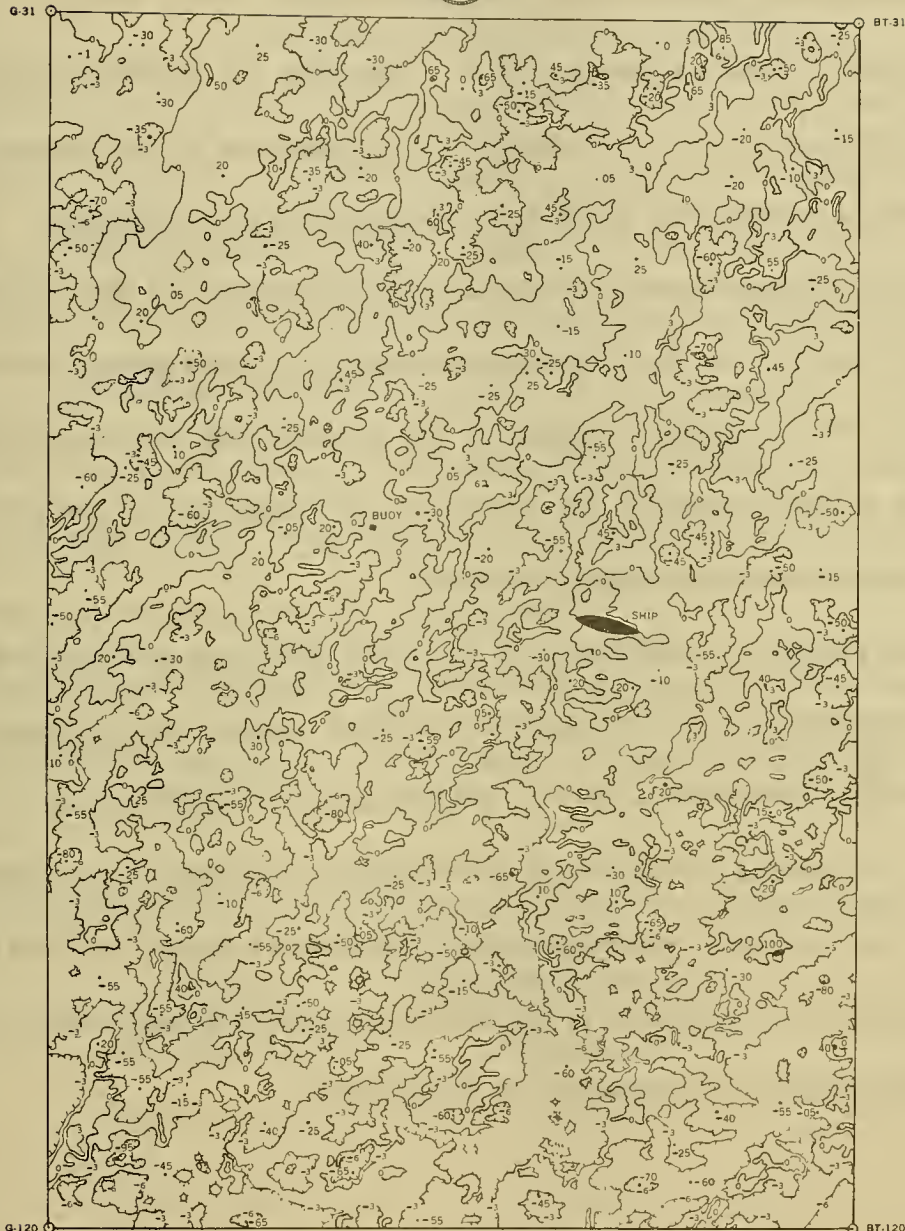
The above described graphics were forwarded to N. Y. U. for analysis and a new vertical datum was derived analytically.* From this information eight spot heights were established along the model periphery. This information was forwarded to the Hydrographic Office and was used to re-establish a vertical datum on the final model set-up. This final model is shown in figure 6.2. Of the eight spot heights, six were held photogrammetrically and two could not be held. One of these was located in the left-center and had an error of -3.0 feet; the other was located in the lower-right corner and had an error of -7.0 feet. Table I shows the (NYU) computed values, the instrument values, and the errors, for all eight points.

Table I. Final level values for the stereo wave data

<u>Point No.</u>	<u>Computed Value (mm)</u>	<u>Instrument Value (mm.)</u>	<u>Error (mm)</u>
G-31	0.00	0.00	0.00
G-68	0.00	-0.30	-0.30
G-120	-0.26	-0.25	0.00
P-120	-0.27	-0.25	0.00
BJ-120	-0.05	0.00	0.00
BS-70	+0.12	+0.10	0.00
BT-31	+0.01	+0.05	0.00
BT-120	+0.08	-0.60	-0.70

*See Part 7.

PROJECT SWOP



Scale 1,3,000

100 0 100 200 300 400 500 ft.

CONTOUR INTERVAL 0.30 mm
(1.0 mm = 9.8425 ft.)

Prepared by the U.S. Navy Hydrographic Office for the Office of Naval Research using stereophotogrammetric methods (stereoplaniograph). April 1956

Contour values given in tenths of a millimeter.
Spot heights given in hundredths of a millimeter.

SHEET NO. 2

Run No. 3, Model No. 6
Date of Photography: 25 October 1956
Time of Photography: 1728 GCT

FIGURE 6.2 GRAPHIC FOR DATA SET No. 2

Accuracy of Results

Reconnaissance-type film was used erroneously in the aerial cameras instead of the more stable topo-base film. The film furnished this Office was not dimensionally stable, and made the recapturing of the precise instrument settings impossible when the last model was re-compiled. Therefore, the final photogrammetric solution could not match all the computed values. This explains the discrepancy in holding all eight points as described above. The computed values for the leveled data are more valid since they are substantiated by the leveled graphic analysis which shows about equal areas above and below sea level.

The final graphic forwarded to N. Y. U. exhibits both contour and spot-height information over the nearly 5 million square feet of ocean surface. The spot height accuracy is ± 0.05 mm (at 1:3,000 scale) or ± 0.5 feet. The contour interval is 3 feet and is accurate to ± 0.2 mm or ± 2 feet. The relatively short distance represented by the ATLANTIS-raft combination is not adequate to assure a precise horizontal scale, and the horizontal accuracy is estimated to be ± 2 feet.

Part 7

PRELIMINARY ANALYSIS, CHOICE OF GRID SPACING AND DISCUSSION OF ALIASING

Weather and Wave Pole Observations

Weather and wave pole observations were made prior to and at the time of the flight of the planes. A running graph of the wind direction and velocity and of the estimated significant wave heights and the dominant wave direction as observed on the R. V. ATLANTIS prior to and at the time of the wave pole and stereo observations is shown in figure 7.1. The times of the wave pole observations and of the two pairs of photos finally chosen for a complete analysis are also shown. The winds 6 hours prior to the time of the stereo observations averaged about 19 or 20 knots.

The significant heights of the uncorrected wave pole observations were computed at WHOI, and the results of these computations yielded the following values.

Table 7.1

Significant heights from uncorrected wave pole observations

<u>Time</u>	<u>Significant Height</u>
1547 to 1610Z	5.02 feet
1652 to 1715Z	5.04 feet
1756 to 1821Z	5.12 feet

A paper by Marks and Chase [1955] summarizes these results and the way the visually observed values seemed to be quite a bit higher than the wave pole values and seemed to remain high for quite a while after the 19 to 20 knot

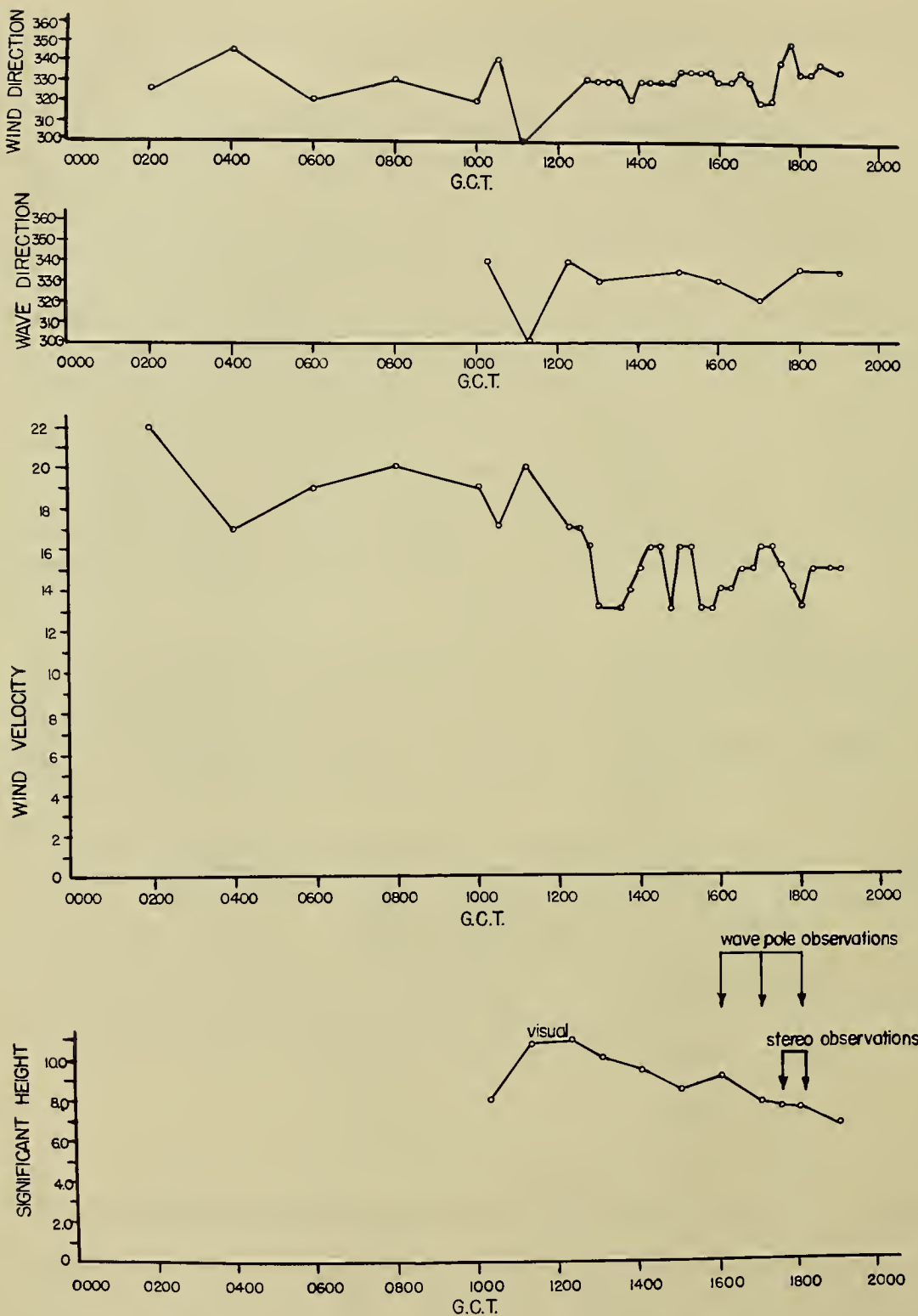


FIGURE 7-1 WIND AND VISUAL WAVE OBSERVATION DATA
OBTAINED BY THE R.V. ATLANTIS

winds had died down. Note that the visual estimate of the significant height was 7.5 feet at 1800Z.

Stereo Contour Data

The first data prepared by the Photogrammetry Division was in the form of a contour analysis of one of the stereo pairs. It was somewhat disconcerting because the expected waves with lengths of from 100 to 300 feet or so could not be seen in the contours and the range of contoured heights was far in excess of anything to be expected from a 20 knot wind.

The first hint of where the difficulty lay came from Woods Hole where line sections of the contoured surface were drawn. These showed almost a straight line tilt along a given section with the waves we were looking for superimposed thereon. A line section with arbitrary scale units from the lower left to the upper right of the contoured surface is shown in figure 7.2. The unforeseen difficulty of determining a true mean zero reference plane on the open ocean with no known reference points had arisen.

It was also pointed out at this time that spot heights could be determined by Hydro with far greater accuracy than the contours could be drawn due to the nature of the techniques involved. The original plan had been to choose an appropriate grid and read spot heights from the contoured data. This now had to be revised, and it was now necessary to find a way to determine the true zero reference plane and to choose a grid, the desired number of points to be read, and the desired resolution and statistical reliability, all on the basis of the data then on hand.

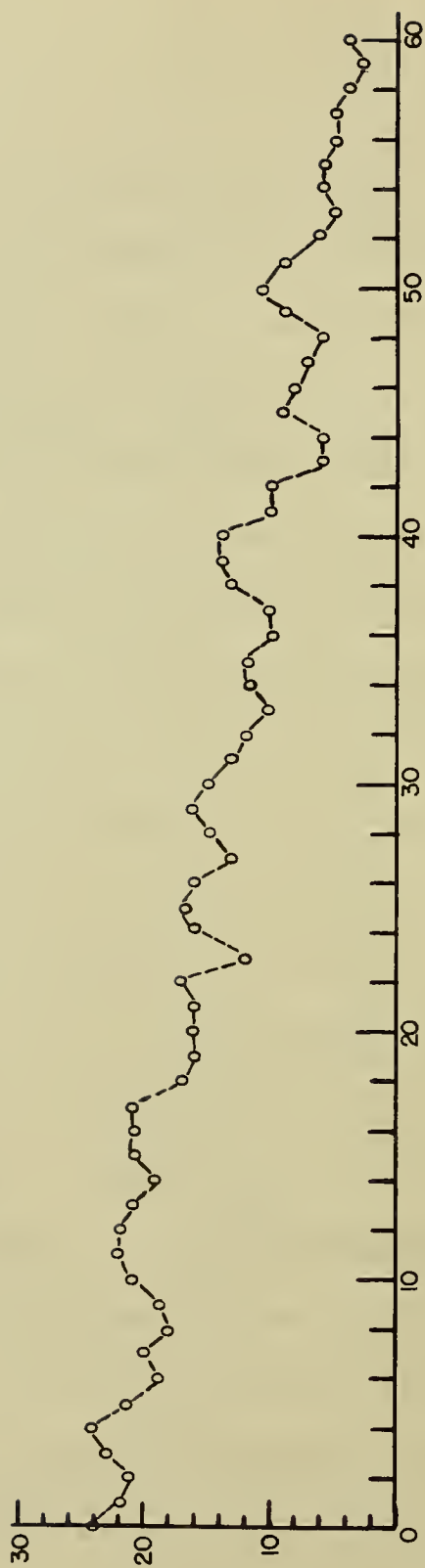


FIG. 7.2
LINE SECTION OF CONTOURED SURFACE PROVIDED BY THE HYDROGRAPHIC OFFICE.

Decision on Grid Interval and Number of Points to be Read

Fortunately the theoretical aspects of the problem had been carried out to the point where the methods for the one-dimensional analyses of time series developed by Tukey [1949] had been extended to the two-dimensional wave number analysis desired in this problem. Thus the formulas for resolution, aliasing, and degrees of freedom were available. They will be derived in Part 8. It was also realized that it was not essential to have the dominant wave direction roughly parallel to the sides of the rectangular grid of points to be used.

The leveling problem was then studied and formulas were derived for determining the true zero reference plane. It was assumed that the spot heights would be reported with reference to some unknown arbitrary reference plane of the form $z = ax + by + c$. If η is the reported value, then $\eta^* = \eta - ax - by - c$ is the value with reference to a true zero reference plane, and $\Sigma(\eta^*)^2$ will be a minimum. By standard least squares techniques, the values for a , b and c can be determined, and the data can be leveled. The derivation and the procedures used are described in the following two parts of this report.

Since leveling was no longer a problem, the problems of statistical reliability, aliasing, and resolution were studied. Suppose that the spot heights are read at an interval of Δx feet on a square grid. Then, due to the nature of the methods of analysis, some spectral components shorter than $2\Delta x$ and all components shorter than $\sqrt{2}\Delta x$ will be aliased so that they appear as

longer waves than they actually are. Suppose that m lags are to be used in the x and y directions of the rectangular grid. Then the E value contributed by the waves with lengths from infinity to $4m\Delta x$ will all be concentrated at the zero wave number of the spectral coordinate system. The next wave number will correspond to a wavelength of $2m\Delta x$ and will actually cover a range from $4m\Delta x$ to $4m\Delta x/3$. On a line at 45° to the grid system of the spectrum, it is necessary to shorten the above wavelengths by $\sqrt{2}/2$. Finally, if N_x and N_y are the number of points on the grid system in the x and y directions, then the number of degrees of freedom is given by

$$f = 1.58 \left(\frac{N_x}{m_x} - \frac{1}{2} \right) \left(\frac{N_y}{m_y} - \frac{1}{2} \right)$$

where for purposes of symmetry it was decided to let $m_x = m_y$.

The significant wave heights reported by the wave pole observations corresponded to a wind of about 17 knots, and an attempt was made to choose a method of analysis such that a theoretical Neumann spectrum (Neumann [1954]) for 17 knots would be adequately resolved. Also since winds of 20 knots had occurred previously, it was decided to guard against wavelengths due to a wind of 20 knots in addition to those due to 17 knots.

It was estimated that periods from 2.25 to 10 seconds would be present and that approximately 10 percent of the energy would be at frequencies above 0.29 cycles per second (or a period of 3.45 seconds). A wavelength of 60 ft corresponds to this period, and hence a spacing of 30 feet between points would be needed to insure no more than 10 percent aliasing.

A grid of 30 feet was therefore chosen. Smaller values of Δx would require a much greater m than that actually chosen and many more spot heights.

The winds at the surface varied from 17 to 20 knots just prior to the time of the observations and hence the values seemed consistent. Spectral periods as high as 11 seconds might have been present in the waves due to the 20 knot winds. This period would correspond to a wavelength of about 600 feet.

With a grid spacing of 30 feet, the area of the stereo analysis for one pair of photographs was found to contain about 60 points on the short side and more than 90 points on the long side. This would imply the determination of 5400 spot heights from each stereo pair.

Various lags were then tested and a value of m equal to 20 was chosen for two reasons. The first was that there would be adequate resolution, and the second was that there would be enough statistical reliability.

With respect to resolution, wavelengths greater than 2400 feet would then show up at the origin and since this corresponds to a period of over 20 seconds the energy at zero wave number should be entirely due to aliasing and white noise reading error on the assumption that the Neumann spectrum was roughly correct. The next wave number would cover a range in lengths from 2400 feet to 800 feet, and it would also not be expected to show any appreciable wave energy.

These values were also checked on the assumption that the peak of the spectrum would fall at an angle of 45 degrees to the coordinates of the spec-

trum. A wavelength of 1680 feet would still not be expected, and a wavelength of 560 feet would just barely be beginning to show up.

On the basis of the transformation needed to go from the theoretical Neumann frequency spectrum to the wave number spectrum, it was estimated that the peak in the spectrum would fall four or five wave numbers away from the origin, and that the range covered would adequately trace out the details of the shape of the spectrum. The full consequences of these decisions will be discussed in a later section.

With respect to statistical reliability, there are 16 degrees of freedom for each point estimated on the spectrum for each set of data. Fifty degrees of freedom are desirable so it was decided to do three pairs of stereo photos, since, with the same grid alignment of all three, the estimates for each set of data could be averaged to obtain final estimates with 48 degrees of freedom. One of the stereo pairs spot heighted by Hydro turned out to have serious "barrel" distortion in addition to tilt, and it had to be discarded so the final results will be based on 32 degrees of freedom.

A choice of a 60 by 90 grid and 20 lags (really 20 to the left, 20 up and 20 down plus all combinations such as, say, 5 to the left and 17 up) implies 861 points to be determined for the co-variance surface and 861 points for the final spectrum. About 4,000,000 multiplications and an equal number of additions are needed to get each of the co-variance surfaces, and about 720,000 multiplications and additions are needed to get each of the raw spectra.

Much the same considerations entered in the above choices as enter in

the choice of time interval, number of lags, resolution and degrees of freedom in the analysis of a wave record as a function of time at a fixed point (Pierson and Marks [1952]) except that far more data processing and numerical computation is necessary. As an example, to double the resolution with the same grid spacing and same number of degrees of freedom would require 40 lags and four times the number of spot heights. The covariance surface would then require about 48 million multiplications and additions. The time required would be more than twelve times greater than was actually used. To have reduced the aliasing by halving Δx , would have required four times the number of spot heights, 40 lags, and the above number of multiplications. Moreover, the total energy over $3/4$ of the area of the spectrum would have been only 10 percent of the total energy of the sea surface.

For these reasons, Hydro was requested to read spot heights on a square grid with 30 feet between intersections. Essentially all of the details of the analysis were decided by this one choice of grid interval.

References

Marks, W., and J. Chase [1955]: Observation of the growth and decay of a wave spectrum. Contribution No. 769, from the Woods Hole Oceanographic Institution.

Part 8

EQUATIONS FOR LEVELING THE DATA, ESTIMATING THE DIRECTIONAL SPECTRUM, AND CORRECTING THE WAVE POLE SPECTRUM

Leveling the Data

The original spot height data reported by Hydro was reassigned a position code for computational purposes such that the points would fall in the first quadrant of a Cartesian coordinate system and such that the first column of 90 points would fall on the y-axis and the bottom row of 60 points would fall on the x-axis. For simplicity in writing the following equations, let the free surface, η , be represented by an N when a spot height is considered. The pattern of the points was as follows:

$N_0, 89 \dots \dots \dots \dots \dots \dots \dots \dots \dots N_{59}, 89$

6

1

6

6

1

6

1

1

10

1

N

N₀, 4

$$N_{0,1} \ N_{1,1}$$

$N_{0,0} \ N_{1,0} \ N_{2,0} \ \dots \ \dots \ \dots \ \dots \ \dots \ \dots \ N_{59,0}$

and the general element will be designated by N_{jk} .

These 5400 points cover an extensive area of the sea surface such that quite a few waves are involved. Were they measured with respect to a zero determined by the level of the water in the absence of the waves, they would average to zero and the sum of their squares would be a minimum. However, they were read with reference to an arbitrary tilted plane instead of with reference to the sea level.

The values desired with respect to zero level are given by equation (8.1) where the unknown constants a , b , and c absorb the effects of the grid spacing.

$$(8.1) \quad N_{jk}^* = N_{jk} - aj - bk - c$$

$$j = 0, \dots, n-1 \quad k = 0, \dots, m-1$$

$$n = 60 \quad m = 90$$

Consider equation (8.2).

$$(8.2) \quad V = \sum_{k=0}^{m-1} \sum_{j=0}^{n-1} (N_{jk}^*)^2 = \sum_{k=0}^{m-1} \sum_{j=0}^{n-1} (N_{jk} - aj - bk - c)^2$$

The value of V should be a minimum with reference to true sea level (if the area covered by the points is large enough), and this can be accomplished if

$$\frac{\partial V}{\partial a} = 0 ,$$

$$\frac{\partial V}{\partial b} = 0 ,$$

$$\text{and} \quad \frac{\partial V}{\partial c} = 0 .$$

Equations (8.3) lead to equations (8.4).

$$\sum_{k=0}^{m-1} \sum_{j=0}^{n-1} (N_{jk} - aj - bk - c)j = 0$$

$$(8.4) \quad \sum_{k=0}^{m-1} \sum_{j=0}^{n-1} (N_{jk} - aj - bk - c)k = 0$$

$$\sum_{k=0}^{m-1} \sum_{j=0}^{n-1} (N_{jk} - aj - bk - c) = 0$$

The last equation simply states that the average of all the points in the plane when truly leveled should be zero. Points on a tilted surface could still average to zero, but V would not be a minimum; and thus the other two equations assure that V will be a minimum.

The indicated summations can be carried out, and the result is three simultaneous linear equations in the three unknowns, a , b , and c .

(8.25)

$$\begin{array}{ccc|c|c} \frac{mn(n-1)(2n-1)}{6} & \frac{n(n-1)m(m-1)}{4} & \frac{mn(n-1)}{2} & a & \sum_{k=0}^{m-1} \sum_{j=0}^{n-1} jN_{jk} \\ \frac{n(n-1)m(m-1)}{4} & \frac{nm(m-1)(2m-1)}{6} & \frac{nm(m-1)}{2} & b & = \sum_{k=0}^{m-1} \sum_{j=0}^{n-1} kN_{jk} \\ \frac{mn(n-1)}{2} & \frac{nm(m-1)}{2} & \frac{nm}{1} & c & \sum_{k=0}^{m-1} \sum_{j=0}^{n-1} N_{jk} \end{array}$$

For $m = 90$, $n = 60$, the determinant is known, and the indicated summations on the right hand side, when performed on the data, then permit the values of a , b and c to be found.

Estimating the Directional Spectrum

In theoretical discussions of wind generated gravity waves, it has been shown by Cox and Munk [1954] and by Pierson [1955] that

$$(8.6) \quad Q(x', y', t') = \lim_{\substack{T \rightarrow \infty \\ X \rightarrow \infty \\ Y \rightarrow \infty}} \frac{1}{XYT} \int_{-\frac{T}{2}}^{\frac{T}{2}} \int_{-\frac{X}{2}}^{\frac{X}{2}} \int_{-\frac{Y}{2}}^{\frac{Y}{2}} \eta(x, y, t) \eta(x+x', y+y', t+t') dx dy dt$$

$$= \frac{1}{2} \int_{-\pi}^{\pi} \left[\int_0^{\infty} [A(\mu, \theta)]^2 \cos \left[\frac{\mu^2}{g} (x' \cos \theta + y' \sin \theta) - \mu t' \right] d\mu d\theta \right]$$

$$= \frac{1}{2} \int_{-\infty}^{\infty} \left[\int_{-\infty}^{\infty} [A^*(\alpha, \beta)]^2 \cos (\alpha x' + \beta y' - \sqrt{g}(\alpha^2 + \beta^2)^{1/4} t') d\beta \right] d\alpha$$

In equation (8.6), $\alpha = \mu^2 \cos \theta / g$, $\beta = \mu^2 \sin \theta / g$, $\mu = \sqrt{g}(\alpha^2 + \beta^2)^{1/4}$,

and $\theta = \tan^{-1}(\beta/\alpha)$. Also

$$(8.7) \quad [A^*(\alpha, \beta)]^2 = \frac{\sqrt{g}}{2} \frac{[A(\sqrt{g}(\alpha^2 + \beta^2)^{1/4}, \tan^{-1} \beta/\alpha)]^2}{[\alpha^2 + \beta^2]^{3/4}}$$

If x' and y' are chosen to be zero, then an average over time can replace an average over space and time, and the result is

$$(8.8) \quad Q(t') = \lim_{T \rightarrow \infty} \frac{1}{T} \int_{-\frac{T}{2}}^{\frac{T}{2}} \eta(x, y, t) \eta(x, y, t+t') dt$$

$$= \frac{1}{2} \int_{-\pi}^{\pi} \int_0^{\infty} [A(\mu, \theta)]^2 \cos \mu t' d\mu d\theta$$

$$= \frac{1}{2} \int_0^{\infty} [A(\mu)]^2 \cos \mu t' d\mu$$

The above is equivalent to observing the waves at a fixed point as a function of time, and all knowledge of the direction of travel of the waves is lost since

$$\int_{-\pi}^{\pi} [A(\mu, \theta)]^2 d\theta = [A(\mu)]^2$$

The procedures for analyzing waves as a function of time at a fixed point have been described by Pierson and Marks [1952], and Ijima [1956] has carried out quite a number of such analyses in Japan with very interesting results. The same techniques are being used by Lewis [1955] to analyze the spectra of model waves and ship motions in a towing tank. The wave pole records will be analyzed using the methods described by Pierson and Marks [1952].

If t' is chosen to be zero, then an average over space can replace an average over time and space and the result is

$$(8.9) \quad Q(x', y') = \lim_{\substack{X \rightarrow \infty \\ Y \rightarrow \infty}} \frac{1}{X} \frac{1}{Y} \int_{-\frac{X}{2}}^{\frac{X}{2}} \int_{-\frac{Y}{2}}^{\frac{Y}{2}} \eta(x, y) \eta(x+x', y+y') dx dy \\ = \frac{1}{2} \int_{-\infty}^{\infty} \int_{-\infty}^{\infty} [A^*(\alpha, \beta)]^2 \cos(\alpha x' + \beta y') d\beta d\alpha$$

In equation (8.9) the same right hand side results if $-x'$ and $-y'$ are substituted for x' and y' , and therefore $Q(x', y') = Q(-x', -y')$.

The above is equivalent to observing the waves at an instant of time over an area. Some knowledge of the direction of travel of the waves is lost. Consider, for example, a progressive simple sine wave observed at an instant

of time. A line parallel to the crests can be determined, and the direction of travel of the wave will be perpendicular to this line, but the direction can be either one of two directions, one the opposite of the other.

This indeterminacy is avoided in this analysis by considering a positive direction, x' , to be the dominant direction of the wind and by assuming that the spectral components of the waves being studied are all traveling with an angle of $\pm 90^\circ$ to the wind. Then $[A(\mu', \theta')]^2$ would be zero for $\pi/2 < \theta' < \pi$ and for $-\pi/2 < \theta' < -\pi$, and $[A(\alpha', \beta')]^2$ would be zero for $-\infty < \beta' < 0$. (Note μ', θ', α' and β' would have to be redefined with respect to the x' direction.) When these assumptions are applied to the results to be obtained the directions will be completely determined.

Consider equation (8.9) again. One can form the indicated operation given by equation (8.10).

$$(8.10) \lim_{\substack{M \rightarrow \infty \\ N \rightarrow \infty}} \int_{-\frac{M}{2}}^{\frac{M}{2}} \int_{-\frac{N}{2}}^{\frac{N}{2}} Q(x'y') \cos(\alpha*x' + \beta*y') dx' dy'$$

$$= \lim_{\substack{M \rightarrow \infty \\ N \rightarrow \infty}} \frac{1}{2} \int_{-\frac{M}{2}}^{\frac{M}{2}} \int_{-\frac{N}{2}}^{\frac{N}{2}} [\int_{-\infty}^{\infty} \int_{-\infty}^{\infty} [A*(\alpha, \beta)]^2 \cos(\alpha x' + \beta y') \cos(\alpha*x' + \beta*y') d\alpha d\beta] dx' dy'$$

The term after the equals sign can also be written

$$(8.11) \quad \lim_{\substack{M \rightarrow \infty \\ N \rightarrow \infty}} \int_{-\infty}^{\infty} \int_{-\infty}^{\infty} \int_{-\frac{M}{2}}^{\frac{M}{2}} \int_{-\frac{N}{2}}^{\frac{N}{2}} \frac{1}{4} [A^*(\alpha, \beta)]^2 \left[\cos[x'(\alpha + \alpha^*) + y'(\beta + \beta^*)] + \cos[x'(\alpha - \alpha^*) + y'(\beta - \beta^*)] \right] dx' dy' d\alpha d\beta$$

$$= \lim_{\substack{M \rightarrow 0 \\ N \rightarrow 0}} \int_{-\infty}^{\infty} \int_{-\infty}^{\infty} [A^*(\alpha, \beta)]^2 \left[\frac{\sin \frac{N}{2}(\alpha + \alpha^*) \sin \frac{M}{2}(\beta + \beta^*)}{(\alpha + \alpha^*)(\beta + \beta^*)} + \frac{\sin \frac{N}{2}(\alpha - \alpha^*) \sin \frac{M}{2}(\beta - \beta^*)}{(\alpha - \alpha^*)(\beta - \beta^*)} \right] d\alpha d\beta$$

When Dirichlet's formula is applied, the result is finally that equation (8.12) is obtained.

$$(8.12) \quad [A^*(\alpha^*, \beta^*)]^2 + [A^*(-\alpha^*, -\beta^*)]^2 = \frac{1}{\pi^2} \int_{-\infty}^{\infty} \int_{-\infty}^{\infty} Q(x', y') \cos(\alpha^* x' + \beta^* y') dx' dy'$$

Note that substituting $-\alpha^*$ and $-\beta^*$ for α^* and β^* leaves equation (8.12) unchanged.

Equations (8.9) and (8.12) are the x, y plane analogues of the classical time series equations which state that the covariance function is the Fourier transform of the power spectrum and conversely that the Fourier transform of the power spectrum is the covariance function. When applied to the problem of finding the directional spectrum of a wind generated sea from discrete data, the integrals have to be replaced by summations and formulas analogous to the Tukey formulas for time series have to be derived.

In deriving the equations used to determine the directional spectrum, the analogy to the one-dimensional case given by Tukey [1949] will be shown. The

theoretical equations in the one-dimensional case are given by

$$(8.13) \quad Q(t') = \lim_{t \rightarrow \infty} \frac{1}{T} \int_{-\frac{T}{2}}^{\frac{T}{2}} \eta(t) \eta(t + t') dt$$

and

$$(8.14) \quad [A(\mu)]^2 = \frac{1}{\pi} \int_{-\infty}^{\infty} Q(t') \cos \mu t' dt'$$

The equations due to Tukey [1949] are given by equations (8.15) to (8.17)

where $N_1, N_2, N_3, \dots, N_n$ are given values equally spaced usually in time.

$$(8.15) \quad Q(p) = \frac{1}{n-p} \sum_{k=1}^{n-p} N(k) N(k+p) \quad p = 0, 1, \dots, m.$$

$$Q_o^* = Q_o, \quad Q_p^* = 2Q_p, \quad (p = 1 \text{ to } m-1), \quad \text{and} \quad Q_m^* = Q_m.$$

$$(8.16) \quad L_h = \frac{1}{m} \sum_{p=0}^m Q_p^* \cos \frac{\pi ph}{m} \quad h = 0, 1, \dots, m.$$

$$\text{Let } L_{-1}^* = L_{+1}^*, \quad \text{and} \quad L_{m-1} = L_{m+1}.$$

$$(8.17) \quad U_h = 0.23 L_{h-1} + 0.54 L_h + 0.23 L_{h+1}. \quad h = 0, 1, \dots, m.$$

$$\text{Define } U_o^* = U_o/2, \quad U_h^* = U_h \quad (h = 1 \text{ to } 19), \quad U_m^* = U_m/2,$$

In the above equations (8.15) is the discrete approximation to equation

(8.13). Also in equation (8.13), $Q(t')$ equals $Q(-t')$ and to obtain the

discrete approximation to (8.14), $Q(p)$ is expanded as a periodic even function about p equal to zero. Thus Q_0 received a weight of one, Q_1 through Q_{m-1} receive double weight, and Q_m received a weight of one.

The values of L are the discrete estimates of the Fourier coefficients of the even expansion of Q .

Due to the fact that the L 's are only estimates of the spectrum since the series of readings is finite, they have to be filtered to recover a smoothed estimate of the spectrum in terms of the U 's.

There is, of course, another way to estimate the spectrum. The original series of points could be expanded in a Fourier series. Sine and cosine coefficients a_n and b_n , for periods of $n\Delta t/1$, $n\Delta t/2$, $n\Delta t/3$, etc. would then be computed. The quantity $c_n^2 = a_n^2 + b_n^2$ is then a very unstable estimate of the energy at that particular frequency. A proper running weighted average of the values of c_n^2 would then recover the spectrum as determined by the Tukey method. The number of degrees of freedom (f) is a measure of the number of values of c_n^2 weighted in the average and of the shape of the weighting process. The U 's have a Chi Square distribution with f degrees of freedom.

The values of U have the dimensions of $(\text{length})^2$, and U_h as given above is an estimate of the contribution to the total variance made by frequencies in the range from $2\pi(h - \frac{1}{2})/\Delta tm$ to $2\pi(h + \frac{1}{2})/\Delta tm$.⁺

The theoretical equations in this two-variable problem are given by

⁺For $h = 0$ and $h = m$ the values of U must be halved since one of the frequencies defined above is not applicable.

$$(8.18) \quad Q(x'y') = \lim_{\substack{X \rightarrow \infty \\ Y \rightarrow \infty}} \int_{-\frac{X}{2}}^{\frac{X}{2}} \int_{-\frac{Y}{2}}^{\frac{Y}{2}} \eta(x, y) \eta(x + x', y + y') dx dy$$

and

$$(8.19) \quad [A^*(\alpha^*, \beta^*)]^2 + [A^*(-\alpha^*, -\beta^*)]^2 = \frac{1}{\pi^2} \int_{-\infty}^{\infty} \int_{-\infty}^{\infty} Q(x', y') \cos(\alpha x' + \beta y') dx' dy'$$

The analogous summation formula for the covariance surface over the set of leveled readings N_{jk}^* is given by

$$(8.20) \quad Q(p, q) = \sum_{k=0}^{m-1-|q|} \sum_{j=0}^{n-1-p} \frac{N_{jk}^* N_{j+p, k+q}^*}{(n-p)(m-|q|)}$$

$$p = 0, 1, \dots, 20$$

$$q = -20, -19, -18, \dots, -1, 0, 1, \dots, 20$$

This determines the estimates of the covariance surface for the first and fourth quadrants of the q, p plane (really x', y'). Since $Q(p, q) = Q(-p, -q)$, the results can be extended into all four quadrants of the q, p plane.

The function must now be extended into the entire q, p plane so that its Fourier coefficients can be determined, and the property that $Q(p, q) = Q(-p, -q)$ must be preserved. This is accomplished by simply translating the covariance surface parallel to itself to fill the whole plane.

As a consequence, the Q 's have to be redefined slightly in order to weight them properly. The definitions are that

$$Q^*(p, q) = 2Q(p, q)$$

for $p = 1$ to 19 , $q = -19$ to $+19$

that

$$Q^*(0, q) = Q(0, q) \quad q = -19 \text{ to } +19$$

$$Q^*(20, q) = Q(20, q) \quad q = -19 \text{ to } +19$$

$$Q^*(p, 20) = Q(p, 20) \quad p = 1 \text{ to } 19$$

$$Q^*(p, -20) = Q(p, -20) \quad p = 1 \text{ to } 19$$

and that

$$Q^*(0, 20) = \frac{1}{2} Q(0, 20)$$

$$Q^*(0, -20) = \frac{1}{2} Q(0, -20)$$

$$Q^*(20, 20) = \frac{1}{2} Q(20, 20)$$

$$Q^*(20, -20) = \frac{1}{2} Q(20, -20) .$$

Thus points on the q -axis have unit weight (but since $Q(0, q) = Q(0, -q)$, they could be considered as one set of values weighted twice). Points off the p -axis in the first and fourth quadrants are weighted twice due to extension into the $-p$ quadrants, points on the sides are weighted once, (really $1/2$ on four sides of the full expansion) and corner points are weighted one half (really $1/4$ on the four corners).

The raw estimates of the spectrum are then found from equation (8.21).

$$(8.21) \quad L(r, s) = \frac{1}{800} \sum_{q=-20}^{+20} \sum_{p=0}^{20} Q^*(p, q) \cos \left[\frac{\pi}{20} (rp + sq) \right]$$

where

$$r = 0, 1, 2, \dots, 20$$

$$s = -20, -19, \dots, +20 .$$

Note that $L(r, s) = L(-r, -s)$ and that the spectral estimates have the same property as equation (8.12).

A check of the computations can be made at this point by defining the quantities, L^* , as below. The sum of the 861 values of L^* thus obtained should equal $Q(0, 0)$. Thus

$$L^*(r, s) = L(r, s)$$

$$\text{for } r = 1, \dots, 19, \quad s = -19 \text{ to } +19$$

and

$$L^*(0, s) = \frac{1}{2} L(0, s) \quad s = -19 \text{ to } +19$$

$$L^*(20, s) = \frac{1}{2} L(20, s) \quad s = -19 \text{ to } +19$$

$$L^*(r, 20) = \frac{1}{2} L(r, 20) \quad r = 1 \text{ to } 19$$

$$L^*(r, -20) = \frac{1}{2} L(r, -20) \quad r = 1 \text{ to } 19$$

and

$$L^*(0, 20) = \frac{1}{4} L(0, 20)$$

$$L^*(0, -20) = \frac{1}{4} L(0, -20)$$

$$L^*(20, 20) = \frac{1}{4} L(20, 20)$$

$$L^*(20, -20) = \frac{1}{4} L(20, -20).$$

Also, in order to smooth on the line $r = 0$ and on the edges, the values of L are continued by the following equations.

$$L(-1, b) = L(1, -b) \quad a = 0, 1, \dots, +20$$

$$L(a, 21) = L(a, 19) \quad b = -20, -19, \dots, 0, \dots, +20.$$

$$L(a, -21) = L(a, -19)$$

$$L(21, b) = L(19, b)$$

$$L(-21, -21) = L(-19, -19)$$

$$L(21, 21) = L(19, 19)$$

The smoothing filter is a straightforward extension of the smoothing

filter used in the one-dimensional case as shown by the following scheme where the product of the two one-dimensional smoothing filters give the filter values over a square grid of nine points.

Table 8.1. The Smoothing Filter

	0. 23	0. 54	0. 23
0. 23	0. 053	0. 124	0. 053
0. 54	0. 124	0. 292	0. 124
0. 23	0. 053	0. 124	0. 053

The smoothed spectral estimates are finally obtained from equation (8.23).

$$(8.22) \quad U(r, s) = 0.053[L(r+1, s+1) + L(r+1, s-1) + L(r-1, s+1) + L(r-1, s-1)] \\ + 0.124[L(r, s+1) + L(r, s-1) + L(r+1, s) + L(r-1, s)] \\ + 0.292[L(r, s)]$$

where again $U(r, s) = U(-r, -s)$ and $r = 1, 2, \dots, 20$

$$s = -20, \dots, +20.$$

The U 's are estimates of that contribution to the total variance of the sea surface made by waves with frequency components between $2\pi(r - \frac{1}{2})/40\Delta x$ and $2\pi(r + \frac{1}{2})/40\Delta x$ in the r direction, and between $2\pi(s - \frac{1}{2})/40\Delta x$ and $2\pi(s + \frac{1}{2})/40\Delta x$ in the s direction.⁺

One difficulty with estimating power spectra by these techniques is that the operations on the original data described by the above equations do not guarantee that the spectral estimates will be positive, and yet in the theory they should be. This is because a term of the form

$$\frac{\sin \alpha X}{X} \cdot \frac{\sin \beta Y}{Y}$$

operates on the spectrum in the complete derivation when X and Y are kept

⁺ Except at the borders--see Part II.

finite in equation (8.9). This term can have negative values which can make the L's and the U's come out negative. The L's in particular can be negative quite frequently because of the operation of the above term on the estimated spectrum. The purpose of the smoothing filter is in part to eliminate as much as possible some of the negative values. Usually the negative values are quite small and do not materially affect the analysis.

In time series theory in general, the spectrum is usually defined so that an integral over a given frequency band represents that contribution to the total variance of the process being studied made by the frequencies in that band. In ocean wave theory, another convenient way to define the spectrum is so that an integral over a given frequency band represents the sum of the squares of the amplitudes of those simple harmonic progressive waves which lie in that frequency band. This is the definition used by Pierson [1955] and Pierson, Neumann and James [1956]. The E value thus defined is equal to twice the variance of the process under study.

Equations (8.6) through (8.14) and equations (8.18) and (8.19) are derived with the definition of the spectrum used in ocean wave theory. Equations (8.15), (8.16), (8.17), (8.20), (8.21) and (8.22), have been derived in terms of variance. To place all equations in terms of ocean wave theory equations (8.15) and (8.12) should be multiplied by 2 on the right hand side and then all results would be obtained in terms of E values.

In what follows, all results will be discussed in terms of variances and covariances as far as the directional spectra are concerned except that

when the U values for the two independently obtained estimates of the spectrum are added together to get the best final estimate, the results will be in terms of E values.

Degrees of Freedom

In the single variable case, each of the final spectral estimates has a Chi Square distribution with f degrees of freedom where f as given by Tukey is determined by equation (8.23).

$$(8.23) \quad f = 2 \left(\frac{N}{m} - \frac{1}{4} \right)$$

This result is obtained from rather complex considerations of all of the operations on the original time series which have led to the final values of the U 's. In the case of an electronic analogue analyzer, the procedure is described by Pierson [1954], and the results depend on the shape of the smoothing filter.

In the two variable case under consideration here, the smoothing filter is known only at 9 points as given in Table 8.1.

The values of $U(r, s)$ for a particular r and s is a random variable with a Chi Square distribution with an as yet to be determined number of degrees of freedom. When U is considered as a random variable the degrees of freedom can be found from the following equation.

$$(8.24) \quad f = \frac{2(E(U))^2}{E(U^2)} = \frac{(\sum W_K)^2}{4(\sum W_K)^2} \frac{M_x M_y}{m_x m_y}$$

In equation (8.24), the W_K 's are given by Table 8.1, M_x is the average number of x points, and M_y is the average number of y points used in computing a value of Q .

It can be shown that the average number of x points used in computing the Q values is $N_x - (m/2)$ and the average number of y points is $N_y - (m_y/2)$. All of the Q 's enter in each value of U . The number of x points used for the individual Q 's ranges by integer steps from N_x to $N_x - m_x$ with an average value of $N_x - (m_x/2)$, and similarly for the y points.

The value of $(\sum W_K)^2 / 4(\sum W_K^2)$ is equal to 1.58, and hence the final expression for the number of degrees of freedom is given by equation (8.25).

$$(8.25) \quad f = 1.58 \left[\frac{N_x}{m_x} - \frac{1}{2} \right] \left[\frac{N_y}{m_y} - \frac{1}{2} \right]$$

Equation (8.25) may underestimate the number of degrees of freedom. Instead of $(\frac{N}{m} - \frac{1}{4})$ as in equation (8.23), it has the product of two terms $(\frac{N_x}{m_x} - \frac{1}{2})$ and $(\frac{N_y}{m_y} - \frac{1}{2})$ and instead of a factor of 2 it has a 1.58. The values of Q near $Q(0,0)$ are much larger than the values of Q on the edges, and therefore values of 1/4 instead of 1/2 might weight them more properly in equation (8.25).

A Correction for the Wave Pole Spectrum

The wave pole used by the R. V. ATLANTIS was free floating, and its dimensions are shown in figure 8.1. Therefore it probably underwent a rather complex non-linear motion in heave, pitch and surge. If the motions can be linearized, the heaving motion is the most important, and the pitch

and surge can be neglected.

The heaving motion in response to simple harmonic waves of amplitude a_0 can be described by equation (8.26).

$$(8.26) \quad M \ddot{z} + f \dot{z} + \rho g A_1 z = \rho g A_1 [\Phi(\mu)] a_0 \cos \mu t$$

where $\Phi(\mu)$ is determined from the wave pressures on the horizontal areas of the wave pole, and M includes the added mass of the water set in motion by the moving wave pole.

$\Phi(\mu)$ is given by equation (8.27).

$$(8.27) \quad \Phi(\mu) = e^{-\frac{8\mu^2}{g}} + \frac{A_2}{A_1} \left(e^{-\frac{28\mu^2}{g}} - e^{-\frac{8\mu^2}{g}} \right) + \frac{A_3}{A_1} \left(e^{-\frac{50\mu^2}{g}} - e^{-\frac{30\mu^2}{g}} \right)$$

where A_1 , A_2 , and A_3 are the cross sectional areas of the top, middle, and bottom portions of the wave pole respectively.

Note that as μ approaches infinity $\Phi(\mu)$ approaches zero and there is no force on the wave pole. As μ approaches zero $\Phi(\mu)$ approaches one and the wave pole follows the wave profile exactly.

For this particular wave pole as shown in figure 8.1, $(A_2/A_1) = (6/2.5)^2$, and $(A_3/A_1) = (12/2.5)^2$. The function $\Phi(\mu)$ is graphed in figure 8.2. Because of the greater magnitude of the areas of the larger submerged tanks and the rate of change of the wave pressure with depth, a wave crest actually produces a downward force instead of an upward force for most wave frequencies and this force is $5\frac{1}{2}$ times greater than that which would have been produced by a very long wave acting on a pole of constant diameter A_1 .

The wave pole was calibrated in still water by measuring the period of

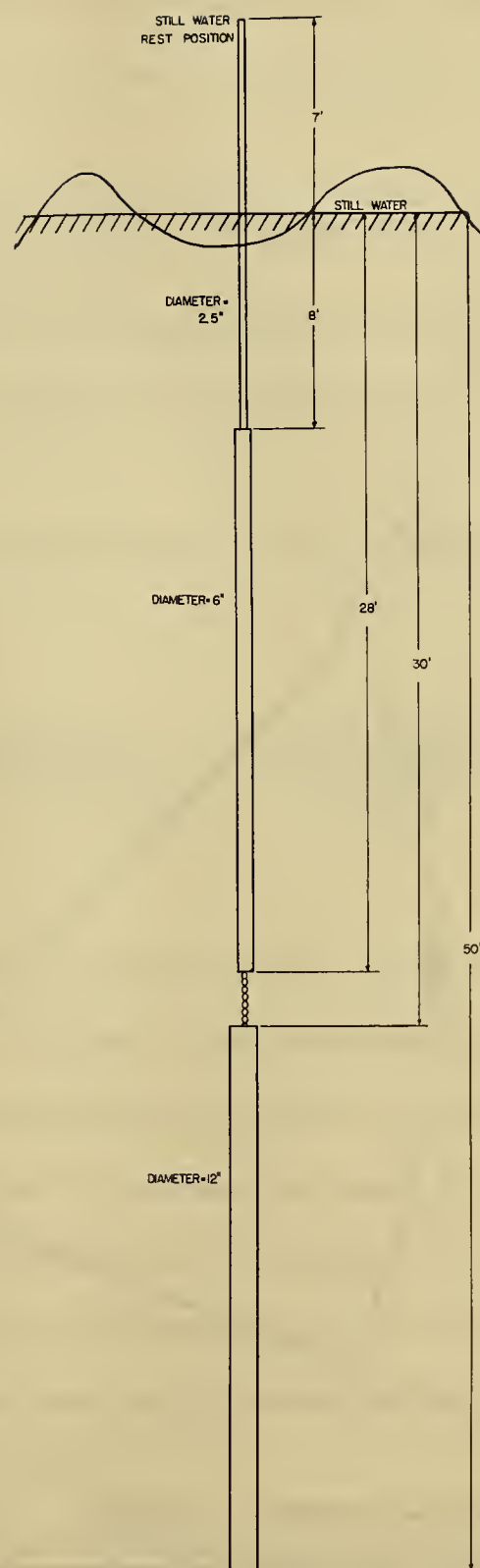


FIGURE 8.1 CAPACITANCE WAVE POLE USED BY THE R.V. ATLANTIS

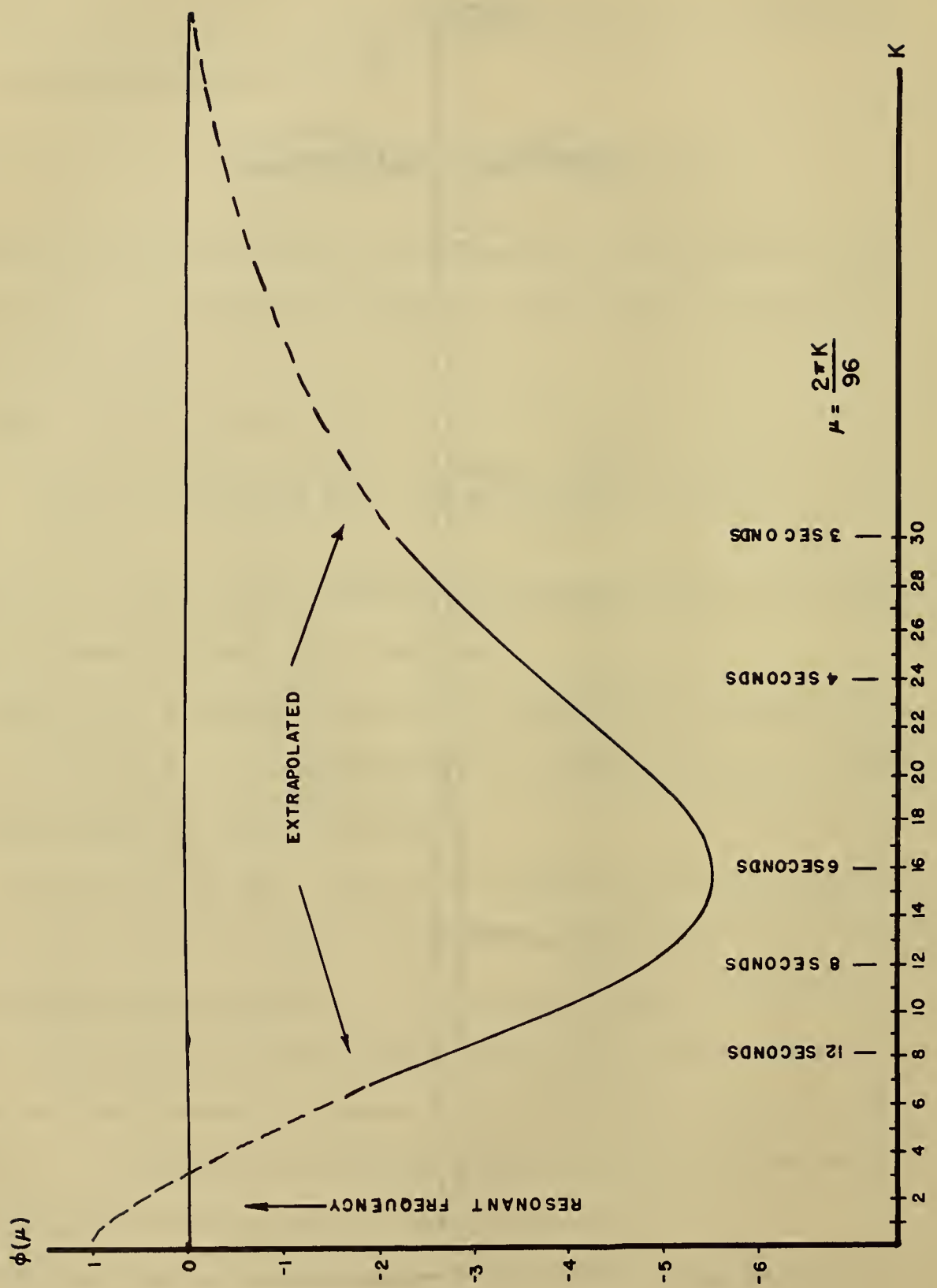


FIG. 82 THE FUNCTION $\Phi(\mu)$

oscillation and the damping. The resonant frequency was between $\mu_0 = 2\pi/41$ and $\mu_0 = 2\pi/42$ and the ratio of observed damping to critical damping was 0.16. When these calibration values are used, equation (8.26) can be put in the form given by equation (8.28).

$$(8.28) \quad \frac{\ddot{z}}{\mu_0^2} + \frac{0.32}{\mu_0} \dot{z} + z = a_0 \Phi(\mu) \cos \mu t$$

in which μ_0 is $2\pi/41$. The true resonant frequency works out to be $2\pi/41.5$ (a period half way between the two observed values) and the damping is 0.16 of critical damping.

The motion of the wave pole under the above conditions is given by equation (8.29).

$$(8.29) \quad z(t) = \frac{[1 - (\mu/\mu_0)^2] a_0 \Phi(\mu) \cos \mu t}{[1 - (\mu/\mu_0)^2]^2 + K^2(\mu/\mu_0)^2} + \frac{K(\mu/\mu_0) a_0 \Phi(\mu)}{[1 - (\mu/\mu_0)^2]^2 + K^2(\mu/\mu_0)^2} \sin \mu t$$

in which K equals 0.32.

For μ corresponding to a period of ten seconds, the coefficient of the cosine is positive, and the sine term is small compared to the cosine term. Therefore the wave pole will move up as the crest of a wave passes and the height of the recorded wave will be less than the height of the actual wave. The forcing function tends to force the pole downward in a wave crest, but the left hand side of the equation is so far past resonance at the high frequency end that an additional 180 degree phase shift is introduced, and the wave pole moves up in a passing wave crest.

The height of the water on the moving wave pole was recorded, and the spectrum of this function is to be obtained. What is desired is the spectrum of

the function that would have been obtained had the wave pole been stationary.

Let $\eta^*(t)$ be the recorded wave height and let $\eta(t)$ be the true wave height. Then equation (8.30) can be obtained.

$$(8.30) \quad \eta^*(t) = \eta(t) - z(t)$$

It states that if the pole were stationary, ($z(t) \equiv 0$), $\eta^*(t)$ would equal $\eta(t)$ and that if the wave pole followed the wave profile exactly, ($\eta(t) = z(t)$), $\eta^*(t)$ would be zero.

From equations (8.29) and (8.30) the result is that

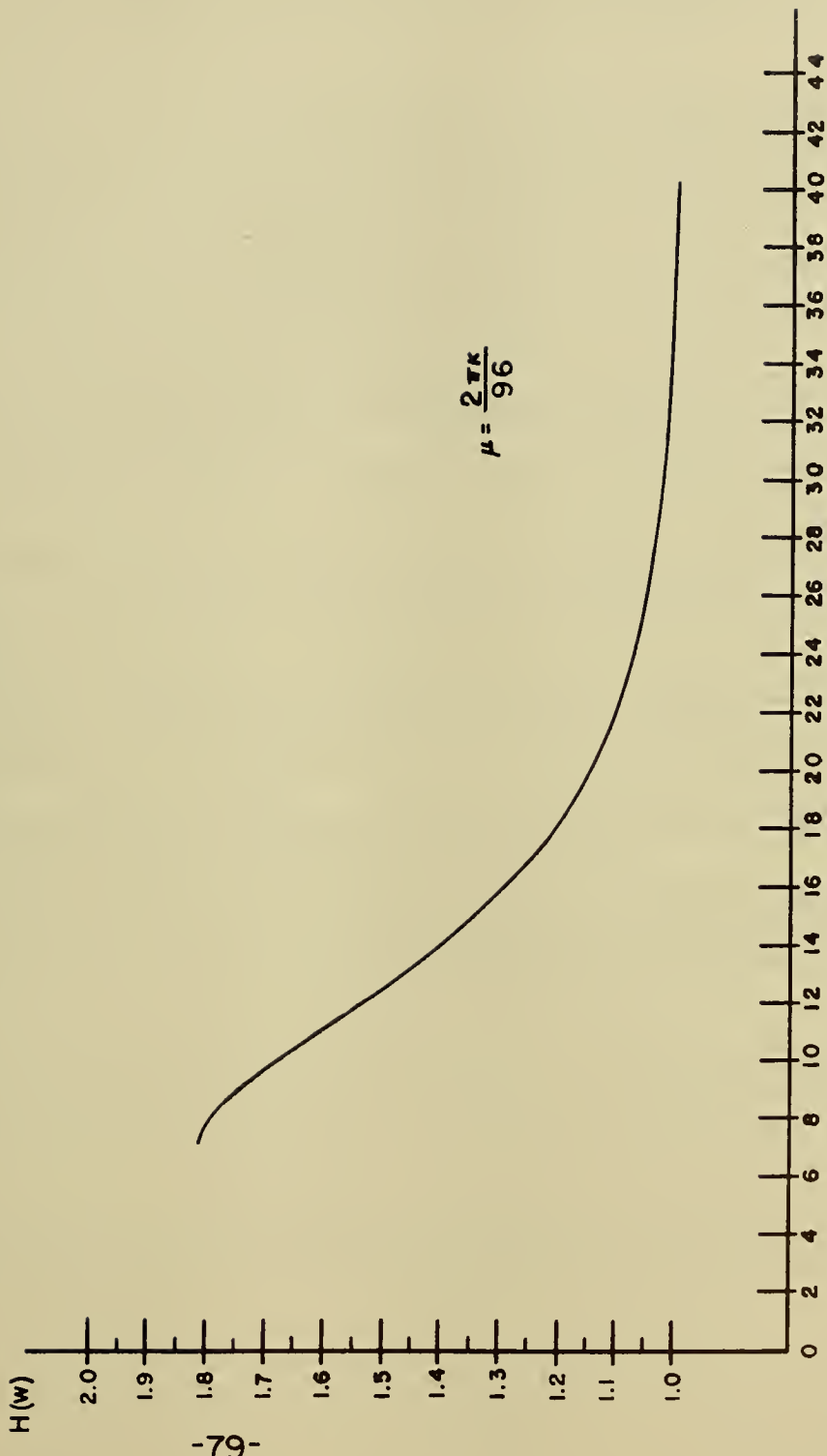
$$(8.31) \quad \eta^*(t) = \left[1 - \frac{[1 - (\mu/\mu_o)^2] \phi(\mu)}{D(\mu)} \right] a_o \cos \mu t - \left[\frac{[K(\mu/\mu_o)] \phi(\mu)}{D(\mu)} \right] a_o \sin \mu t$$

where $D(\mu)$ is the denominator of the terms in (8.28).

If the wave pole response is linear, and if the free surface can be represented by a stationary Gaussian process with the spectrum $[A(\mu)]^2$, it then follows that the spectrum of the recorded function is related to the spectrum of the waves by equation (8.32). The term in brackets is just the sum of the squares of the two coefficients in (8.31).

$$(8.32) \quad [A^*(\mu)]^2 = \left[\frac{[(\mu/\mu_o)^2 - 1 + \phi(\mu)]^2 + K^2(\mu/\mu_o)^2}{[(\mu/\mu_o)^2 - 1]^2 + K^2(\mu/\mu_o)^2} \right] [A(\mu)]^2$$

Over the range of frequencies expected in the wave record, the numerator of this expression is always less than the denominator. Therefore the waves recorded by the instrument will be too low and the spectrum computed from the wave record will have to be amplified to get the correct spectrum. The final equation given that $[A^*(\mu)]^2$ is known permits one to find $[A(\mu)]^2$.



-79-

FIG. 8.3

CORRECTION FACTOR FOR THE WHOI WAVE POLE SPECTRUM.

$$(8.33) \quad [A(\mu)]^2 = \left[\frac{[(\mu^2/\mu_0^2) - 1]^2 + K^2(\mu^2/\mu_0^2)}{[(\mu/\mu_0)^2 - 1 + \phi(\mu)]^2 + K^2(\mu/\mu_0)^2} \right] [A^*(\mu)]^2$$

The form of the correction curve is shown in figure 8.3.

The spectrum actually determined will be discussed in a later part of the report. The authors are indebted to Professor B. V. Korvin-Kroukovsky of the Experimental Towing Tank at Stevens Institute of Technology, and Harlow Farmer of Woods Hole Oceanographic Institution for the derivation, discussion and clarification of equation (8.26) and to Mr. Farmer again for calibration data. Prof. Korvin-Kroukovsky found from purely theoretical considerations using an added mass of unity that the resonant frequency should be near 38 seconds. Tucker [1956] has discussed the calibration of essentially the same wave pole except that the depth of submergence of the tanks is different, and the derivation follows his results. Tucker's results show that a change in the depth of submergence of the tanks by a few feet one way or the other changes the results markedly.

References

- Cox, C. and W. H. Munk [1954]: Statistics of the sea surface derived from sun glitter. Journal of Marine Research, v. 13, pp. 198-227.
- Ijima, T., T. Takahashi, and K. Nakamura [1956]: On the results of wave observations at the Port of Onahama in August, September, and October 1955. (Measurements of Ocean Waves VIII. Transportation Technical Research Institute, Ministry of Transportation. In Japanese--summary in English.)
- Lewis, E. V. [1955]: Ship model tests to determine bending moments in waves. TsNAME, vol. 62.
- Nakagawa, M. and T. Ijima [1956]: "On Waves at Sakata Harbor." The First Sakata-Harbor Construction Office, Regional Harbor Construction Bureau and Transportation Technics Research Institute, Ministry of Transportation, Tokyo. (In Japanese.)
- Pierson, W. J. [1954]: An electronic wave spectrum analyzer and its use in engineering problems. Tech. Memo. No. 56, Beach Erosion Board, Washington, D. C.
- Pierson, W. J. [1955]: Wind Generated Gravity Waves in Advances in Geophysics, vol. 2. Academic Press, Inc.
- Pierson, W. J. and W. Marks [1952]: The power spectrum analysis of ocean wave records. Trans. Amer. Geophys. Union, 33, no. 6.
- Pierson, W. J., G. Neumann, and R. W. James [1955]: Practical methods for observing and forecasting ocean waves by means of wave spectra and statistics. H. O. Pub. No. 603, U. S. Navy Hydrographic Office.
- Tucker, M. J. [1956]: Comparison of wave spectra as measured by the NIO ship-borne wave recorder installed on the R. V. "Atlantis" and the Woods Hole Oceanographic Institution wave pole. NIO Internal Report No. A6.
- Tukey, J. W. [1949]: The sampling theory of power spectrum estimates. Symposium on Applications of Autocorrelation Analysis to Physical Problems. Woods Hole, Mass. (Office of Naval Research, Washington, D. C.)

Part 9

THE LEVELED DATA, THE NUMERICAL ANALYSIS AND THE NUMERICAL RESULTS

The Leveled Data

The first numerical task was to level the data using the equations derived in Part 8. Missing data was a complicating factor. For the most part this was caused by the presence of the ATLANTIS. The missing coordinates are given below:

<u>Data Set 2</u>	<u>Data Set 3</u>
<u>j</u>	<u>k</u>
(39, 45)	(2, 45)
(40, 45)	(39, 50)
(41, 45)	(44, 63)
(42, 45)	(45, 63)
	(46, 63)
	(45, 62)
	(46, 62)

where j is the index running from 0 to 59 and k is the index running from 0 to 89.

With missing points in the data, there are two possible ways to level the data. One would be to minimize the sum of the squares of the deviations of the known values of the spot heights from an unknown tilted plane. The other would be to interpolate the unknown values from the known data; use them in the equations given in Part 8; and level the data. The first

of the two procedures described above was employed, but it will also be shown that the second procedure is simpler and that it gives substantially the same results.

The original set of equations for the assumed complete set of data is given by the matrix equation (see Part 8);

$$(9.1) \quad AX = B$$

where A is the matrix:

$$(9.2) \quad \begin{pmatrix} \Sigma j^2 & \Sigma jk & \Sigma j \\ \Sigma jk & \Sigma k^2 & \Sigma k \\ \Sigma j & \Sigma k & \Sigma l \end{pmatrix}$$

and where Σ represents the double sum:

$$(9.3) \quad \sum_{k=0}^{89} \sum_{j=0}^{59}$$

A calculation shows A to be:

$$(9.4) \quad \begin{pmatrix} 6,318,900 & 7,088,850 & 159,300 \\ 7,088,850 & 14,337,900 & 240,300 \\ 159,300 & 240,300 & 5,400 \end{pmatrix}$$

B is defined as the vector:

$$(9.5) \quad \begin{aligned} & \Sigma j N_{jk} \\ & \Sigma k N_{jk} \\ & \Sigma N_{jk} \end{aligned}$$

where Σ is defined by (9.3).

The column vector, X, is given by

(9.6)

$$X = \begin{vmatrix} a \\ b \\ c \end{vmatrix}$$

where a , b , and c determine the coefficients of the unknown tilted reference plane.

The equation for the leveled data is

$$N_{jk}^* = N_{jk} - aj - bk - c$$

The modified equations which take into account the missing data are given by eqn. (9.7) where the summations omit the missing points.

(9.7)

$$A'X = B''$$

The numerical results for sets 2 and 3 are as follows:

	<u>Set 2</u>			<u>Set 3</u>		
A'	6,312,334	7,081,560	159,138	6,307,157	7,072,663	159,033
	7,081,560	14,329,800	240,120	7,072,663	14,313,780	239,892
	159,138	240,120	5,396	159,033	239,892	5,393
B'	767,640.680			847,416.000		
	1,184,012.640			1,261,367.290		
	26,618.730			28,650.330		
X	-.010744			+.001575		
	-.000140			-.003584		
	+5.256144			+5.425500		

The final equations for the leveled data, N_{jk} , are given by:

$$(9.8) \quad N_{jk}^* = N_{jk} + .010744j + .000140k - 5.256144$$

$$(9.9) \quad N_{jk}^* = N_{jk} - .001575j + .003584k + 5.425500$$

The leveled data are given in Tables 9.1 and 9.2. Data at the missing points were determined by interpolating the leveled data at the neighboring points.

The preceding can be simplified by interpolating the data at the start for the missing points. It will be shown that this method yields the same results to at least five significant figures. From equation (9.8) the missing data in the second run are given by:

$$(39, 45) : 4.830825$$

$$(40, 45) : 4.820081$$

$$(41, 45) : 4.809338$$

$$(42, 45) : 4.789590$$

if N_{jk}^* is assumed to be zero at the missing points. By interpolation at the neighboring points, one could assume the missing data to be given by:

$$(39, 45) : 5.02$$

$$(40, 45) : 5.03$$

$$(41, 45) : 4.92$$

$$(42, 45) : 4.77$$

If one were to start the leveling over again, with the missing data tabulated above under the assumption that N_{jk}^* were zero at the missing points thus using the entire 5400 points and the matrix A, there would be no change in the results. This is a fundamental property of a least square

solution. However, if one were to level with the interpolated data, the results would be almost indistinguishable, because the vectors B for both cases agree to at least 5 significant figures. Hence the solutions agree. Thus in a repetition of this problem, missing data could simply be averaged at the start. The column vector B for Set 2 for the case in which N_{jk}^* is assumed to be zero is given by

$$B = \begin{pmatrix} 768,420.609 \\ 1,184,879.288 \\ 26,637.989 \end{pmatrix}$$

and if the interpolated points are used, B for Set 2 is given by

$$B = \begin{pmatrix} 768,440.13 \\ 1,184,901.39 \\ 26,638.49 \end{pmatrix}$$

The missing data for Set 3 under the assumption that N_{jk}^* is zero at each of the missing points is given by

j k

(2, 45) : 5.26735

(39, 50) : 5.30770

(44, 63) : 5.26898

(45, 63) : 5.27056

(46, 63) : 5.27213

(45, 62) : 5.27414

(46, 62) : 5.27572

By interpolation at the neighboring points one could assume the missing data to be given by

j k

- (2, 45) : 5.15
- (39, 50) : 5.11
- (44, 63) : 5.28
- (45, 63) : 5.39
- (46, 63) : 5.59
- (45, 62) : 5.43
- (46, 62) : 5.53

The column vector B for Set 3 for the case in which N_{jk}^* is assumed to be zero is given by

$$B = \begin{pmatrix} 848,825.093 \\ 1,263,519.932 \\ 28,687.267 \end{pmatrix} ;$$

and if the interpolated points are used, B for Set 3 is given by

$$B = \begin{pmatrix} 848,856.34 \\ 1,263,558.44 \\ 28,687.81 \end{pmatrix}$$

The leveling equations for the two different ways of leveling each set of data were actually obtained. The greatest difference in the two sets of data between the two methods was -0.02 ft which was far below the level of accuracy in the original spot heights.

The preceding calculations were carried out on the Univac, a large

digital computer. The actual computation took only a few minutes; however the clerical work involved in correcting errors in the data and in the program consumed almost two hours. Were the problem to be done for a new set of data, only a few minutes of Univac time would be needed, as the program already exists, and the data can be made ready by a card to tape converter.

Spectrum Computation by Means of the Univac

The computation of the covariance surface is an extremely long computation, involving many millions of multiplications. Thus it could be most speedily handled by the IBM 704, the NORC, or the LARC.

Programming the covariance surface on the Univac was especially difficult because of its limited memory. Since many numbers must be available almost simultaneously, it was deemed inefficient to store the data on tape, as tape time would add considerably to the program's running time. The way out of this dilemma was to break up the 90 by 60 array into three arrays: 44 x 60, 2 x 60, and 44 x 60. There is considerable overlap. Since we want a lag of 20, the middle group must contain 20 rows above and below; thus it contains 42 rows in all. These data were packed 4 on a line. In this way, it was possible to pack an entire section in the memory, and still have enough instructions for the program. Since no room was left for sign, a constant was added to all the data to make them positive. The reader may perceive how these factors added materially to the length of the computation run. Every two numbers had to be isolated by an ingenious system of shifts, then the same constant had to be subtracted out. Only then could the numbers be multiplied and the product accumulated in a counter. Then the calculation

of the covariance surface is accomplished by means of three programs yielding three 21×41 matrices. The sum of these three matrices equals $Q(p, q)(90 - |q|)(60 - p)$, and a division will obtain the required values for the covariance surface. Since the problem is quite long, procedures have been established in case of machine trouble. The program can be restarted by typing on supervisory control the initial desired two-dimensional lag. The computer will pick it up from that point. A flow chart for this program is given in figure 9.1.

The spectrum program did not present such difficulties because the entire data could be easily written in the memory.

These programs were compiled by means of Generalized Programming, a particular system of automatic programming developed by the Univac Division of the Sperry Rand Corp. These programs for a general array can be found in the G. P. Library under the call letters AUC2, and COSM. They are available at the Univac Division of Sperry Rand, Inc., 19th and Allegheny Avenue, Philadelphia, Pennsylvania.

To complete the program, an input-output routine must be added. This program has been written. It exists on tape at the College of Engineering, New York University. Further checking is deemed desirable before a production run is attempted.

The complete Univac procedure for determining the spectrum from leveled data has thus been set up. After further checking, it could be used given about twenty hours of Univac time for each set of data.

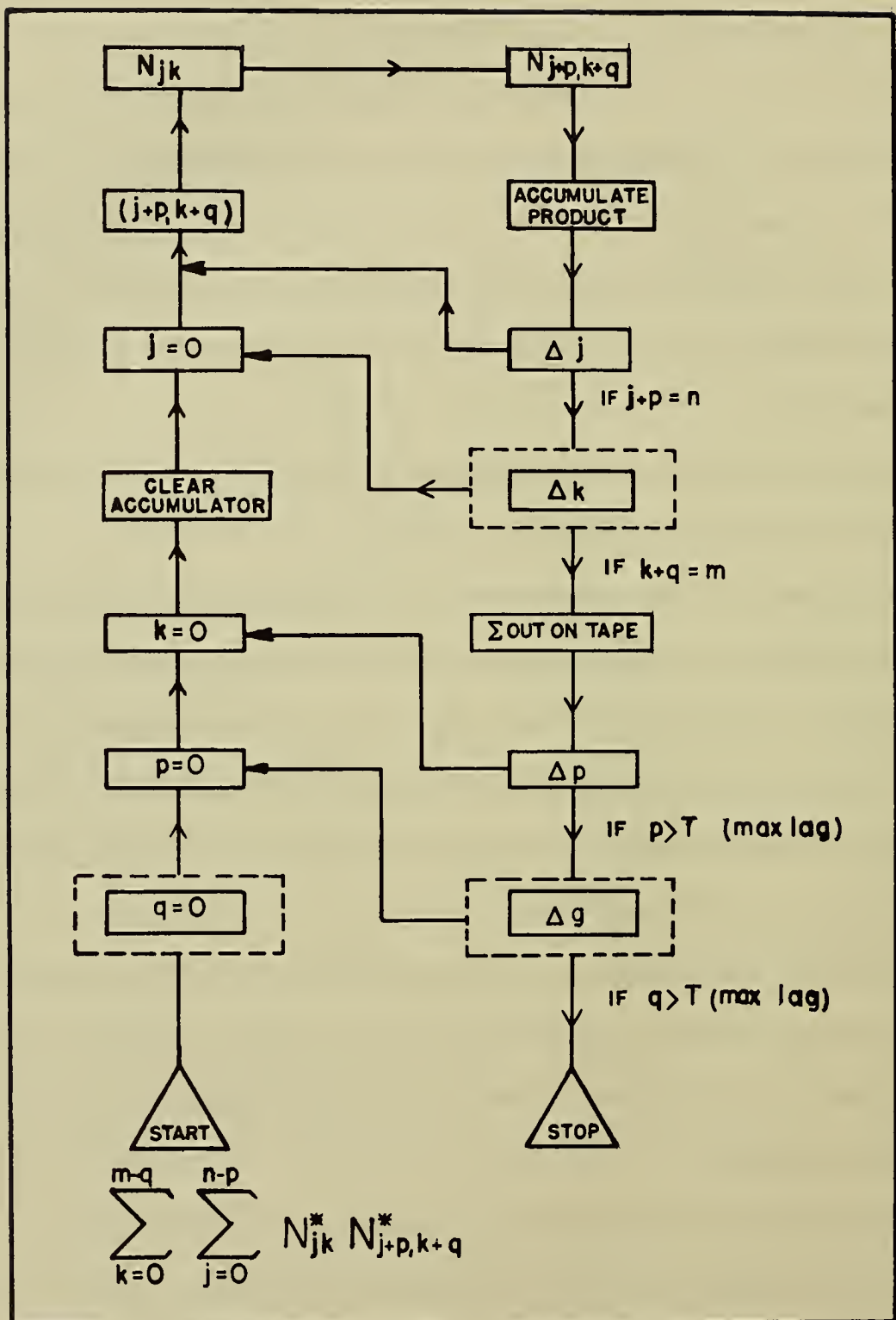


Fig. 9.1 FLOW CHART FOR UNNORMALIZED COVARIANT SURFACE

Spectrum Computation by Means of the Logistics Computer

The problem was eventually run on the Logistics Computer, owned by the Office of Naval Research and operated by the George Washington University Logistics Research Project. Time was made available by ONR. This computer is a plugboard controlled electronic digital computer with a large internal drum memory of approximately 175,000 decimal digits. For this computation a word length of 12 decimal digits (in reality 11 1/2, since negative numbers are represented by 9's complements) was used, providing over 14,000 words of memory, more than enough to store all the necessary data at each stage of computation.

The leveled data N_{jk}^* were provided on punched cards for both data sets 2 and 3. A later computation was made on Data Set 2A derived from Data Set 2 by the deletion of all j from 50 to 59 and all k from 0 to 19 inclusive, providing a 50×70 array; and on Data Set 3C derived from Data Set 3 by the deletion of all j from 0 to 9 and 50 to 59, inclusive, providing a 40×90 array. The N_{jk}^* were converted from cards to paper tape. Conversion and input were checked by comparing $\sum_{j,k} N_{jk}^*$ on the drum with a check sum of the punched cards. As each value of $Q(p, q)(90 - |q|)(60 - p)$ was computed, it was punched out on paper tape, ready for further input. Total computation time for Data Sets 2 and 3 was about 30 hours apiece, each computation involving 3,433,500 multiplications and 6,867,000 drum references. For Sets 2A and 3C the computation time was about 18 hours each. The computer was allowed to run overnight unattended without encountering too many difficulties. Due to lack

of time no check on the above computation was made for Sets 2 and 3 other than visual observation of the results for reasonableness. For Sets 2A and 3C, however, a check computation of $\sum_{p,q} Q(p,q)(90 - |q|(60 - p))$ was made, two minor errors being discovered and corrected in the results for Set 3C. This check computation required about 6 1/2 hours for each set and would have required about 11 hours for Data Sets 2 and 3. Since the Logistics Computer does not include division as a basic operation, this had to be subroutineed in order to find the values of $Q(p,q)$, a matter of a few minutes. This division was checked by repetition of the program. The values of $Q(p,q)$ were converted from tape to punched cards for listing, the conversion being checked in the case of Data Sets 2A and 3C by comparing the sum of the $Q(p,q)$ on tape with the corresponding card sum.

The $Q(p,q)$ were fed back into the computer, being doubled before being stored. Each side of the resulting matrix was then multiplied by 1/2, the corner elements belonging to two sides, being multiplied twice. In this manner the covariance surface $Q^*(p,q)$ was stored on the drum. $1.21095 \cos \frac{\pi j}{20}$ ($j = 0, 1, \dots, 39$) were also stored on the drum. The factor 1.21095×10^{-7} was introduced to divide by 800, to locate the decimal point (since, say, 0.311 was entered as 311), and to convert from the scale of the stereo planigraph to feet (0.1016 mm = 1 foot). During the computation of the spectrum $rp + sq$ was reduced modulo 40 to the least non-negative residue. Because of the ranges of p, q, r , and s , resetting of $rp + sq$ at the limit of the range of any variable was quite easy. The total computation time for each spectrum was

about 7 hours. In the case of Data Sets 2A and 3C the $L(r,s)$ were punched into cards, the conversion from tape to cards being checked by summation. In the earlier computation of Data Sets 2 and 3, due to an error made with derivation of the equations in Part 8, the values of $L^*(r,s)$ were computed and punched into cards. As a check $\sum L^*(r,s)$ was compared with $Q(0,0)/(1.016)^2$, to which it should be equal. This check was made by hand for Data Sets 2 and 3 and by machine for 2A and 3C. In all cases there was agreement to four significant figures, the values for Data Sets 2, 3, 2A, and 3C being 4.614, 4.299, 4.105, and 4.049, respectively.

For Data Sets 2 and 3 the final smoothing was performed incorrectly, due to the above mentioned error, on the $L^*(r,s)$ matrix rather than the $L(r,s)$ matrix. This error was corrected by the time Data Sets 2A and 3C were run, and correct procedures are described in Part 8. The $L(r,s)$ matrix on the drum was bordered to provide the proper values for $r = -1, 21$ and $s = -21, 21$. A final computation of approximately 15 minutes per data set provides the $U(r,s)$. For Data Sets 2 and 3 $U(r,s)$ (incorrect in the two outer columns and rows because of the use of $L^*(r,s)$) was punched on tape and converted to cards. Many of these values were checked by hand, and no errors were discovered. For Data Sets 2A and 3C $U(r,s)$ (correctly computed from $L(r,s)$) was used to obtain $U^*(r,s)$ (the borders being multiplied by 1/2), punched out on the tape, and converted to cards. For both of these sets as a check $\sum L^*(r,s)$ was compared to $\sum U^*(r,s)$, agreement being obtained to seven significant figures.

Although computation time was greater than it would have been on the Univac or other large machine, the problem as done on the Logistics Computer was conceptually simpler, because of the ability to store ultimately all data needed at any computation stage, and more economical (even if the problem had been charged for) due to the smaller cost per hour of this machine.

In conclusion, the authors would like to thank Louis Grey, Anatole Holt and William Turanski for the help and advice they have given in the Univac programming, Gordon J. Morgan of the Logistics Research Project, William W. Ellis and Bernard Chasin who helped with the IBM card operations needed to provide the tables in this report.

The original spot height data furnished by the U. S. Navy Hydrographic Office, the leveled data, the values of $Q(p, q)$, $L^*(r, s)$, and $U(r, s)$ for the original computations, and the values of $Q(p, q)$, $L(r, s)$, and $U(r, s)$ for the reduced data, are given in the following tables. (Note that in order to compute the $U(r, s)$ values, the $L(r, s)$ values must be used, and not the $L^*(r, s)$ values.) The tabulated values of $L^*(r, s)$ should be doubled on all borders except at the corners where they should be quadrupled to obtain the $L(r, s)$ values. These values are also available in a deck of IBM punched cards at the Research Division of the College of Engineering, New York University. The raw data and the leveled data are given in 540 cards per run, for Data Sets 2 and 3 and 350 and 360 cards for Data Sets 2A and 3C, respectively; and the covariance surface, the spectrum, and the smoothed spectrum are given on 841 cards per run. Thus 11,882 cards are available in all. All Logistics Computer programs used are in the possession of George Stephenson.

	<u>Index to Tables</u>	Page
Table 9.1	Leveled Spot Height Data for Data Set No. 2 .	98
Table 9.2	Leveled Spot Height Data for Data Set No. 3 .	103
Table 9.3	Covariance Surface for Data Set No. 2 .	108
Table 9.4	Covariance Surface for Data Set No. 3 .	109
Table 9.5	Table 9.3 plus Table 9.4 .	110
Table 9.6	$L^*(r, s)$ Values for Data Set No. 2 .	111
Table 9.7	$L^*(r, s)$ Values for Data Set No. 3 .	112
Table 9.8	Spectral Estimates $U(r, s)$ for Data Set No. 2 .	113
Table 9.9	Spectral Estimates $U(r, s)$ for Data Set No. 3 .	114
Table 9.10	Table 9.8 plus Table 9.9 .	115
Table 9.11	Unleveled Raw Data for Data Set No. 2 .	116
Table 9.12	Unleveled Raw Data for Data Set No. 3 .	121
Table 9.13	Errata Sheet for Table 9.8 .	126
Table 9.14	Errata Sheet for Table 9.9 .	127
Table 9.15	Covariance Surface for Data Set No. 2A.	128
Table 9.16	Covariance Surface for Data Set No. 3C.	129
Table 9.17	$L(r, s)$ Values for Data Set No. 2A.	130
Table 9.18	$L(r, s)$ Values for Data Set No. 3C.	131
Table 9.19	Spectral Estimates $U(r, s)$ for Data Set No. 2A.	132
Table 9.20	Spectral Estimates $U(r, s)$ for Data Set No. 3C.	133

Explanation of Tables

The decimal point is not shown in any of the tables. The units for each table are given below. Negative numbers in all tables are shown by an asterisk (*).

Tables 9.1 and 9.2.

The value of $N(00, 00)$ in Table 9.1 (the number in the upper left corner of the first page) can be read as -2.56 feet (approximately). To get feet exactly divide 2.56 by 1.016. All other numbers can be similarly interpreted.

Tables 9.3, 9.4, 9.15, and 9.16.

The value of $Q(0, 0)$ in Table 9.3 is 4.763 (ft)^2 (approximately). To get (ft)^2 exactly divide 4.763 by $(1.016)^2$.

Tables 9.6, 9.7, 9.17, and 9.18.

The value of $L(0, 20)$ in Table 9.17 is 0.0013 (ft)^2 . All other $L(r, s)$ values can be interpreted similarly. To convert the $L^*(r, s)$ values in Table 9.6 and 9.7 to $L(r, s)$ values, double all entries that have 20 as a coordinate, double the first column, and redouble the entries at the four corners.

Tables 9.8, 9.9, 9.19, and 9.20.

The value of $U(1, 00)$ in Table 9.19 is 0.0302 (ft)^2 . All other values can be interpreted the same way for Tables 9.19 and 9.20 in which the values of U are bordered.

Note Tables 9.13 and 9.14 in connection with Tables 9.8 and 9.9

in which the corrected values of $U(r, s)$ are not bordered.

Tables 9.11 and 9.12 $N(0, 00)$ is 50.0 feet approximately. To convert to feet exactly, divide by 1.016. Other entries can be interpreted similarly.

Table 9.1(0) Leveled Spot Height Data for Date Set No. 2 (n=0-19)

1	2	3	4	5	6	7	8
0	256*	175*	144	604	415	95	155*
01	245*	176*	105*	695	355	105*	155*
02	245*	175*	095	485	396	026	124*
03	234*	174*	095	036	686	013*	123*
04	197	134*	184*	173*	697	547	177*
05	197	134*	121*	193*	528	548	177*
06	18*	083*	121*	121*	079	189	140*
07	18*	083*	042*	042*	019	140*	020*
08	18*	010*	101*	091*	050	120*	010*
09	18*	010*	211*	361*	120*	190*	011*
10	18*	010*	210*	250*	091	101*	011*
11	18*	010*	210*	250*	038*	123*	011*
12	18*	010*	210*	250*	038*	123*	011*
13	196	175*	121*	177*	123	123	175*
14	196	175*	104*	174*	123	123	175*
15	196	175*	074	174*	123	123	175*
16	196	175*	074	174*	123	123	175*
17	196	175*	074	174*	123	123	175*
18	196	175*	074	174*	123	123	175*
19	196	175*	074	174*	123	123	175*

Table 9.1(2). Leveled Spot Height Data for Sete Set No. 2 ($k = 20-39$)

Table 9.1(4). Laveled Spot Height Data for Data Set No. 2 (k = 40-59)

40	41	42	43	44	45	46	47	48	49	50	51	52	53	54	55	56	57	58
0.0	0.50*	0.10	1.20*	1.11	2.10*	1.09*	3.29*	1.50*	1.51	2.71	2.35*	2.64*	2.48*	2.48*	2.48*	1.50*	0.68*	0.68*
0.02	0.59*	0.71	0.40	1.61	1.28*	2.12*	3.08*	3.28*	1.12*	1.12*	0.93*	0.93*	1.47*	1.47*	1.47*	0.67*	1.17*	1.23*
0.03	1.12*	0.72	0.42	0.62	1.52*	2.12*	2.77*	1.07*	0.53	1.53	1.53	1.24	2.53*	1.24	1.46*	0.76*	1.66*	1.56*
0.04	2.63	0.73	2.23	1.74	0.37*	0.54	0.24	3.06*	1.66*	1.45*	1.45*	1.24	0.25*	1.25*	1.25*	1.46*	1.66*	1.86*
0.05	2.53	2.44	1.94	1.74	0.54	0.24	3.06*	3.06*	1.76*	1.76*	1.76*	1.76*	0.76*	0.76*	0.76*	1.46*	1.25*	1.25*
0.06	1.24	1.75	2.25	1.75	0.45	0.15	0.15	0.15	0.15	0.15	0.15	0.15	0.15	0.15	0.15	0.15	0.15	0.15
0.07	0.25	1.24	1.92	1.75	0.46	0.15	0.16	0.16	0.16	0.16	0.16	0.16	0.16	0.16	0.16	0.16	0.16	0.16
0.08	1.45*	0.26	1.88	1.86	0.26	0.26	0.26	0.26	0.26	0.26	0.26	0.26	0.26	0.26	0.26	0.26	0.26	0.26
0.09	1.64*	0.24*	0.23*	1.63*	1.63*	0.24*	0.24*	0.24*	0.24*	0.24*	0.24*	0.24*	0.24*	0.24*	0.24*	0.24*	0.24*	0.24*
1.10	0.03*	0.83*	1.38*	0.28	0.88	0.32*	1.62*	1.62*	0.49	0.49	0.89	0.21*	0.15*	0.15*	0.15*	0.15*	0.15*	0.15*
1.11	1.98	0.31*	0.31*	0.09*	0.69	1.21*	1.21*	0.21*	0.21*	0.21*	0.21*	0.21*	0.21*	0.21*	0.21*	0.21*	0.21*	0.21*
1.12	1.28	0.21*	0.21*	1.39	0.01*	1.51*	1.00*	0.80*	0.80	0.80	0.80	0.80	0.80	0.80	0.80	0.80	0.80	0.80
1.13	0.21*	1.74	1.94	1.74	0.30*	2.20*	2.20*	2.20*	2.20*	2.20*	2.20*	2.20*	2.20*	2.20*	2.20*	2.20*	2.20*	2.20*
1.14	1.00*	2.40	0.30*	2.10	0.31*	1.79*	0.49*	0.49*	0.49*	0.49*	0.49*	0.49*	0.49*	0.49*	0.49*	0.49*	0.49*	0.49*
1.15	2.91	0.61	0.61	0.42	1.88*	1.88*	1.88*	1.88*	1.88*	1.88*	1.88*	1.88*	1.88*	1.88*	1.88*	1.88*	1.88*	1.88*
1.16	0.42	0.42	0.38*	0.38*	2.07*	2.07*	2.07*	2.07*	2.07*	2.07*	2.07*	2.07*	2.07*	2.07*	2.07*	2.07*	2.07*	2.07*
1.17	2.63	0.53	0.53	1.23*	1.23*	1.23*	1.23*	1.23*	1.23*	1.23*	1.23*	1.23*	1.23*	1.23*	1.23*	1.23*	1.23*	1.23*
1.18	0.53	0.53	1.23*	1.23*	1.23*	1.23*	1.23*	1.23*	1.23*	1.23*	1.23*	1.23*	1.23*	1.23*	1.23*	1.23*	1.23*	1.23*
1.19	1.16*	1.16*	1.16*	1.16*	0.53	0.53	0.53	0.53	0.53	0.53	0.53	0.53	0.53	0.53	0.53	0.53	0.53	0.53
2.20	0.34	1.55	1.25	1.25	0.14*	0.46	0.27*	0.27*	0.27*	0.27*	0.27*	0.27*	0.27*	0.27*	0.27*	0.27*	0.27*	0.27*
2.21	1.05*	1.45	1.14*	1.14*	0.56	1.54*	1.27*	1.27*	1.27*	1.27*	1.27*	1.27*	1.27*	1.27*	1.27*	1.27*	1.27*	1.27*
2.22	0.64	1.04*	1.04*	1.04*	1.97	1.17	1.17	1.17	1.17	1.17	1.17	1.17	1.17	1.17	1.17	1.17	1.17	1.17
2.23	2.07*	0.07*	1.97	1.27	1.17	1.17	1.17	1.17	1.17	1.17	1.17	1.17	1.17	1.17	1.17	1.17	1.17	1.17
2.24	1.03*	2.13*	1.03*	1.03*	1.18*	0.72*	1.28	1.28	1.28	1.28	1.28	1.28	1.28	1.28	1.28	1.28	1.28	1.28
2.25	1.58	0.92*	0.92*	2.42*	1.81*	2.09*	3.79*	2.29*	1.59	1.59	1.59	1.59	1.59	1.59	1.59	1.59	1.59	1.59
2.26	1.09	0.01*	2.59	1.20	0.04*	0.60	2.70	2.70	2.41*	2.41*	2.41*	2.41*	2.41*	2.41*	2.41*	2.41*	2.41*	2.41*
2.27	2.80	0.23	1.20	0.40	0.60	0.60	0.60	0.60	0.60	0.60	0.60	0.60	0.60	0.60	0.60	0.60	0.60	0.60
2.28	0.30*	3.79*	1.19*	0.69*	0.81	0.81	0.81	0.81	0.81	0.81	0.81	0.81	0.81	0.81	0.81	0.81	0.81	0.81
2.29	1.48*	1.48*	1.48*	1.48*	1.48*	1.48*	1.48*	1.48*	1.48*	1.48*	1.48*	1.48*	1.48*	1.48*	1.48*	1.48*	1.48*	1.48*
3.0	1.07*	1.77*	1.17*	1.17*	1.17*	1.17*	1.17*	1.17*	1.17*	1.17*	1.17*	1.17*	1.17*	1.17*	1.17*	1.17*	1.17*	1.17*
3.2	0.07*	1.77*	1.17*	1.17*	1.17*	1.17*	1.17*	1.17*	1.17*	1.17*	1.17*	1.17*	1.17*	1.17*	1.17*	1.17*	1.17*	1.17*
3.3	1.16*	1.16*	1.16*	1.16*	1.16*	1.16*	1.16*	1.16*	1.16*	1.16*	1.16*	1.16*	1.16*	1.16*	1.16*	1.16*	1.16*	1.16*
3.4	1.55*	1.55*	1.55*	1.55*	1.55*	1.55*	1.55*	1.55*	1.55*	1.55*	1.55*	1.55*	1.55*	1.55*	1.55*	1.55*	1.55*	1.55*
3.5	1.64*	2.84*	2.84*	2.84*	2.84*	2.84*	2.84*	2.84*	2.84*	2.84*	2.84*	2.84*	2.84*	2.84*	2.84*	2.84*	2.84*	2.84*
3.6	2.17	2.17	2.17	2.17	2.17	2.17	2.17	2.17	2.17	2.17	2.17	2.17	2.17	2.17	2.17	2.17	2.17	2.17
3.8	1.09	1.09	1.09	1.09	1.09	1.09	1.09	1.09	1.09	1.09	1.09	1.09	1.09	1.09	1.09	1.09	1.09	1.09
3.9	1.07*	1.07*	1.07*	1.07*	1.07*	1.07*	1.07*	1.07*	1.07*	1.07*	1.07*	1.07*	1.07*	1.07*	1.07*	1.07*	1.07*	1.07*
4.0	1.90	1.90	1.90	1.90	1.90	1.90	1.90	1.90	1.90	1.90	1.90	1.90	1.90	1.90	1.90	1.90	1.90	1.90
4.1	1.55*	1.55*	1.55*	1.55*	1.55*	1.55*	1.55*	1.55*	1.55*	1.55*	1.55*	1.55*	1.55*	1.55*	1.55*	1.55*	1.55*	1.55*
4.2	1.90	1.90	1.90	1.90	1.90	1.90	1.90	1.90	1.90	1.90	1.90	1.90	1.90	1.90	1.90	1.90	1.90	1.90
4.3	4.43	4.43	4.43	4.43	4.43	4.43	4.43	4.43	4.43	4.43	4.43	4.43	4.43	4.43	4.43	4.43	4.43	4.43
4.4	4.44	4.44	4.44	4.44	4.44	4.44	4.44	4.44	4.44	4.44	4.44	4.44	4.44	4.44	4.44	4.44	4.44	4.44
4.5	4.45	4.45	4.45	4.45	4.45	4.45	4.45	4.45	4.45	4.45	4.45	4.45	4.45	4.45	4.45	4.45	4.45	4.45
4.6	4.46	4.46	4.46	4.46	4.46	4.46	4.46	4.46	4.46	4.46	4.46	4.46	4.46	4.46	4.46	4.46	4.46	4.46
4.7	4.47	4.47	4.47	4.47	4.47	4.47	4.47	4.47	4.47	4.47	4.47	4.47	4.47	4.47	4.47	4.47	4.47	4.47
4.8	4.48	4.48	4.48	4.48	4.48	4.48	4.48	4.48	4.48	4.48	4.48	4.48	4.48	4.48	4.48	4.48	4.48	4.48
4.9	5.50	5.50	5.50	5.50	5.50	5.50	5.50	5.50	5.50	5.50	5.50	5.50	5.50	5.50	5.50	5.50	5.50	5.50
5.0	5.51	5.51	5.51	5.51	5.51	5.51	5.51	5.51	5.51	5.51	5.51	5.51	5.51	5.51	5.51	5.51	5.51	5.51
5.1	5.52	5.52	5.52	5.52	5.52	5.52	5.52	5.52	5.52	5.52	5.52	5.52	5.52	5.52	5.52	5.52	5.52	5.52
5.2	5.53	5.53	5.53	5.53	5.53	5.53	5.53	5.53	5.53	5.53	5.53	5.53	5.53	5.53	5.53	5.53	5.53	5.53
5.3	5.54	5.54	5.54	5.54	5.54	5.54	5.54	5.54	5.54	5.54	5.54	5.54	5.54	5.54	5.54	5.54	5.54	5.54
5.4	5.55	5.55	5.55	5.55	5.55	5.55	5.55	5.55	5.55	5.55	5.55	5.55	5.55	5.55	5.55	5.55	5.55	5.55
5.5	5.56	5.56	5.56	5.56	5.56	5.56	5.56	5.56	5.56	5.56	5.56	5.56	5.56	5.56	5.56	5.56	5.56	5.56
5.6	5.57	5.57	5.57	5.57	5.57	5.57	5.57	5.57	5.57	5.57	5.57	5.57	5.57	5.57	5.57	5.57	5.57	5.57
5.7	5.58	5.58	5.58	5.58	5.58	5.58	5.58	5.58	5.58	5.58	5.58	5.58	5.58	5.58	5.58	5.58	5.58	5.58
5.8	5.59	5.59	5.59	5.59	5.59	5.59	5.59	5.59	5.59	5.59	5.59	5.59	5.59	5.59	5.59	5.59	5.59	5.59
5.9	5.60	5.60	5.60	5.60	5.60	5.60	5.60	5.60	5.60	5.60	5.60	5.60	5.60	5.60	5.60	5.60	5.60	5.60

Tab. 9.1(6). Layered Spot Height Data for Data Set No. 2 (k = 68-79)	
60	61
62	63
64	65
66	67
68	69
70	71
72	73
74	75
76	77
78	79
80	81
82	83
84	85
86	87
88	89
90	91
92	93
94	95
96	97
98	99
100	101
102	103
104	105
106	107
108	109
110	111
112	113
114	115
116	117
118	119
120	121
122	123
124	125
126	127
128	129
130	131
132	133
134	135
136	137
138	139
140	141
142	143
144	145
146	147
148	149
150	151
152	153
154	155
156	157
158	159
160	161
162	163
164	165
166	167
168	169
170	171
172	173
174	175
176	177
178	179
180	181
182	183
184	185
186	187
188	189
190	191
192	193
194	195
196	197
198	199
200	201
202	203
204	205
206	207
208	209
210	211
212	213
214	215
216	217
218	219
220	221
222	223
224	225
226	227
228	229
230	231
232	233
234	235
236	237
238	239
240	241
242	243
244	245
246	247
248	249
250	251
252	253
254	255
256	257
258	259
260	261
262	263
264	265
266	267
268	269
270	271
272	273
274	275
276	277
278	279
280	281
282	283
284	285
286	287
288	289
290	291
292	293
294	295
296	297
298	299
300	301
302	303
304	305
306	307
308	309
310	311
312	313
314	315
316	317
318	319
320	321
322	323
324	325
326	327
328	329
330	331
332	333
334	335
336	337
338	339
340	341
342	343
344	345
346	347
348	349
350	351
352	353
354	355
356	357
358	359
360	361
362	363
364	365
366	367
368	369
370	371
372	373
374	375
376	377
378	379
380	381
382	383
384	385
386	387
388	389
390	391
392	393
394	395
396	397
398	399
400	401
402	403
404	405
406	407
408	409
410	411
412	413
414	415
416	417
418	419
420	421
422	423
424	425
426	427
428	429
430	431
432	433
434	435
436	437
438	439
440	441
442	443
444	445
446	447
448	449
450	451
452	453
454	455
456	457
458	459
460	461
462	463
464	465
466	467
468	469
470	471
472	473
474	475
476	477
478	479
480	481
482	483
484	485
486	487
488	489
490	491
492	493
494	495
496	497
498	499
500	501
502	503
504	505
506	507
508	509
510	511
512	513
514	515
516	517
518	519
520	521
522	523
524	525
526	527
528	529
530	531
532	533
534	535
536	537
538	539
540	541
542	543
544	545
546	547
548	549
550	551
552	553
554	555
556	557
558	559
560	561
562	563
564	565
566	567
568	569
570	571
572	573
574	575
576	577
578	579
580	581
582	583
584	585
586	587
588	589
590	591
592	593
594	595
596	597
598	599
600	601
602	603
604	605
606	607
608	609
610	611
612	613
614	615
616	617
618	619
620	621
622	623
624	625
626	627
628	629
630	631
632	633
634	635
636	637
638	639
640	641
642	643
644	645
646	647
648	649
650	651
652	653
654	655
656	657
658	659
660	661
662	663
664	665
666	667
668	669
670	671
672	673
674	675
676	677
678	679
680	681
682	683
684	685
686	687
688	689
690	691
692	693
694	695
696	697
698	699
700	701
702	703
704	705
706	707
708	709
710	711
712	713
714	715
716	717
718	719
720	721
722	723
724	725
726	727
728	729
730	731
732	733
734	735
736	737
738	739
740	741
742	743
744	745
746	747
748	749
750	751
752	753
754	755
756	757
758	759
760	761
762	763
764	765
766	767
768	769
770	771
772	773
774	775
776	777
778	779
780	781
782	783
784	785
786	787
788	789
790	791
792	793
794	795
796	797
798	799
799	800
801	802
803	804
805	806
807	808
809	810
811	812
813	814
815	816
817	818
819	820
821	822
823	824
825	826
827	828
829	830
831	832
833	834
835	836
837	838
839	840
841	842
843	844
845	846
847	848
849	850
851	852
853	854
855	856
857	858
859	860
861	862
863	864
865	866
867	868
869	870
871	872
873	874
875	876
877	878
879	880
881	882
883	884
885	886
887	888
889	890
891	892
893	894
895	896
897	898
899	900
901	902
903	904
905	906
907	908
909	910
911	912
913	914
915	916
917	918
919	920
921	922
923	924
925	926
927	928
929	930
931	932
933	934
935	936
937	938
939	940
941	942
943	944
945	946
947	948
949	950
951	952
953	954
955	956
957	958
959	960
961	962
963	964
965	966
967	968
969	970
971	972
973	974
975	976
977	978
979	980
981	982
983	984
985	986
987	988
989	990
991	992
993	994
995	996
997	998
999	1000

Tabl. 9.1(6). Levelad Spot Height Data for Data Set No. 2 ($k = 60-79$)

Table 9.1(8). Levelled Spot Height Data for Date Set No. 2 ($k = 80-89$)

	81	82	83	84	85	86	87	88	89
80	0.0	1.35	1.65	0.34*	1.14*	0.04*	0.56	0.74*	0.04*
	0.86	1.56	0.34*	0.76	1.04*	0.04*	1.03*	0.74*	0.04*
0.1	0.87	1.07	1.67	0.77	2.33*	2.03*	0.53*	2.67	3.17
0.2	0.87	1.37	2.86	0.88	1.22*	1.32*	1.35*	1.68	2.68
0.3	0.18	2.72*	0.42*	1.31*	3.31*	0.02*	0.98	2.08	3.98
0.4	0.51*	0.41*	2.01*	2.31*	2.81*	1.50*	0.11*	0.29	0.01*
0.5	0.80*	1.40*	1.10*	1.50*	1.70*	0.50*	0.25*	0.60*	1.40*
0.6	1.20*	1.60*	1.59*	2.49*	0.49*	1.49*	1.69*	1.09*	3.79*
0.7	2.09*	3.69*	1.38*	2.28*	1.88*	2.28*	3.48*	2.78*	2.48*
0.8	0.93	1.08*	1.38*	2.28*	1.88*	2.28*	4.07*	4.77*	5.08*
0.9	1.33	1.13	0.73	1.57*	1.57*	2.23	0.17*	2.86*	2.16*
1.0	1.73	3.24	2.74	2.04	2.64	2.04	1.14	2.66*	2.95*
1.1	0.94	2.05	1.84	2.35	2.85	2.85	2.65	4.46	1.24*
1.2	1.05*	2.25	1.75	2.95	1.66	1.66	3.26	3.46	0.43*
1.3	0.96*	1.46	1.67	1.07	1.07	2.27	1.37	2.17	0.68
1.4	0.74*	0.67	0.57	1.77	1.77	2.27	2.48	3.47	0.48
1.5	1.37	1.37	0.77	1.28	0.98	1.18	0.79	1.89	2.29
1.6	2.07	1.18	1.28	1.28	0.58	1.18	0.79	1.81	2.29
1.7	2.78	2.89	1.59	1.49	0.09	0.79	1.09	1.60*	2.50*
1.8	2.38	1.09	1.10	0.20*	0.50	0.00*	3.00*	4.00*	2.10*
1.9	3.70*	3.60*	1.10	1.10	1.70	0.59*	3.09*	3.09*	2.10*
2.0	2.21	2.91	0.41	0.29*	0.39*	0.39*	0.22*	0.08*	2.69*
2.1	1.49*	1.22	1.12	0.72*	1.38*	1.38*	0.42*	1.29*	1.28*
2.2	0.98*	0.38*	0.53	1.27*	1.73*	1.37*	2.47*	2.97*	3.03
2.3	3.28*	2.88*	0.38*	1.27*	1.73*	1.73*	2.47*	2.97*	3.03
2.4	2.67*	1.67*	1.67*	1.76*	1.76*	0.44*	2.47*	2.97*	3.15*
2.5	0.46*	1.46*	1.46*	1.76*	1.76*	1.76*	2.36*	2.95*	2.16*
2.6	4.14	1.75	3.55	3.36	0.55	1.85*	2.05*	2.45*	2.04*
2.7	3.75	1.56	3.76	4.46	4.16	3.26	3.06	3.06	2.04*
2.8	2.07	4.97	1.67	4.57	5.37	5.37	2.17	2.48	2.04*
2.9	2.98	3.08	3.08	1.17	1.17	2.48	2.48	2.18	0.38
3.0	0.68	0.58	0.58	2.17	1.48	6.29	6.29	6.29	2.49
3.1	1.21*	0.91*	0.91*	1.21*	1.21*	0.69	1.21*	1.17	1.70
3.2	1.30*	1.70*	1.70*	3.50*	0.14*	1.90*	1.60*	1.60*	1.41
3.3	2.30*	2.59*	2.59*	5.09*	4.08*	1.58*	1.04*	1.04*	1.12
3.4	3.49*	3.08*	1.68*	3.68*	0.28*	1.07*	1.07*	1.07*	1.07*
3.5	3.6	3.03	0.53	0.53	0.28*	0.07*	0.07*	0.07*	0.07*
3.6	3.7	0.57*	0.57*	0.57*	0.28*	0.10*	0.10*	0.10*	0.10*
3.7	3.8	0.146*	0.146*	0.146*	1.65*	1.65*	1.34*	1.34*	1.34*
3.8	3.9	1.454*	1.454*	1.454*	1.24*	1.24*	1.24*	1.24*	1.24*
3.9	4.0	1.044*	1.044*	1.044*	1.23*	1.23*	1.23*	1.23*	1.23*
4.0	4.1	1.57*	1.57*	1.57*	1.20*	1.20*	1.18*	1.18*	1.18*
4.1	4.2	1.75*	1.75*	1.75*	1.18*	1.18*	1.18*	1.18*	1.18*
4.2	4.3	4.45	4.45	4.45	4.09	4.09	3.39	3.29	1.19
4.3	4.46	1.61	1.61	1.61	3.40	3.40	3.70	3.50	2.40
4.4	4.47	1.64	1.64	1.64	4.70	6.60	5.70	6.30	3.71
4.5	4.48	1.50*	1.50*	1.50*	0.19*	3.01	2.41	2.52	2.52
4.6	4.49	1.48*	1.48*	1.48*	0.58*	1.02*	1.02*	7.02	5.92
4.7	5.0	3.98*	3.98*	3.98*	1.77*	1.77*	2.53	3.12	3.33
4.8	5.1	0.87*	0.87*	0.87*	0.53	0.53	2.93	3.03	0.94
4.9	5.2	0.56	0.56	0.56	1.26*	1.26*	3.36*	5.34	6.64
5.0	5.3	0.25	0.25	0.25	1.85	1.85	3.25*	4.85	3.65
5.1	5.4	0.85	1.15	1.15	2.86	2.86	0.76	2.05*	0.84*
5.2	5.5	0.66	1.64*	1.64*	0.64*	0.64*	0.04*	0.04*	0.97
5.3	5.5	0.91*	1.03*	1.03*	0.73*	0.73*	4.53*	2.63*	0.87
5.4	5.6	1.88*	1.42*	1.42*	0.73*	0.73*	1.12*	3.22*	1.62*
5.5	5.7	1.28	0.88	0.88	0.48	0.48	0.08	1.02*	2.51**
5.6	5.8	1.28	0.88	0.88	0.11*	0.11*	0.69	0.91*	0.90*
5.7	5.9	0.89	0.69	0.69	0.59	0.59	3.40	0.20*	0.90

Table 9.2(0). Levelled Spot Height Data for Date Set No. 3 ($k = 0.19$)

	1	2	3	4	5	6	7	8	9	10	11	12	13	14	15	16	17	18	19
0	4.25	15.2	54.9	19.2	12.6	29.0	35.3	0.43*	0.75	0.22	29.4	21.2	20.5	1.02	2.59	3.23	5.91	7.19	10.3
0.1	4.48	15.0	54.7	18.9	10.41*	28.8	0.22	0.75	0.36	0.21	21.4	12.8	0.53	1.02	2.17	3.04	4.66*	7.07	10.16
0.2	4.57	15.0	3.52	0.84*	0.91*	0.23	0.34	0.86	0.21	0.15	1.41	2.33	0.59	0.71	0.72	0.74	0.77	0.79	0.81
0.3	4.21	15.0	2.95	0.84*	0.938	0.23	0.34	0.86	0.21	0.15	1.41	2.33	0.59	0.71	0.72	0.74	0.77	0.79	0.81
0.4	0.77*	15.0	2.31	0.84*	0.84	0.23	0.34	0.86	0.21	0.15	1.41	2.33	0.59	0.71	0.72	0.74	0.77	0.79	0.81
0.5	0.22	15.0	0.65*	0.47	0.249	0.241	0.205	0.205*	0.215	0.215	1.48	2.34	0.60	0.64	0.64	0.64	0.64	0.64	0.64
0.6	0.07	15.0	0.15*	0.142	0.142*	0.142*	0.142*	0.142*	0.142*	0.142*	1.49	2.35	0.61	0.65	0.65	0.65	0.65	0.65	0.65
0.7	0.05	15.0	0.075*	0.1425	0.1425*	0.1425*	0.1425*	0.1425*	0.1425*	0.1425*	1.50	2.36	0.62	0.66	0.66	0.66	0.66	0.66	0.66
0.8	0.09	15.0	0.025	0.064	0.064*	0.064*	0.064*	0.064*	0.064*	0.064*	1.51	2.37	0.63	0.67	0.67	0.67	0.67	0.67	0.67
0.9	0.10	15.0	0.052	0.045	0.045*	0.045*	0.045*	0.045*	0.045*	0.045*	1.52	2.38	0.64	0.68	0.68	0.68	0.68	0.68	0.68
1.0	0.12	15.0	0.157	0.157	0.157*	0.157*	0.157*	0.157*	0.157*	0.157*	1.53	2.39	0.65	0.69	0.69	0.69	0.69	0.69	0.69
1.1	0.12	15.0	0.156	0.156	0.156*	0.156*	0.156*	0.156*	0.156*	0.156*	1.54	2.40	0.66	0.70	0.70	0.70	0.70	0.70	0.70
1.2	0.12	15.0	0.156	0.156	0.156*	0.156*	0.156*	0.156*	0.156*	0.156*	1.55	2.41	0.67	0.71	0.71	0.71	0.71	0.71	0.71
1.3	0.12	15.0	0.156	0.156	0.156*	0.156*	0.156*	0.156*	0.156*	0.156*	1.56	2.42	0.68	0.72	0.72	0.72	0.72	0.72	0.72
1.4	0.12	15.0	0.156	0.156	0.156*	0.156*	0.156*	0.156*	0.156*	0.156*	1.57	2.43	0.69	0.73	0.73	0.73	0.73	0.73	0.73
1.5	0.12	15.0	0.156	0.156	0.156*	0.156*	0.156*	0.156*	0.156*	0.156*	1.58	2.44	0.70	0.74	0.74	0.74	0.74	0.74	0.74
1.6	0.12	15.0	0.156	0.156	0.156*	0.156*	0.156*	0.156*	0.156*	0.156*	1.59	2.45	0.71	0.75	0.75	0.75	0.75	0.75	0.75
1.7	0.12	15.0	0.156	0.156	0.156*	0.156*	0.156*	0.156*	0.156*	0.156*	1.60	2.46	0.72	0.76	0.76	0.76	0.76	0.76	0.76
1.8	0.12	15.0	0.156	0.156	0.156*	0.156*	0.156*	0.156*	0.156*	0.156*	1.61	2.47	0.73	0.77	0.77	0.77	0.77	0.77	0.77
1.9	0.12	15.0	0.156	0.156	0.156*	0.156*	0.156*	0.156*	0.156*	0.156*	1.62	2.48	0.74	0.78	0.78	0.78	0.78	0.78	0.78
2.0	0.12	15.0	0.156	0.156	0.156*	0.156*	0.156*	0.156*	0.156*	0.156*	1.63	2.49	0.75	0.79	0.79	0.79	0.79	0.79	0.79
2.1	0.12	15.0	0.156	0.156	0.156*	0.156*	0.156*	0.156*	0.156*	0.156*	1.64	2.50	0.76	0.80	0.80	0.80	0.80	0.80	0.80
2.2	0.12	15.0	0.156	0.156	0.156*	0.156*	0.156*	0.156*	0.156*	0.156*	1.65	2.51	0.77	0.81	0.81	0.81	0.81	0.81	0.81
2.3	0.12	15.0	0.156	0.156	0.156*	0.156*	0.156*	0.156*	0.156*	0.156*	1.66	2.52	0.78	0.82	0.82	0.82	0.82	0.82	0.82
2.4	0.12	15.0	0.156	0.156	0.156*	0.156*	0.156*	0.156*	0.156*	0.156*	1.67	2.53	0.79	0.83	0.83	0.83	0.83	0.83	0.83
2.5	0.12	15.0	0.156	0.156	0.156*	0.156*	0.156*	0.156*	0.156*	0.156*	1.68	2.54	0.80	0.84	0.84	0.84	0.84	0.84	0.84
2.6	0.12	15.0	0.156	0.156	0.156*	0.156*	0.156*	0.156*	0.156*	0.156*	1.69	2.55	0.81	0.85	0.85	0.85	0.85	0.85	0.85
2.7	0.12	15.0	0.156	0.156	0.156*	0.156*	0.156*	0.156*	0.156*	0.156*	1.70	2.56	0.82	0.86	0.86	0.86	0.86	0.86	0.86
2.8	0.12	15.0	0.156	0.156	0.156*	0.156*	0.156*	0.156*	0.156*	0.156*	1.71	2.57	0.83	0.87	0.87	0.87	0.87	0.87	0.87
2.9	0.12	15.0	0.156	0.156	0.156*	0.156*	0.156*	0.156*	0.156*	0.156*	1.72	2.58	0.84	0.88	0.88	0.88	0.88	0.88	0.88
3.0	0.12	15.0	0.156	0.156	0.156*	0.156*	0.156*	0.156*	0.156*	0.156*	1.73	2.59	0.85	0.89	0.89	0.89	0.89	0.89	0.89
3.1	0.12	15.0	0.156	0.156	0.156*	0.156*	0.156*	0.156*	0.156*	0.156*	1.74	2.60	0.86	0.90	0.90	0.90	0.90	0.90	0.90
3.2	0.12	15.0	0.156	0.156	0.156*	0.156*	0.156*	0.156*	0.156*	0.156*	1.75	2.61	0.87	0.91	0.91	0.91	0.91	0.91	0.91
3.3	0.12	15.0	0.156	0.156	0.156*	0.156*	0.156*	0.156*	0.156*	0.156*	1.76	2.62	0.88	0.92	0.92	0.92	0.92	0.92	0.92
3.4	0.12	15.0	0.156	0.156	0.156*	0.156*	0.156*	0.156*	0.156*	0.156*	1.77	2.63	0.89	0.93	0.93	0.93	0.93	0.93	0.93
3.5	0.12	15.0	0.156	0.156	0.156*	0.156*	0.156*	0.156*	0.156*	0.156*	1.78	2.64	0.90	0.94	0.94	0.94	0.94	0.94	0.94
3.6	0.12	15.0	0.156	0.156	0.156*	0.156*	0.156*	0.156*	0.156*	0.156*	1.79	2.65	0.91	0.95	0.95	0.95	0.95	0.95	0.95
3.7	0.12	15.0	0.156	0.156	0.156*	0.156*	0.156*	0.156*	0.156*	0.156*	1.80	2.66	0.92	0.96	0.96	0.96	0.96	0.96	0.96
3.8	0.12	15.0	0.156	0.156	0.156*	0.156*	0.156*	0.156*	0.156*	0.156*	1.81	2.67	0.93	0.97	0.97	0.97	0.97	0.97	0.97
3.9	0.12	15.0	0.156	0.156	0.156*	0.156*	0.156*	0.156*	0.156*	0.156*	1.82	2.68	0.94	0.98	0.98	0.98	0.98	0.98	0.98
4.0	0.12	15.0	0.156	0.156	0.156*	0.156*	0.156*	0.156*	0.156*	0.156*	1.83	2.69	0.95	0.99	0.99	0.99	0.99	0.99	0.99
4.1	0.12	15.0	0.156	0.156	0.156*	0.156*	0.156*	0.156*	0.156*	0.156*	1.84	2.70	0.96	1.00	1.00	1.00	1.00	1.00	1.00
4.2	0.12	15.0	0.156	0.156	0.156*	0.156*	0.156*	0.156*	0.156*	0.156*	1.85	2.71	0.97	1.01	1.01	1.01	1.01	1.01	1.01
4.3	0.12	15.0	0.156	0.156	0.156*	0.156*	0.156*	0.156*	0.156*	0.156*	1.86	2.72	0.98	1.02	1.02	1.02	1.02	1.02	1.02
4.4	0.12	15.0	0.156	0.156	0.156*	0.156*	0.156*	0.156*	0.156*	0.156*	1.87	2.73	0.99	1.03	1.03	1.03	1.03	1.03	1.03
4.5	0.12	15.0	0.156	0.156	0.156*	0.156*	0.156*	0.156*	0.156*	0.156*	1.88	2.74	1.00	1.04	1.04	1.04	1.04	1.04	1.04
4.6	0.12	15.0	0.156	0.156	0.156*	0.156*	0.156*	0.156*	0.156*	0.156*	1.89	2.75	1.01	1.05	1.05	1.05	1.05	1.05	1.05
4.7	0.12	15.0	0.156	0.156	0.156*	0.156*	0.156*	0.156*	0.156*	0.156*	1.90	2.76	1.02	1.06	1.06	1.06	1.06	1.06	1.06
4.8	0.12	15.0	0.156	0.156	0.156*	0.156*	0.156*	0.156*	0.156*	0.156*	1.91	2.77	1.03	1.07	1.07	1.07	1.07	1.07	1.07
4.9	0.12	15.0	0.156	0.156	0.156*	0.156*	0.156*	0.156*	0.156*	0.156*	1.92	2.78	1.04	1.08	1.08	1.08	1.08	1.08	1.08
5.0	0.12	15.0	0.156	0.156	0.156*	0.156*	0.156*	0.156*	0.156*	0.156*	1.93	2.79	1.05	1.09	1.09	1.09	1.09	1.09	1.09
5.1	0.12	15.0	0.156	0.156	0.156*	0.156*	0.156*	0.156*	0.156*	0.156*	1.94	2.80	1.06	1.10	1.10	1.10	1.10	1.10	1.10
5.2	0.12	15.0	0.156	0.156	0.156*	0.156*	0.156*	0.156*	0.156*	0.156*	1.95	2.81	1.07	1.11	1.11	1.11	1.11	1.11	1.11
5.3	0.12	15.0	0.156	0.156	0.156*	0.156*	0.156*	0.156*	0.156*	0.156*	1.96	2.82	1.08	1.12	1.12	1.12	1.12	1.12	1.12
5.4	0.12	15.0	0.156	0.156	0.156*	0.156*	0.156*	0.156*	0.156*	0.156*	1.97	2.83	1.09	1.13	1.13	1.13	1.13	1.13	1.13
5.5	0.12	15.0	0.156	0.156	0.156*	0.156*	0.156*	0.156*	0.156*	0.156*	1.98	2.84	1.10	1.14	1.14	1.14	1.14	1.14	1.14
5.6	0.12	15.0	0.156	0.156	0.156*	0.156*	0.156*	0.156*	0.156*	0.156*	1.99	2.85	1.11	1.15	1.15	1.15	1.15	1.15	1.15
5.7	0.12	15.0	0.156	0.156	0.156*	0.156*	0.156*	0.156*	0.156*	0.156*	2.00	2.86	1.12	1.16	1.16	1.16	1.16	1.16	1.16
5.8	0.12	15.0	0.156	0.156	0.156*	0.156*	0.156*	0.156*	0.156*	0.156*	2.01	2.87	1.13	1.17	1.17	1.17	1.17	1.17	1.17
5.9	0.12	15.0	0.156	0.156	0.156*	0.156*	0.156*	0.156*	0.156*	0.156*	2.02	2.88	1.14	1.18	1.18	1.18	1.18	1.18	1.18

Table 9.2(2) Leveled Spot Height Data for Data Set No. 2 ($k = 20-39$)

38	33	32	31	30	29	28	27	26	25	24	23	22	21	20	19	18	17	16	15	14	13	12	11	10	9	8	7	6	5	4	3	2	1		
37	35	34	33	32	31	30	29	28	27	26	25	24	23	22	21	20	19	18	17	16	15	14	13	12	11	10	9	8	7	6	5	4	3	2	1
36	34	33	32	31	30	29	28	27	26	25	24	23	22	21	20	19	18	17	16	15	14	13	12	11	10	9	8	7	6	5	4	3	2	1	
35	34	33	32	31	30	29	28	27	26	25	24	23	22	21	20	19	18	17	16	15	14	13	12	11	10	9	8	7	6	5	4	3	2	1	
34	33	32	31	30	29	28	27	26	25	24	23	22	21	20	19	18	17	16	15	14	13	12	11	10	9	8	7	6	5	4	3	2	1		
33	32	31	30	29	28	27	26	25	24	23	22	21	20	19	18	17	16	15	14	13	12	11	10	9	8	7	6	5	4	3	2	1			
32	31	30	29	28	27	26	25	24	23	22	21	20	19	18	17	16	15	14	13	12	11	10	9	8	7	6	5	4	3	2	1				
31	30	29	28	27	26	25	24	23	22	21	20	19	18	17	16	15	14	13	12	11	10	9	8	7	6	5	4	3	2	1					
30	29	28	27	26	25	24	23	22	21	20	19	18	17	16	15	14	13	12	11	10	9	8	7	6	5	4	3	2	1						
29	28	27	26	25	24	23	22	21	20	19	18	17	16	15	14	13	12	11	10	9	8	7	6	5	4	3	2	1							
28	27	26	25	24	23	22	21	20	19	18	17	16	15	14	13	12	11	10	9	8	7	6	5	4	3	2	1								
27	26	25	24	23	22	21	20	19	18	17	16	15	14	13	12	11	10	9	8	7	6	5	4	3	2	1									
26	25	24	23	22	21	20	19	18	17	16	15	14	13	12	11	10	9	8	7	6	5	4	3	2	1										
25	24	23	22	21	20	19	18	17	16	15	14	13	12	11	10	9	8	7	6	5	4	3	2	1											
24	23	22	21	20	19	18	17	16	15	14	13	12	11	10	9	8	7	6	5	4	3	2	1												
23	22	21	20	19	18	17	16	15	14	13	12	11	10	9	8	7	6	5	4	3	2	1													
22	21	20	19	18	17	16	15	14	13	12	11	10	9	8	7	6	5	4	3	2	1														
21	20	19	18	17	16	15	14	13	12	11	10	9	8	7	6	5	4	3	2	1															
20	19	18	17	16	15	14	13	12	11	10	9	8	7	6	5	4	3	2	1																
19	18	17	16	15	14	13	12	11	10	9	8	7	6	5	4	3	2	1																	
18	17	16	15	14	13	12	11	10	9	8	7	6	5	4	3	2	1																		
17	16	15	14	13	12	11	10	9	8	7	6	5	4	3	2	1																			
16	15	14	13	12	11	10	9	8	7	6	5	4	3	2	1																				
15	14	13	12	11	10	9	8	7	6	5	4	3	2	1																					
14	13	12	11	10	9	8	7	6	5	4	3	2	1																						
13	12	11	10	9	8	7	6	5	4	3	2	1																							
12	11	10	9	8	7	6	5	4	3	2	1																								
11	10	9	8	7	6	5	4	3	2	1																									
10	9	8	7	6	5	4	3	2	1																										
9	8	7	6	5	4	3	2	1																											
8	7	6	5	4	3	2	1																												
7	6	5	4	3	2	1																													
6	5	4	3	2	1																														
5	4	3	2	1																															
4	3	2	1																																
3	2	1																																	
2	1																																		
1																																			

Table 9.2(4). Labeled Spot Height Data for Data Set No. 3 ($k = 40-59$)

Table 9.2(6). Leveled Spot Height Data for Date Set no. 3. (K = 60-79)

60	61	62	63	64	65	66	67	68	69	70	71	72	73	74	75	76	77	78	79	
0.0	3.80	2.63	1.24	1.10	0.54	1.03*	1.69*	0.95*	1.12*	2.08*	0.79	2.05*	2.27*	2.17*	2.15*	0.46*	0.02*	0.02*	0.02*	
0.023	3.58	2.62	1.32*	1.06*	1.58*	0.95*	1.21*	1.02*	0.63*	1.87*	0.89*	1.19*	0.51*	0.51*	0.51*	0.04*	0.92	1.86	0.92	
0.024	0.86	1.32	*	1.05	1.58	0.46*	1.19	1.02	0.65	1.02	0.89	1.19	0.51	0.51	0.51	0.04*	1.01	1.01	1.01	
0.025	2.87	4.22	*	4.05	4.46	4.46	4.46	4.46	4.46	4.46	4.46	4.46	4.46	4.46	4.46	4.46	4.46	4.46	4.46	
0.026	0.02	1.31	*	1.86	4.03	4.03	4.03	4.03	4.03	4.03	4.03	4.03	4.03	4.03	4.03	4.03	4.03	4.03	4.03	
0.027	0.93	3.69	*	2.07	1.96	1.96	1.96	1.96	1.96	1.96	1.96	1.96	1.96	1.96	1.96	1.96	1.96	1.96	1.96	
0.028	4.15	1.93	*	3.24	2.19	2.19	2.19	2.19	2.19	2.19	2.19	2.19	2.19	2.19	2.19	2.19	2.19	2.19	2.19	
0.029	1.0	1.46	*	1.64	1.88	1.88	1.88	1.88	1.88	1.88	1.88	1.88	1.88	1.88	1.88	1.88	1.88	1.88	1.88	
0.030	1.11	1.64	*	1.64	1.64	1.64	1.64	1.64	1.64	1.64	1.64	1.64	1.64	1.64	1.64	1.64	1.64	1.64	1.64	
0.031	1.49	3.33	*	0.06	1.06	1.06	1.06	1.06	1.06	1.06	1.06	1.06	1.06	1.06	1.06	1.06	1.06	1.06	1.06	
0.032	0.77	2.16	*	2.23	1.67	1.67	1.67	1.67	1.67	1.67	1.67	1.67	1.67	1.67	1.67	1.67	1.67	1.67	1.67	
0.033	1.6	4.04	*	3.88	1.20	1.20	1.20	1.20	1.20	1.20	1.20	1.20	1.20	1.20	1.20	1.20	1.20	1.20	1.20	
0.034	3.23	0.06	*	1.20	1.56	1.56	1.56	1.56	1.56	1.56	1.56	1.56	1.56	1.56	1.56	1.56	1.56	1.56	1.56	
0.035	0.89	3.74	*	0.06	0.62	0.62	0.62	0.62	0.62	0.62	0.62	0.62	0.62	0.62	0.62	0.62	0.62	0.62	0.62	
0.036	1.12	1.64	*	0.06	0.91	0.91	0.91	0.91	0.91	0.91	0.91	0.91	0.91	0.91	0.91	0.91	0.91	0.91	0.91	
0.037	1.14	0.77	*	1.55	1.55	1.55	1.55	1.55	1.55	1.55	1.55	1.55	1.55	1.55	1.55	1.55	1.55	1.55	1.55	
0.038	0.38	1.30	*	1.30	0.76	0.76	0.76	0.76	0.76	0.76	0.76	0.76	0.76	0.76	0.76	0.76	0.76	0.76	0.76	
0.039	2.21	0.25	*	0.25	0.76	0.76	0.76	0.76	0.76	0.76	0.76	0.76	0.76	0.76	0.76	0.76	0.76	0.76	0.76	
0.040	0.40	0.37	*	0.37	0.07	0.07	0.07	0.07	0.07	0.07	0.07	0.07	0.07	0.07	0.07	0.07	0.07	0.07	0.07	
0.041	2.1	0.24	*	0.24	0.76	0.76	0.76	0.76	0.76	0.76	0.76	0.76	0.76	0.76	0.76	0.76	0.76	0.76	0.76	
0.042	0.25	2.25	*	1.27	1.80	1.80	1.80	1.80	1.80	1.80	1.80	1.80	1.80	1.80	1.80	1.80	1.80	1.80	1.80	
0.043	2.4	4.40	*	2.15	0.41	0.41	0.41	0.41	0.41	0.41	0.41	0.41	0.41	0.41	0.41	0.41	0.41	0.41	0.41	
0.044	2.5	2.54	*	0.87	1.12	1.12	1.12	1.12	1.12	1.12	1.12	1.12	1.12	1.12	1.12	1.12	1.12	1.12	1.12	
0.045	2.6	1.97	*	1.31	1.31	1.31	1.31	1.31	1.31	1.31	1.31	1.31	1.31	1.31	1.31	1.31	1.31	1.31	1.31	
0.046	1.97	1.11	*	1.11	1.11	1.11	1.11	1.11	1.11	1.11	1.11	1.11	1.11	1.11	1.11	1.11	1.11	1.11	1.11	
0.047	2.28	0.88	*	0.29	0.67	0.67	0.67	0.67	0.67	0.67	0.67	0.67	0.67	0.67	0.67	0.67	0.67	0.67	0.67	
0.048	0.88	2.27	*	0.27	0.76	0.76	0.76	0.76	0.76	0.76	0.76	0.76	0.76	0.76	0.76	0.76	0.76	0.76	0.76	
0.049	3.0	2.39	*	2.74	1.11	1.11	1.11	1.11	1.11	1.11	1.11	1.11	1.11	1.11	1.11	1.11	1.11	1.11	1.11	
0.050	3.2	2.37	*	2.19	2.94	2.94	2.94	2.94	2.94	2.94	2.94	2.94	2.94	2.94	2.94	2.94	2.94	2.94	2.94	
0.051	3.4	2.45	*	2.54	2.42	2.42	2.42	2.42	2.42	2.42	2.42	2.42	2.42	2.42	2.42	2.42	2.42	2.42	2.42	
0.052	3.5	3.07	*	3.07	3.05	3.05	3.05	3.05	3.05	3.05	3.05	3.05	3.05	3.05	3.05	3.05	3.05	3.05	3.05	
0.053	3.6	1.52	*	1.52	1.52	1.52	1.52	1.52	1.52	1.52	1.52	1.52	1.52	1.52	1.52	1.52	1.52	1.52	1.52	
0.054	3.7	1.01	*	1.01	1.01	1.01	1.01	1.01	1.01	1.01	1.01	1.01	1.01	1.01	1.01	1.01	1.01	1.01	1.01	
0.055	3.8	0.62	*	0.62	0.97	0.97	0.97	0.97	0.97	0.97	0.97	0.97	0.97	0.97	0.97	0.97	0.97	0.97	0.97	
0.056	3.9	0.63	*	0.63	1.28	1.28	1.28	1.28	1.28	1.28	1.28	1.28	1.28	1.28	1.28	1.28	1.28	1.28	1.28	
0.057	4.0	0.83	*	0.00	1.11	1.11	1.11	1.11	1.11	1.11	1.11	1.11	1.11	1.11	1.11	1.11	1.11	1.11	1.11	
0.058	4.1	0.47	*	0.47	1.11	1.11	1.11	1.11	1.11	1.11	1.11	1.11	1.11	1.11	1.11	1.11	1.11	1.11	1.11	
0.059	4.2	0.47	*	0.47	1.85	1.85	1.85	1.85	1.85	1.85	1.85	1.85	1.85	1.85	1.85	1.85	1.85	1.85	1.85	
0.060	4.3	1.64	*	1.64	0.97	0.97	0.97	0.97	0.97	0.97	0.97	0.97	0.97	0.97	0.97	0.97	0.97	0.97	0.97	
0.061	4.4	4.45	*	0.61	1.92	1.92	1.92	1.92	1.92	1.92	1.92	1.92	1.92	1.92	1.92	1.92	1.92	1.92	1.92	
0.062	4.5	3.17	*	3.17	3.91	3.91	3.91	3.91	3.91	3.91	3.91	3.91	3.91	3.91	3.91	3.91	3.91	3.91	3.91	
0.063	4.6	1.26	*	1.26	3.09	3.09	3.09	3.09	3.09	3.09	3.09	3.09	3.09	3.09	3.09	3.09	3.09	3.09	3.09	
0.064	4.7	1.39	*	1.39	3.32	3.32	3.32	3.32	3.32	3.32	3.32	3.32	3.32	3.32	3.32	3.32	3.32	3.32	3.32	
0.065	4.8	4.38	*	4.38	3.44	3.44	3.44	3.44	3.44	3.44	3.44	3.44	3.44	3.44	3.44	3.44	3.44	3.44	3.44	
0.066	4.9	5.0	*	1.29	2.06	2.06	2.06	2.06	2.06	2.06	2.06	2.06	2.06	2.06	2.06	2.06	2.06	2.06	2.06	
0.067	5.0	1.71	*	1.71	1.27	1.27	1.27	1.27	1.27	1.27	1.27	1.27	1.27	1.27	1.27	1.27	1.27	1.27	1.27	
0.068	5.1	1.38	*	1.38	0.64	0.64	0.64	0.64	0.64	0.64	0.64	0.64	0.64	0.64	0.64	0.64	0.64	0.64	0.64	
0.069	5.2	0.16	*	0.16	1.10	1.10	1.10	1.10	1.10	1.10	1.10	1.10	1.10	1.10	1.10	1.10	1.10	1.10	1.10	
0.070	5.3	0.16	*	0.16	0.64	0.64	0.64	0.64	0.64	0.64	0.64	0.64	0.64	0.64	0.64	0.64	0.64	0.64	0.64	
0.071	5.4	0.16	*	0.16	1.10	1.10	1.10	1.10	1.10	1.10	1.10	1.10	1.10	1.10	1.10	1.10	1.10	1.10	1.10	
0.072	5.5	0.16	*	0.16	0.64	0.64	0.64	0.64	0.64	0.64	0.64	0.64	0.64	0.64	0.64	0.64	0.64	0.64	0.64	
0.073	5.6	0.16	*	0.16	1.10	1.10	1.10	1.10	1.10	1.10	1.10	1.10	1.10	1.10	1.10	1.10	1.10	1.10	1.10	
0.074	5.7	2.02	*	2.02	0.70	0.70	0.70	0.70	0.70	0.70	0.70	0.70	0.70	0.70	0.70	0.70	0.70	0.70	0.70	
0.075	5.8	2.48	*	2.48	1.06	1.06	1.06	1.06	1.06	1.06	1.06	1.06	1.06	1.06	1.06	1.06	1.06	1.06	1.06	1.06
0.076	5.9	1.15	*	1.15	1.15	1.15	1.15	1.15	1.15	1.15	1.15	1.15	1.15	1.15	1.15	1.15	1.15	1.15	1.15	

Table 9.2(B). Levelon Spot Height Data for Data Set No. 3 ($k = 80-89$)

Table 9.3 Covariance Surface for Data Set No. 2

	1	2	3	4	5	6	7	8	9	10	11	12	13	14	15	16	17	18	19	20
0	0.430	0.383	0.261	0.253	0.285	0.205	0.031	0.019	0.094	0.036	0.017	0.017	0.002	0.002	0.002	0.002	0.002	0.002	0.002	
1	0.465	0.328	0.207	0.180	0.085	0.021	0.003	0.001	0.001	0.001	0.001	0.001	0.001	0.001	0.001	0.001	0.001	0.001	0.001	
2	0.480	0.431	0.244	0.030	0.110	0.159	0.007	0.003	0.001	0.001	0.001	0.001	0.001	0.001	0.001	0.001	0.001	0.001	0.001	
3	0.436	0.415	0.191	0.061	0.066	0.066	0.005	0.005	0.005	0.005	0.005	0.005	0.005	0.005	0.005	0.005	0.005	0.005	0.005	
4	0.366	0.366	0.151	0.015	0.015	0.015	0.005	0.005	0.005	0.005	0.005	0.005	0.005	0.005	0.005	0.005	0.005	0.005	0.005	
5	0.376	0.376	0.156	0.056	0.056	0.056	0.005	0.005	0.005	0.005	0.005	0.005	0.005	0.005	0.005	0.005	0.005	0.005	0.005	
6	0.377	0.377	0.157	0.057	0.057	0.057	0.005	0.005	0.005	0.005	0.005	0.005	0.005	0.005	0.005	0.005	0.005	0.005	0.005	
7	0.377	0.377	0.157	0.057	0.057	0.057	0.005	0.005	0.005	0.005	0.005	0.005	0.005	0.005	0.005	0.005	0.005	0.005	0.005	
8	0.377	0.377	0.157	0.057	0.057	0.057	0.005	0.005	0.005	0.005	0.005	0.005	0.005	0.005	0.005	0.005	0.005	0.005	0.005	
9	0.377	0.377	0.157	0.057	0.057	0.057	0.005	0.005	0.005	0.005	0.005	0.005	0.005	0.005	0.005	0.005	0.005	0.005	0.005	
10	0.377	0.377	0.157	0.057	0.057	0.057	0.005	0.005	0.005	0.005	0.005	0.005	0.005	0.005	0.005	0.005	0.005	0.005	0.005	
11	0.377	0.377	0.157	0.057	0.057	0.057	0.005	0.005	0.005	0.005	0.005	0.005	0.005	0.005	0.005	0.005	0.005	0.005	0.005	
12	0.377	0.377	0.157	0.057	0.057	0.057	0.005	0.005	0.005	0.005	0.005	0.005	0.005	0.005	0.005	0.005	0.005	0.005	0.005	
13	0.377	0.377	0.157	0.057	0.057	0.057	0.005	0.005	0.005	0.005	0.005	0.005	0.005	0.005	0.005	0.005	0.005	0.005	0.005	
14	0.377	0.377	0.157	0.057	0.057	0.057	0.005	0.005	0.005	0.005	0.005	0.005	0.005	0.005	0.005	0.005	0.005	0.005	0.005	
15	0.377	0.377	0.157	0.057	0.057	0.057	0.005	0.005	0.005	0.005	0.005	0.005	0.005	0.005	0.005	0.005	0.005	0.005	0.005	
16	0.377	0.377	0.157	0.057	0.057	0.057	0.005	0.005	0.005	0.005	0.005	0.005	0.005	0.005	0.005	0.005	0.005	0.005	0.005	
17	0.377	0.377	0.157	0.057	0.057	0.057	0.005	0.005	0.005	0.005	0.005	0.005	0.005	0.005	0.005	0.005	0.005	0.005	0.005	
18	0.377	0.377	0.157	0.057	0.057	0.057	0.005	0.005	0.005	0.005	0.005	0.005	0.005	0.005	0.005	0.005	0.005	0.005	0.005	
19	0.377	0.377	0.157	0.057	0.057	0.057	0.005	0.005	0.005	0.005	0.005	0.005	0.005	0.005	0.005	0.005	0.005	0.005	0.005	
20	0.377	0.377	0.157	0.057	0.057	0.057	0.005	0.005	0.005	0.005	0.005	0.005	0.005	0.005	0.005	0.005	0.005	0.005	0.005	

Table 2.4 Covariance Surface for Data Set No. 3

Table 9.3(0) plus Table 9.4(0).

Table 9-6

L ^o values for Date Set No. 2	
0	0.0003*
1	0.0113*
2	0.0002*
3	0.0013*
4	0.00025*
5	0.0005*
6	0.00045*
7	0.0003*
8	0.0002*
9	0.00018*
10	0.00015*
11	0.00012*
12	0.0001*
13	0.00008*
14	0.00006*
15	0.00004*
16	0.00003*
17	0.00002*
18	0.000015*
19	0.00001*
20	0.000005*
0	0.0003*
1	0.0113*
2	0.0002*
3	0.0013*
4	0.00025*
5	0.0005*
6	0.00045*
7	0.0003*
8	0.0002*
9	0.00018*
10	0.00015*
11	0.00012*
12	0.0001*
13	0.00008*
14	0.00006*
15	0.00004*
16	0.00003*
17	0.00002*
18	0.000015*
19	0.00001*
20	0.000005*

Table 9.7 V_0 values for Data Set No. 3

Table 9.8 Spectral Estimates, $(\hat{U}(r,s))$, for Data Set No.2

0	1	2	3	4	5	6	7	8	9	10	11	12	13	14	15	16	17	18	19	20
2.0	0.005*	0.009*	0.006*	0.009*	0.006*	0.007*	0.007*	0.008*	0.007*	0.007*	0.013*	0.011*	0.011*	0.009*	0.009*	0.010*	0.009*	0.009*	0.007*	
1.9	0.001*	0.001*	0.001*	0.001*	0.001*	0.001*	0.001*	0.001*	0.001*	0.001*	0.001*	0.001*	0.001*	0.001*	0.001*	0.001*	0.001*	0.001*	0.001*	
1.8	0.0005	0.0005	0.0005	0.0005	0.0005	0.0005	0.0005	0.0005	0.0005	0.0005	0.0005	0.0005	0.0005	0.0005	0.0005	0.0005	0.0005	0.0005	0.0005	
1.7	0.0004	0.0004	0.0004	0.0004	0.0004	0.0004	0.0004	0.0004	0.0004	0.0004	0.0004	0.0004	0.0004	0.0004	0.0004	0.0004	0.0004	0.0004	0.0004	
1.6	0.0004	0.0004	0.0004	0.0004	0.0004	0.0004	0.0004	0.0004	0.0004	0.0004	0.0004	0.0004	0.0004	0.0004	0.0004	0.0004	0.0004	0.0004	0.0004	
1.5	0.0005*	0.0005*	0.0005*	0.0005*	0.0005*	0.0005*	0.0005*	0.0005*	0.0005*	0.0005*	0.0005*	0.0005*	0.0005*	0.0005*	0.0005*	0.0005*	0.0005*	0.0005*	0.0005*	
1.4	0.0005*	0.0005*	0.0005*	0.0005*	0.0005*	0.0005*	0.0005*	0.0005*	0.0005*	0.0005*	0.0005*	0.0005*	0.0005*	0.0005*	0.0005*	0.0005*	0.0005*	0.0005*	0.0005*	
1.3	0.0006*	0.0006*	0.0006*	0.0006*	0.0006*	0.0006*	0.0006*	0.0006*	0.0006*	0.0006*	0.0006*	0.0006*	0.0006*	0.0006*	0.0006*	0.0006*	0.0006*	0.0006*	0.0006*	
1.2	0.0019	0.0025	0.0032	0.0033	0.0026	0.0018*	0.0018*	0.0024	0.0025	0.0025	0.0023	0.0023	0.0023	0.0023	0.0023	0.0023	0.0023	0.0023	0.0023	
1.1	0.0044	0.0050	0.0062	0.0063	0.0061	0.0044	0.0042	0.0045	0.0050	0.0050	0.0047	0.0047	0.0047	0.0047	0.0047	0.0047	0.0047	0.0047	0.0047	
1.0	0.0059	0.0063	0.0066	0.0066	0.0066	0.0054	0.0060	0.0060	0.0061	0.0061	0.0056	0.0056	0.0056	0.0056	0.0056	0.0056	0.0056	0.0056	0.0056	
0.9	0.0056	0.0056	0.0064	0.0064	0.0064	0.0065	0.0065	0.0065	0.0065	0.0065	0.0067	0.0067	0.0067	0.0067	0.0067	0.0067	0.0067	0.0067	0.0067	
0.8	0.0055	0.0055	0.0064	0.0064	0.0064	0.0066	0.0066	0.0066	0.0066	0.0066	0.0066	0.0066	0.0066	0.0066	0.0066	0.0066	0.0066	0.0066	0.0066	
0.7	0.0060	0.0073	0.0076	0.0076	0.0076	0.0067	0.0073	0.0071	0.0071	0.0071	0.0067	0.0067	0.0067	0.0067	0.0067	0.0067	0.0067	0.0067	0.0067	
0.6	0.0091	0.0119	0.0122	0.0122	0.0122	0.0107	0.0109	0.0099	0.0091	0.0091	0.0066	0.0066	0.0066	0.0066	0.0066	0.0066	0.0066	0.0066	0.0066	
0.5	0.0150	0.0201	0.0214	0.0201	0.0159	0.0159	0.0139	0.0117	0.0112	0.0112	0.0111	0.0111	0.0107	0.0099	0.0092	0.0089	0.0080	0.0072	0.0065	
0.4	0.0165	0.0262	0.0290	0.0290	0.0236	0.0179	0.0120	0.0103	0.0103	0.0103	0.0104	0.0105	0.0105	0.0096	0.0073	0.0067	0.0065	0.0065	0.0057	
0.3	0.0066	0.0128	0.0200	0.0177	0.0108	0.0071	0.0071	0.0060	0.0059	0.0059	0.0060	0.0060	0.0060	0.0046	0.0034	0.0033	0.0027	0.0022	0.0019	
0.2	0.0002*	0.0002*	0.0002*	0.0002*	0.0002*	0.0071	0.0071	0.0054	0.0057	0.0061	0.0059	0.0059	0.0059	0.0056	0.0057	0.0057	0.0057	0.0057	0.0042	
0.1	0.0043	0.0052	0.0051	0.0051	0.0051	0.0066	0.0066	0.0063	0.0063	0.0063	0.0060	0.0060	0.0060	0.0060	0.0060	0.0060	0.0060	0.0060	0.0042	
-0.1	0.0131	0.0143	0.0147	0.0147	0.0147	0.0165	0.0165	0.0165	0.0165	0.0165	0.0170	0.0170	0.0170	0.0167	0.0167	0.0167	0.0167	0.0167	0.0167	
-0.2	0.0042	0.0042	0.0042	0.0042	0.0042	0.0122	0.0122	0.0122	0.0122	0.0122	0.0122	0.0122	0.0122	0.0122	0.0122	0.0122	0.0122	0.0122	0.0122	
-0.3	0.0002	0.0002	0.0002	0.0002	0.0002	0.0146	0.0146	0.0146	0.0146	0.0146	0.0146	0.0146	0.0146	0.0146	0.0146	0.0146	0.0146	0.0146	0.0146	
-0.4	0.0010	0.0010	0.0010	0.0010	0.0010	0.0147	0.0147	0.0147	0.0147	0.0147	0.0147	0.0147	0.0147	0.0147	0.0147	0.0147	0.0147	0.0147	0.0147	
-0.5	0.0010	0.0010	0.0010	0.0010	0.0010	0.0148	0.0148	0.0148	0.0148	0.0148	0.0148	0.0148	0.0148	0.0148	0.0148	0.0148	0.0148	0.0148	0.0148	
-0.6	0.0010	0.0010	0.0010	0.0010	0.0010	0.0149	0.0149	0.0149	0.0149	0.0149	0.0149	0.0149	0.0149	0.0149	0.0149	0.0149	0.0149	0.0149	0.0149	
-0.7	0.0010	0.0010	0.0010	0.0010	0.0010	0.0150	0.0150	0.0150	0.0150	0.0150	0.0150	0.0150	0.0150	0.0150	0.0150	0.0150	0.0150	0.0150	0.0150	
-0.8	0.0010	0.0010	0.0010	0.0010	0.0010	0.0151	0.0151	0.0151	0.0151	0.0151	0.0151	0.0151	0.0151	0.0151	0.0151	0.0151	0.0151	0.0151	0.0151	
-0.9	0.0010	0.0010	0.0010	0.0010	0.0010	0.0152	0.0152	0.0152	0.0152	0.0152	0.0152	0.0152	0.0152	0.0152	0.0152	0.0152	0.0152	0.0152	0.0152	
-1.0	0.0010	0.0010	0.0010	0.0010	0.0010	0.0153	0.0153	0.0153	0.0153	0.0153	0.0153	0.0153	0.0153	0.0153	0.0153	0.0153	0.0153	0.0153	0.0153	
-1.1	0.0010	0.0010	0.0010	0.0010	0.0010	0.0154	0.0154	0.0154	0.0154	0.0154	0.0154	0.0154	0.0154	0.0154	0.0154	0.0154	0.0154	0.0154	0.0154	
-1.2	0.0010	0.0010	0.0010	0.0010	0.0010	0.0155	0.0155	0.0155	0.0155	0.0155	0.0155	0.0155	0.0155	0.0155	0.0155	0.0155	0.0155	0.0155	0.0155	
-1.3	0.0010	0.0010	0.0010	0.0010	0.0010	0.0156	0.0156	0.0156	0.0156	0.0156	0.0156	0.0156	0.0156	0.0156	0.0156	0.0156	0.0156	0.0156	0.0156	
-1.4	0.0010	0.0010	0.0010	0.0010	0.0010	0.0157	0.0157	0.0157	0.0157	0.0157	0.0157	0.0157	0.0157	0.0157	0.0157	0.0157	0.0157	0.0157	0.0157	
-1.5	0.0010	0.0010	0.0010	0.0010	0.0010	0.0158	0.0158	0.0158	0.0158	0.0158	0.0158	0.0158	0.0158	0.0158	0.0158	0.0158	0.0158	0.0158	0.0158	
-1.6	0.0010	0.0010	0.0010	0.0010	0.0010	0.0159	0.0159	0.0159	0.0159	0.0159	0.0159	0.0159	0.0159	0.0159	0.0159	0.0159	0.0159	0.0159	0.0159	
-1.7	0.0010	0.0010	0.0010	0.0010	0.0010	0.0160	0.0160	0.0160	0.0160	0.0160	0.0160	0.0160	0.0160	0.0160	0.0160	0.0160	0.0160	0.0160	0.0160	
-1.8	0.0010	0.0010	0.0010	0.0010	0.0010	0.0161	0.0161	0.0161	0.0161	0.0161	0.0161	0.0161	0.0161	0.0161	0.0161	0.0161	0.0161	0.0161	0.0161	
-1.9	0.0010	0.0010	0.0010	0.0010	0.0010	0.0162	0.0162	0.0162	0.0162	0.0162	0.0162	0.0162	0.0162	0.0162	0.0162	0.0162	0.0162	0.0162	0.0162	
-2.0	0.0005*	0.0005*	0.0005*	0.0005*	0.0005*	0.0005*	0.0005*	0.0005*	0.0005*	0.0005*	0.0005*	0.0005*	0.0005*	0.0005*	0.0005*	0.0005*	0.0005*	0.0005*	0.0005*	

Table 9.9 Spectral Estimates, $(\hat{U}(r,s))$, for Data Set No. 3

Table 9.10. Table 9.8 plus Table 9.9

Table 9.11(0). Unelevated Raw Data for Data Set No. 2. ($X \approx 0.19$)

Table 9.11(2). Unleveled Raw Data for Data Set No. 2 $k = 20-39$

Table 9.1(2). Unleveled Raw Data for Data Set No. 2 k = 20-39)	
0	1.3
1	1.5
2	0.86
3	0.38
4	0.32
5	0.22
6	0.20
7	0.17
8	0.15
9	0.13
10	0.09
11	0.07
12	0.05
13	0.04
14	0.03
15	0.02
16	0.01
17	0.00
18	0.00
19	0.00
20	0.00
21	0.00
22	0.00
23	0.00
24	0.00
25	0.00
26	0.00
27	0.00
28	0.00
29	0.00
30	0.00
31	0.00
32	0.00
33	0.00
34	0.00
35	0.00
36	0.00
37	0.00
38	0.00
39	0.00
40	0.00
41	0.00
42	0.00
43	0.00
44	0.00
45	0.00
46	0.00
47	0.00
48	0.00
49	0.00
50	0.00
51	0.00
52	0.00
53	0.00
54	0.00
55	0.00
56	0.00
57	0.00
58	0.00
59	0.00
60	0.00
61	0.00
62	0.00
63	0.00
64	0.00
65	0.00
66	0.00
67	0.00
68	0.00
69	0.00
70	0.00
71	0.00
72	0.00
73	0.00
74	0.00
75	0.00
76	0.00
77	0.00
78	0.00
79	0.00
80	0.00
81	0.00
82	0.00
83	0.00
84	0.00
85	0.00
86	0.00
87	0.00
88	0.00
89	0.00
90	0.00
91	0.00
92	0.00
93	0.00
94	0.00
95	0.00
96	0.00
97	0.00
98	0.00
99	0.00
100	0.00
101	0.00
102	0.00
103	0.00
104	0.00
105	0.00
106	0.00
107	0.00
108	0.00
109	0.00
110	0.00
111	0.00
112	0.00
113	0.00
114	0.00
115	0.00
116	0.00
117	0.00
118	0.00
119	0.00
120	0.00
121	0.00
122	0.00
123	0.00
124	0.00
125	0.00
126	0.00
127	0.00
128	0.00
129	0.00
130	0.00
131	0.00
132	0.00
133	0.00
134	0.00
135	0.00
136	0.00
137	0.00
138	0.00
139	0.00
140	0.00
141	0.00
142	0.00
143	0.00
144	0.00
145	0.00
146	0.00
147	0.00
148	0.00
149	0.00
150	0.00
151	0.00
152	0.00
153	0.00
154	0.00
155	0.00
156	0.00
157	0.00
158	0.00
159	0.00
160	0.00
161	0.00
162	0.00
163	0.00
164	0.00
165	0.00
166	0.00
167	0.00
168	0.00
169	0.00
170	0.00
171	0.00
172	0.00
173	0.00
174	0.00
175	0.00
176	0.00
177	0.00
178	0.00
179	0.00
180	0.00
181	0.00
182	0.00
183	0.00
184	0.00
185	0.00
186	0.00
187	0.00
188	0.00
189	0.00
190	0.00
191	0.00
192	0.00
193	0.00
194	0.00
195	0.00
196	0.00
197	0.00
198	0.00
199	0.00
200	0.00
201	0.00
202	0.00
203	0.00
204	0.00
205	0.00
206	0.00
207	0.00
208	0.00
209	0.00
210	0.00
211	0.00
212	0.00
213	0.00
214	0.00
215	0.00
216	0.00
217	0.00
218	0.00
219	0.00
220	0.00
221	0.00
222	0.00
223	0.00
224	0.00
225	0.00
226	0.00
227	0.00
228	0.00
229	0.00
230	0.00
231	0.00
232	0.00
233	0.00
234	0.00
235	0.00
236	0.00
237	0.00
238	0.00
239	0.00
240	0.00
241	0.00
242	0.00
243	0.00
244	0.00
245	0.00
246	0.00
247	0.00
248	0.00
249	0.00
250	0.00
251	0.00
252	0.00
253	0.00
254	0.00
255	0.00
256	0.00
257	0.00
258	0.00
259	0.00
260	0.00
261	0.00
262	0.00
263	0.00
264	0.00
265	0.00
266	0.00
267	0.00
268	0.00
269	0.00
270	0.00
271	0.00
272	0.00
273	0.00
274	0.00
275	0.00
276	0.00
277	0.00
278	0.00
279	0.00
280	0.00
281	0.00
282	0.00
283	0.00
284	0.00
285	0.00
286	0.00
287	0.00
288	0.00
289	0.00
290	0.00
291	0.00
292	0.00
293	0.00
294	0.00
295	0.00
296	0.00
297	0.00
298	0.00
299	0.00
300	0.00
301	0.00
302	0.00
303	0.00
304	0.00
305	0.00
306	0.00
307	0.00
308	0.00
309	0.00
310	0.00
311	0.00
312	0.00
313	0.00
314	0.00
315	0.00
316	0.00
317	0.00
318	0.00
319	0.00
320	0.00
321	0.00
322	0.00
323	0.00
324	0.00
325	0.00
326	0.00
327	0.00
328	0.00
329	0.00
330	0.00
331	0.00
332	0.00
333	0.00
334	0.00
335	0.00
336	0.00
337	0.00
338	0.00
339	0.00
340	0.00
341	0.00
342	0.00
343	0.00
344	0.00
345	0.00
346	0.00
347	0.00
348	0.00
349	0.00
350	0.00
351	0.00
352	0.00
353	0.00
354	0.00
355	0.00
356	0.00
357	0.00
358	0.00
359	0.00
360	0.00
361	0.00
362	0.00
363	0.00
364	0.00
365	0.00
366	0.00
367	0.00
368	0.00
369	0.00
370	0.00
371	0.00
372	0.00
373	0.00
374	0.00
375	0.00
376	0.00
377	0.00
378	0.00
379	0.00
380	0.00
381	0.00
382	0.00
383	0.00
384	0.00
385	0.00
386	0.00
387	0.00
388	0.00
389	0.00
390	0.00
391	0.00
392	0.00
393	0.00
394	0.00
395	0.00
396	0.00
397	0.00
398	0.00
399	0.00
400	0.00
401	0.00
402	0.00
403	0.00
404	0.00
405	0.00
406	0.00
407	0.00
408	0.00
409	0.00
410	0.00
411	0.00
412	0.00
413	0.00
414	0.00
415	0.00
416	0.00
417	0.00
418	0.00
419	0.00
420	0.00
421	0.00
422	0.00
423	0.00
424	0.00
425	0.00
426	0.00
427	0.00
428	0.00
429	0.00
430	0.00
431	0.00
432	0.00
433	0.00
434	0.00
435	0.00
436	0.00
437	0.00
438	0.00
439	0.00
440	0.00
441	0.00
442	0.00
443	0.00
444	0.00
445	0.00
446	0.00
447	0.00
448	0.00
449	0.00
450	0.00
451	0.00
452	0.00
453	0.00
454	0.00
455	0.00
456	0.00
457	0.00
458	0.00
459	0.00
460	0.00
461	0.00
462	0.00
463	0.00
464	0.00
465	0.00
466	0.00
467	0.00
468	0.00
469	0.00
470	0.00
471	0.00
472	0.00
473	0.00
474	0.00
475	0.00
476	0.00
477	0.00
478	0.00
479	0.00
480	0.00
481	0.00
482	0.00
483	0.00
484	0.00
485	0.00
486	0.00
487	0.00
488	0.00
489	0.00
490	0.00
491	0.00
492	0.00
493	0.00
494	0.00
495	0.00
496	0.00
497	0.00
498	0.00
499	0.00
500	0.00
501	0.00
502	0.00
503	0.00
504	0.00
505	0.00
506	0.00
507	0.00
508	0.00
509	0.00
510	0.00
511	0.00
512	0.00
513	0.00
514	0.00
515	0.00
516	0.00
517	0.00
518	0.00
519	0.00
520	0.00
521	0.00
522	0.00
523	0.00
524	0.00
525	0.00
526	0.00
527	0.00
528	0.00
529	0.00
530	0.00
531	0.00
532	0.00
533	0.00
534	0.00
535	0.00
536	0.00
537	0.00
538	0.00
539	0.00
540	0.00
541	0.00
542	0.00
543	0.00
544	0.00
545	0.00
546	0.00
547	0.00
548	0.00
549	0.00
550	0.00
551	0.00
552	0.00
553	0.00
554	0.00
555	0.00
556	0.00
557	0.00
558	0.00
559	0.00
560	0.00
561	0.00
562	0.00
563	0.00
564	0.00
565	0.00
566	0.00
567	0.00
568	0.00
569	0.00
570	0.00
571	0.00
572	0.00
573	0.00
574	0.00
575	0.00
576	0.00
577	0.00
578	0.00
579	0.00

Table 9.11(4). Unleveled Raw Data for Data Set No. 2. ($k = 40-59$)

Table 9.11(6). Unevaluated Raw Data for Data Set No. 2. ($k = 60\text{-}79$)

60	54.0	53.6	52.0	53.1	52.7	52.0	50.6	4.9.9	52.6	52.6	51.4	53.2	53.3
61	54.1	52.2	50.4	51.4	52.6	53.1	49.5	4.9.5	49.5	49.5	49.1	50.2	50.8
62	50.4	52.2	52.0	51.2	50.8	51.0	50.4	50.4	50.4	50.4	49.7	50.5	50.8
63	51.9	52.0	51.8	51.2	50.9	51.3	51.7	51.7	51.7	51.7	51.7	51.7	51.7
64	51.7	52.2	52.7	51.2	50.9	51.3	51.7	51.7	51.7	51.7	51.7	51.7	51.7
65	51.0	51.2	50.4	51.4	51.8	51.9	51.6	51.6	51.6	51.6	51.6	51.6	51.6
66	51.2	51.4	50.9	51.4	51.8	51.9	51.6	51.6	51.6	51.6	51.6	51.6	51.6
67	51.2	51.4	51.2	51.4	51.8	51.9	51.6	51.6	51.6	51.6	51.6	51.6	51.6
68	51.0	51.2	50.8	51.3	51.7	51.9	51.6	51.6	51.6	51.6	51.6	51.6	51.6
69	51.4	51.6	51.2	51.4	51.8	51.9	51.6	51.6	51.6	51.6	51.6	51.6	51.6
70	51.4	51.6	51.2	51.4	51.8	51.9	51.6	51.6	51.6	51.6	51.6	51.6	51.6
71	51.4	51.6	51.2	51.4	51.8	51.9	51.6	51.6	51.6	51.6	51.6	51.6	51.6
72	51.4	51.6	51.2	51.4	51.8	51.9	51.6	51.6	51.6	51.6	51.6	51.6	51.6
73	51.4	51.6	51.2	51.4	51.8	51.9	51.6	51.6	51.6	51.6	51.6	51.6	51.6
74	51.4	51.6	51.2	51.4	51.8	51.9	51.6	51.6	51.6	51.6	51.6	51.6	51.6
75	51.4	51.6	51.2	51.4	51.8	51.9	51.6	51.6	51.6	51.6	51.6	51.6	51.6
76	51.4	51.6	51.2	51.4	51.8	51.9	51.6	51.6	51.6	51.6	51.6	51.6	51.6
77	51.4	51.6	51.2	51.4	51.8	51.9	51.6	51.6	51.6	51.6	51.6	51.6	51.6
78	51.4	51.6	51.2	51.4	51.8	51.9	51.6	51.6	51.6	51.6	51.6	51.6	51.6
79	51.4	51.6	51.2	51.4	51.8	51.9	51.6	51.6	51.6	51.6	51.6	51.6	51.6

Table 9.11(8). Unelevated Raw Data for Data Set No. 2 ($k = 80-89$).

Table 9.11(8). Unleaded Raw Data for Data Set No. 2 (k = 80-89).									
	89	88	87	86	85	84	83	82	81
80	52.8	53.2	53.1	53.0	52.9	52.8	52.7	52.6	52.5
81	54.3	53.9	52.5	52.0	51.6	51.0	49.5	49.0	48.5
82	52.5	51.6	51.1	50.9	50.5	50.7	50.2	49.2	49.5
83	53.0	53.1	51.6	51.6	50.9	50.7	50.5	49.2	49.5
84	52.0	51.6	51.3	50.9	50.5	50.1	49.9	49.2	49.5
85	52.4	52.0	51.3	50.9	50.5	50.1	49.9	49.2	49.5
86	53.0	52.4	51.8	51.0	50.7	50.3	49.9	49.2	49.5
87	52.4	51.3	51.0	50.9	50.7	50.3	49.9	49.2	49.5
88	51.7	51.5	51.0	50.9	50.7	50.3	49.9	49.2	49.5
89	52.4	51.3	51.0	50.9	50.7	50.3	49.9	49.2	49.5

Table 9.12(0). Unleveled Raw Data for Data Set No. 1. ($k = 0-19$)

Table 4.1(2d). Unveiled Data Set No. 3 (A = 20-37)	Data	
	Row	Column
20	5654	526
21	5635	527
22	5623	528
23	5614	529
24	5604	530
25	5594	531
26	5584	532
27	5574	533
28	5564	534
29	5554	535
30	5544	536
31	5534	537
32	5524	538
33	5514	539
34	5504	540
35	5494	541
36	5484	542
37	5474	543
38	5464	544
39	5454	545
40	5444	546
41	5434	547
42	5424	548
43	5414	549
44	5404	550
45	5394	551
46	5384	552
47	5374	553
48	5364	554
49	5354	555
50	5344	556
51	5334	557
52	5324	558
53	5314	559
54	5304	560
55	5294	561
56	5284	562
57	5274	563
58	5264	564
59	5254	565
60	5244	566
61	5234	567
62	5224	568
63	5214	569
64	5204	570
65	5194	571
66	5184	572
67	5174	573
68	5164	574
69	5154	575
70	5144	576
71	5134	577
72	5124	578
73	5114	579
74	5104	580
75	5094	581
76	5084	582
77	5074	583
78	5064	584
79	5054	585
80	5044	586
81	5034	587
82	5024	588
83	5014	589
84	5004	590
85	4994	591
86	4984	592
87	4974	593
88	4964	594
89	4954	595
90	4944	596
91	4934	597
92	4924	598
93	4914	599
94	4904	600
95	4894	601
96	4884	602
97	4874	603
98	4864	604
99	4854	605
100	4844	606
101	4834	607
102	4824	608
103	4814	609
104	4804	610
105	4794	611
106	4784	612
107	4774	613
108	4764	614
109	4754	615
110	4744	616
111	4734	617
112	4724	618
113	4714	619
114	4704	620
115	4694	621
116	4684	622
117	4674	623
118	4664	624
119	4654	625
120	4644	626
121	4634	627
122	4624	628
123	4614	629
124	4604	630
125	4594	631
126	4584	632
127	4574	633
128	4564	634
129	4554	635
130	4544	636
131	4534	637
132	4524	638
133	4514	639
134	4504	640
135	4494	641
136	4484	642
137	4474	643
138	4464	644
139	4454	645
140	4444	646
141	4434	647
142	4424	648
143	4414	649
144	4404	650
145	4394	651
146	4384	652
147	4374	653
148	4364	654
149	4354	655
150	4344	656
151	4334	657
152	4324	658
153	4314	659
154	4304	660
155	4294	661
156	4284	662
157	4274	663
158	4264	664
159	4254	665
160	4244	666
161	4234	667
162	4224	668
163	4214	669
164	4204	670
165	4194	671
166	4184	672
167	4174	673
168	4164	674
169	4154	675
170	4144	676
171	4134	677
172	4124	678
173	4114	679
174	4104	680
175	4094	681
176	4084	682
177	4074	683
178	4064	684
179	4054	685
180	4044	686
181	4034	687
182	4024	688
183	4014	689
184	4004	690
185	3994	691
186	3984	692
187	3974	693
188	3964	694
189	3954	695
190	3944	696
191	3934	697
192	3924	698
193	3914	699
194	3904	700
195	3894	701
196	3884	702
197	3874	703
198	3864	704
199	3854	705
200	3844	706
201	3834	707
202	3824	708
203	3814	709
204	3804	710
205	3794	711
206	3784	712
207	3774	713
208	3764	714
209	3754	715
210	3744	716
211	3734	717
212	3724	718
213	3714	719
214	3704	720
215	3694	721
216	3684	722
217	3674	723
218	3664	724
219	3654	725
220	3644	726
221	3634	727
222	3624	728
223	3614	729
224	3604	730
225	3594	731
226	3584	732
227	3574	733
228	3564	734
229	3554	735
230	3544	736
231	3534	737
232	3524	738
233	3514	739
234	3504	740
235	3494	741
236	3484	742
237	3474	743
238	3464	744
239	3454	745
240	3444	746
241	3434	747
242	3424	748
243	3414	749
244	3404	750
245	3394	751
246	3384	752
247	3374	753
248	3364	754
249	3354	755
250	3344	756
251	3334	757
252	3324	758
253	3314	759
254	3304	760
255	3294	761
256	3284	762
257	3274	763
258	3264	764
259	3254	765
260	3244	766
261	3234	767
262	3224	768
263	3214	769
264	3204	770
265	3194	771
266	3184	772
267	3174	773
268	3164	774
269	3154	775
270	3144	776
271	3134	777
272	3124	778
273	3114	779
274	3104	780
275	3094	781
276	3084	782
277	3074	783
278	3064	784
279	3054	785
280	3044	786
281	3034	787
282	3024	788
283	3014	789
284	3004	790
285	2994	791
286	2984	792
287	2974	793
288	2964	794
289	2954	795
290	2944	796
291	2934	797
292	2924	798
293	2914	799
294	2904	800
295	2894	801
296	2884	802
297	2874	803
298	2864	804
299	2854	805
300	2844	806
301	2834	807
302	2824	808
303	2814	809
304	2804	810
305	2794	811
306	2784	812
307	2774	813
308	2764	814
309	2754	815
310	2744	816
311	2734	817
312	2724	818
313	2714	819
314	2704	820
315	2694	821
316	2684	822
317	2674	823
318	2664	824
319	2654	825
320	2644	826
321	2634	827
322	2624	828
323	2614	829
324	2604	830
325	2594	831
326	2584	832
327	2574	833
328	2564	834
329	2554	835
330	2544	836
331	2534	837
332	2524	838
333	2514	839
334	2504	840
335	2494	841
336	2484	842
337	2474	843
338	2464	844
339	2454	845
340	2444	846
341	2434	847
342	2424	848
343	2414	849
344	2404	850
345	2394	851
346	2384	852
347	2374	853
348	2364	854
349	2354	855
350	2344	856
351	2334	857
352	2324	858
353	2314	859
354	2304	860
355	2294	861
356	2284	862
357	2274	863
358	2264	864
359	2254	865
360	2244	866
361	2234	867
362	2224	868
363	2214	869
364	2204	870
365	2194	871
366	2184	872
367	2174	873
368	2164	874
369	2154	875
370	2144	876
371	2134	877
372	2124	878
373	2114	879
374	2104	880
375	2094	881
376	2084	882
377	2074	883
378	2064	884
379	2054	885
380	2044	886
381	2034	887
382	2024	888
383	2014	889
384	2004	890
385	1994	891
386	1984	892
387	1974	893
388	1964	894
389	1954	895
390	1944	896
391	1934	897
392	1924	898
393	1914	899
394	1904	900
395	1894	901
396	1884	902
397	1874	903
398	1864	904
399	1854	905
400	1844	906
401	1834	907
402	1824	908
403	1814	909
404	1804	910
405	1794	911
406	1784	912
407	1774	913
408	1764	914
409	1754	915
410	1744	916
411	1734	917
412	1724	918
413	1714	919
414	1704	920
415	1694	921
416	1684	922
417	1674	923
418	1664	924
419	1654	925
420	1644	926
421	1634	927
422	1624	928
423	1614	929
424	1604	930
425	1594	931
426	1584	932
427	1574	933
428	1564	934
429	1554	935
430	1544	936
431	1534	937
432	1524	938
433	1514	939
434	1504	940
435	1494	941
436	1484	942

Table 9.12(2). Unleveled Data for Data Set No. 3. ($k = 20-39$)

Table 9.12(4). Unleveled Data for Data Set No. 3. ($k = 40-55$)

Table 9.12(6). Unelevated Data for Data Set No. 3. ($k = 60\text{-}79$)

60	559	547	523	531	534	545	505	525	525	509	502	502	509	507	497	545	517	512	514
61	555	530	527	519	523	524	512	521	521	500	512	512	500	502	497	517	512	514	516
62	523	531	525	525	525	525	525	525	525	525	525	525	525	525	502	525	525	525	525
63	64	65	66	67	68	69	70	71	72	73	74	75	76	77	78	79	79	78	79
64	525	525	525	525	525	525	525	525	525	525	525	525	525	525	525	525	525	525	525
65	540	521	521	521	521	521	521	521	521	521	521	521	521	521	521	521	521	521	521
66	531	531	531	531	531	531	531	531	531	531	531	531	531	531	531	531	531	531	531
67	536	536	536	536	536	536	536	536	536	536	536	536	536	536	536	536	536	536	536
68	527	527	527	527	527	527	527	527	527	527	527	527	527	527	527	527	527	527	527
69	519	519	519	519	519	519	519	519	519	519	519	519	519	519	519	519	519	519	519
70	512	512	512	512	512	512	512	512	512	512	512	512	512	512	512	512	512	512	512
71	513	513	513	513	513	513	513	513	513	513	513	513	513	513	513	513	513	513	513
72	513	513	513	513	513	513	513	513	513	513	513	513	513	513	513	513	513	513	513
73	513	513	513	513	513	513	513	513	513	513	513	513	513	513	513	513	513	513	513
74	513	513	513	513	513	513	513	513	513	513	513	513	513	513	513	513	513	513	513
75	513	513	513	513	513	513	513	513	513	513	513	513	513	513	513	513	513	513	513
76	513	513	513	513	513	513	513	513	513	513	513	513	513	513	513	513	513	513	513
77	513	513	513	513	513	513	513	513	513	513	513	513	513	513	513	513	513	513	513
78	513	513	513	513	513	513	513	513	513	513	513	513	513	513	513	513	513	513	513
79	513	513	513	513	513	513	513	513	513	513	513	513	513	513	513	513	513	513	513

Table 9.12(B) - Unleveled Data for Data Set No. 3 ($N = 80-69$).-

80	81	82	83	84	85	86	87	88	89	90
0.0	4.92	4.97	5.12	5.13	5.12	5.23	5.19	5.17	5.33	5.30
0.2	5.09	5.14	5.00	5.08	5.26	5.06	5.11	5.25	5.36	5.34
0.3	5.25	4.95	4.75	4.86	5.07	4.92	4.79	4.82	4.84	4.82
0.4	5.15	5.11	5.06	5.14	5.13	4.90	4.88	4.82	4.74	4.74
0.5	5.16	4.92	4.92	4.81	5.07	4.74	4.86	4.82	4.90	4.76
0.6	5.20	4.81	4.84	4.65	5.23	5.13	5.06	5.04	4.99	4.79
0.7	5.04	5.23	5.05	4.98	5.37	5.42	5.30	5.24	4.80	4.92
0.8	5.31	5.16	5.10	5.18	5.32	5.20	5.40	5.04	5.04	4.92
0.9	5.32	5.43	5.05	4.93	5.16	4.90	5.07	5.24	5.04	5.21
1.0	5.12	5.29	5.05	4.85	5.14	4.95	5.03	5.12	5.11	5.29
1.1	4.73	4.93	5.20	5.25	5.31	4.84	4.79	4.90	5.12	5.51
1.2	4.82	4.66	4.66	4.74	4.88	4.77	4.66	4.92	4.72	5.02
1.3	4.79	4.68	4.69	4.75	4.79	4.85	4.77	4.98	5.03	4.90
1.4	4.84	4.98	4.89	4.87	4.78	4.64	4.64	4.90	5.06	4.92
1.5	5.10	4.96	4.98	5.02	4.92	4.96	5.04	4.80	4.83	5.06
1.6	5.08	5.00	5.19	5.18	5.32	5.13	5.13	5.05	5.05	5.50
1.7	5.48	5.34	5.46	5.35	5.16	5.14	5.24	5.07	5.05	5.25
1.8	4.90	5.34	5.14	5.36	5.41	5.24	5.47	5.05	5.05	5.29
1.9	4.93	5.03	5.20	5.25	5.31	5.26	5.25	5.13	5.03	4.98
2.0	5.00	4.96	4.99	4.97	4.98	5.02	5.02	5.03	5.03	5.02
2.1	5.25	4.99	5.02	5.17	5.04	5.12	5.26	5.21	5.18	5.16
2.2	5.22	5.20	4.99	5.02	5.07	5.02	5.12	5.12	5.16	5.16
2.3	5.14	5.14	5.10	5.07	5.05	5.07	5.16	5.16	5.16	5.16
2.4	5.21	5.18	5.13	5.17	5.15	5.15	5.16	5.05	5.05	5.41
2.5	5.37	5.37	5.26	5.43	5.25	5.07	5.16	5.09	5.09	5.16
2.6	5.37	5.37	5.36	5.26	5.30	5.22	5.16	5.20	5.20	5.00
2.7	5.31	5.31	5.40	5.47	5.32	5.32	5.16	5.26	5.26	5.25
2.8	5.30	5.30	5.28	5.23	5.23	5.15	5.14	5.12	5.12	5.23
2.9	5.29	5.30	5.28	5.20	5.16	5.16	5.12	5.16	5.16	5.23
3.0	5.31	5.10	5.00	4.92	4.69	4.81	4.83	4.96	4.96	5.23
3.1	5.49	5.37	5.37	5.37	5.37	5.37	5.37	5.37	5.37	5.37
3.2	5.33	5.33	5.37	5.37	5.37	5.37	5.37	5.37	5.37	5.37
3.3	5.04	4.99	4.86	4.76	5.01	4.86	4.77	4.81	4.88	5.23
3.4	5.26	5.08	5.08	5.03	5.03	4.92	4.81	5.06	5.02	5.05
3.5	5.56	5.41	5.28	5.24	4.95	5.12	5.12	5.16	5.19	5.19
3.6	5.50	5.65	5.73	5.60	5.33	5.22	5.31	5.18	5.25	5.25
3.7	5.74	5.70	5.73	5.92	5.64	5.44	5.47	5.30	5.20	5.23
3.8	5.35	5.30	5.37	5.42	5.71	5.53	5.27	5.13	5.20	5.29
3.9	5.05	5.06	5.07	5.19	5.47	5.37	5.30	5.32	5.44	5.22
4.0	5.18	5.10	5.13	5.09	5.13	5.05	5.55	5.69	5.56	5.26
4.1	4.99	4.93	5.05	4.97	5.13	5.17	5.27	5.48	5.35	5.29
4.2	4.87	4.87	4.90	4.89	5.02	5.22	5.23	5.23	5.23	5.46
4.3	5.12	5.10	4.90	5.00	5.00	5.20	5.40	5.62	5.62	5.61
4.4	4.92	4.96	4.85	4.98	4.99	5.14	5.16	5.55	5.55	5.36
4.5	5.32	5.12	4.87	4.86	4.93	5.14	5.17	5.37	5.52	5.14
4.6	5.40	5.36	5.37	5.20	5.31	5.25	5.22	5.25	5.25	5.19
4.7	5.50	5.49	5.43	5.35	5.52	5.27	5.36	5.24	5.24	5.30
4.8	5.51	5.60	5.40	5.27	5.22	5.20	5.28	5.18	5.04	5.26
4.9	5.42	5.49	5.49	5.45	5.35	5.02	5.18	5.04	5.05	5.23
5.0	5.40	5.25	5.20	5.25	5.28	5.32	5.35	5.35	5.37	5.37
5.1	5.25	5.37	5.50	5.32	5.19	5.32	5.27	5.30	5.12	5.08
5.2	5.38	5.40	5.40	5.40	5.40	5.40	5.40	5.67	5.67	5.67
5.3	5.54	5.47	5.47	5.47	5.47	5.47	5.47	5.83	5.77	5.77
5.4	5.55	5.57	5.57	5.57	5.57	5.57	5.57	5.80	5.75	5.75
5.5	5.56	5.44	5.44	5.44	5.44	5.44	5.44	5.48	5.48	5.48
5.6	5.57	5.59	5.59	5.59	5.59	5.59	5.59	5.60	5.60	5.60
5.7	5.58	5.59	5.59	5.59	5.59	5.59	5.59	5.61	5.61	5.61
5.8	5.59	5.59	5.59	5.59	5.59	5.59	5.59	5.62	5.62	5.62
5.9	5.59	5.59	5.59	5.59	5.59	5.59	5.59	5.62	5.62	5.62

Table 9.13
 Errata Sheet for Table 9.8
 $(U(r,s)$ values for Data Set 2)

<u>Column 0</u>	<u>Column 1</u>	<u>Column 19</u>	<u>Column 20</u>	<u>Row 20</u>	<u>Row -20</u>
20	-0011	-0015	-0014	-0013	1 -0016 -0011
19	+0006	-0009	-0010	-0009	2 -0012 -0008
18	-0002	-0001	-0005	-0004	3 -0008 -0005
17	0003	0002	-0002	-0001	4 -0010 -0007
16	0002	0005	-0006	-0004	5 -0012 -0012
15	0003	-0004	-0017	-0016	6 -0012 -0013
14	0002	-0006	-0016	-0017	7 -0012 -0010
13	0009	0007	-0002	-0005	8 -0014 -0010
12	0028	0028	0022	0018	9 -0014 -0010
11	0062	0058	0044	0041	10 -0013 -0010
10	0081	0073	0058	0054	11 -0013 -0014
9	0075	0070	0058	0056	12 -0018 -0016
8	0074	0072	0057	0058	13 -0017 -0016
7	0083	0083	0062	0064	14 -0013 -0015
6	0122	0133	0073	0076	15 -0014 -0015
5	0190	0231	0082	0084	16 -0014 -0016
4	0204	0278	0070	0070	17 -0015 -0016
3	0131	0147	0021	0024	18 -0015 -0016
2	0087	0032	-0049	-0049	19 -0015 -0016
1	0143	0095	-0081	-0062	
0	0202	0218	-0052	-0024	
-1	0143	0280	-0064	-0056	
-2	0087	0448	-0048	-0046	
-3	0131	0449	0022	0024	
-4	0204	0280	0071	0071	
-5	0190	0202	0086	0088	
-6	0122	0136	0073	0077	
-7	0083	0093	0056	0060	
-8	0074	0078	0052	0055	
-9	0075	0079	0055	0054	
-10	0081	0084	0052	0050	
-11	0062	0065	0041	0040	
-12	0028	0029	0021	0021	
-13	0009	0007	-0004	-0004	
-14	0002	0004	-0021	-0019	
-15	0003	0004	-0020	-0018	
-16	0002	-0008	-0010	-0008	
-17	0003	-0001	-0003	-0004	
-18	-0002	-0002	-0004	-0003	
-19	-0006	-0007	-0010	-0009	
-20	-0011	-0011	-0016	-0013	

Table 9.14
 Errata Sheet for Table 9.9
 ($U(r,s)$ values for Data Set 3)

<u>Column 0</u>	<u>Column 1</u>	<u>Column 19</u>	<u>Column 20</u>	<u>Row 20</u>	<u>Row -20</u>
20	-0004	-0004	-0006	1	-0006
19	-0002	-0002	-0003	2	-0003
18	-0006	-0006	-0008	3	0002
17	-0010	-0009	-0010	4	0004
16	-0013	-0012	-0011	5	0000
15	-0006	-0007	-0008	6	-0003
14	0000	-0004	-0007	7	-0005
13	0013	0010	0001	8	-0004
12	0026	0026	0016	9	-0004
11	0041	0033	0031	10	-0003
10	0076	0060	0346	11	-0003
9	0089	0075	0060	12	-0007
8	0094	0093	0071	13	-0010
7	0120	0100	0071	14	-0009
6	0152	0145	0077	15	-0006
5	0152	0204	0059	16	-0-007
4	0128	0183	0046	17	-0003
3	0076	0097	0027	18	-0008
2	0165	0136	0028	19	-0006
1	0742	0386	-0083		-0004
0	1286	0872	-0216		-0230
-1	0742	0651	-0086		-0094
-2	0165	0337	0021		0020
-3	0076	0361	0029		0028
-4	0128	0266	0049		0049
-5	0152	0163	0059		0058
-6	0152	0152	0076		0073
-7	0120	0125	0071		0074
-8	0094	0096	0070		0074
-9	0089	0087	0057		0056
-10	0076	0075	0045		0042
-11	0041	0049	0029		0026
-12	0026	0030	0016		0014
-13	0013	0018	0002		0002
-14	0000	0001	-0007		-0007
-15	-0006	-0007	-0011		-0011
-16	-0013	-0014	-0013		-0013
-17	-0010	-0007	-0011		-0011
-18	-0006	-0005	-0010		-0011
-19	-0002	-0002	-0005		-0005
-20	-0004	-0004	-0007		-0008

Table 9.15 Covariance Surface for Data Set No. 2A

Table 9.16 Covariance Surface for Data Set No. 3C

	1	2	3	4	5	6	7	8	9	10	11	12	13	14	15	16	17	18	19	20
0	1151	0239	0148	0005*	0064	0075*	0038	0153*	0011*	0064*	0016*	0167	0121	0242	0005*	0172*	0150*	0023	0186	
1	0218	0133	0149	0095	0050*	0014	0024*	0039	0087*	0064*	0014	0071*	0081	0238*	0150*	0071*	0023	0150		
2	0216	0217	0219	0337	0329	0170	0078	0032*	0009	0059*	0014	0073*	0055	0275*	0166*	0129*	0048	0150		
3	0197	0198	0198	0317	0317	0198	0122	0034*	0010	0086	0175*	0080*	0054	0162*	0166*	0102*	0064	0144		
4	0145	0145	0145	0317	0317	0198	0122	0034*	0010	0123	0048	0079*	0054	0132*	0163	0207*	0153*	0087*		
5	0329	0329	0329	0285	0320	0156	0141	0046	0066	0125	0023*	0135*	0058	0293	0185	0045*	0142*	0144		
6	0453	0453	0453	0453	0453	0200	0120	0064	0066	0125	0174*	0232*	0085*	0596	0347	0124	0075*	0148*		
7	0453	0453	0453	0453	0453	0175	0155	0051*	0051	0132*	0132*	0121*	0102	0325	0508	0391	0076*	0010		
8	0453	0453	0453	0453	0453	0216	0166	0095	0095	0122*	0122*	0122*	0080*	0350	0112	0077	0096*	0010		
9	0453	0453	0453	0453	0453	0187	0187	0051*	0051	0252*	0252*	0195	0195	0252	0252	0091	0077	0191		
10	0453	0453	0453	0453	0453	0187	0187	0051*	0051	0252*	0252*	0195	0195	0252	0252	0091	0077	0191		
11	0453	0453	0453	0453	0453	0187	0187	0051*	0051	0252*	0252*	0195	0195	0252	0252	0091	0077	0191		
12	0453	0453	0453	0453	0453	0187	0187	0051*	0051	0252*	0252*	0195	0195	0252	0252	0091	0077	0191		
13	0453	0453	0453	0453	0453	0187	0187	0051*	0051	0252*	0252*	0195	0195	0252	0252	0091	0077	0191		
14	0453	0453	0453	0453	0453	0187	0187	0051*	0051	0252*	0252*	0195	0195	0252	0252	0091	0077	0191		
15	0453	0453	0453	0453	0453	0187	0187	0051*	0051	0252*	0252*	0195	0195	0252	0252	0091	0077	0191		
16	0453	0453	0453	0453	0453	0187	0187	0051*	0051	0252*	0252*	0195	0195	0252	0252	0091	0077	0191		
17	0453	0453	0453	0453	0453	0187	0187	0051*	0051	0252*	0252*	0195	0195	0252	0252	0091	0077	0191		
18	0453	0453	0453	0453	0453	0187	0187	0051*	0051	0252*	0252*	0195	0195	0252	0252	0091	0077	0191		
19	0453	0453	0453	0453	0453	0187	0187	0051*	0051	0252*	0252*	0195	0195	0252	0252	0091	0077	0191		
20	0453	0453	0453	0453	0453	0187	0187	0051*	0051	0252*	0252*	0195	0195	0252	0252	0091	0077	0191		

Table 9.17 L{r, s} Values for Data Set 2A

Table 9.18 L(r,s) Values for Data Set 3C

Table 9.19 Spectral Estimates ($\hat{U}(\mathbf{f}_r, s)$) for Data Set 2A

	0	1	2	3	4	5	6	7	8	9	10	11	12	13	14	15	16	17	18	19	20
0.0003	0.0005	0.0007	0.0008	0.0004	0.0005	0.0004	0.0005	0.0005	0.0004	0.0006	0.0004	0.0005	0.0004	0.0005	0.0004	0.0005	0.0004	0.0005	0.0003	0.0003	
0.0007	0.0012	0.0013	0.0014	0.0012	0.0010	0.0008	0.0008	0.0008	0.0008	0.0009	0.0010	0.0009	0.0009	0.0009	0.0009	0.0009	0.0009	0.0009	0.0009	0.0006	
0.0017	0.0013	0.0014	0.0014	0.0012	0.0007	0.0006	0.0006	0.0006	0.0006	0.0007	0.0008	0.0008	0.0008	0.0008	0.0008	0.0008	0.0008	0.0008	0.0008	0.0004	
0.0016	0.0010	0.0011	0.0015	0.0015	0.0013	0.0010	0.0010	0.0010	0.0010	0.0009	0.0014	0.0008	0.0008	0.0008	0.0008	0.0008	0.0008	0.0008	0.0008	0.0004	
0.0015	0.0011	0.0012	0.0024	0.0019	0.0023	0.0018	0.0018	0.0018	0.0018	0.0017	0.0017	0.0016	0.0016	0.0016	0.0016	0.0016	0.0016	0.0016	0.0016	0.0005	
0.0014	0.0010	0.0010	0.0020	0.0020	0.0018	0.0015	0.0015	0.0015	0.0015	0.0015	0.0017	0.0017	0.0017	0.0017	0.0017	0.0017	0.0017	0.0017	0.0017	0.0007	
0.0013	0.0012	0.0012	0.0023	0.0017	0.0017	0.0016	0.0016	0.0016	0.0016	0.0015	0.0015	0.0015	0.0015	0.0015	0.0015	0.0015	0.0015	0.0015	0.0015	0.0007	
0.0012	0.0011	0.0011	0.0018	0.0017	0.0017	0.0016	0.0016	0.0016	0.0016	0.0015	0.0015	0.0015	0.0015	0.0015	0.0015	0.0015	0.0015	0.0015	0.0015	0.0005	
0.0011	0.0010	0.0010	0.0016	0.0016	0.0016	0.0015	0.0015	0.0015	0.0015	0.0015	0.0014	0.0014	0.0014	0.0014	0.0014	0.0014	0.0014	0.0014	0.0014	0.0004	
0.0010	0.0009	0.0009	0.0009	0.0009	0.0009	0.0009	0.0009	0.0009	0.0009	0.0009	0.0010	0.0010	0.0010	0.0010	0.0010	0.0010	0.0010	0.0010	0.0010	0.0004	
0.0009	0.0008	0.0008	0.0008	0.0008	0.0008	0.0008	0.0008	0.0008	0.0008	0.0009	0.0009	0.0009	0.0009	0.0009	0.0009	0.0009	0.0009	0.0009	0.0009	0.0003	
0.0008	0.0007	0.0007	0.0007	0.0007	0.0007	0.0007	0.0007	0.0007	0.0007	0.0007	0.0008	0.0008	0.0008	0.0008	0.0008	0.0008	0.0008	0.0008	0.0008	0.0003	
0.0007	0.0006	0.0006	0.0006	0.0006	0.0006	0.0006	0.0006	0.0006	0.0006	0.0006	0.0006	0.0006	0.0006	0.0006	0.0006	0.0006	0.0006	0.0006	0.0006	0.0003	
0.0006	0.0005	0.0005	0.0005	0.0005	0.0005	0.0005	0.0005	0.0005	0.0005	0.0005	0.0005	0.0005	0.0005	0.0005	0.0005	0.0005	0.0005	0.0005	0.0005	0.0003	
0.0005	0.0004	0.0004	0.0004	0.0004	0.0004	0.0004	0.0004	0.0004	0.0004	0.0004	0.0004	0.0004	0.0004	0.0004	0.0004	0.0004	0.0004	0.0004	0.0004	0.0003	
0.0004	0.0003	0.0003	0.0003	0.0003	0.0003	0.0003	0.0003	0.0003	0.0003	0.0003	0.0003	0.0003	0.0003	0.0003	0.0003	0.0003	0.0003	0.0003	0.0003	0.0003	
0.0003	0.0002	0.0002	0.0002	0.0002	0.0002	0.0002	0.0002	0.0002	0.0002	0.0002	0.0002	0.0002	0.0002	0.0002	0.0002	0.0002	0.0002	0.0002	0.0002	0.0002	
0.0002	0.0001	0.0001	0.0001	0.0001	0.0001	0.0001	0.0001	0.0001	0.0001	0.0001	0.0001	0.0001	0.0001	0.0001	0.0001	0.0001	0.0001	0.0001	0.0001	0.0001	
0.0001	0.0000	0.0000	0.0000	0.0000	0.0000	0.0000	0.0000	0.0000	0.0000	0.0000	0.0000	0.0000	0.0000	0.0000	0.0000	0.0000	0.0000	0.0000	0.0000	0.0000	

Table 9.20 Spectral Estimates ($\hat{U}(r, \theta)$) for Data Set 3C

PART 10

ANALYSIS OF WAVE POLE DATA

Determination of spectra and correction for wave pole motion

Three wave pole records were taken at the times shown in Part 7. The records had been read at an 0.2 second interval at Woods Hole for another purpose, and the numbers were made available to us by Harlow Farmer of Woods Hole. Every fourth point in the sequence was used in the determination of the spectrum, and the result was that the first series had 1,758 points, the second had 1,686 points and the third had 1,764 points. Sixty points were estimated for each of the spectra. The formulas given by Tukey and described in Part 8 were used to compute the spectra. Since the points on the record were 0.8 seconds apart, and since 60 lags were used, the result was that the ΔE values of the spectrum for frequencies between $\mu = 2\pi(k - \frac{1}{2})/96$ and $\mu = 2\pi(k + \frac{1}{2})/96$ would be estimated and plotted at the point $\mu = 2\pi(k)/96$ as k ranges from 0 to 60. Frequencies above $2\pi/1.6$ would be aliased.

The values for the three spectra which were obtained were averaged after a study of the individual values showed no statistically significant variation at the 5 percent level from record to record. Nevertheless, there may have been fluctuations from record to record due to variations in the wind field which would show up at a lower level of significance. The average was multiplied by the correction factor derived in Part 8 in order to obtain the true spectrum of the waves.

The result is shown in figure 10.1. The solid curve is the estimate of

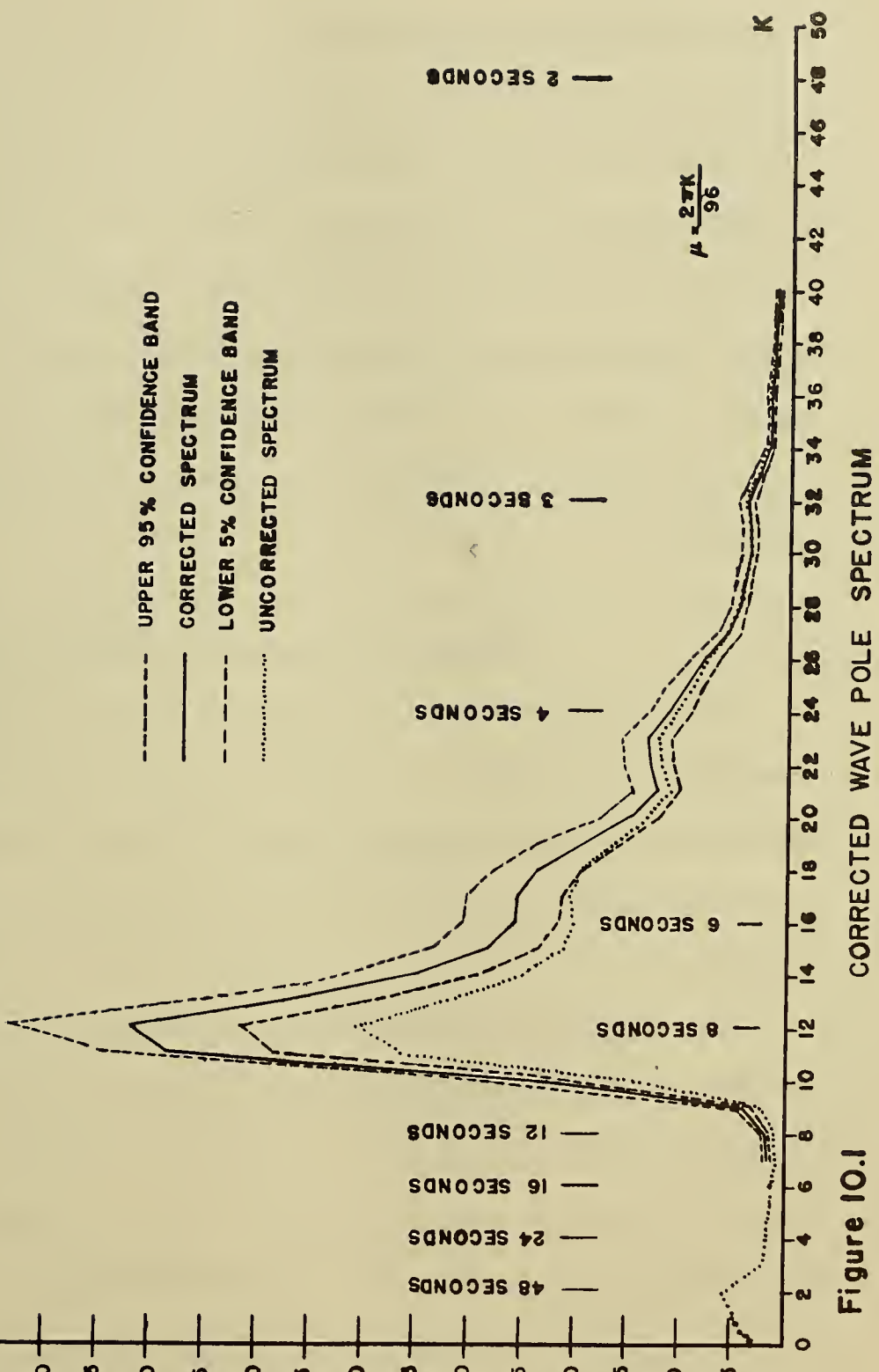


Figure 10.1

the true wave spectrum. From the above lengths of record, one can compute that each spectral estimate has 174 degrees of freedom so that the dashed curves above and below the solid curve show the upper 95 percent and the lower 5 percent confidence bands for portions of the spectrum where it is not rapidly varying. The bounds are probably quite a bit broader at the point $k = 10$. Stated another way, the true spectrum would lie between the bounds shown for nine points out of ten, where it is not varying too rapidly, given that it could be determined from a much larger record under which conditions were stationary.

Comparison with the Neumann Spectrum

This spectrum was compared with the theoretical spectrum derived by Neumann [1954] in two different ways. The first was by plotting the theoretical Neumann spectrum against the observed spectrum, and the second was by computing the co-cumulative spectrum.

The comparison of the spectrum was obtained by evaluating the Neumann spectrum with dimensions of $\text{ft}^2\text{-sec}$ for a set of different wind speeds at the frequencies given by $\mu = 2\pi k / 96$ and multiplying by $2\pi / 96$ with dimensions of sec^{-1} to get an estimate of the ΔE value with dimensions of ft^2 between $\mu = 2\pi(k - \frac{1}{2}) / 96$ and $\mu = 2\pi(k + \frac{1}{2}) / 96$. The quantities are thus directly comparable.

From Figure 10.1, one can see that the energy for frequencies less than $2\pi/96$ is negligible and is probably due to such effects as a slow drift of the recording instrument and a tilting back and forth of the wave pole due to the varying pressures of the wind acting on it. The total E value for the spectrum (E equals twice the variance of the wave record, and it also equals the sum of the squares of the amplitudes of the spectral components) for frequencies equal to or greater than $2\pi/96$ is 4.94 ft^2 . When the upper and lower confidence bounds are taken into consideration, as will be explained shortly, one can conclude that the true value probably lies between 5.28 ft^2 and 4.59 ft^2 . (See also Table 10.1.)

Since

$$(10.1) \quad E = 0.242 \left(\frac{v}{10}\right)^5$$

as given in Pierson, Neumann and James [1955], where E is in ft^2 and v is in knots, an E value of 4.94 ft^2 implies a wind speed of 18.25 knots, and E value of 5.28 ft^2 implies a wind of about 18.5 knots, and an E value of 4.59 ft^2 implies a wind speed of about 18.0 knots.

The Neumann spectra for 19.00. 18.5. 18.25, 18.00 and 17.5 knots were computed in order to cover the above range, and a little extra, and plotted against the observed spectrum. The results are

shown in figure 10.2.

Figure 10.2 shows that no single theoretical curve for a particular wind velocity lies completely within the bounds of the 90 percent confidence bands. In general the values for the observed spectrum are too high for $\mu = 2\pi(11)/96$ and $2\pi(12)/96$ and too low near $\mu = 2\pi(15)/96$.

However, it is also evident that at least one of the five points plotted for the five different theoretical spectra falls within the 90 percent confidence bands on the observed spectrum for all values of k between 10 and 30. A variation in wind velocity of ± 5 percent about a value of 18.25 knots is more than sufficient to explain the observed spectrum at each of these points.

At values above $k = 30$, the observed spectrum is a little above the theoretical spectrum. This may in part be due to a small amount of white noise.

An appeal to the meteorological turbulent variation of the wind speed and to the theory of wave generation and propagation must be made in order to clarify this point. The observations of the ATLANTIS as plotted in

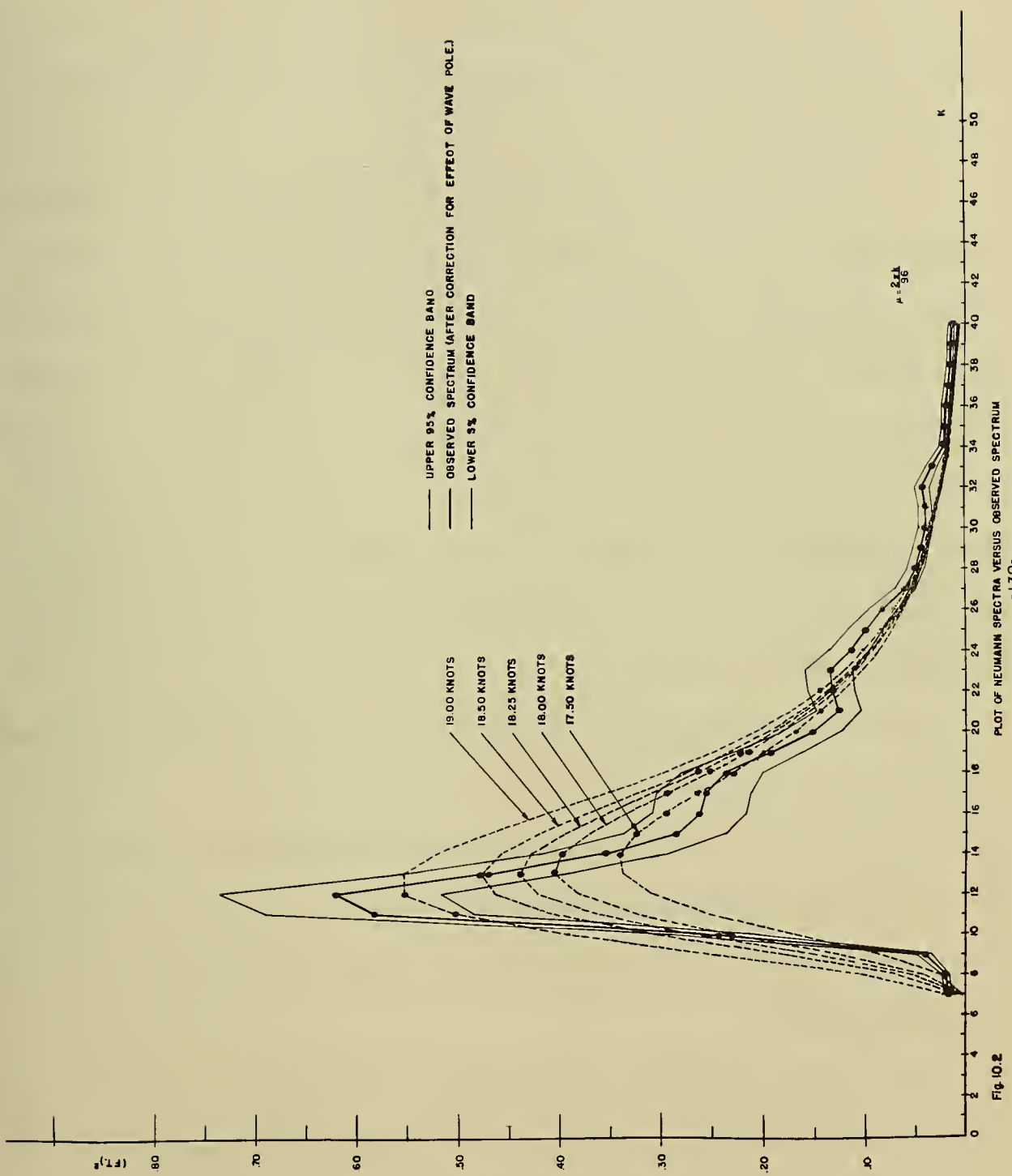


FIG. 10.2
PLOT OF NEUMANN SPECTRA VERSUS OBSERVED SPECTRUM

figure 7.1 show that the wind speed have values of 22 knots, 17 knots, 19 knots, 20 knots, 19 knots, 17 knots, 20 knots, and 17 knots between 0200Z and 1200Z on the day of the observations. Thereafter the wind died down and fluctuated between 13 and 16 knots until after the observations were completed at 1800Z.

The Neumann theory of wave generation requires a duration of 8.3 hours and a fetch of 55 NM in order to produce a fully developed sea at 18 knots, and a duration of 10 hours and a fetch of 75 NM to produce a fully developed sea at 20 knots. An average of the wind speeds from 0400 to 1230Z, as read at half-hour intervals from the lines connecting the actual observations, gives an average wind speed of about 18.7 knots which compares favorably with the values used above. The duration of 9 hours would be enough to produce a fully developed sea at this wind speed, and it certainly seems plausible that the fetch was at least 75 NM.

Over the ocean area upwind of the point of observation (a distance of about 250 NM) it can be stated that due to turbulent variations in the wind there should be areas of the dimensions of 50 to 75 NM where the mean wind speed would vary over a range from 17.5 to 19 knots as averaged over the nine or ten hours previous to the time that the winds died down at the ATLANTIS station.

Then, given a decrease in wind speed, each of the areas would have to be treated according to the methods of Pierson, Neumann and James [1955] as if it were a Filter IV case and the spectrum at the point where the observations were made reconstructed.

A frequency of $2\pi(10)/96$ would still be present at the point of observation if it had been produced by a 19 knot wind 150 NM upwind of the point of observation 6 hours prior to the time of observation. Were the fetch a little shorter, this would result in the low frequency cutoff and the sharp steep forward fact of the observed spectrum.

The spectrum which was observed could easily have resulted from a combination of these effects, although the sparsity of oceanographic observations makes it difficult to demonstrate the exact disposition of the generating area which would lead to the observed spectrum.

The figures given in Part 5 which describe the wind field were the operational maps for the project. Additional ship reports for the area were obtained by checking back through the data, and weather maps showing these reports are plotted in figures 10.3a through 10.3h. The wind as reported in knots is inserted in the feather of the arrow showing the wind direction.

From a study of the winds upwind of the ATLANTIS, it is possible to conclude that the above argument is quite plausible and that therefore variations in wind speed from place to place explain the variation in the observed spectrum.

Comparison with the C. C. S. curves

If the sum of the ΔE values for $\mu = 2\pi k/96$ to $2\pi 60/96$ is computed, an estimate of the point on the co-cumulative spectrum curve for $\mu = 2\pi(k - \frac{1}{2})/96$ is obtained. The estimates of the spectral curve can be

FIG.10.3 WEATHER OBSERVATIONS FOR OCTOBER 24, 1954

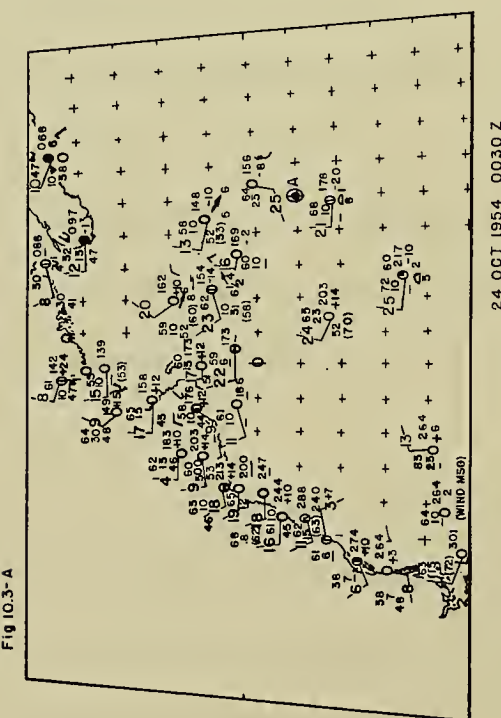


Fig 10.3-A

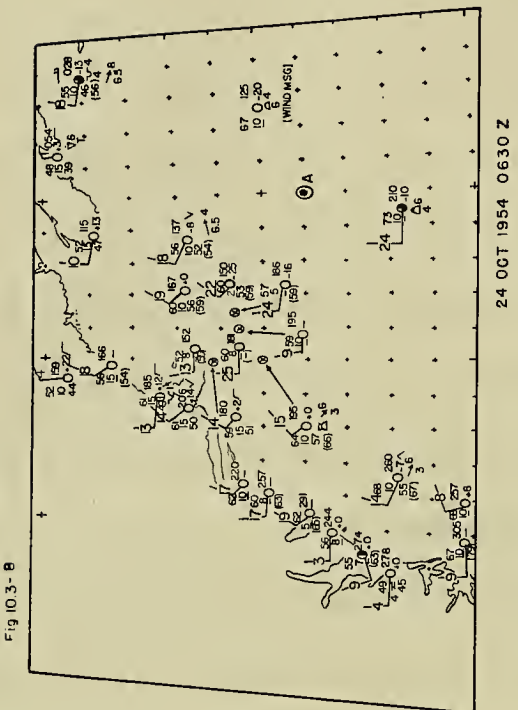


Fig 10.3-8

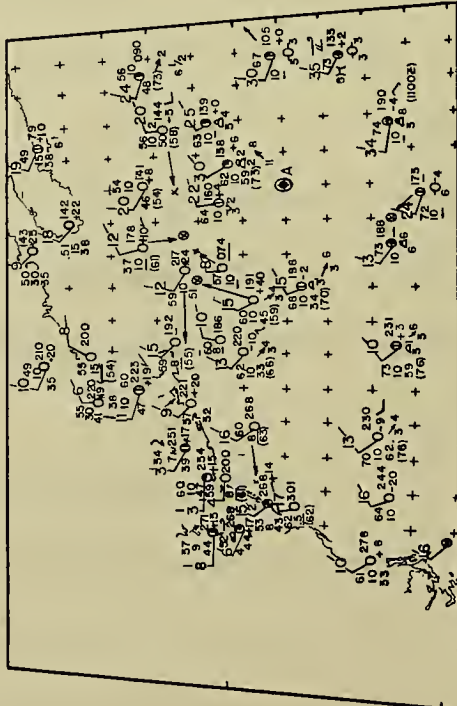


Fig 10.3- C

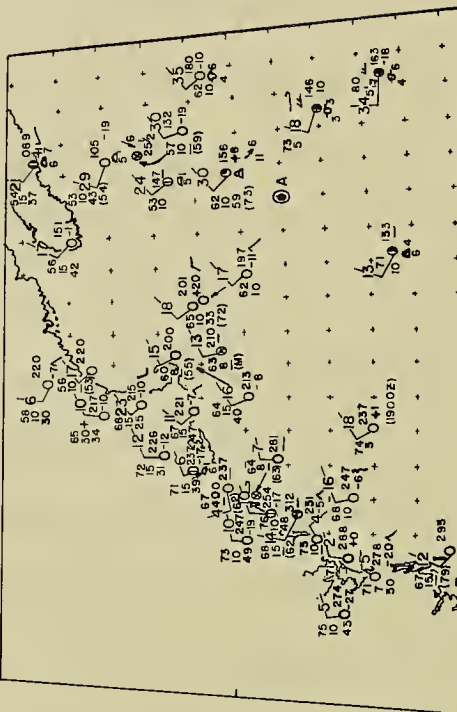


Fig 10.3-D

FIG. 10.3 WEATHER OBSERVATIONS FOR OCTOBER 25, 1954

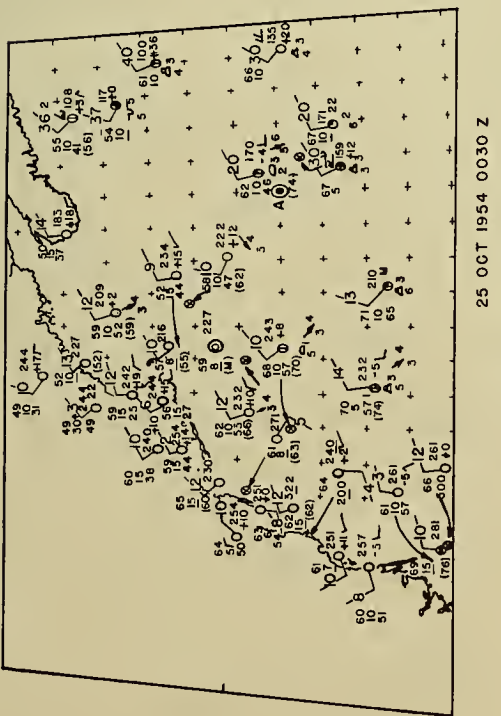


Fig 10.3-G

-143-

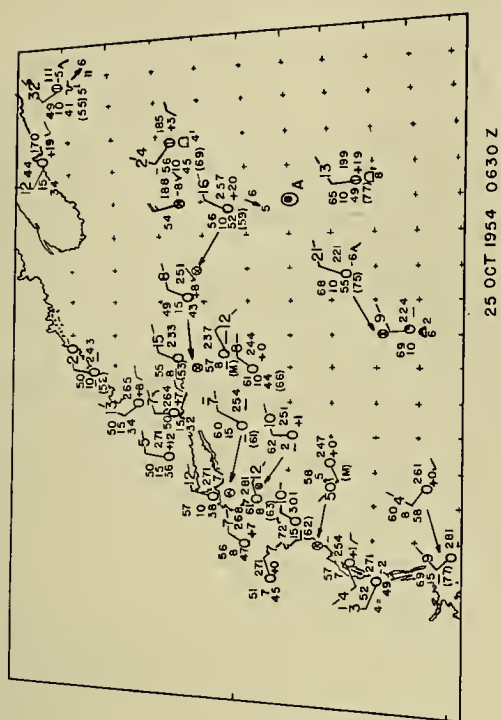
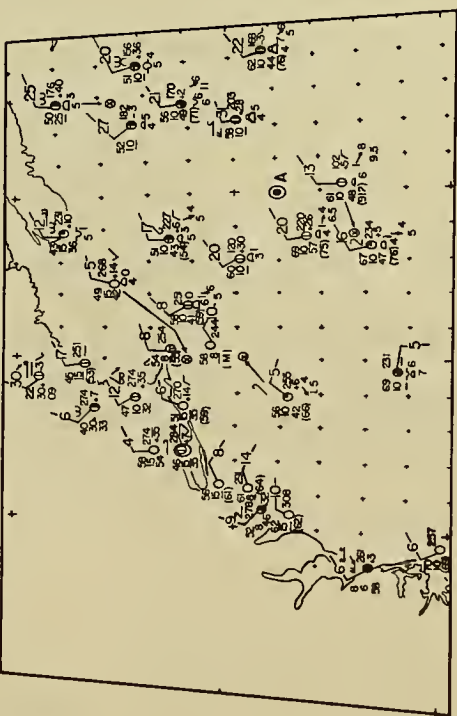


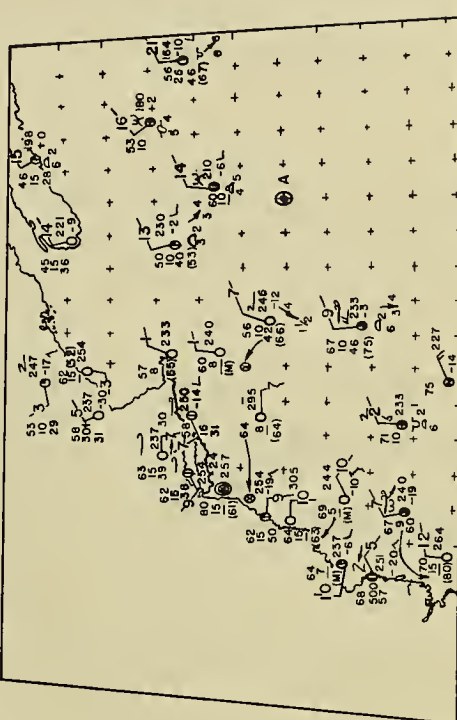
Fig 10.3 - F

Fig. 10.3-H

25 OCT 1954 0630 Z



25 OCT 1954 1230 7



三

treated as if every other one was independent, and since they are distributed according to Chi Square with f degrees of freedom, the point on the CCS curve is approximately distributed according to Chi Square with

$$(10.2) \quad N_k = \frac{f}{2} \left[\frac{\left(\sum_{n=k}^{60} \Delta E_n \right)^2}{\left(\sum_{n=k}^{60} \Delta E_n^2 \right)} \right]$$

degrees of freedom (see Pierson [1954]). Then the confidence bands according to Tukey for large N are approximately given by multiplying the point on the CCS curve by

$$10^{+1/\sqrt{N}} \quad \text{and} \quad 10^{-1/\sqrt{N}}$$

The observed CCS curve is shown in figure 10.4 as plotted on the theoretical family of curves given by Pierson, Neumann and James [1955]. The agreement for some CCS curve slightly in excess of 18 knots is quite striking although the agreement is not perfect.

The CCS curve is too high at the frequency side of the scale. This may in part be due to the summation of white noise errors at high frequencies. Also if the pole surges back and forth in the long period waves, it may encounter shorter period chop while moving back in a trough in such a way as to falsely assign their height contribution to a higher frequency.

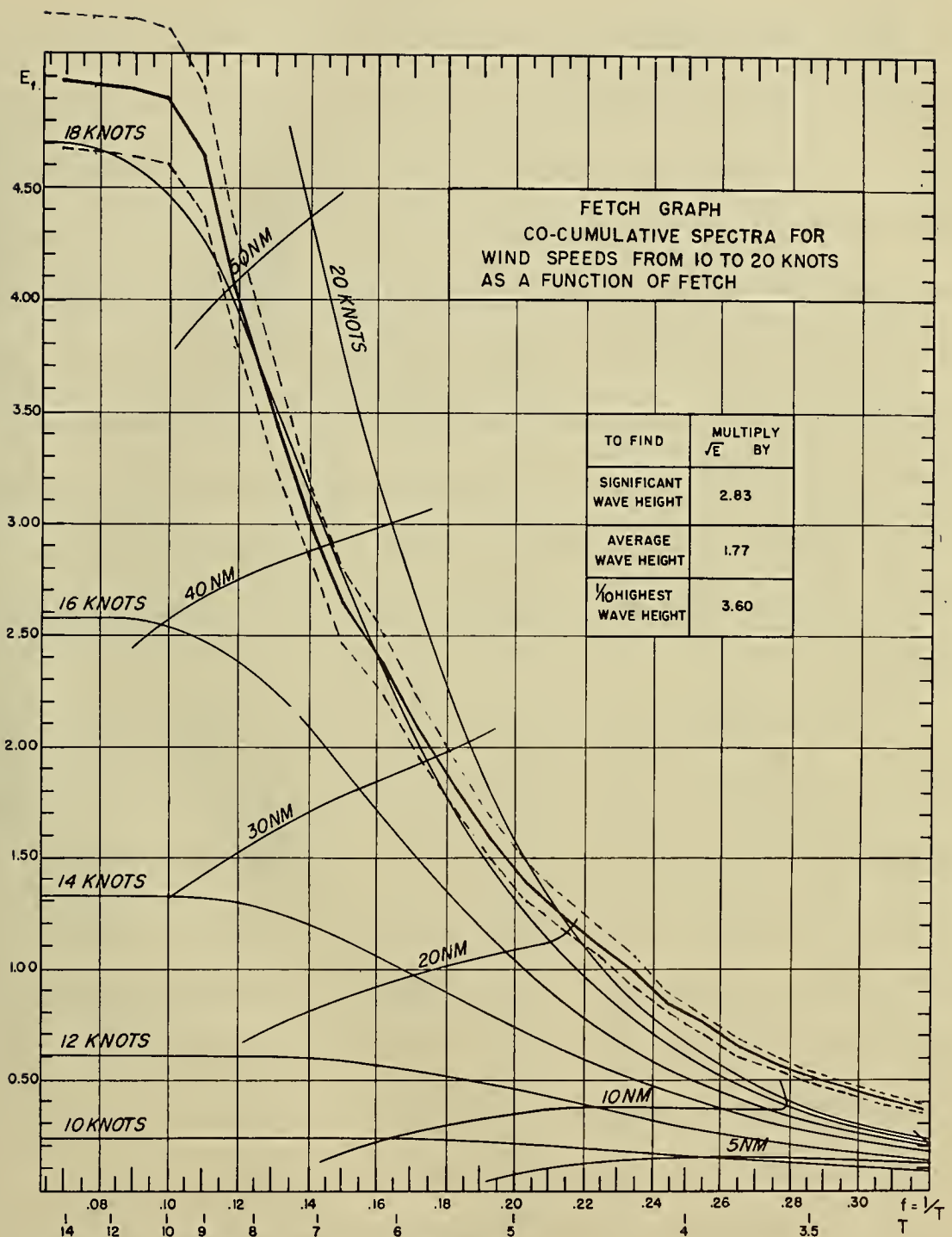


Fig 10.4 OBSERVED C.C.S. CURVE

DASHED LINES ARE 5% AND 95% CONFIDENCE BANDS

Tabulation of Data

The spectral data on which the above figures are based is given in Table 10.1. The frequency is determined by the formula $\mu = 2\pi k/96$, and the entries are given in terms of k . The first column gives the period ($96/k$) which corresponds to the appropriate frequency. The next three columns give the three spectra actually obtained in terms of the contribution to the total variance in $(ft)^2$ of the record made by frequencies within the band. (The values should be doubled to get ΔE values.) The fifth column is the average of the three observed spectra. The sixth column gives the function $\phi(\mu)$ as derived in Part 8, and the seventh gives the function (designated by $H(\mu)$) by which the observed spectrum must be multiplied to obtain the corrected spectrum.

The next column gives the ΔE values in $(ft)^2$ which are the estimates of the area under the spectrum from $\mu = 2\pi(k - \frac{1}{2})/96$ to $\mu = 2\pi(k + \frac{1}{2})/96$. The column fourth from the right gives the sum of the ΔE values in the previous column from the given value of k to 60 and this estimates the point on the CCS curve given by $\mu = 2\pi(k - \frac{1}{2})/96$. The column third from the right gives the value of $2N_k$ (eqn. 10.2) for that point on the CCS curve just obtained. The last two columns give the upper 95 percent and the lower 5 percent confidence bounds on the ΔE values.

The original series of points from which the spectra were computed are not reproduced in this report. They can be made available on request to the Department of Meteorology and Oceanography at N. Y. U.

[For references see Part 11.]

Table 10.1. Spectrum values from the wave pole data.

k	PERIOD	RECORD #1	RECORD #2	RECORD #3	AVERAGE	$\phi(\mu)$	H(μ)	ΔE	Co-Cumulative E	Twice the Degrees of Freedom for Cumulative E	Upper 95% Confidence Band on ΔE	Lower 5% Confidence Band on ΔE
0		0.02054	0.0399	0.0118	0.0241							
1	96	0.0242	0.0309	0.0160	0.0237							
2	48	0.0260	0.0178	0.0191	0.0293							
3	32	0.0142	0.0089	0.0103	0.0111							
4	24	0.0116	0.0068	0.0055	0.0080							
5	19.2	0.0097	0.0068	0.0051	0.0072							
6	16	0.0074	0.0057	0.0073	0.0068							
7	13.7	0.0047	0.0042	0.0060	0.0050	-2.050	1.8119	0.018	4.98	2773	0.021	0.015
8	12	0.0068	0.0041	0.0057	0.0055	-2.719	1.7974	0.020	4.96	2754	0.23	0.016
9	10.7	0.0187	0.0107	0.0060	0.0118	-3.357	1.7470	0.041	4.94	2732	0.049	0.034
10	9.6	0.1045	0.0713	0.0444	0.0734	-3.890	1.6660	0.245	4.90	2690	0.289	0.203
11	8.7	0.2004	0.1853	0.1570	0.1809	-4.443	1.6044	0.580	4.65	2525	0.687	0.482
12	8	0.1826	0.1954	0.2292	0.2024	-4.864	1.5321	0.620	4.07	2499	0.734	0.515
13	7.4	0.1534	0.1563	0.1704	0.1600	-5.168	1.4629	0.468	3.45	2692	0.554	0.389
14	6.86	0.1311	0.1340	0.1102	0.1251	-5.380	1.4110	0.353	2.98	2811	0.418	0.293
15	6.4	0.1029	0.1033	0.1057	0.1057	-5.487	1.3430	0.284	2.63	2823	0.336	0.236
16	6	0.1012	0.1042	0.0977	0.1010	-5.500	1.2921	0.261	2.35	2769	0.309	0.217
17	5.6	0.0939	0.1062	0.1078	0.1026	-5.433	1.2483	0.256	2.09	2723	0.303	0.213
18	5.3	0.0793	0.0937	0.1194	0.0975	-5.274	1.2094	0.236	1.83	2743	0.279	0.196
19	5.05	0.0705	0.0722	0.1024	0.0817	-5.094	1.1775	0.192	1.59	2819	0.238	0.159
20	4.8	0.0648	0.0508	0.0812	0.0656	-4.857	1.1500	0.151	1.40	2852	0.179	0.125
21	4.57	0.0596	0.0552	0.0519	0.0556	-4.585	1.1264	0.125	1.25	2804	0.148	0.104
22	4.36	0.0568	0.0731	0.0492	0.0597	-4.292	1.1060	0.132	1.12	2707	0.156	0.110
23	4.17	0.0568	0.0651	0.0622	0.0614	-3.993	1.0891	0.134	0.99	2683	0.158	0.111
24	4	0.0580	0.0484	0.0522	0.0529	-3.696	1.0751	0.114	0.86	2786	0.134	0.094
25	3.84	0.0575	0.0403	0.0401	0.0460	-3.449	1.0640	0.098	0.75	2911	0.116	0.081
26	3.6	0.0498	0.0391	0.0271	0.0387	-3.128	1.0532	0.082	0.65	3083	0.096	0.068
27	3.55	0.0325	0.0316	0.0209	0.0283	-2.863	1.0448	0.059	0.57	3272	0.070	0.049
28	3.42	0.0236	0.0250	0.0225	0.0237	-2.620	1.0379	0.049	0.51	3300	0.058	0.041
29	3.3	0.0201	0.0230	0.0213	0.0215	-2.391	1.0321	0.044	0.46	3273	0.052	0.037
30	3.2	0.0184	0.0197	0.0195	0.0192	-2.181	1.0273	0.040	0.41	3240	0.047	0.033
31	3	0.0151	0.0190	0.0233	0.0191		1.0264	0.039	0.37	3189	0.046	0.033
32	3	0.0166	0.0212	0.0240	0.0206		1.0300	0.042	0.33	3197	0.050	0.035
33	2.9	0.0163	0.0172	0.0148	0.0161		1.0180	0.033	0.29	3439	0.039	0.027
34	2.82	0.0131	0.0101	0.0082	0.0105		1.0140	0.021	0.26	3609	0.025	0.018
35	2.74	0.0118	0.0078	0.0091	0.0096		1.0110	0.019	0.24	3533	0.023	0.016
36	2.66	0.0113	0.0083	0.0103	0.0100		1.0090	0.020	0.22	3447	0.024	0.017
37	2.59	0.0107	0.0083	0.0072	0.0087		1.0080	0.018	0.20	3419	0.021	0.015
38	2.52	0.0095	0.0086	0.0054	0.0078		1.0070	0.016	0.18	3361	0.019	0.013
39	2.46	0.0082	0.0083	0.0061	0.0075		1.0050	0.015	0.17	3287	0.018	0.013
40	2.40	0.0053	0.0071	0.0082	0.0068		1.0020	0.014	0.15	3223	0.016	0.011
41	2.34	0.0035	0.0054	0.0084	0.0057			0.011	0.15	3156	0.014	0.010
42	2.28	0.0036	0.0051	0.0064	0.0050			0.010	0.13	3035	0.012	0.008
43	2.23	0.0039	0.0060	0.0043	0.0048			0.010	0.12	2891	0.011	0.008
44	2.18	0.0035	0.0062	0.0043	0.0046			0.009	0.11	2745	0.011	0.008
45	2.13	0.0038	0.0050	0.0049	0.0046			0.009	0.10	2603	0.011	0.008
46	2.08	0.0036	0.0042	0.0049	0.0042			0.008	0.09	2466	0.010	0.007
47	2.04	0.0041	0.0045	0.0037	0.0041			0.008	0.08	2324	0.010	0.007
48	2	0.0044	0.0042	0.0031	0.0039			0.008	0.07	2182	0.010	0.006
49	1.96	0.0036	0.0036	0.0033	0.0035			0.007	0.06	2039	0.008	0.006
50	1.94	0.0038	0.0029	0.0027	0.0031			0.006	0.06	1884	0.007	0.005
51	1.88	0.0038	0.0027	0.0025	0.0030			0.006	0.05	1719	0.007	0.005
52	1.85	0.0032	0.0018	0.0025	0.0025			0.005	0.04	1553	0.006	0.004
53	1.81	0.0030	0.0016	0.0027	0.0024			0.005	0.04	1379	0.006	0.004
54	1.78	0.0026	0.0023	0.0028	0.0026			0.005	0.03	1206	0.006	0.004
55	1.75	0.0026	0.0029	0.0027	0.0027			0.005	0.03	1033	0.006	0.004
56	1.71	0.0023	0.0026	0.0024	0.0024			0.005	0.02	863	0.006	0.004
57	1.68	0.0018	0.0027	0.0024	0.0024			0.005	0.02	690	0.005	0.004
58	1.66	0.0020	0.0029	0.0025	0.0024			0.005	0.01	516	0.006	0.004
59	1.63	0.0018	0.0024	0.0025	0.0022			0.004	0.01	345	0.005	0.004
60	1.60	0.0015	0.0021	0.0021	0.0019			0.004	0.004	174	0.004	0.003

Part II

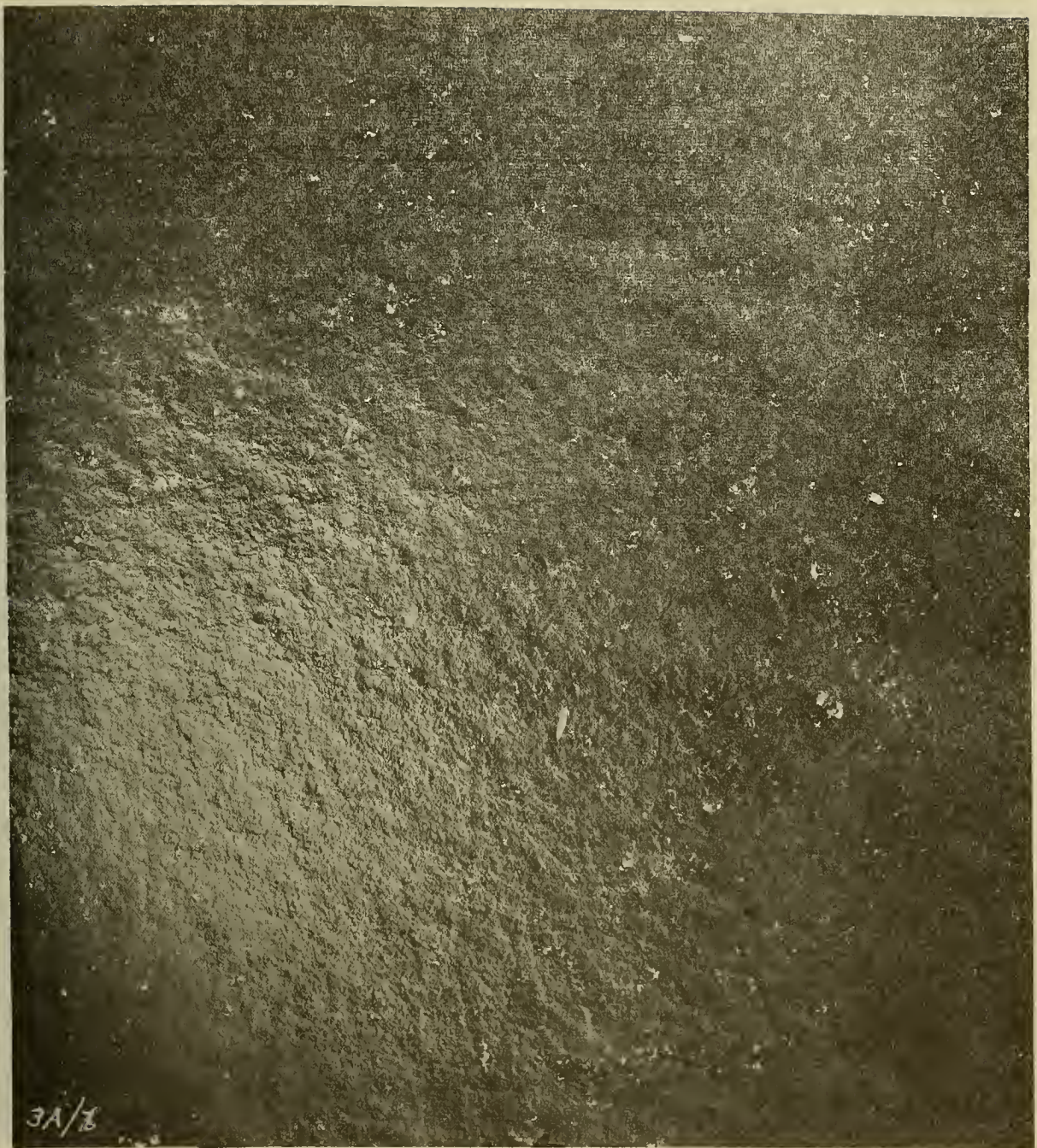
THE STEREO PAIRS, AND THE INTERPRETATION AND ANALYSIS OF THE DIRECTIONAL SPECTRUM IN TERMS OF WAVE THEORY

Introduction

Of the one hundred stereo pairs of photographs taken by the two aircraft, three were selected by the Photogrammetry Division for spot height readings on the basis of picture quality and lack of cloud shadow areas. After leveling, Data Set 1 was found to have a serious barrel distortion so it had to be abandoned. The original numerical analysis of the two remaining sets and the numerical analysis of the reduced data were described in Part 9. In this part, the difficulties which were encountered in analyzing the original results, the way the decision was reached to use a smaller area of points, and the results of the analysis of the modified data will be described.

The stereo pairs

The two sets of stereo pairs chosen for analysis are shown in figures 11.1(A), 11.1(B), 11.2(A), and 11.2(B) where the lead plane picture is the first one of the pair. In order to be sure that the photographs chosen were not chosen, say, for high waves in the vicinity of the ATLANTIS, 10 photographs as taken from one of the planes were picked at random from the 100 photographs available and the wave patterns in the vicinity of the ATLANTIS were compared qualitatively with each other and the two photographs chosen for analysis. There was no apparent difference in wave heights or wave patterns, so that it seemed safe to assume that the two pairs chosen for numerical analysis were representative within usual sampling variation of the sea state.



3A/1

FIG. II.1
STEREO PHOTOGRAPH FOR DATA SET N_o 2
(LEAD PLANE.)



FIG. II.I
STEREO PHOTOGRAPH FOR DATA SET N_o 2
(FOLLOWING PLANE.)

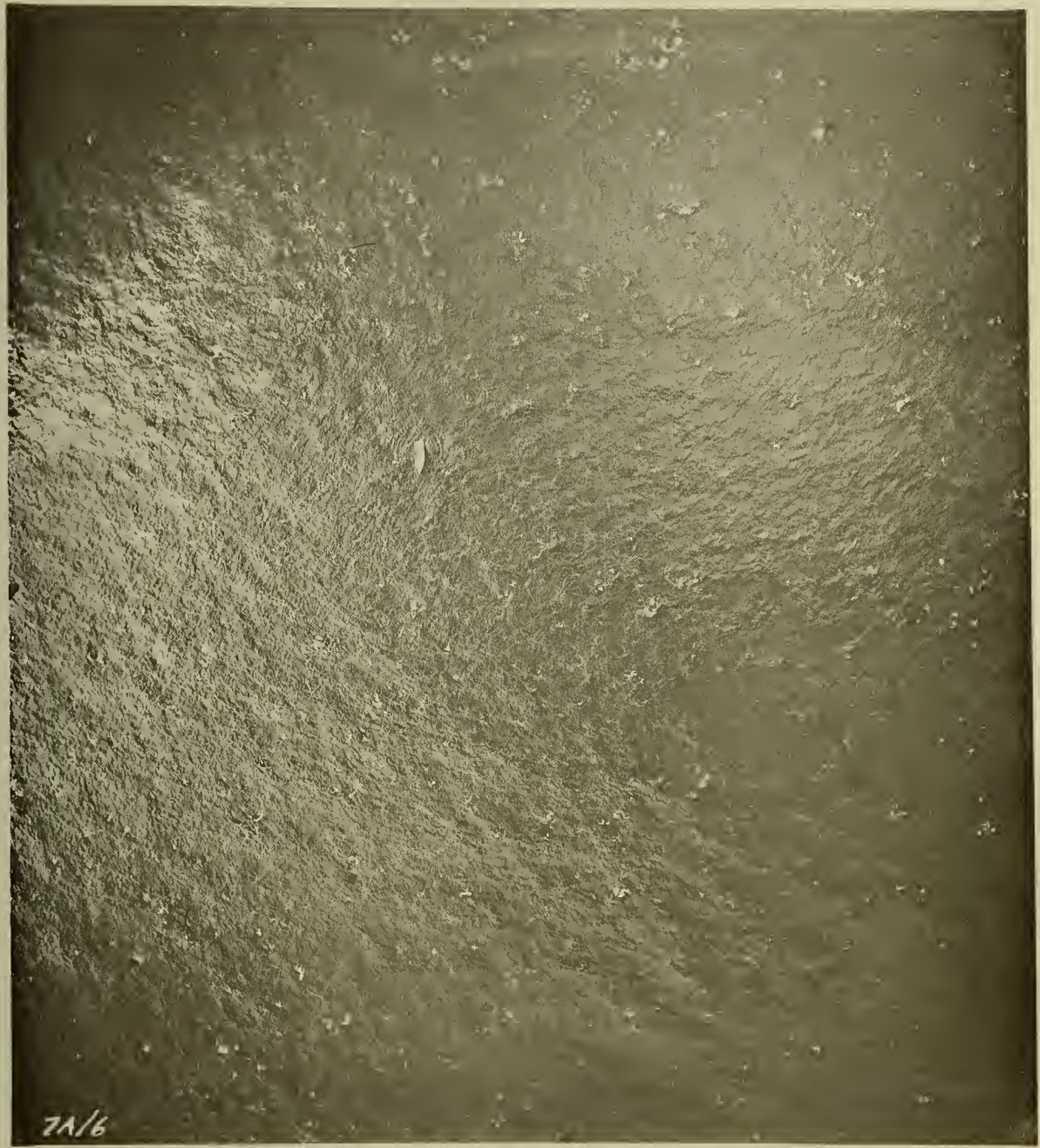


FIG. II.2
STEREO PHOTOGRAPH FOR DATA SET N. 3
(LEAD PLANE.)



FIG. II.2
STEREO PHOTOGRAPH FOR DATA SET N^o 3
(FOLLOWING PLANE)

It should be noted that the exact pattern of the waves shown in figures 11.1 and 11.2 will never occur again and never occurred previous to the time of the photographs. However, patterns with the same statistical properties should occur every time the gross meteorological conditions are the same.

The leveled data

The spot height data after leveling according to the procedure described previously was plotted on a grid 90 points high by 60 points wide. The values as given in mm ($\times 10$) were then contoured. The contouring was done by interpolating to the contour value along the lines joining the points where the data were plotted and connecting the interpolated points by straight line segments. Figure 11.3 illustrates the procedure employed. The contours can be roughly interpreted in feet. To convert to feet exactly the values shown should be divided by 1.016.

The contouring procedure illustrates the effect of the spot height readings. Any irregularities in the sea surface of shorter wave length than 60 feet are essentially undetectable. The exact position of the height contours cannot be determined, but if they could, they would wiggle all around about the straight line segments shown, break off into little closed contour patterns, and show a fine structure all the way down to the capillary level.

The contours for Data Set 2 are shown in figure 11.4. The contours for Data Set 3 are shown in figure 11.5.

The spot height readings are inaccurate by the very nature of the stereo process just as any system of obtaining data has inaccuracies in it. The contoured values and the values tabulated in the tables given before should be

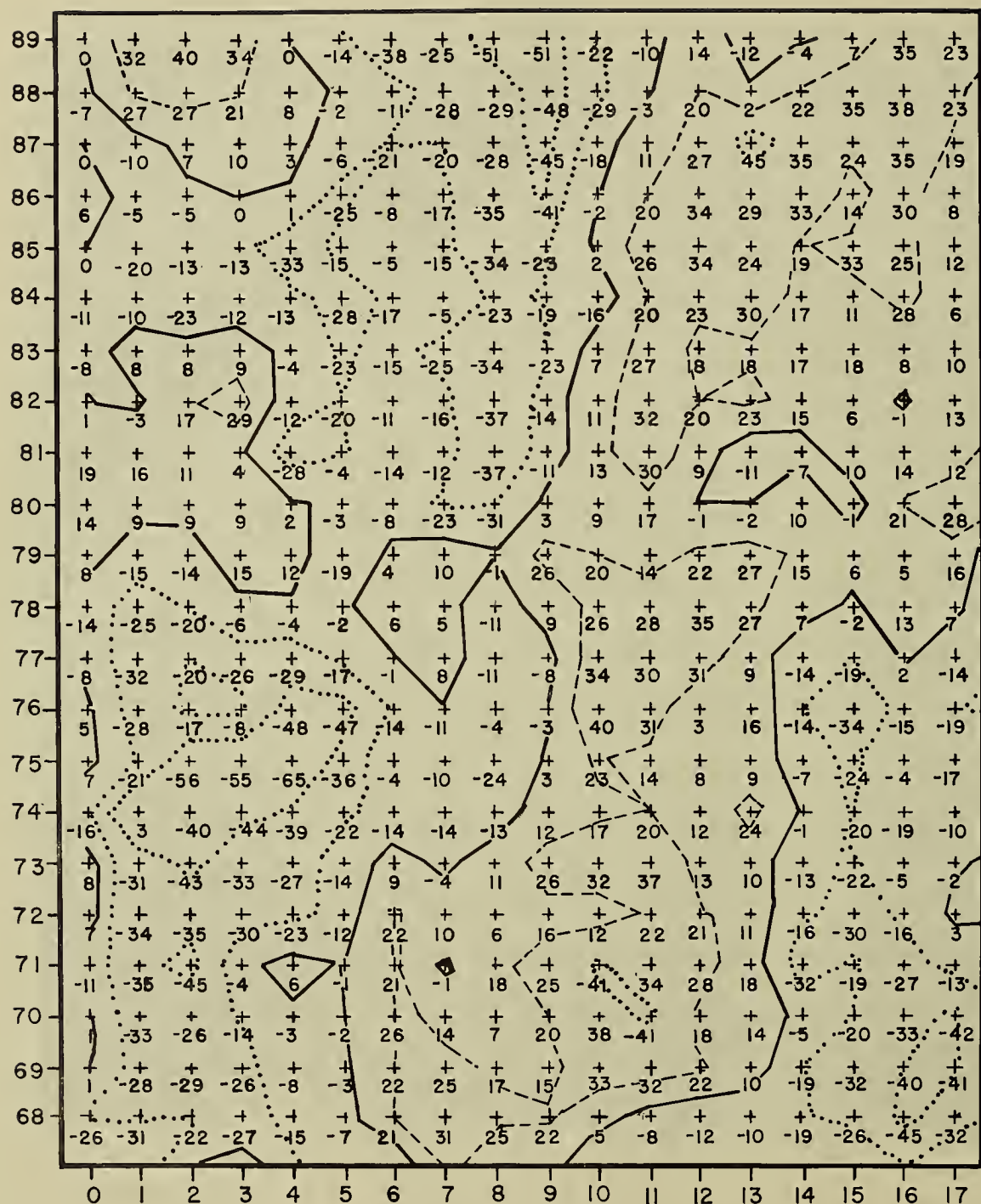


FIGURE 11.3 EXAMPLE OF CONTOURING PROCEDURE



CONTOUR INTERVAL 0.2 mm.
0.1016 mm. = 1 foot
AREA COVERED IS 2670 by 1770 FEET

LEVELED CONTOUR ANALYSIS SET No.2

SHADED AREAS BELOW SEA LEVEL
CLEAR AREAS ABOVE SEA LEVEL



CONTOUR INTERVAL 0.2 mm

0.1016mm = 1 foot

AREA COVERED IS 2570 by 1770 feet

LEVELED CONTOUR ANALYSIS SET No. 3

FIGURE 11.5

156

SHADeD AREAS BELOW SEA LEVEL

CLEAR AREAS ABOVE SF' . LEVEL

considered to be of the form

$$(11.1) \quad \eta_{jk}^* = \eta_{jk(\text{true})} + \epsilon_{jk}$$

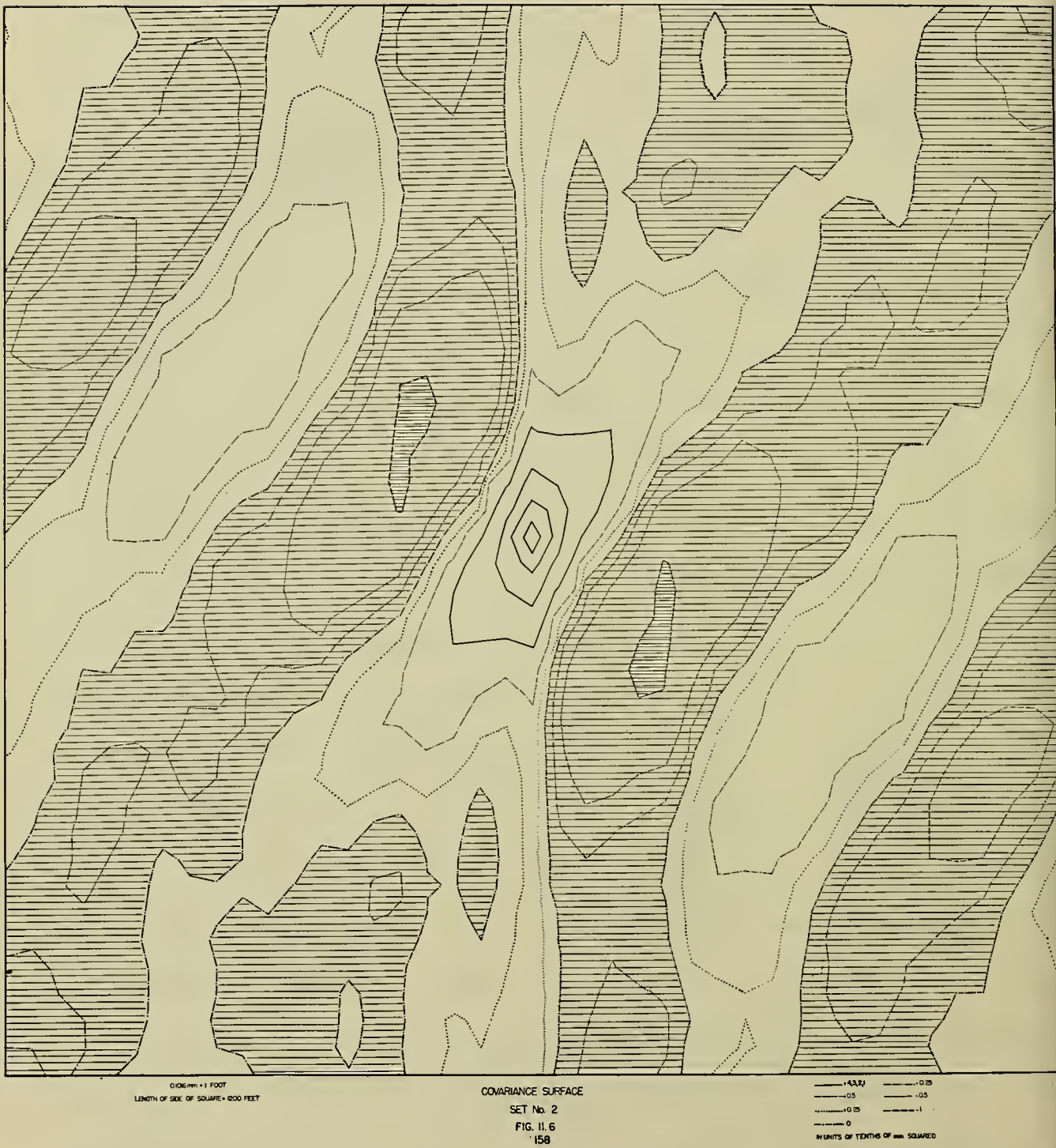
where η_{jk}^* is the tabulated value; $\eta_{jk(\text{true})}$ is the true value and ϵ_{jk} is a random error picked according to some probability scheme to be discussed in detail later.

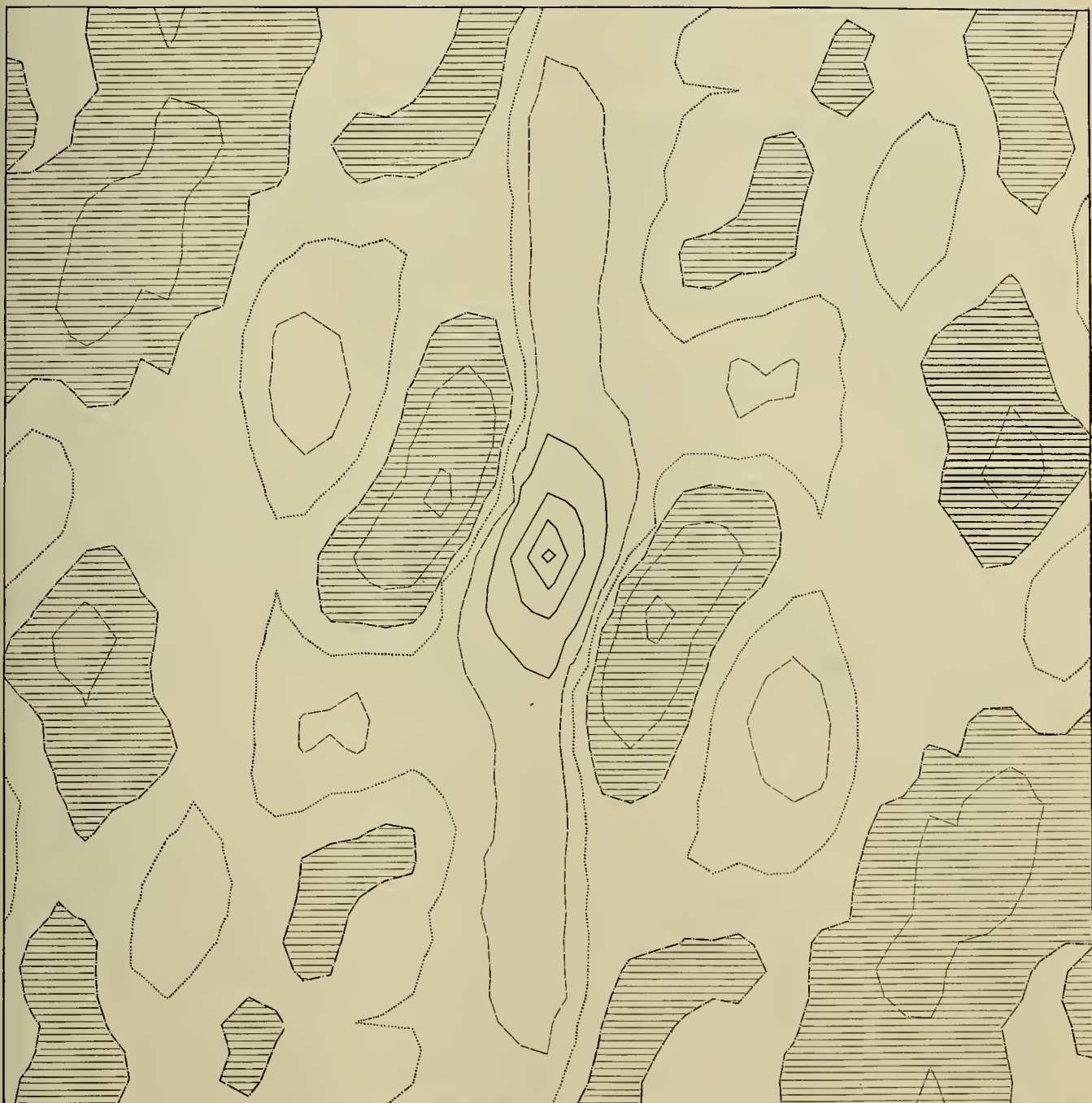
The values of ϵ_{jk} will turn out to be appreciable, and they have the effect of making the pattern shown fuzzy in detail. Due to the size of ϵ_{jk} , statistical evaluations of the patterns shown should be interpreted with considerable caution.

There are other errors of a more serious nature in the data as shown in figures 11.4 and 11.5. These errors will be analyzed in the following paragraphs of this part of the report.

The covariance surfaces

The covariances were computed according to the equations given in Part 8 and plotted on a square grid of points 41 points on a side. The covariance surface for Data Set 2 is shown in figure 11.6, the surface for Data Set 3 is shown in figure 11.7, and the average of the two is shown in figure 11.8. The units of the contours are $(\text{mm})^2 \times 100$. Shaded areas are negative. The figures show an estimate of the correlation (when each value is divided by the value at the center) of the sea surface with itself over distances of the order of 600 feet in any direction. Roughly the correlation is less than ± 0.10 in any direction at a distance of 600 feet. Again the effects of errors in the data have distorted the pattern. The covariances would have the dimensions of $(\text{ft})^2$, if each number shown were divided by $(1.016)^2$.





0.106 m = 1 FOOT
LENGTH OF SIDE OF SQUARE = 200 FEET

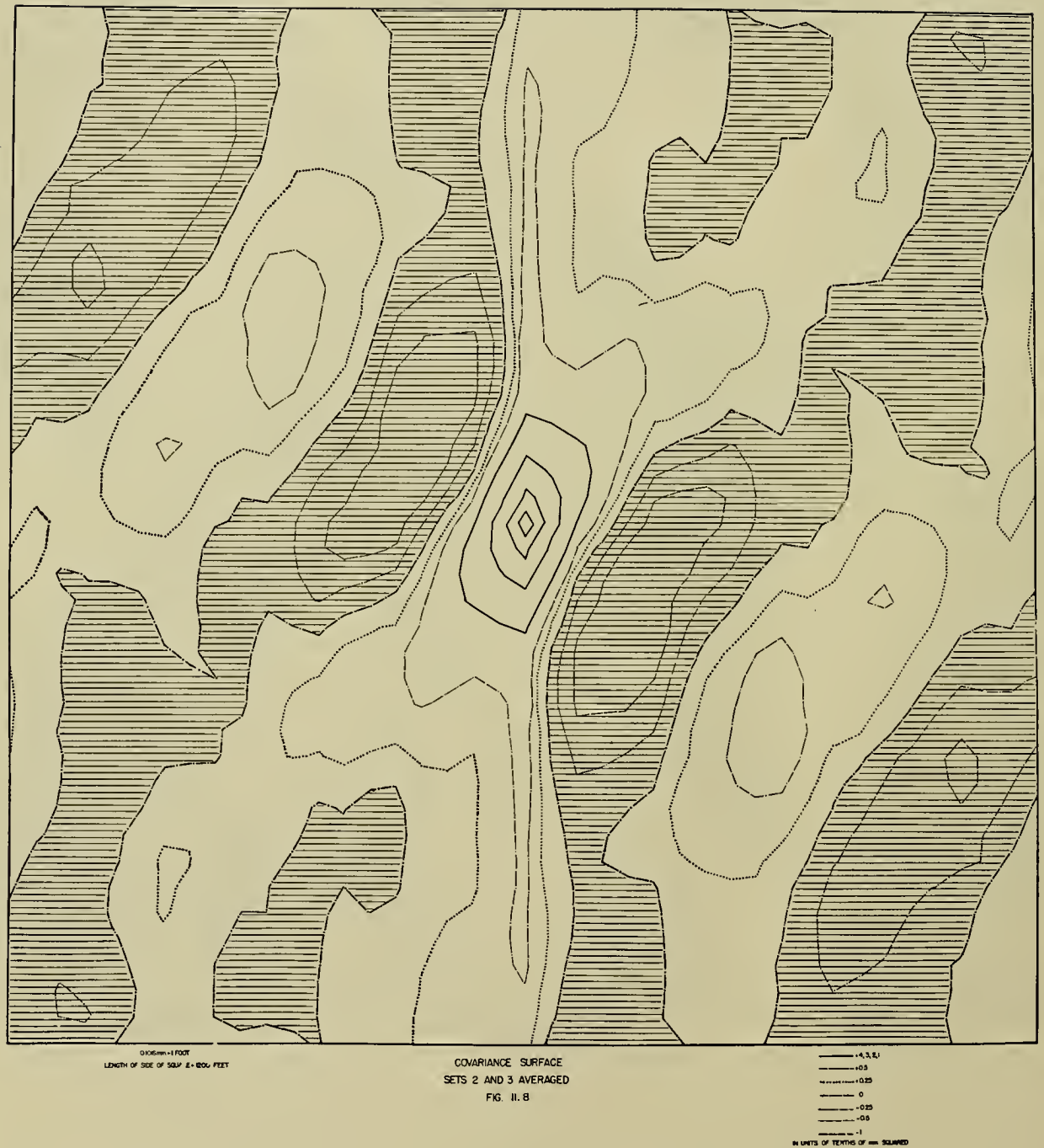
COVARIANCE SURFACE

SET No. 3

FIG. II.7

159

+0.3
-0.5
+0.25
0
-0.25
-0.5
IN UNITS OF TENTHS OF mm. SQUARED



The spectral estimates

The spectral estimates $U(r, s)$ are shown in figures 11.9, 11.10, and 11.11. Figure 11.11 is the average of figures 11.9 and 11.10. The values plotted at the grid intersections should be divided by 1000 to put them in units of $(ft)^2$. The contours are correctly labeled in units of $(ft)^2$. As described in Part 8, the spectra have the property that the same value is obtained at $U(-r, -s)$ as was obtained at $U(r, s)$. If these figures are cut in half by a line through the origin, the sum of the $U(r, s)$ values on one side of the line will equal the variance of the spot height data.

The contours do not give a true representation of the shape of the spectrum. As drawn, they represent an estimate of the volume under the true spectrum when integrated over a square of the size shown in the figure and centered at the contour position. Thus steep slopes in the spectral surface tend to be smoothed out.

These spectra due to the errors hinted at above also have errors in them. The region of analysis should be exactly square. The area shown is rectangular and in actuality the area analyzed should be as high as it is wide. Seven rows of numbers have been omitted from the top and bottom of the figures. At the top of the figure above the dash dot line and at the bottom of the figure below the dash dot line the omitted numbers were all slightly negative. Near the bottom and top edges they were of the order of $-0.002 (ft)^2$. Moreover, near the left and right edges along the r axis of the figures there are considerable areas of negative values with some values of $-0.024 (ft)^2$.

FIG. II.9
DIRECTIONAL SPECTRUM FOR
DATA SET NUMBER 2

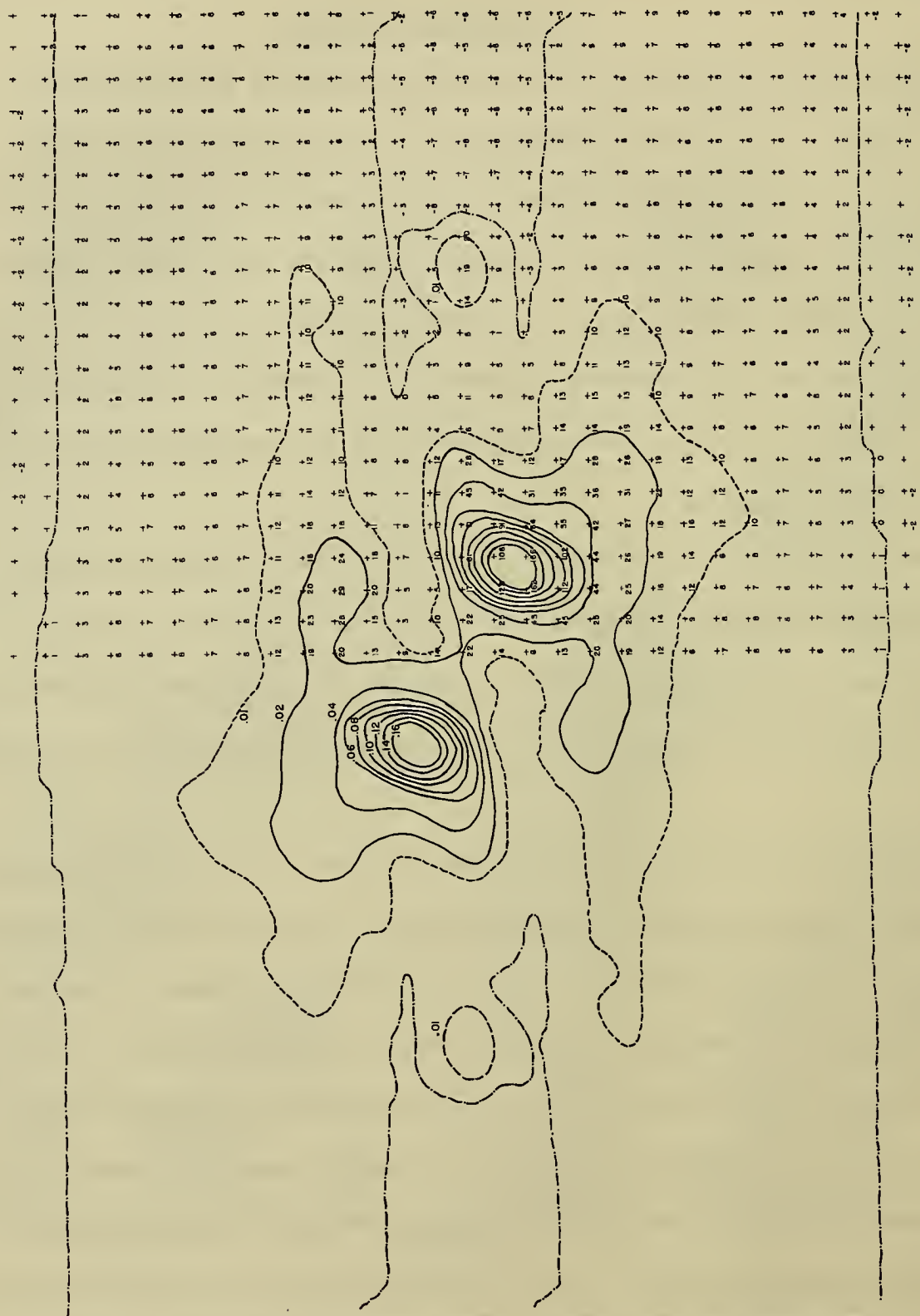




FIG. II.10 DIRECTIONAL SPECTRUM FOR DATA SET NUMBER 3.



FIG. II.11

Although it is not impossible to obtain a negative value in a power spectrum computed according to the techniques described, it is highly improbable that such consistent patterns of negative numbers should occur. Given that the computations are correct, one possible explanation of what occurred is that the original data have been distorted by some unknown and undetected source of error to such an extent that they no longer represent a sample from a stationary Gaussian process in two variables. (Another very disturbing possible conclusion is that the ocean waves cannot be satisfactorily approximated by a stationary Gaussian process in three variables.)

Moreover since the sum of all the values of $U(r, s)$ must add up to the variance of the original data (in these figures), the negative values have the effect of adding erroneous positive values to the already positive estimates in the other parts of the figure.

A study of the figures and the data shows that the gross features of the analysis appear to be correct but that there seems to be a background distortion in the pattern which is difficult to define precisely.

Analysis of original results

Various tests of the results were made at this point, and it soon became evident that there were serious discrepancies between the wave pole frequency spectrum and the average of the two directional spectra. The average of the sums of the values shown in the directional spectra (which in turn equals $[\Omega(00)_2 + \Omega(00)_3]/[2(1.016)^2]$) should give a number which when corrected for possible sources of error should be nearly the same as one half the E value

for the wave pole spectrum.

There were two possible sources of error considered in the stereo data. Even after their removal, there was still a considerable discrepancy.

The first possible source of error was what is called white noise reading error by Tukey [1949]* for the one dimensional case. It can be easily generalized to the two dimensional case. Let

$$(11.2) \quad \eta_{jk} = \eta_{jk}(\text{true}) + \epsilon_j^* + \epsilon_k^* + \epsilon_{jk}^*$$

where η_{jk} is the actual reading, $\eta_{jk}(\text{true})$ is the reading that would be obtained from the stereo data with the stereo planigraph if there were absolutely no sources of photographic, machine or human error, and ϵ_j^* , ϵ_k^* and ϵ_{jk}^* are random errors.

More precisely, let ϵ_j^* be numbers picked at random from a normal population with zero mean with an unknown variance and added to every value of a column of $\eta_{jk}(\text{true})$; let ϵ_k^* be similar number with perhaps a different variance added to every row, and let ϵ_{jk}^* be numbers picked at random from still a third different normal population with a zero mean and a different variance and added to the appropriate value of $\eta_{jk}(\text{true}) + \epsilon_j^* + \epsilon_k^*$. The errors just described will be referred to as column noise, row noise, and white noise, respectively.

* For a more recent and more readily available reference, see Press and Tukey [1957].

The effect of the random errors on Q_{pq} can then be determined under the assumption that the different types of errors are small and independent.

$$(11.3) \quad Q_{pq} = Q_{pq(\text{true})} + S_{oq} + S_{po} + S_{oo}$$

where $S_{oq} = E(\epsilon_j^*)^2$ if $p = 0$ for any q and is zero if $p \neq 0$;

$S_{po} = E(\epsilon_k^*)^2$ if $q = 0$ for any p and is zero if $q \neq 0$;

$S_{oo} = E(\epsilon_{jk}^*)^2$ if $p = 0$ and $q = 0$ and is zero if $p \neq 0$ and $q \neq 0$.

The effect of a random error along a column of the data is thus to cause a constant error to be added to every value on the vertical axis of the coordinate system of the covariance surface; an error along a row adds a constant error to each value on the horizontal axis; and a random error over the whole plane is concentrated as a spike at the origin.

The values of $L(r, s)$ can then be found from the values of $Q(pq)$

$$(11.4) \quad L(r, s) = L(r, s)_{(\text{true})} + W_{os} + W_{ro} + W_{rs}$$

where $W_{os} = \frac{1}{20} E(\epsilon_j^*)^2$ if $r = 0$ for any s and zero if $r \neq 0$;

$W_{ro} = \frac{1}{20} E(\epsilon_k^*)^2$ if $s = 0$ for any r and zero if $s \neq 0$;

and $W_{rs} = \frac{1}{800} E(\epsilon_{jk}^*)^2$, for every value of r and s .

Thus, random errors along columns in the original data show up as a constant error along the horizontal coordinate axis in the $L(r, s)$ plane; errors along rows show up as a constant error along the vertical axis, and random errors show up as a constant error at each point in the spectral plane. Of course, since the data are really a finite sample, there will be fluctuations from point to point in the $L(r, s)$ plane.

Finally the computation of $U(r, s)$ smooths the values of W_{os} and W_{ro} into three rows or columns and assigns weights of 0.54 to the values given along to the axes and 0.23 to the row or column on either side of the axis. Random fluctuations in W_{rs} are smoothed out so that $U(r, s)$ is more nearly a constant at every point and equal to 1/800 of the white noise variance.

The other source of error lies in the possibility of background curvature of the plane of the stereo data. It will be recalled that one set of data was so severely distorted by background curvature that it had to be abandoned. Although no curvature is detectable in figures 11.4 and 11.5, a very slight amount of curvature would produce high values for the spectral estimates near the origin.

The effect of pure white noise can be estimated from the information given in Part 7. The accuracy of the spot height readings is considered to be ± 0.5 feet. Under the assumption that the errors are normally distributed this can be interpreted to mean that

$$(11.5) \quad P(-0.5 < H_T - H_o < 0.5) = 0.5$$

which can be read that the probability is one half that the difference between the true height and the observed height lies between -0.5 and +0.5 feet.

This implies that

$$(11.6) \quad \frac{1}{\sqrt{2\pi}\sigma} \int_0^{0.5} e^{-x^2/2\sigma^2} dx = 0.25$$

and that

$$(11.7) \quad \sigma^2 = 0.54 \text{ (approximately)}$$

Thus the total variance of the white noise reading error is approximately 0.54 (ft)^2 , and the quantity $0.54/800 \text{ (ft)}^2$ should be subtracted from each of the tabulated values of $U(r, s)$ to correct for this effect.

Moreover the spectrum for data Set 3 at the origin definitely shows the effects of curvature. The average spectrum also shows an effect of curvature in the peak at the origin of the spectrum and in the distortion of the contours near the origin. The magnitude of the effect can be estimated from the spectrum.

There is a hint of column noise in both of the covariance surfaces and in the average covariance surface. There is a fairly strong ridge along the vertical axis of all three figures. However, these ridges do not produce the predicted effect of a ridge along the horizontal axis of the spectra. Thus if the column noise is present it is masked by some other more serious source of error.

White noise and curvature error both add positive quantities to the spectrum when they occur. Corrections to the total variance of the original data can be calculated from the above information and the results are tabulated in Table 11.1.

As seen from Table 11.1 the corrected variance of the combined data is 3.80 (ft)^2 . From the study of the wave pole spectrum, assuming correct calibration, confidence bounds on the E value were set and it can therefore be calculated (by taking half the value) that the range from 2.23 (ft)^2 to 2.64 (ft)^2 would enclose the true value of the variance of the wave pole data nine times out of ten. The true variances of the wave pole data and the stereo data should

Table 11.1. Corrections to variances of the original stereo data.

	Original value	White noise	Curvature	Lower 5 percent confidence value on corrected variance	Corrected for white noise and curvature on corrected variance	Upper 95 percent confidence value on corrected variance
$Q(00)_2$ [(mm) ² (x 100)]	4.76		0.56	0.00		
(ft) ²	4.61		0.54	0.00	3.62	4.07
						4.55
$Q(00)_3$ [(mm) ² (x 100)]	4.44		0.56	0.26		
(ft) ²	4.30		0.54	0.25	3.12	3.51
						3.93
$\bar{Q}(00)$ [(mm) ² (x 100)]	4.60		0.56	0.13		
(ft) ²	4.46		0.54	0.12	3.48	3.80
						4.13

be equal, and yet the estimates obtained from the samples are not. The variance of the stereo data is 1.54 times the estimated variance of the wave pole data and 1.48 times the upper confidence bound of the estimated variance of the wave pole data.

This result is not necessarily highly improbable. If the number of effective degrees of freedom of the 10,800 points in the stereo data is very low due to their correlation with each other, the result would be possible. Thus it is necessary to obtain an estimate of the degrees of freedom of the estimated variances of the stereo data.

This can be done by applying a formula similar to the one used on the wave pole spectrum in Part 10 except that now every fourth point is truly independent and there are 16 degrees of freedom per point for each of the original spectra and 32 degrees of freedom per point for the average spectrum.

The total variance was found to have at least 800 degrees of freedom by means of a computation using the average spectrum and grouping data so as always to decrease the computed degrees of freedom. The variances of the individual data sets as a consequence have about 400 degrees of freedom. Additional entries in Table 11.1 give the upper 95 percent and lower 5 percent confidence bounds on the estimates of the variance based on the above degrees of freedom.

The lower 5 percent confidence bounds for the stereo data are greater than the upper 95 percent confidence bounds for the wave pole data. The hypothesis that the wave pole data and the stereo data are samples (free from any sources of additional error) from the population with the same variance must

therefore be rejected at least at the 5 percent significance level, and of course the probability that either variance would be obtained, given that the other is correct, is much less than 0.05.

An application of the F test to the ratio of the two variances, that is, 1.54, with 1000 degrees of freedom for the wave pole data and 500 degrees of freedom for the stereo data, yields a rejection of the hypothesis that the variances are from the same population at the 1 percent significance level.

The directional spectra given in figures 11.9, 11.10, and 11.11 therefore do not have gross properties which agree with independently determined data from the wave pole. If the wave pole data are assumed to be correct since in the original planning the wave pole data were thought of as a primary source of calibration, it must then be concluded that the directional spectra are in error. Moreover, the directional spectra have negative values which is a definite indication of something wrong.

Of course, there would be one way to force the two spectra to agree. It would be to assume that the estimate of the white noise error was too low approximately by a factor of 4. It would then be necessary to subtract about 0.0025 (ft)^2 from each spectra estimate. The effect would be to increase the size of the negative areas. Such a solution would only serve to increase the error in the result due to the negative areas of the spectrum.

Various attempts were made to correct the results by making changes in the covariance surface and calculating their effect on the spectrum and making changes in the spectrum and calculating their effect on the covariance surface.

For example, quasi column noise whose effect would disappear at plus or minus ten lags in the vertical direction on the covariance surface could produce the negative areas in the spectra found on the horizontal axis.

However the attempts were in general unsatisfactory as the different types of corrections propagated very oddly from one system to another. No notable success was achieved by these attempts.

Detailed analysis of leveled spot height data

The analysis of the data had reached an impasse. After a number of conferences with Leo Tick and Prof. Max Woodbury, Prof. Woodbury suggested that the original data be studied to see if they could be corrected. Such a procedure would involve re-computation of the results, but the use of the Logistics computer at George Washington University was assured, and the problem was deemed so important that the added effort to obtain a satisfactory solution should be made.

The ridge along the vertical axes of the covariance surfaces suggested some source of error in the vertical direction of the stereo data. Figures 11.4 and 11.5 and the leveled spot height values as tabulated were then studied very carefully to see if any discrepancies could be found.

In fig. 11v4, it had been noted that the diagonally oriented wave crest-wave trough pattern on the left side and in the center of the figure changed to a vertical orientation on the right hand edge of the pattern. Very strong vertically oriented crests are especially pronounced in the lower right corner. This variation had been thought to be a possible perfectly natural variation in the data, but now this assumption was checked.

The ten columns of numbers on the far right of the figure and the twenty rows of numbers on the bottom of the figure were set apart from the main part of the figure, because of this tendency toward a vertical distortion, and divided into three groups with the rest of the data comprising a fourth group.

The breakdown was as follows:

89,0, 89,1	89,49	89,50	89,59
.	.	.	.
.	AREA A 3500 points	.	AREA B 700 points
.	.	.	.
21,0			
20,0, 20,1	20,49	20,50	20,59
-----	-----	-----	-----
19,0	19,49	19,50	19,59
.	AREA D 1000 points	.	AREA C 200 points
.	.	.	.
2,0			
1,0			
0,0, 0,1, 0,2	0,49	0,50, 0,51	0,59

The variances of the sub-areas were computed, and probability histograms were drawn. The variances of areas B, C and D were all greater than the variance of A, and since it was known that the total variance of Data Set 2 had about 400 degrees of freedom, these 400 degrees of freedom were apportioned in the ratio of the total number of points in each area. It was then possible to apply the F test to the ratios of the variances. Table 11.2 shows the results which were obtained.

Table 11.2. Analysis of Sub Areas in Data Set 2.

Area	ΣN^2	No points	Variance (mm) ² $\times 100$	Ratio to A	F test significance level			Confidence factors			Confidence bounds		
					used	5%	1%	5%	95%	Lower	Upper		
A	14,913	3500	4.26					0.865	1.155	3.68	4.92		
B	3,639	700	5.20	1.22	52	<u>50</u> 200	1.48	1.76	0.725	1.38	3.77	7.18	
C	1,982	200	9.92	2.30	15	<u>15</u> <u>200</u>	2.10	2.92	0.484	1.67	<u>4.80</u>	16.55	
D	5,160	1000	5.16	1.21	73	<u>70</u> 200	1.40	1.62	0.762	1.31	3.93	6.76	
Total	25,704	5400	4.76		400				
B+C	5,621	900	6.26	1.47	67	<u>65</u> 200	1.42	1.64	0.755	1.32	<u>4.73</u>	8.25	
D+C	7,142	1200	5.95	1.39	88	<u>80</u> 200	1.38	1.57	0.782	1.28	<u>4.65</u>	7.62	
B+C+D	10,781	1900	5.67	1.33	140	<u>125</u> 200	1.31	1.46	0.825	1.21	<u>4.68</u>	6.85	

The variance of area A was $0.50[(\text{mm})^2 \times 100]$ less than the variance of the total area. The variance of area C was over twice as large as that of area A. The degrees of freedom actually used in the F test were less than the computed degrees of freedom, and yet at the 5 percent significance level the hypothesis that the sample of points from area C is from the same population as the sample of points from area A must be rejected.

The grid of points for the numerical analysis must be rectangular. Areas B and C, D and C; and B, C, and D were combined, and their combined variances were tested against area A. In all combinations, the areas could be rejected at the 5 percent level. Moreover the lower confidence bounds on the variances of area C, areas B+C, C+D, and B + C + D were all greater than the upper confidence bound on area A.

Figure 11.12 shows a comparison of the probability histograms (number of points in class interval divided by total number of points) from areas B, C, and D, with the probability histogram from area A. Area C is quite a bit different from area A. Note also that the histogram for area A appears to be normal.

The spot heights for Data Set 3 were analyzed in a similar way. A study of the contours suggested that a tendency toward vertical instead of diagonal crest orientation existed on both edges of the area of analysis and the points in Data Set 3 were broken up into five areas as indicated below.

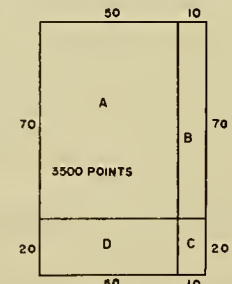
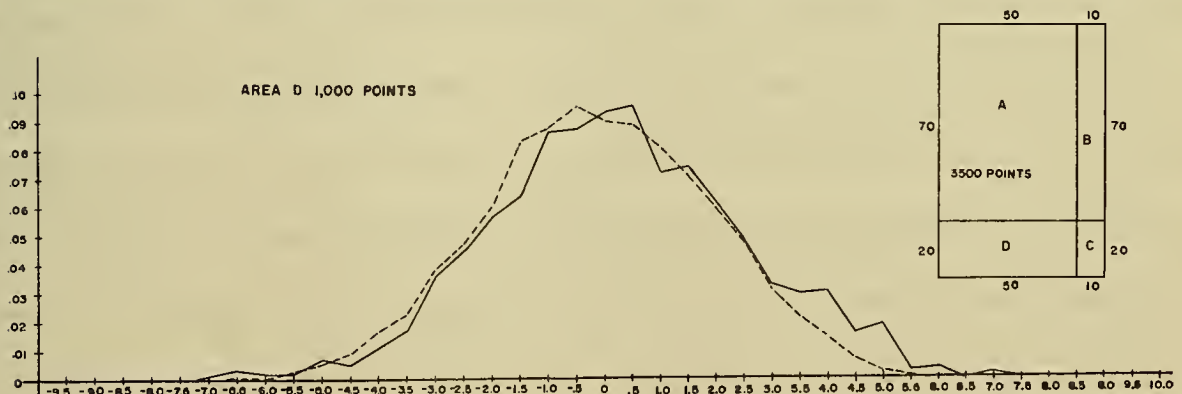
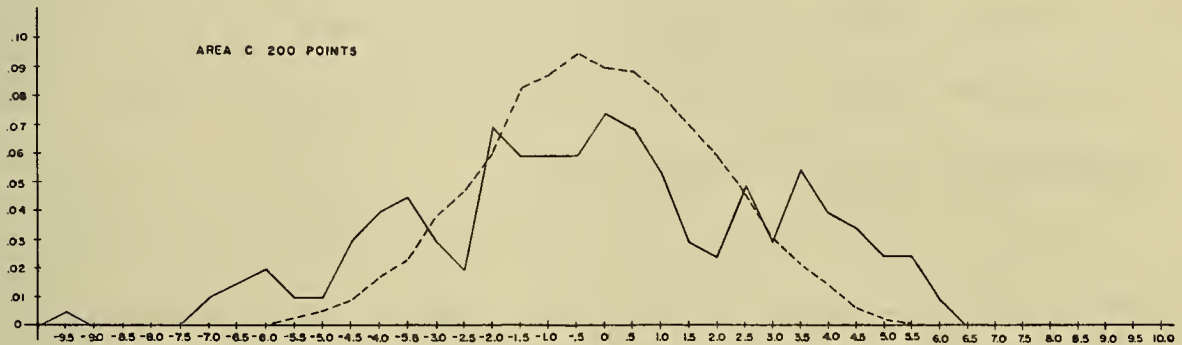


Fig. 11.12 EMPIRICAL PROBABILITY HISTOGRAMS FOR AREAS B,C, AND D FOR DATA SET 2 COMPARED WITH AREA A.(TO CONVERT TO FEET DIVIDE HORIZONTAL SCALE BY 1.016.)

89,0	89,5 ... 89,9	89,10 ... 89,49	89,50 ... 89,54	89,55... 89,59
AREA A 450 points	AREA B 450 points	AREA C 3600 points	AREA D 450 points	AREA E 450 points
0,0, 0,1, .. 0,4	0,5, 0,9	0,10 ... 0,49	0,50... 0,54	0,55.. 0,59

The results of the analysis are shown in Table 11.3. Area C in this set of data had the smallest variance (a reduction of about $0.24[(mm)^2 (x100)]$) over the various points. However there is no significant discrepancy with any combination of areas at the 5 percent level.

The above results show something definitely wrong with Data Set 2 and suggest something wrong in Data Set 3, especially since some spectral estimates are negative in Set 3. It was therefore decided to do the computations over again on a reduced portion of the data. The computations were performed on area A (with 3500 points) in Data Set 2, and on area C (with 3600 points) in Data Set 3. Some badly needed degrees of freedom were sacrificed by this procedure, but the results were quite encouraging. For example, the covariances actually became negative on the vertical axis of the covariance surface of Data Set 2, and there were no negative values in the smoothed spectral estimates for either data set. A discussion of the corrected computations will follow.

Table 11.3. Analysis of Sub Areas in Data Set 3.

Area	No points	ΣN^2	Variance	Ratio to C	d of f used	d of f used	F test		Confidence factors		Confidence bounds	
							significance level	5 1	5 95	5 95	Lower	Upper
A	450	2,148	4.77	1.12	33	$\frac{32}{200}$	1.64	2.02	0.62	1.45	2.94	6.80
B	450	2,408	5.35	1.27	33	$\frac{32}{200}$	1.64	2.02	0.62	1.45	3.30	7.75
C	3600	15,124	4.20		268				0.87	1.15	3.66	4.83
D	450	2,224	4.94	1.17	33	$\frac{32}{200}$	1.64	2.02	0.62	1.45	3.04	7.15
E	450	2,072	4.60	1.09	33	$\frac{32}{200}$	1.64	2.02	0.62	1.45	2.84	6.66
Total	5400	23,976										
A+B	900	4,556	5.06	1.20	66	$\frac{65}{200}$	1.42	1.64	0.75	1.33	3.80	6.73
D+E	900	4,296	4.77	1.13	66	$\frac{65}{200}$	1.42	1.64	0.75	1.33	3.57	6.35
A+B+D+E	1800	8,852	4.92	1.17	132	$\frac{125}{200}$	1.31	1.46	1.82	1.23	3.68	6.05

Before the analysis of the corrected results is made, a discussion of what went wrong with the original results is needed. The basic source of the difficulty can be traced back to a statement made in Part 6. The photographs were taken with reconnaissance type film instead of the more dimensionally stable topographic base film. The film magazines used in the cameras were labeled to contain the correct film but they had actually been loaded with the wrong film. Such a mistake would not be detectable until after the film had been developed. This dimensionally unstable film then underwent differential changes in areas (that is, small areas of the film shrank by greater amounts than others) which introduced a complicated error pattern in the spot height data. Fortunately most of the error (but possibly not all) appears to have been concentrated on the edges of the areas analyzed.

The question might be asked as to why the errors in the original leveled spot heights were not detected prior to making the laborious computations of the covariances and spectra given above. A close comparison of figures 11.1 and 11.3 suggests, since hindsight is always better than foresight, that the error in the spot heights might have been detectable simply on a comparison basis. To be really sure, however, computations similar to the ones given above would have had to have been made, and they could not have been made without a knowledge of the effective number of degrees of freedom of the sub-samples. This effective number of degrees of freedom was estimated from the incorrect spectra. The use of theories valid for correct data on incorrect data to show that the data are incorrect is quite similar to pulling

oneself up by one's own bootstraps (with perhaps the bootstraps being broken in this case). Thus all of the above analyses and comments serve only to suggest the nature and source of the error and a possible way to remove it. What was done did remove the error, so in this sense the analysis of the error was correct.

All of the numerical results obtained in the original analyses of the full sets of stereo spot heights were kept in the tables along with the preceding figures in order that this report would be complete. They represent a wealth of data which can be used for additional analysis and study. This report is unique in that it is a study of a random process in a plane, and the complete set of original data and computations should be of value to geophysicists, statisticians and physicists.

Re-analysis of reduced areas

As stated above both spectral computations were carried out over again for reduced sets of spot height data. For Data Set 2 the area was area A as defined before as bounded on the four corners by the points 20, 0; 20, 49; 89, 0; and 89, 49. In what follows these 3500 numbers will be called Data Set 2A. Similarly for Data Set 3, area C (consisting of 3600 points) bounded by 0, 10; 0, 49; 89, 10; and 89, 49 will be called Data Set 3C.

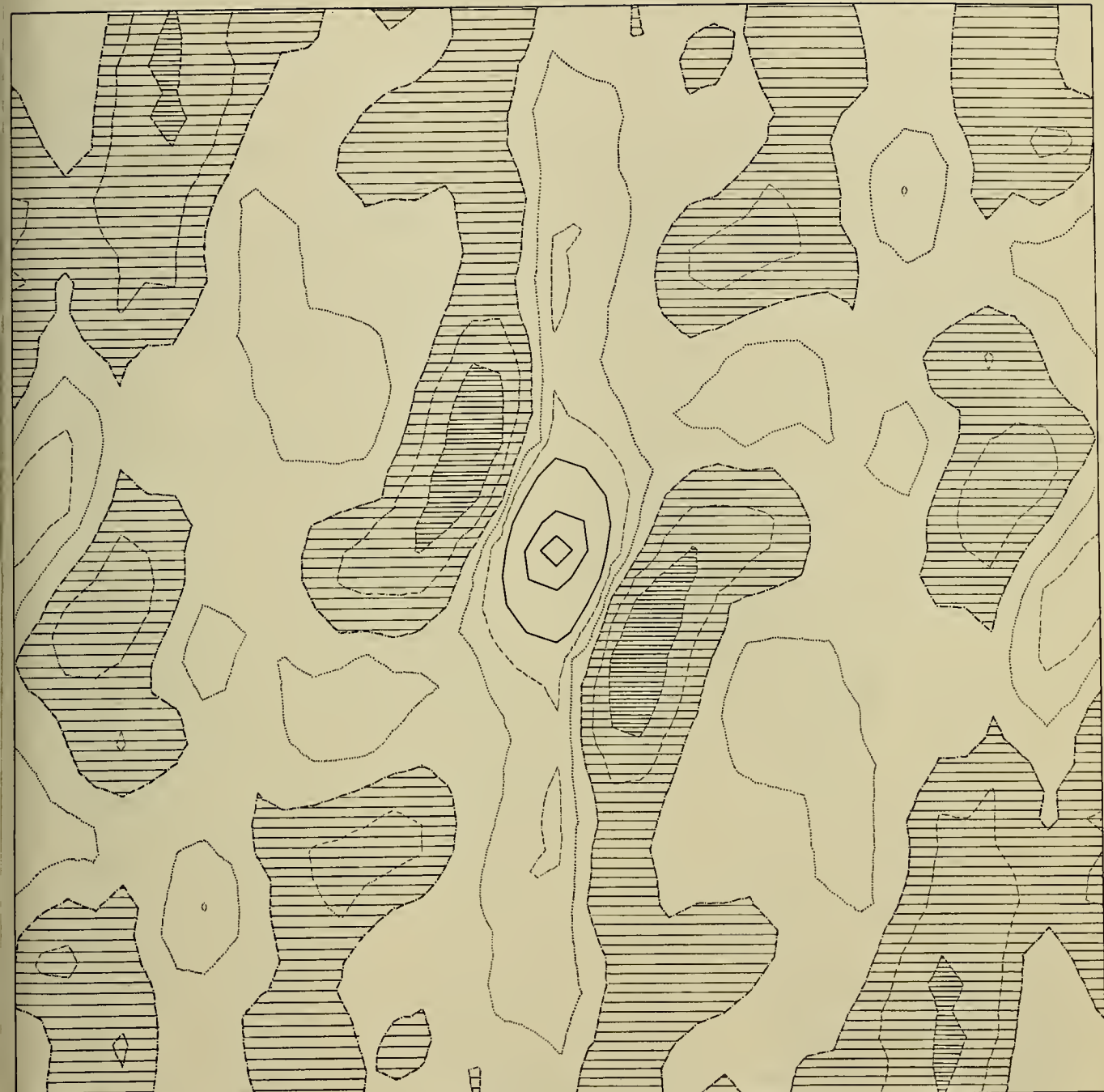
The covariance surfaces for the reduced data

The covariance surfaces for Data Sets 2A and 3C and the average of the values for the two data sets are shown in figures 11.13, 11.14, and 11.15. The patterns are better defined than they were for the surfaces given previously



COVARIANCE SURFACE
SET 2A
FIGURE II.13

-4, -3, -2, -1
-0.6
-0.26
0
0.26
0.6
1
IN UNITS OF TENTHS OF mm. SQUARED



0.1016 mm = 1 FOOT
LENGTH OF SIDE OF SQUARE = 1200 FEET

COVARIANCE SURFACE
SET 3C
FIGURE II.14

+0.5 to +1
-0.5 to -1
-0.25 to -0.5
0
IN UNITS OF TENTHS OF MM SQUARED



0.1018 MM. = 1 FOOT
LENGTH OF SIDE OF SQUARE = 1200 FEET

COVARIANCE SURFACE
SETS 2A AND 3C
AVERAGED
FIGURE II.15

— +4.3, 2, 1 — 0.25
— -0.5 — -0.5
— -0.25 — -1
.....
IN UNITS OF TENTHS OF MM. SQUARED

in figures 11.6, 11.7, and 11.8. The negative areas are better defined. The ridge along the vertical axis is weakened although there is still a trace of column noise. For Data Set 2A, the covariance surface actually becomes slightly negative on the vertical axis. The covariance surfaces still need some minor corrections, but they will not be too difficult to make.

The spectra for the reduced data sets

The spectra for Data Sets 2A and 3C (in terms of variance) and the sum of the values for the two (in terms of E value) are shown in figures 11.16, 11.17, and 11.18. There are no negative values! The numbers at the grid intersections should be divided by 10^4 to put them in units of $(\text{ft})^2$. The contours are labeled in units of $(\text{ft})^2$, and as mentioned before they should be interpreted as the integral over the spectrum on a square of the same size as the grid of the plotted numbers.

These spectra definitely show the effects of column noise. There is a strong ridge along the horizontal axis of the spectral coordinate system. The spectrum for Data Set 3C shows a decrease in the effect of curvature in producing high values at the origin.

In general the above two spectra appear consistent with each other. The 0.0100 and 0.0050 contours are in roughly the same positions on the two spectra. The peak in the spectrum for Data Set 2A has a value of 0.2052 $(\text{ft})^2$ whereas the corresponding value in the spectrum for Data Set 3C is 0.0797. The ratio of 0.2052 to 0.0797 is equal to 2.57.

For Data Set 2A, the number of degrees of freedom is given by equation (11.8).



FIGURE II.16 VARIANCE SPECTRUM FOR DATA SET 2A

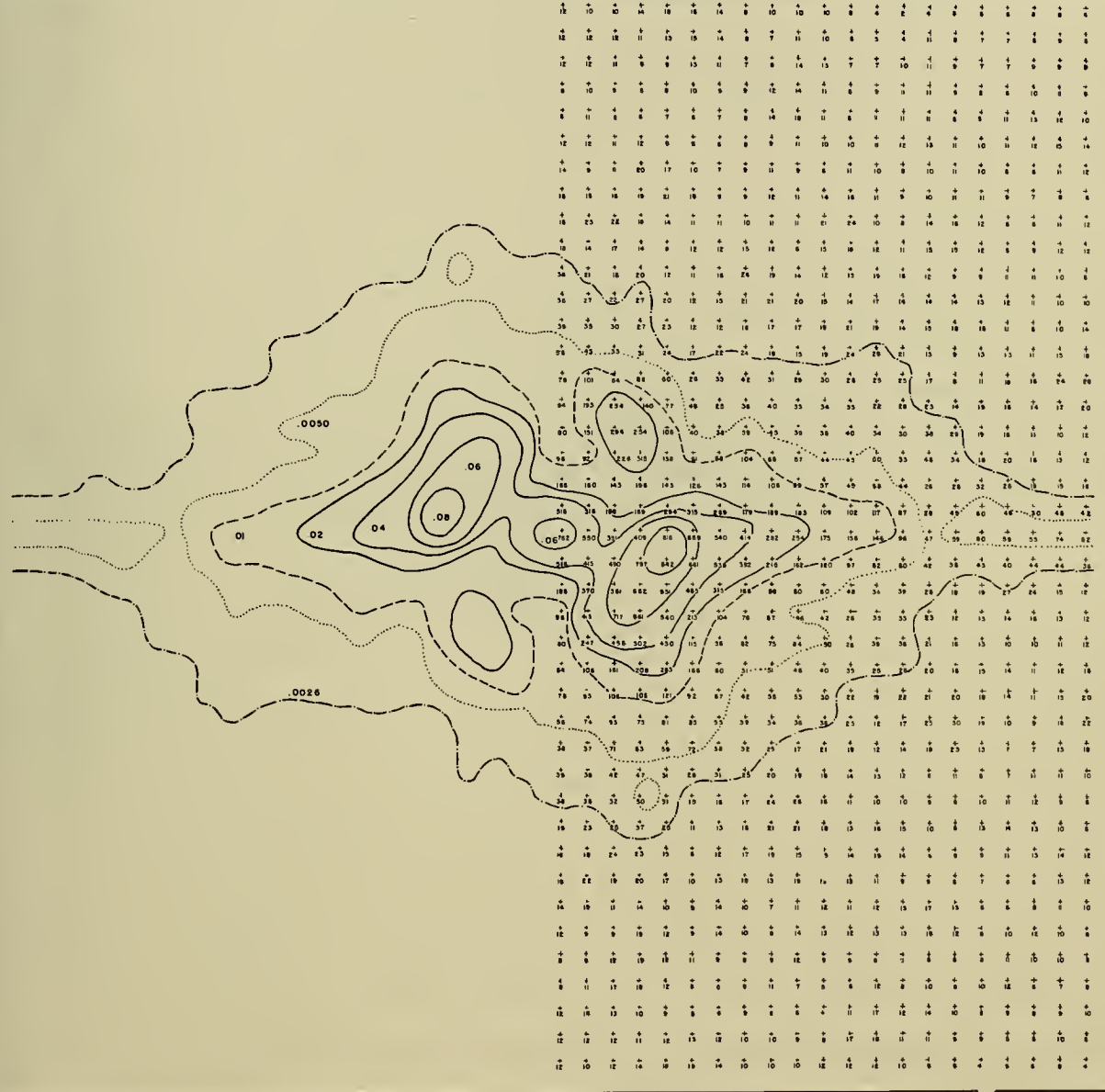


Figure II.I7 VARIANCE SPECTRUM FOR DATA SET 3C

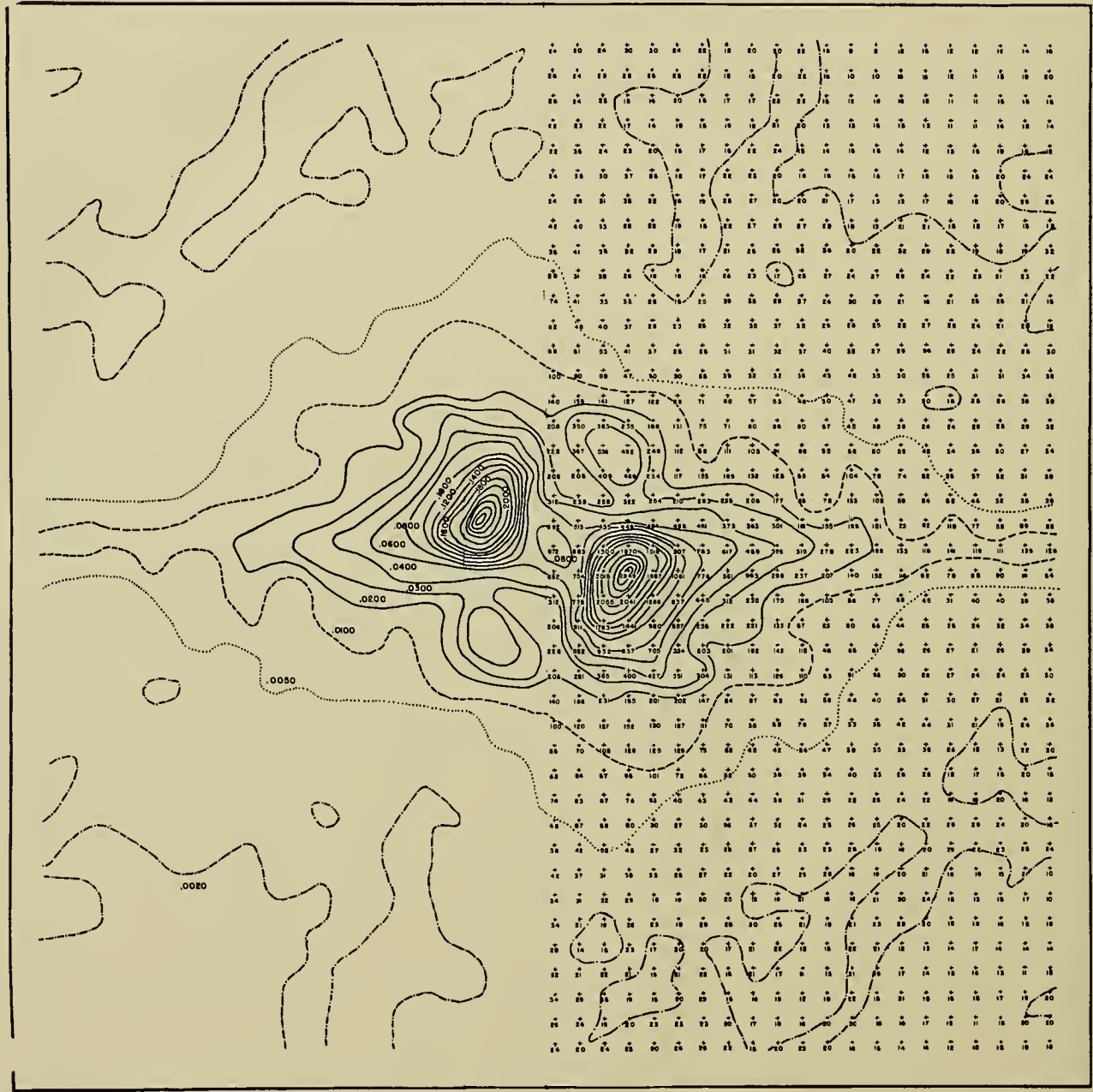


Fig. 11.18

$$U_{2A}(r,s) + U_{3C}(r,s)$$

(11.8)

$$f = 1.58 \left[\frac{50}{20} - \frac{1}{2} \right] \left[\frac{70}{20} - \frac{1}{2} \right]$$

$$= 1.58(6) = 9.48$$

For Data Set 3C, the number of degrees of freedom is given by equation

(11.9).

$$(11.9) \quad F = 1.58 \left[\frac{40}{20} - \frac{1}{2} \right] \left[\frac{90}{20} - \frac{1}{2} \right]$$
$$= 9.48$$

Thus each individual spectral estimate is distributed according to a Chi-square distribution with slightly more than 9 degrees of freedom. A ratio as large as 2.57 for two variances so distributed is quite possible since at the 5 percent level of significance the ratio can be 3.18, and therefore these values are not unusual. They simply represent sampling variation.

The plan for the analysis of the results

The average of the two covariance surfaces as shown in figure 11.15 is the best available estimate of the covariance surface. The sum of the two independently determined spectra as shown in figure 11.18 is the best available estimate of the energy spectrum. This energy spectrum has only 19 degrees of freedom per spectral estimate. Also it obviously has some distortions in it caused by column noise (mainly) and curvature. It also has a white noise background due to the original spot height reading errors. The plan of the analysis of the data as represented by figures 11.15 and 11.18 is to:

1. Remove the column noise from the directional spectrum.
2. Sum around circles of constant frequency in order to compare the

results of the wave pole spectrum with the stereo spectrum and verify the estimate of the amount of the white noise error.

3. Study the angular variation for bands of constant frequency.

4. Compute the confidence bounds for the bands of constant frequency and compare the frequency spectrum obtained from the directional spectrum with the wave pole spectrum and various theoretical spectra.

5. Remove the white noise from the directional spectrum and analyze the spectrum both in an unsmoothed and smoothed form.

6. Fit the angular variation for bands of constant frequency by means of a Fourier series approximation and determine a smoothed analytic form for the spectrum.

7. Correct the covariance surface for the effects of column noise and white noise.

Column noise correction

The ridge along the horizontal axis of figure 11.18 is rather well defined especially for $U(17, 0)$, $U(18, 0)$ and $U(19, 0)$. A vertical line, say, along the values $U(17, 3)$, $U(17, 2)$, $U(17, 1)$, $U(17, 0)$, $U(17, -1)$, $U(17, -2)$, and $U(17, -3)$ shows that there is a definite ridge produced by the values of $U(17, 1)$, $U(17, 0)$, and $U(17, -1)$. The ridge is quite possibly due to column noise as given by the random errors, ϵ_k^* , and it has shown up in the final spectrum as the filtered effect of the contribution of W_{r_0} to $L(r, s)$ in equation (11.4). By inspection, if 0.0100 (ft)^2 is subtracted from each value of $U(r, o)$ the central part of the ridge will disappear and become approximately equal to the value of U two rows above and below the horizontal axis.

This implies that

$$(11.10) \quad 0.54 W_{ro} = 0.0100$$

and that

$$W_{ro} = 0.0185.$$

When W_{ro} is multiplied by 0.23 the result is 0.0043. This quantity must be subtracted from each value of $U(r, l)$ and $U(r, -l)$ as r varies from zero to 20 (before bordering).

A total of $0.0186 (\text{ft})^2$ times 20 is subtracted from the total E value of the stereo data when this correction is made. The total reduction of E value is $0.372 (\text{ft})^2$.

The reanalyzed spectrum for this correction is not shown in any figure. It was used however, in subsequent analyses, and the correction will be incorporated in subsequent plots.

This correction as made to the spectrum also implies that a correction must be applied to the covariance surface. The correction is to subtract 0.186 from $Q(0, q)$ as q varies from +20 to -20. This correction removes the effect of column noise from the covariance surface.

Comparison with the wave pole spectrum

The problem of transforming a spectrum of the form $[A(\alpha, \beta)]^2$ into the form $[A(\mu, \theta)]^2$ in order to integrate out θ so that the directional spectrum can be compared with the wave pole spectrum is difficult. The α 's and β 's are proportional to the square of the wave frequency. One system is in Cartesian coordinates and the other is in polar coordinates. The spectral estimates in both systems have considerable sampling variation.

One way to solve the problem would be to fit the directional spectrum by an analytic function of α and β and carry out the transformation and integration formally so as to obtain the spectrum as a function of frequency. It was decided that this was too difficult so it was assumed that the directional spectrum was a constant over a unit square in the $U(r, s)$ plane. Figure 11.19 illustrates schematically the assumed shape of the directional spectrum.

The wave pole spectrum was determined in Part 10, and the ΔE values for frequencies between $2\pi(K - \frac{1}{2})/96$ and $2\pi(K + \frac{1}{2})/96$ were found. A frequency of $2\pi(K - \frac{1}{2})/96$ corresponds to a period of $96/(K - \frac{1}{2})$ and this in terms of wavelength corresponds to a wave $5.12(96/K - \frac{1}{2})^2$ feet long. Consequently the circle with a radius R^* given by equation (11.11) defines one boundary of that area in the $U(r, s)$ plane which corresponds to a frequency bound of the wave pole spectrum.

$$(11.11) \quad R^* = \frac{2\pi(K - \frac{1}{2})^2}{(96)^2(5.12)}$$

The other boundary for a particular K is given by (11.12)

$$(11.12) \quad R^* = \frac{2\pi(K + \frac{1}{2})^2}{(96)^2(5.12)}$$

In the above, coordinates of the directional spectrum have been

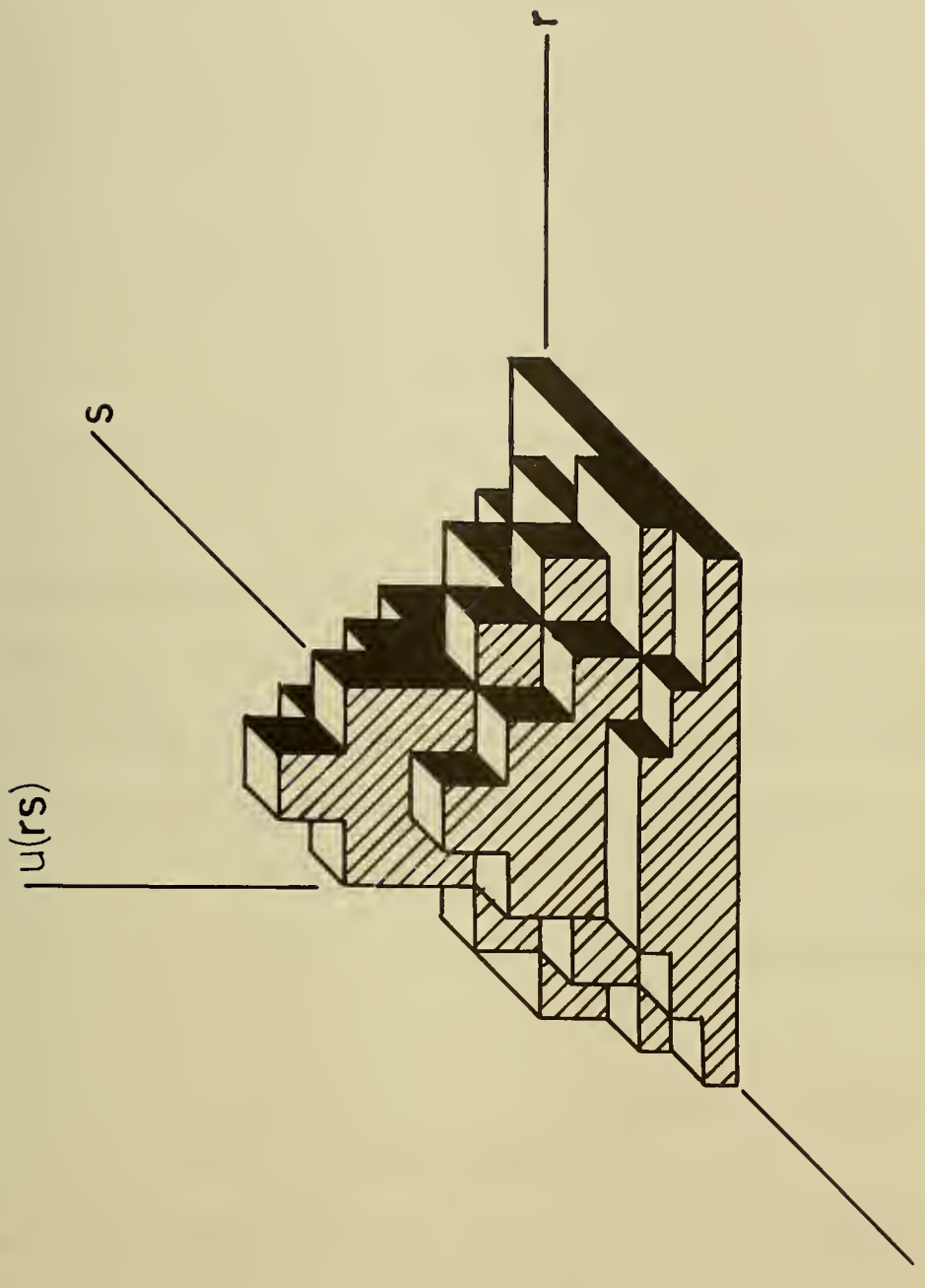


FIGURE 11.19 ASSUMED SHAPE OF DIRECTIONAL SPECTRUM
(SCHEMATIC)

assigned the values

$$0, \quad \frac{2\pi}{1200}, \quad \frac{2\pi(2)}{1200}, \quad \frac{2\pi(3)}{1200}, \quad \text{etc.}$$

on both the horizontal and vertical axes ($1200 = 30 \times 2 \times 20$).

A simpler system of notation will be used by assigning the values 0, 1, ..., etc. to the spectral coordinates just as the values of k were used in studying the wave pole spectrum.

Then R is given by R^* times $1200/2\pi$, and it becomes

$$(11.13) \quad R = \frac{1200(k - \frac{1}{2})^2}{(96)^2 (5.12)}$$
$$= 0.025429(k - \frac{1}{2})^2 = C(k - \frac{1}{2})^2.$$

The values of R for $k - \frac{1}{2}$ and $k + \frac{1}{2}$ determine two concentric circles.

The total contribution to the value of E of all estimates within these two circles should correspond to the value determined from the wave pole spectrum except for residual errors of white noise and curvature. To estimate this, the value of one half of the area between the inner circle and the outer circle is needed.

The area of the inner circle is

$$\pi[C(k - \frac{1}{2})^2]$$

and the area of the outer circle is

$$\pi[C(k + \frac{1}{2})^2].$$

One half of the difference is the area of one half the circular ring as given by

$$\begin{aligned}
 (11.14) \quad A &= \frac{\pi}{2} C^2 \left[\left(k + \frac{1}{2} \right)^4 - \left(k - \frac{1}{2} \right)^4 \right] \\
 &= \frac{\pi}{2} C^2 \left[k^4 + \frac{4k^3}{2} + \frac{6k^2}{4} + \frac{4k}{8} + \frac{1}{16} - k^4 + \frac{4k^3}{2} - \frac{6k^2}{4} + \frac{4k}{8} - \frac{1}{16} \right] \\
 &= \pi C^2 \left[2k^3 + \frac{k}{2} \right] \\
 &= 20.315 \cdot 10^{-4} \left(2k^3 + \frac{k}{2} \right)
 \end{aligned}$$

The values of A are tabulated in Table 11.4 for future reference. A value of k equal to 27 corresponds to the largest circle that can be drawn in the plane of the directional spectrum. The values of A increase slightly more rapidly than the cube of the values of k . Also tabulated in Table 11.4 are the values of A divided by 36 for future reference.

A Cartesian coordinate grid was constructed by drawing heavy lines at the values of r and s corresponding to 0.5, 1.5, 2.5, ..., 19.5. This divided the plane of the spectrum into 741 squares assigned unit area, 116 half squares, and 4 quarter squares for a total of 800 full squares.

The radii given by setting k equal to 1, 2, 3, ... and 28 in equation (11.3) were then computed and semicircles with these radii were superimposed on the grid.

The semi-circles divided the squares into pieces. The number and size of the pieces depended on the geometry of the system.

The areas of the pieces were then computed from geometrical considerations which depended essentially on differences between areas of sectors of circles and triangles. The squares along the r axis, the squares at 45° to the r axis and those in between out to the largest radius were the ones that were analyzed because all others could be obtained by reflection in either

Table 11.4. Half the areas of the circular rings associated with the different values of k.

<u>k</u>	<u>A</u>	<u>A/36</u>
1	0.0051	---
2	0.0345	---
3	0.1127	---
4	0.2641	---
5	0.5130	0.0142
6	0.8837	0.0244
7	1.4007	0.0389
8	2.0681	0.0575
9	2.9711	0.0825
10	4.0732	0.1131
11	5.4190	0.1506
12	7.0331	0.1953
13	8.9396	0.2483
14	11.1631	0.3100
15	13.7279	0.3814
16	16.6583	0.4628
17	19.9788	0.5550
18	23.7137	0.6586
19	27.8874	0.7747
20	32.5243	0.9033
21	37.6488	1.0458
22	43.2852	1.2024
23	49.4579	1.3738
24	56.1913	1.5609
25	63.5098	1.7642
26	71.4377	1.9844
27	79.9995	2.2222

the r axis or the 45° line. The final result was that each piece of each square as cut up by the circles was assigned a percentage between zero and 100. The calculations depended on the difference between large numbers, and the results on summing around circles did not check with the results of Table 11.4. Small adjustments of the order of one or two percent were made to the various areas so that the sum around circles would check with Table 11.4.

The pattern employed, the values of the radii, and the numbers finally obtained are shown in figure 11.20 for a quarter sector of the full area of the directional spectrum. All other points can be obtained by symmetry. Note that half the values on the horizontal axis should be used on the vertical axis.

The values of $U_{2A}(r, s) + U_{3C}(r, s)$ corrected for column noise were then entered in the corresponding squares. To determine $U(k)$, the percentages of the squares falling between circles with radii corresponding to $k - \frac{1}{2}$ and $k + \frac{1}{2}$ were multiplied by the ΔE values for the appropriate squares and all contributions for that particular semicircular ring were summed.

The results are shown in Figure 11.21. The values of ΔE in $(ft)^2$ obtained upon summation are plotted as a function of k in the upper curve. The spectrum obtained from the wave pole data is also shown.

An additional correction is needed before the two curves can be compared. The effect of the white noise variance of $0.54 (ft)^2$ must be removed. Since this error variance is spread evenly over the entire plane of the directional spectrum each square in this analysis has an expected value of $1.08/800 (ft)^2$ assigned to it in terms of E value. When the entries in Table 11.4 are multiplied by $1.08/800$ and subtracted from the values shown on the top curve in figure 11.21 the result is the middle curve which shows the frequency spectrum corrected for the white noise estimate given previously. The effect of assuming that the white noise error variance is twice as great is shown by a third curve in the figure. Such a correction would be much too big.

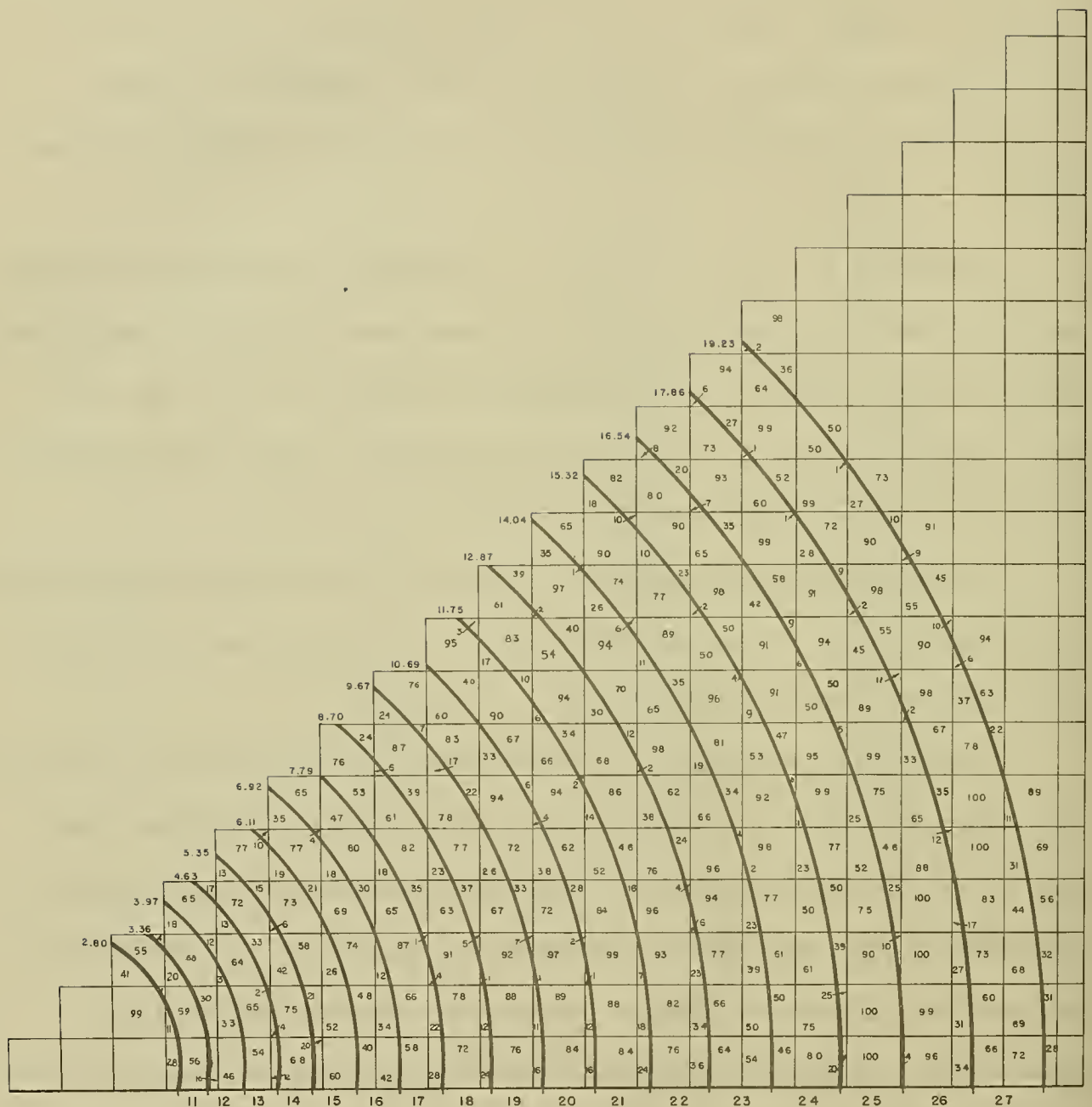


FIG. 11.20
TRANSFORMATION FROM
RECTANGULAR TO POLAR COORDINATES.
198

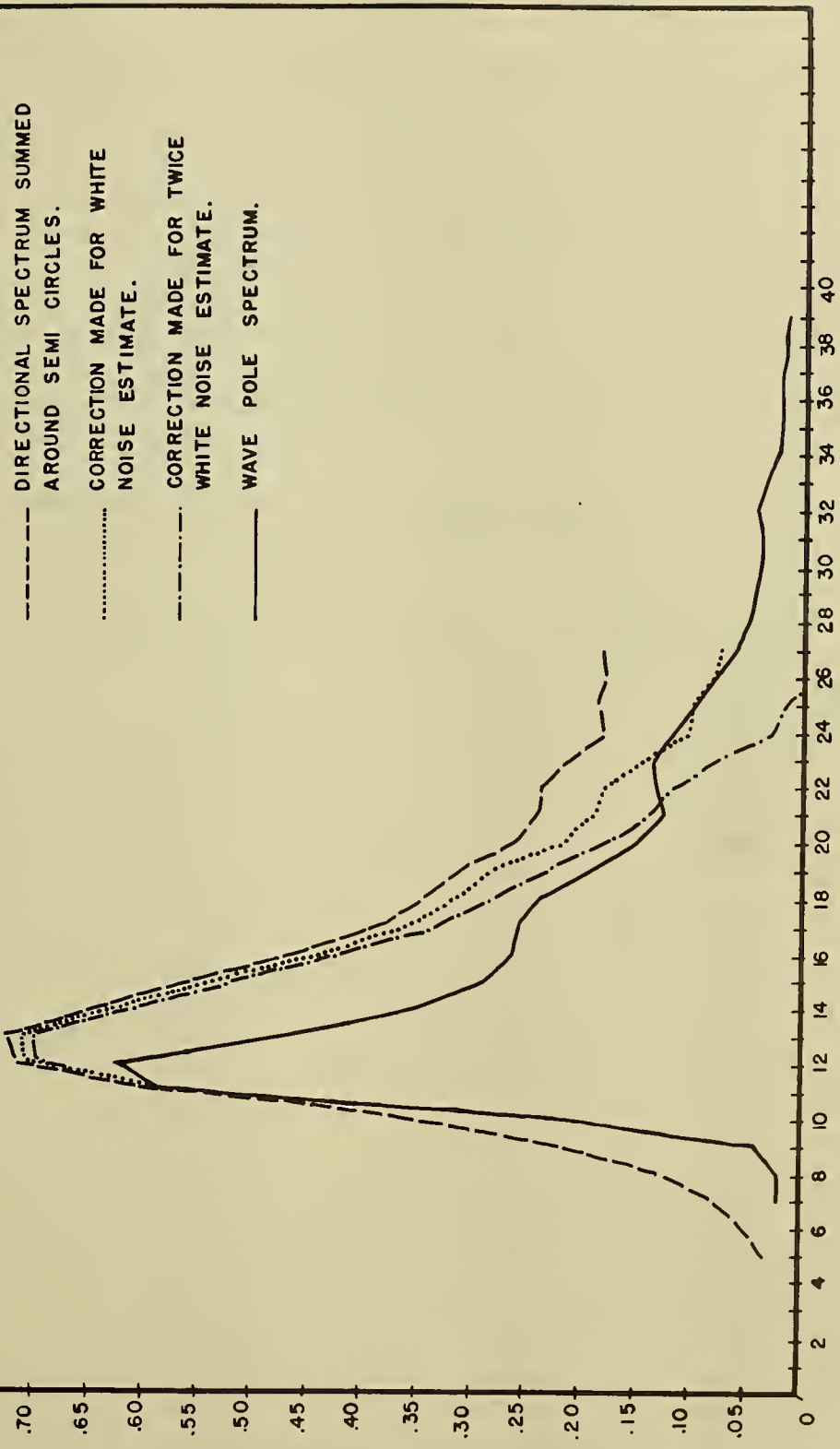


FIG. II.21
 COMPARISON OF WAVE POLE SPECTRUM WITH
 DIRECTIONAL SPECTRUM AS SUMMED AROUND SEMI CIRCLES.

The curve to use for further analysis then is the middle curve of the three curves for the directional spectrum. The agreement at first sight is not too striking since the only points that are close are $k = 11, 23, 24, 25, 26$, and 27. A further study of these results will be made later.

Table 11.5 shows the values obtained for different k by summing around the semicircular rings and the effect of applying the corrections due to white noise.

Table 11.5. ΔE values as a function of k summed around semicircular rings in the directional spectrum.

k	ΔE	ΔE -white noise	ΔE -2 white noise
0, 1, 2, 3, 4	.0357	.0351	.0346
5	.0338	.0331	.0324
6	.0536	.0524	.0512
7	.0850	.0831	.0812
8	.1412	.1384	.1356
9	.2432	.2392	.2352
10	.3771	.3716	.3661
11	.5898	.5825	.5752
12	.7111	.7016	.6921
13	.7202	.7081	.6961
14	.6345	.6194	.6044
15	.5500	.5315	.5129
16	.4544	.4319	.4094
17	.3823	.3553	.3284
18	.3423	.3103	.2783
19	.3086	.2710	.2333
20	.2621	.2194	.1743
21	.2402	.1894	.1385
22	.2355	.1771	.1186
23	.2100	.1432	.0765
24	.1791	.1032	.0274
25	.1836	.0979	.0121
26	.1760	.0796	-.0169
27	.1817	.0737	-.0343

The angular variation

In order to study the angular variation of the spectrum, the results shown in figure 11.20 were employed. Radii at 5 degree intervals were superimposed on the figure by overlays. The plane of the directional spectrum was thus divided into small areas bounded by arcs of two circles and two adjacent radii. Two adjacent circles bounded 36 such small areas, and the areas are tabulated in Table 11.4. Since the effect of the circles in breaking the squares up into sub-areas had already been computed, it was not too difficult to compute the effect of the radii since each small area had to have a known value. The percentages which resulted were then multiplied by the appropriate $U(r, s)$ values and summed for each small area. The number thus obtained is an estimate of the contribution to the total E value of the short crested sea for spectral components with frequencies between $2\pi(k - \frac{1}{2})/96$ and $2\pi(k + \frac{1}{2})/96$ and with directions between θ and $\theta + 5^\circ$ as k varies from 11 through 27 and as θ varies from -90° to $+85^\circ$. The results of this computation are shown in figure 11.22. The white noise estimate has been removed by subtracting $(A/36)(1/800)(1.08)$ from each value.

The curves are erratic, mainly due to sampling variation, but there is a rather definite indication of the presence of a swell for curves corresponding to $k = 11$ through 17. The swell was removed by estimating the shape that the curve would have had, had the swell not been there.

This estimate is shown by the dashed lines in figure 11.22. Tables 11.6 and 11.7 show the resolution of the data into frequency and direction intervals.

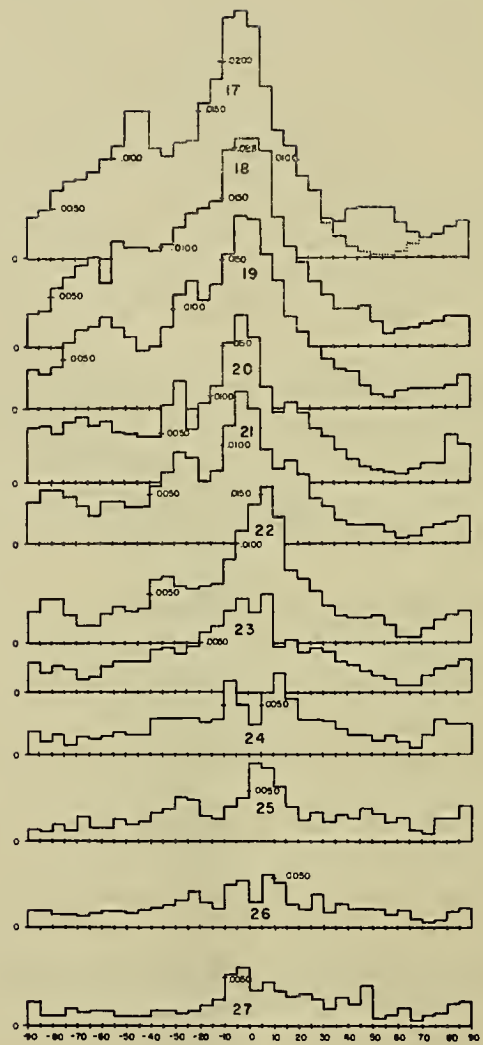
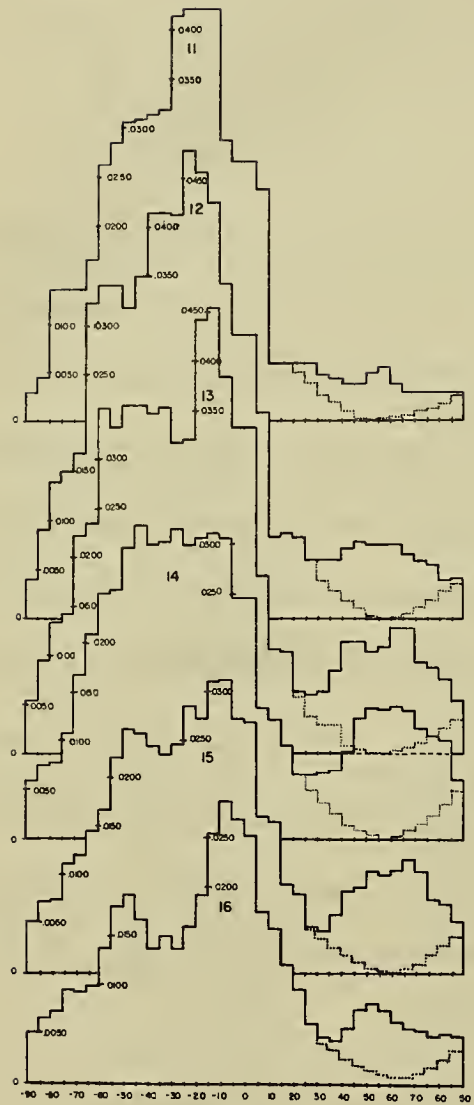


FIG. II.22
ANGULAR VARIATION FOR A CONSTANT FREQUENCY
IN THE DIRECTIONAL SPECTRUM.

Table 11.6. Resolution of directional spectrum into frequency and direction intervals, swell, white noise and column noise removed.

k → Angle	11	12	13	14	15	16	17	18	19	20	21	22	23	24	25	26	27
87.5	.0025	.0035	.0034	.0047	.0039	.0035	.0040	.0031	.0034	.0039	.0027	.0032	.0032	.0029	.0035	.0019	.0025
82.5	.0017	.0028	.0025	.0033	.0030	.0026	.0034	.0030	.0022	.0048	.0022	.0028	.0026	.0028	.0023	.0015	.0022
77.5	.0011	.0018	.0016	.0022	.0020	.0018	.0026	.0026	.0020	.0018	.0020	.0023	.0023	.0035	.0022	.0006	.0012
72.5	.0009	.0011	.0010	.0014	.0011	.0012	.0022	.0022	.0020	.0019	.0016	.0015	.0017	.0020	.0007	.0005	.0010
67.5	.0004	.0005	.0005	.0007	.0006	.0008	.0015	.0019	.0018	.0013	.0008	.0006	.0007	.0007	.0010	.0009	.0006
62.5	.0002	.0001	.0002	.0001	.0002	.0008	.0008	.0017	.0016	.0009	.0006	.0006	.0006	.0012	.0022	.0017	.0018
57.5	.0001	0	0	0	.0003	.0010	.0004	.0014	.0010	.0010	.0012	.0017	.0014	.0018	.0019	.0012	.0011
52.5	0	.0002	0	.0003	.0006	.0014	.0004	.0025	.0014	.0012	.0018	.0028	.0016	.0014	.0027	.0019	.0008
47.5	.0001	.0011	.0003	.0008	.0012	.0019	.0006	.0040	.0024	.0019	.0019	.0026	.0022	.0026	.0032	.0018	.0041
42.5	.0010	.0017	.0008	.0014	.0019	.0026	.0013	.0039	.0028	.0023	.0019	.0025	.0028	.019	.0022	.0019	.0022
37.5	.0019	.0028	.0029	.0027	.0027	.0035	.0024	.0039	.0040	.0034	.0023	.0027	.0031	.0025	.0026	.0024	.0029
32.5	.0026	.0038	.0028	.0037	.0036	.0042	.0027	.0052	.0050	.0046	.0037	.0037	.0041	.0033	.0018	.0015	.0017
27.5	.0038	.0049	.0038	.0051	.0045	.0062	.0071	.0066	.0064	.0055	.0046	.0052	.0045	.0035	.0028	.0033	.0027
22.5	.0049	.0083	.0058	.0065	.0081	.0097	.0085	.0086	.0076	.0071	.0071	.0065	.0040	.0035	.0022	.0019	.0033
17.5	.0059	.0087	.0103	.0095	.0091	.0122	.0115	.0102	.0092	.0081	.0085	.0074	.0054	.0056	.0034	.0023	.0031
12.5	.0059	.0084	.0107	.0122	.0155	.0158	.0131	.0131	.0128	.0071	.0076	.0127	.0046	.0082	.0055	.0045	.0035
7.5	.0236	.0211	.0181	.0134	.0160	.0175	.0175	.0199	.0156	.0097	.0095	.0158	.0100	.0062	.0073	.0054	.0044
2.5	.0265	.0290	.0333	.0246	.0257	.0254	.0236	.0211	.0192	.0147	.0137	.0140	.0081	.0030	.0079	.0026	.0036
-2.5	.0265	.0290	.0333	.0246	.0260	.0269	.0252	.0211	.0196	.0169	.0154	.0113	.0096	.0051	.0044	.0047	.0060
-7.5	.0287	.0342	.0384	.0306	.0299	.0288	.0246	.0199	.0156	.0142	.0121	.0085	.0084	.0075	.0035	.0043	.0052
-12.5	.0421	.0425	.0455	.0312	.0298	.0255	.0183	.0147	.0126	.0098	.0074	.0060	.0067	.0035	.0022	.0019	.0026
-17.5	.0421	.0457	.0443	.0306	.0262	.0192	.0159	.0141	.0110	.0080	.0064	.0057	.0062	.0033	.0025	.0025	.0021
-22.5	.0421	.0479	.0321	.0300	.0273	.0160	.0120	.0135	.0130	.0054	.0088	.0055	.0047	.0036	.0038	.0036	.0015
-27.5	.0413	.0413	.0317	.0315	.0234	.0136	.0119	.0123	.0116	.0103	.0094	.0058	.0040	.0036	.0044	.0027	.0013
-32.5	.0319	.0415	.0353	.0303	.0224	.0150	.0104	.0103	.0084	.0079	.0073	.0067	.0046	.0037	.0032	.0023	.0016
-37.5	.0314	.0415	.0347	.0300	.0232	.0138	.0113	.0097	.0064	.0047	.0059	.0064	.0044	.0037	.0029	.0020	.0011
-42.5	.0308	.0351	.0354	.0321	.0245	.0167	.0151	.0102	.0060	.0046	.0039	.0035	.0033	.0022	.0020	.0017	.0010
-47.5	.0306	.0318	.0355	.0298	.0250	.0192	.0150	.0101	.0074	.0050	.0038	.0032	.0033	.0021	.0017	.0015	.0011
-52.5	.0285	.0341	.0333	.0255	.0220	.0131	.0115	.0108	.0082	.0052	.0043	.0037	.0032	.0023	.0022	.0017	.0011
-57.5	.0262	.0341	.0352	.0250	.0167	.0138	.0101	.0065	.0094	.0062	.0043	.0030	.0027	.0018	.0014	.0016	.0015
-62.5	.0165	.0324	.0235	.0209	.0146	.0100	.0089	.0091	.0084	.0058	.0039	.0019	.0016	.0013	.0015	.0015	.0015
-67.5	.0135	.0169	.0222	.0167	.0121	.0094	.0082	.0083	.0080	.0068	.0039	.0018	.0014	.0019	.0025	.0012	.0014
-72.5	.0135	.0150	.0142	.0109	.0112	.0096	.0079	.0071	.0068	.0062	.0048	.0029	.0024	.0010	.0011	.0013	.0018
-77.5	.0135	.0139	.0134	.0077	.0075	.0073	.0070	.0060	.0042	.0050	.0054	.0045	.0027	.0021	.0017	.0013	.0011
-82.5	.0044	.0091	.0095	.0075	.0073	.0066	.0050	.0036	.0036	.0057	.0055	.0044	.0021	.0013	.0010	.0016	.0010
-87.5	.0029	.0040	.0053	.0060	.0054	.0052	.0043	.0034	.0040	.0055	.0042	.0032	.0031	.0024	.0013	.0017	.0024

Table 11.7. Swell contribution to directional spectrum, white noise and column noise removed.

87.5	.0004	.0005	.0019	-.0013	-.0015	-.0014	0
82.5	.0012	.0011	.0050	-.0067	-.0041	-.0025	0
77.5	.0018	.0036	.0072	-.0082	-.0055	-.0031	0
72.5	.0030	.0047	.0082	-.0099	-.0093	-.0042	0
67.5	.0025	.0060	.0122	-.0123	-.0110	-.0048	-.0012
62.5	.0035	.0075	.0126	-.0134	-.0103	-.0055	-.0030
57.5	.0053	.0077	-.0108	-.0132	+.0097	-.0065	-.0050
52.5	.0048	.0075	-.0103	-.0130	-.0130	-.0068	-.0050
47.5	.0036	.0068	-.0110	-.0115	-.0076	-.0057	-.0047
42.5	.0027	.0054	-.0105	-.0075	-.0065	-.0030	-.0038
37.5	.0023	.0032	-.0055	-.0042	+.0034	-.0010	-.0015
32.5	.0020	.0022	-.0035	-.0030	-.0008	-.0005	-.0005
27.5	.0020	.0010	-.0022	-.0015	-.0003		
22.5	.0010		-.0005				

Table 11.6 shows the local sea and Table 11.7 shows the disturbance from a distance. Corresponding values of Tables 11.6 and 11.7 add up the values graphed by the solid lines in figure 11.22. Table 11.6 corresponds to the solid lines continued by the dashed lines where appropriate. The maximum value for a given k and the minimum value are underlined in Table 11.6. Note that the minimum continues quite smoothly into that region where the swell is not present.

Confidence bounds on the sums around circles

Let the sums of the corresponding entries in Tables 11.6 and 11.7 be designated by $D_{k\theta}$. Each value of $D_{k\theta}$ can be thought to have $19(A/36)$ degrees of freedom if the variation between nearby values of $U(r, s)$ is not too rapid. For example, if a square in the $U(r, s)$ plane were cut in half, then each half would be assigned the value $U(r, s)/2$ and $19/2$ degrees of freedom. The degrees of freedom of the sum of the two values would then be

$$\frac{19}{2} \left[\frac{(U(r, s)/2 + U(r, s)/2)^2}{(U(r, s)/2)^2 + (U(r, s)/2)^2} \right]$$

or 19, and the sum of the two E values would again be $U(r, s)$.

For the sum around a circular ring, this can be generalized to give the degrees of freedom for a ΔE value corresponding to those frequencies between $2\pi(k - \frac{1}{2})/96$ and $2\pi(k + \frac{1}{2})/96$. The equation for the degrees of freedom is then given by equation (11.15).

$$(11.15) \quad f = \frac{19}{4} \frac{A}{36} \frac{[\sum_{k\theta} D_{k\theta}]^2}{[\sum_{k\theta} D_{k\theta}^2]}$$

The factor of 4 enters in the denominator of equation (11.15) because only every fourth value of the spectral estimates is independent.

For a more strict analysis, the degrees of freedom should be computed from the data with the white noise still present since at each value it is also distributed according to Chi square with 19 degrees of freedom. The error made in the above computations is small for low values of k , but for large k the variation in white noise may be falsely reflected into variation in spectral estimates because the white noise is a rather large proportion of the total contribution.

The degrees of freedom for low values of k are quite low. For k equal to 11, there are only 22 degrees of freedom. Had all these stereo pairs been satisfactory for analysis and had there been no distortion at the edges of the stereo data, the 19 degrees of freedom for each value of $U(r,s)$ actually obtained would have been raised to 50 degrees of freedom, and the 22 degrees of freedom for $k = 11$ would have been close to 50 degrees of freedom.

The number of degrees of freedom given by equation (11.15) can be combined with the entries in Table 11.5 to give the 90 percent confidence bounds on the estimates of ΔE as corrected for white noise. The results are shown in Table 11.8. The values given at the 90 percent confidence bounds will enclose the true value of ΔE nine times out of ten in repeated tests of this same type under the same conditions. Of course, for a given set of data, the true value either does or does not fall within the confidence bounds and one can never know whether it did or did not.

The entries shown in Table 11.8 can be combined with the entries in Table 10.1 to compare the wave pole data and the stereo data. The result is

Table 11.8. Confidence bands on data from stereo spectrum

<u>k</u>	<u>Lower 5 percent confidence band</u>	ΔE	<u>Upper 95 percent confidence band</u>
11	.3778	.5825	1.0387
12	.4510	.7016	1.2712
13	.4853	.7081	1.1487
14	.4478	.6194	.9402
15	.3950	.5315	.7715
16	.3279	.4319	.6065
17	.2744	.3553	.4862
18	.2435	.3103	.4089
19	.2235	.2710	.3384
20	.1784	.2194	.1792
21	.1555	.1894	.2379
22	.1466	.1771	.2201
23	.1210	.1432	.1732
24	.0884	.1032	.1228
25	.0845	.0979	.1153
26	.0695	.0796	.0925
27	.0646	.0737	.0852

shown in figure 11.23. For k equal to 11, 12, 13, 22, 23, 24, 25, 26, and 27 the agreement is satisfactory, but for k equal to 14, 15, 16, and 21 the confidence bounds do not even overlap. The two results are therefore inconsistent.

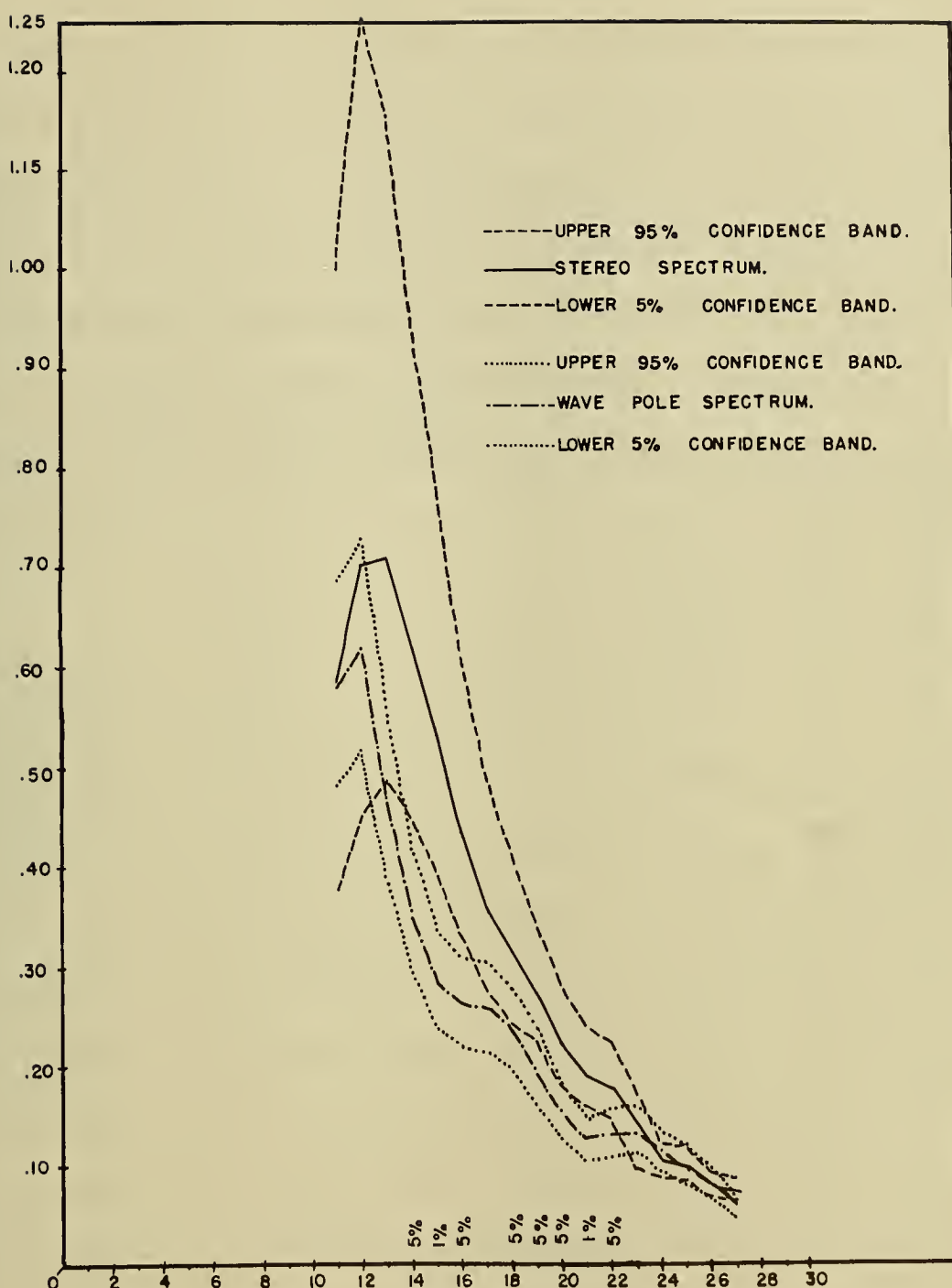


FIG II.23
CONFIDENCE BANDS ON WAVE POLE AND
STEREO SPECTRUM.

Another way to show the lack of agreement in the data is by means of the F test. The ratio of the stereo values to the wave pole values are tabulated in Table 11.9 along with the appropriate degrees of freedom for each estimate. At values of k equal to 15 and 21 there is less than one chance in 100 that the two values of ΔE could have come from the same population.

Table 11.9. F test applied to wave pole and stereo spectra.

k	ddf	Stereo	Wave pole	Ratio	F test significance level		Conclusion
					5 %	1 %	
11	22	.5825	.5804	1.0036	1.82	2.38	Accept at 5 %
12	21	.7016	.6201	1.1314	1.85	2.43	Accept at 5 %
13	30	.7081	.4682	1.5124	1.56	2.08	Accept at 5 %
14	41	.6194	.3530	1.7547	1.56	1.89	Reject at 5 % Accept at 1 %
15	50	.5315	.2838	1.8728	1.49	1.77	Reject at 5 % Reject at 1 %
16	59	.4319	.2611	1.6542	1.45	1.69	Reject at 5 % Accept at 1 %
17	68	.3553	.2562	1.3858	1.41	1.63	Accept at 5 %
18	82	.3103	.2358	1.3159	1.31	1.58	Reject at 5 % Accept at 1 %
19	128	.2710	.1924	1.4085	1.32	1.48	Reject at 5 % Accept at 1 %
20	110	.2194	.1509	1.4539	1.34	1.51	Reject at 5 % Accept at 1 %
21	122	.1894	.1252	1.5128	1.32	1.47	Reject at 1 %
22	133	.1771	.1320	1.3417	1.31	1.47	Reject at 5 % Accept at 1 %
23	171	.1432	.1336	1.0719	1.26	1.41	Accept at 5 %
24	203	.1032	.1137	.9077	1.26	1.39	Accept at 5 %
25	227	.0979	.0979	1.0000	1.26	1.39	Accept at 5 %
26	267	.0796	.0815	.9767	1.26	1.39	Accept at 5 %
27	284	.0737	.0591	1.2470	1.26	1.39	Accept at 5 %

These results are made even more interesting by considering the values obtained by summing the columns in Table 11.6 where the effect of a disturbance from a distance has been removed. These values can be plotted against a Neumann spectrum for 18.7 knots and against the wave pole spectrum as shown in figure 11.24. One could not ask for much better agreement between theory and observation than is shown between the theoretical Neumann spectrum and the frequency spectrum obtained from the directional spectrum. The agreement between the wave pole spectrum and the theoretical spectrum is actually a little (but not much) better than shown because the contribution of the swell for k equal to 11 and 12 will reduce the sharp peak. One disadvantage of wave pole data is evidently that there is no way to see the swell if it has the same frequencies in it as the local sea.

Another question to be asked before entering into a discussion of the above results is what would the wave pole calibration have had to have been in order to provide agreement with it and both the theoretical Neumann spectrum and the directional spectrum. This result can be obtained by dividing the values for the directional spectrum, including swell, by the values for the wave pole spectrum before multiplication by the calibration curve. The result is shown in figure 11.25. There is the possibility of some sort of amplified response in the wave pole, undetected by still water damping and resonance tests, as μ equal to $2\pi(15)/96$. The agreement between the two spectra would be fairly good if something like one of the dashed curves were used for calibration instead of the original theoretical curve.

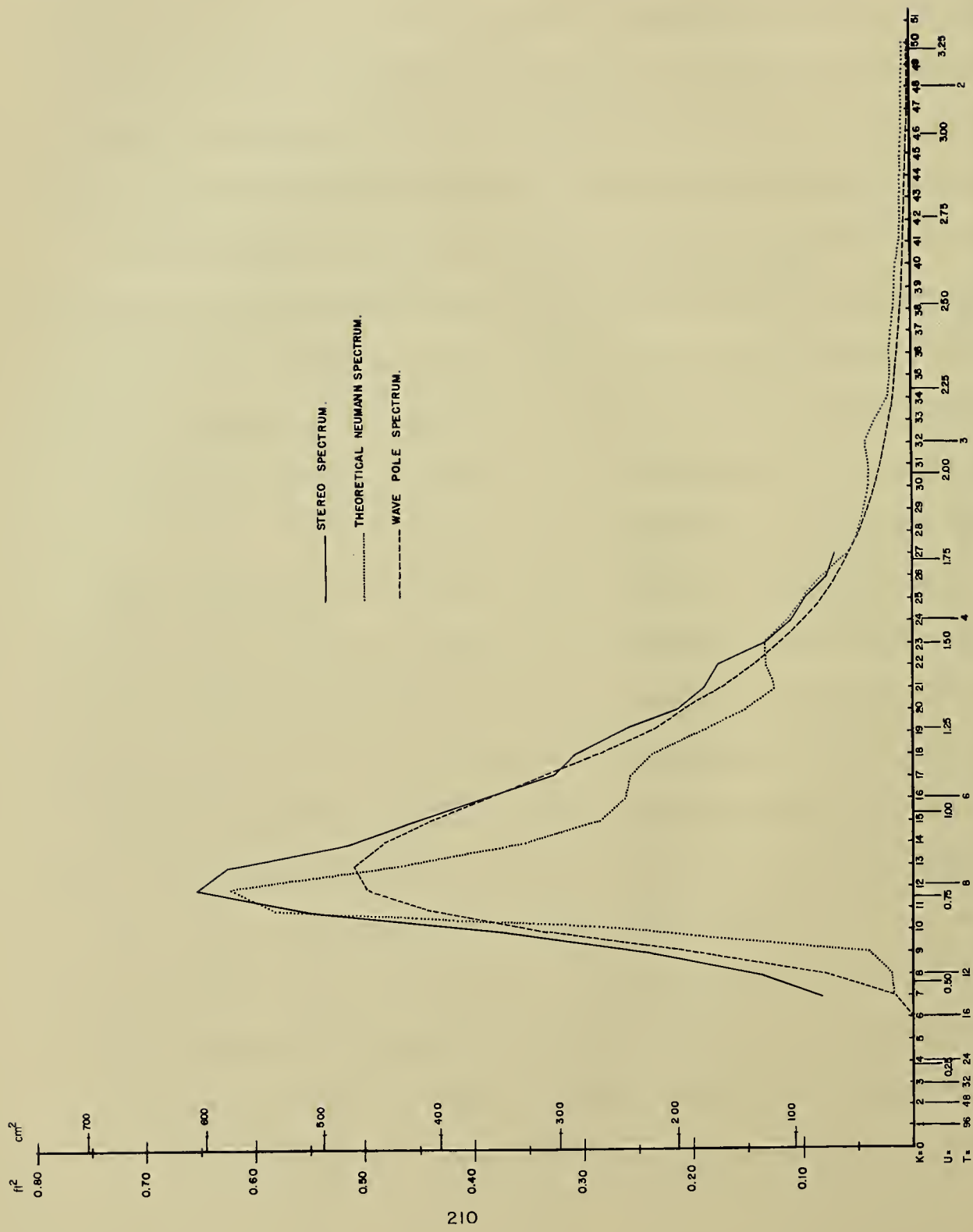


FIGURE 1124 THEORETICAL NEUMANN SPECTRUM FOR AN 18.7 KNOT WIND COMPARED WITH THE SPECTRA OBTAINED FROM THE STEREO DATA AND THE WAVE POLE DATA

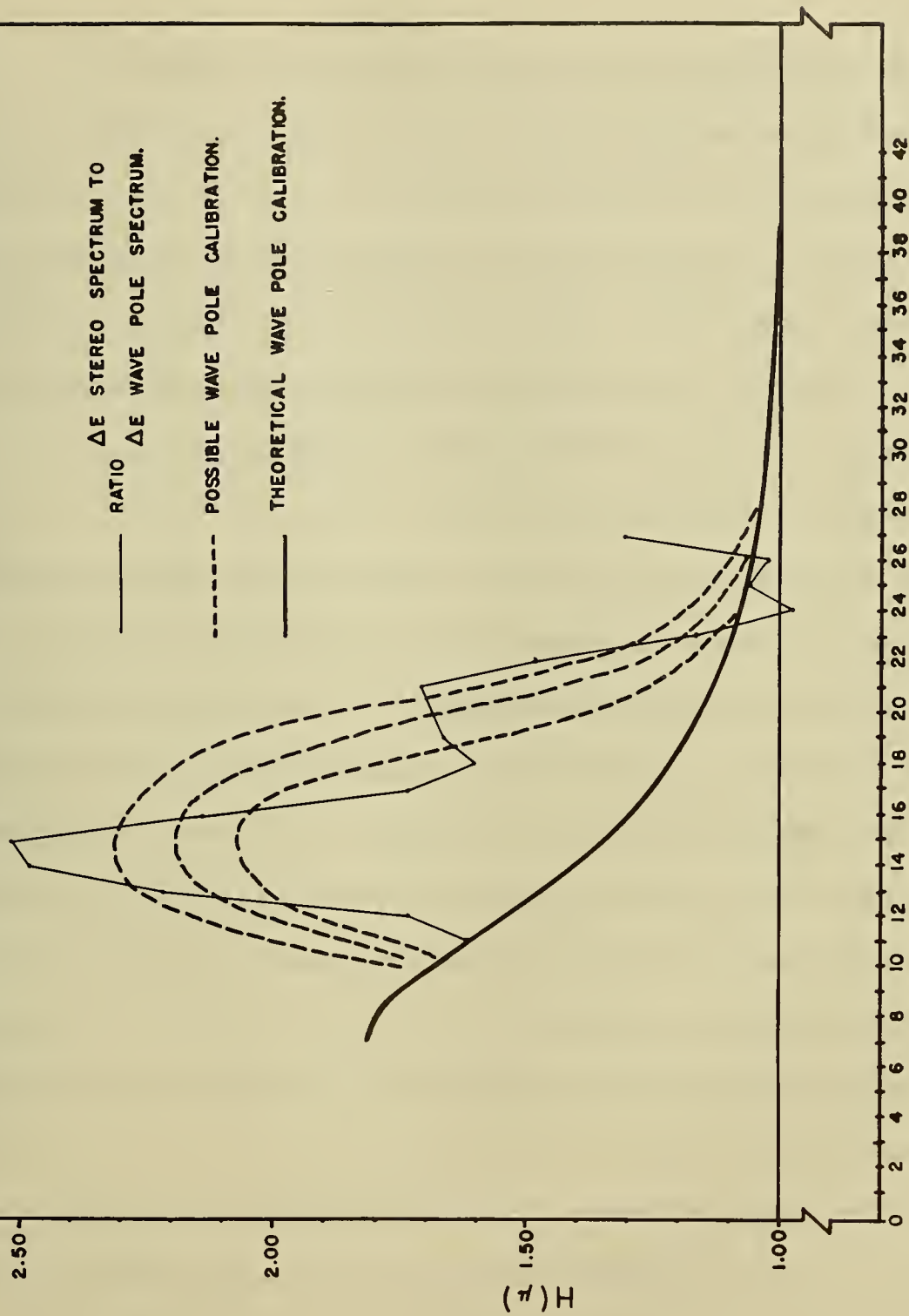


FIG 11.25
 THEORETICAL AND EMPIRICAL
 WAVE POLE CALIBRATION.

Discussion of wave pole, stereo and theoretical spectra

If a physicist were to measure the acceleration of gravity at the same place by two different methods and obtain 980 cm/sec^2 by one method and 1400 cm/sec^2 by another method, he would be positive that there was something wrong with the second method. In this study one is not in so fortunate a position. There is no background of previous experience, and sampling variation must always be recognized as a source of any disagreement.

The results obtained so far are that:

- (1) A frequency spectrum obtained from stereo wave data agrees with a theoretical curve derived by Neumann after correction for the presence of swell and the effects of white noise and column noise in the original data.
- (2) A frequency spectrum obtained from a wave pole observation does not agree with either the one derived theoretically or obtained from the stereo data at two points at the one percent significance level. However, the wave pole spectrum does agree with the theoretical spectra given a one knot variation in the winds as pointed out in Part 10.

The following hypotheses are among those that could be advanced to explain the results:

- (1) The agreement between the stereo spectrum and the theory is fictitious. It has been obtained by choosing just the right weighted average of winds reported quite a few hours before the actual observations of the waves and by rather prejudiced choices of just the right amounts of noise and swell to get agreement. Also the reduced stereo data may still be distorted.

(2) Variability in the winds and background distortion in the stereo data is sufficient to explain the difference in the two different sets of observed values.

(3) Sampling variations at the 1 percent significance level have actually occurred.

(4) The wave pole calibration is incorrect.

(5) Weighted combinations of modifications of the above four hypotheses taken 2, 3, or 4 at a time such as, for example (2-3-4). The wave pole calibration is wrong by 30 percent at $k = 15$, sampling variation was at the 20 percent level and the variability in the winds explains the rest of the differences.

The first hypothesis can be checked by study of the original data as tabulated. The fact that the histogram shown in figure 11.12 shows no effect of distortion in area A at least suggests that most of this effect has been removed. Also the uncorrected spectra come closer to agreeing with the theoretical Neumann spectrum than to agreeing with the theories of Roll and Fischer [1956] and Darbyshire [1955]. The analysis has only served to refine the results by what are in total rather small corrections, and the corrections appear to be logically justifiable in all cases. If agreement with the theoretical Neumann spectrum is not obtained, then the result would be that there is no adequate theoretical wave spectrum in existence.

In the light of these new results, the hypothesis of wind variability is much less attractive than it was in Part 10. The wave pole and stereo observations were simultaneous in the sampling sense. The variation in the three

different wave pole spectra as originally tabulated shows no effect of wind variability at the 5 percent level, and the low value at $k = 15$ occurs in all three cases.

The third hypothesis is one that cannot be tested except by doing the same experiment over again using the same wave pole under similar meteorological conditions. It will be rejected as a working hypothesis solely because it cannot be tested. However, due to the possibility of this hypothesis combining with some of the others in part, the possibility of incorrectly rejecting it with a chance of more than 0.01 (say 0.15) must be borne in mind.

The fourth hypothesis is a very attractive one. If the wave pole calibration curve were more like the one shown by the dashed curves in figure 11.25 than the theoretical one, there would be agreement between both observed curves and the theory. It will therefore be assumed that this hypothesis is the dominant explanation for the discrepancies which have occurred.

This hypothesis can be tested by modeling the wave pole in a scaled down long crested Gaussian sea with the correct model frequencies present, and comparing the record it makes with a record made by a wave pole held fixed in position.

An irregular sea is suggested for the tests because a non-linear effect of considerable magnitude may be present. In Part 8 it was shown that the wave pole moves upward when the crest of a long period wave passes. The submerged tanks are therefore closer to the mean level in the crest of a long period wave. If the crest of a shorter period wave is present at the same

time by superposition, the calibration constants would be considerably modified due to the fact that the depth of the submerged tanks is less. This would cause the wave pole to move up in the crest of the shorter period wave even more than the theory would predict.

This effect is not compensated for by an equal and opposite effect when the trough of a short period wave is present on the crest of a long period wave due to the exponential behavior of these factors. Thus the response may be non-linear and the heights of the shorter period waves may be underestimated. For very short period waves such effects would again be negligible,

If the calibration of the wave pole fails to explain the discrepancy between the two sets of observations then the other possible explanations will have to be investigated. On the basis of the above considerations, a prediction is ventured that the wave pole calibration will explain the discrepancy.

If the above hypothesis is a correct one, then the study of ocean waves is in a very odd position. The wave pole data were to have been a primary calibration for the stereo data. The stereo data appear to have detected, to the contrary, a faulty theoretical calibration of the wave pole. The shipborne wave recorder developed by Tucker [1956 a] has been compared with the WHOI wave pole, and agreement was not obtained in this comparison either (Tucker [1956 b]). This does not necessarily lead to the conclusion that the shipborne instrument is correctly calibrated. In fact, its response at high frequencies is known to be poor (Tucker [1956 a]). Therefore at present, there is no primary instrument capable of measuring waves as a function of time at a fixed point in deep water.

H. G. Farmer in conversations with the author has described how he would modify the WHOI wave pole by putting the tanks at greater depths so as to improve the response of the instrument. This should certainly be a subject for further investigation and study both theoretically and by means of model studies.

Composite frequency spectrum

The results of the frequency analysis of the stereo data and the wave pole data, as given in Tables 11.5, 11.6 and 10.1, can now be combined to yield a composite frequency spectrum over a full range of frequencies. The spectrum for the stereo data is assumed to be correct for low frequencies, and the wave pole spectrum is surely quite reliable at high frequencies except perhaps for a small amount of white noise. As k varies from 0 to 10 the entries in the second column of Table 11.5 from the stereo data will be used. As k varies from 11 to 22 the sums of the columns in Table 11.6 will be used in order to remove swell from the spectrum. One can note small differences between the entries in Tables 11.6 and 11.5 due to round-off errors at high frequencies. The errors are small compared to the variability in the sample. For k from 23 to 27 the stereo values and the wave pole values agree and an average weighted according to the computed number of degrees of freedom is used. For k greater than 27, the wave pole values are used. This composite spectrum is given in Table 11.10.

Table 11.10. Composite frequency spectrum for the local sea determined from the wave pole and the stereo data.

k	ΔE stereo	ΔE wave pole	Com- bined	Degrees of freedom	k	ΔE stereo	ΔE wave pole	Com- bined	Degrees of freedom
7	0.0831				34		0.0212		174
8	0.1384				35		0.0193		174
9	0.2392				36		0.0200		174
10	0.3716				37		0.0180		174
11	0.5496		22		38		0.0160		174
12	0.6498		21		39		0.0150		174
13	0.6208		30		40		0.0140		174
14	0.5135		41		41		0.0110		174
15	0.4545		50		42		0.0100		174
16	0.3818		59		43		0.0100		174
17	0.3272		68		44		0.0090		174
18	0.3056		82		45		0.0090		174
19	0.2656		128		46		0.0080		174
20	0.2144		110		47		0.0080		174
21	0.1894		122		48		0.0080		174
22	0.1766		133		49		0.0070		174
23	0.1373	0.1336	0.1354	345	50		0.0060		174
24	0.1086	0.1137	0.1110	377	51		0.0060		174
25	0.0984	0.0979	0.0982	401	52		0.0050		174
26	0.0769	0.0815	0.0787	441	53		0.0050		174
27	0.0785	0.0591	0.0711	458	54		0.0050		174
28	0.0491		174		55		0.0050		174
29	0.0443		174		56		0.0050		174
30	0.0395		174		57		0.0050		174
31	0.0392		174		58		0.0050		174
32	0.0420		174		59		0.0040		174
33	0.0327		174		60		0.0040		174

The values for the composite spectrum are plotted against the family of theoretical Neumann spectra for various wind speeds in figure 11.26. The agreement is good for an 18.7 knot wind. Note that the family of theoretical spectra grows up to and then through the composite spectrum as the wind speed is varied.

Comparison with other families of theoretical spectra

This composite spectrum can be compared with the families of theoretical spectra derived by Darbyshire [1955] and Roll and Fischer [1956]. In both cases the agreement between the computed spectrum and the theoretical spectrum is poor. There is no value for the wind speed which will give agreement between the theoretical curves and the numbers given in Table 11.10. These comparisons are discussed in greater detail by Neumann and Pierson [1957a] and Neumann and Pierson [1957b].

Removal of white noise from the directional spectrum

Upon summation around semicircles, the predicted effect of the white noise was verified and the original estimate of the error in the spot height readings as made by the Photogrammetry Division of the Hydrographic Office was verified. The total contribution of the white noise to the E value for the waves under study is thus about 1.08 (ft)^2 , and $1.08/800 \text{ (ft)}^2$ must be subtracted from each value of the energy spectrum obtained from summing the values of $U_{2A}(r,s)$ and $U_{3C}(r,s)$, after correction for column noise. This amounts to 0.00135 (ft)^2 per unit square in the spectral plane. Since only four significant figures were tabulated either 0.0013 or 0.0014 was subtracted from each particular square. Each of the above values was subtracted an equal number of times so as to even out the total effect to 1.08 (ft)^2 . A few very small negative values occurred due to extremes of sampling variation in the white noise where it was a large part of the total contribution. The negative values were removed by "borrowing" from nearby points.

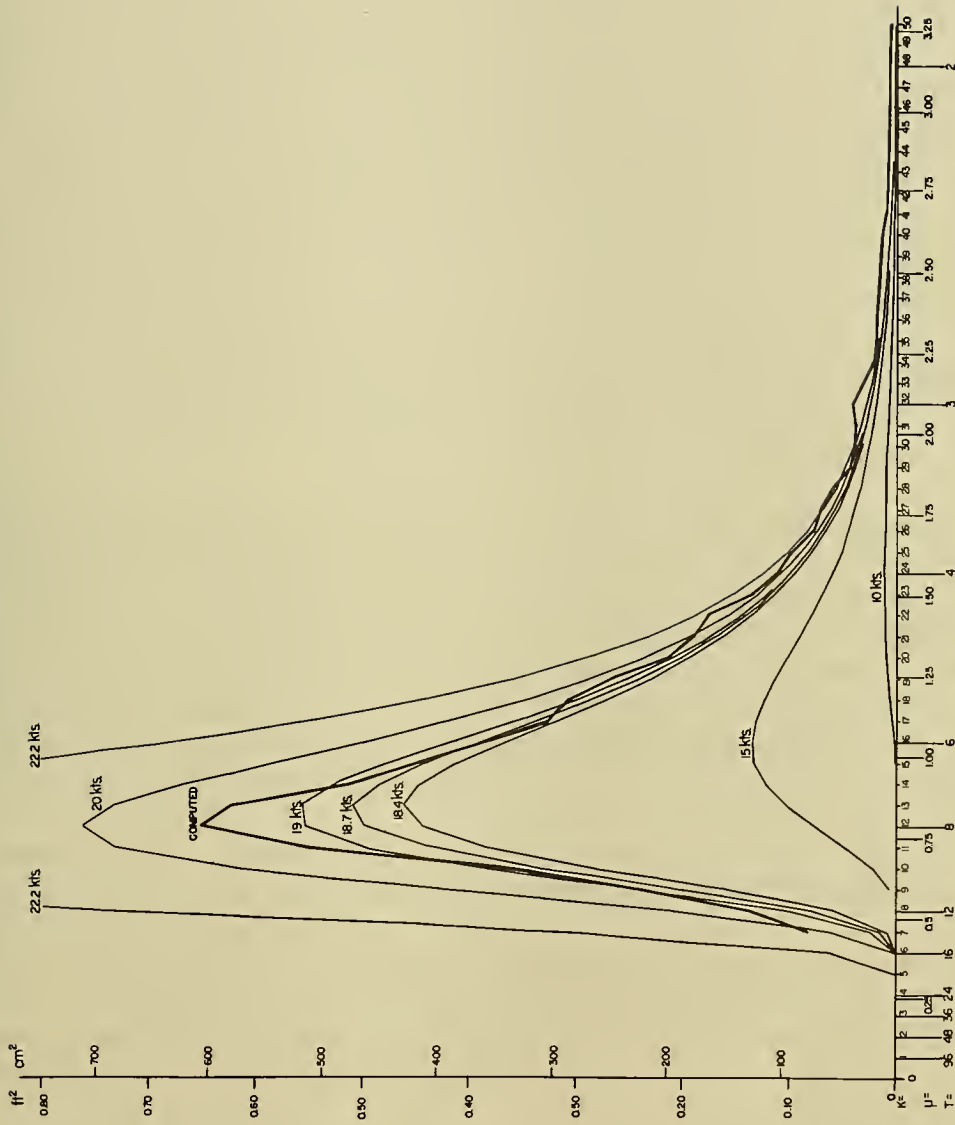


Figure 11.26. Family of theoretical Neumann spectra versus composite spectrum. (The number above each curve is the surface wind in knots.)

Orientation of the sea and swell in the directional spectrum

The heading of the airplanes taking the stereo data for Data Set 2 was 330° . Since the planes flew one behind the other, correctly directed arrows with shafts parallel to the short sides of figure 6.2 will point toward 330° . Since the buoy shown in figure 6.2 drifted generally downwind and since the wind was from 330° , or so, as reported in Part 7, an arrow parallel to the short sides of figure 6.2 and pointing to the left will point toward 330° .

Due to the 180° indeterminacy in direction in the directional spectrum, this is equivalent to letting the positive r axis in the directional spectrum point toward 150° . The peak in the directional spectrum indicates waves traveling toward 180° approximately.

With the direction fixed, the secondary peak in the spectrum indicates that the swell is traveling either toward 90° or toward 270° . It is improbable that the swell is traveling toward 90° because there is no area where it could have been generated between the point of observation and the east coast of the United States.

The assumption that the spectral components are traveling within $\pm 90^{\circ}$ of the direction toward which the wind is blowing is not correct for the swell and thus the final directional spectrum may have to have a range of more than 180° in direction.

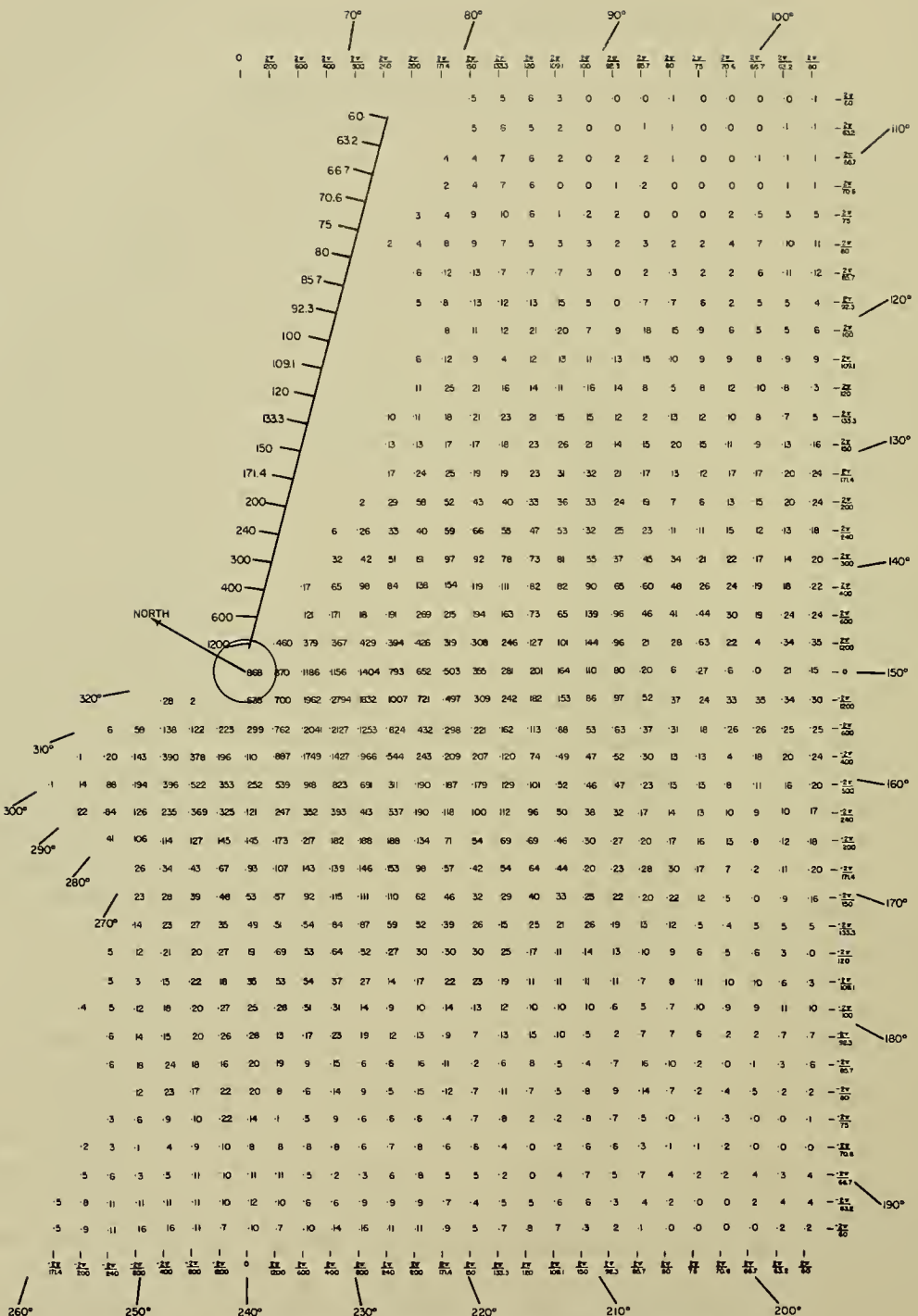
The secondary maximum shown in figure 11.18 should be considered to be composed of two parts. One part is the continuation of the local sea by means of the dashed lines of the energy as a function of direction as shown

in figure 11.22 and tabulated in Table 11.6. Temporarily let all of this energy be assigned to the first quadrant. The contribution from the swell as given in Table 11.7 then belongs in the third quadrant. Tables 11.6 and 11.7 were then recombined separately to provide estimates of each of these contributions to a square area in the $U(r, s)$ plane. The values due to the swell were mapped by reflection through the origin into the third quadrant.

The minima indicated in Table 11.6 were then assumed to be one extreme in the angular range of the sea. A line forming an angle of about 30° with the positive vertical axis could then be determined. Those values of $U(r, s)$ between this line and the vertical axis were then transferred to the third quadrant.

The final spectral estimates in the $U(r, s)$ plane are shown in figure 11.27. The values should be divided by 10^4 to put them in units of $(\text{ft})^2$. The range of directions toward which the spectral components are traveling varies from 80° to 320° . The sea has components traveling toward directions ranging from 80° to 260° . The swell is traveling toward directions ranging from 240° to 320° .

The quantities shown in this figure have been obtained by applying corrections for the effects of column noise and white noise to the original data and by expanding the spectrum to a range of more than 180° from considerations of the local wind direction and the geography of the area where the data were obtained. The effects of curvature do not seem to be very great. The values at the origin must be excluded, and perhaps the



forward face of the spectrum should be somewhat steeper.

If the plotted numbers in figure 11.27, for the third quadrant, are transferred to the first quadrant, and if the column noise and white noise are added to the values obtained, the result would be essentially the numbers shown in figure 11.18.

The sum of the numbers in figure 11.27 will equal the total E value of the sea plus the swell excluding a small circle near the origin. Strictly speaking, the values at the borders of the rectangular area formed by the data in the first and second quadrant before any reflections through the origin should be halved before summing. However, the values on the s axis of the $U(r,s)$ plots are used only once in the direction of 240° . The values at the outer edge are so small that only a minor error is made in not halving these values.

Contours drawn as precisely as possible for the numbers shown in figure 11.27 are shown in figure 11.28. The contours are not very smooth due to sampling variation. The contour analysis can be considerably smoothed when this sampling variation is taken into account.

Each of the original spectral estimates had 19 degrees of freedom. Due to the corrections made so far, the smaller values of the spectral estimates and the values for the transferred swell do not have 19 degrees of freedom, but values near the peak of the spectrum of the sea still have essentially 19 degrees of freedom. If a spectral estimate has 19 degrees of freedom, it can be multiplied by 1.88 and 0.63. Then 9 times out of 10 the true spectral value, as might be obtained by taking a sample with many more degrees of freedom, will lie between these bounds. Similarly, if the spectral estimate is multiplied by



FIGURE II.28 PRECISE CONTOUR ANALYSIS OF THE STEREO SPECTRUM
(CORRECTED FOR WHITE NOISE, COLUMN NOISE, AND WITH THE SWELL TRANPOSED)

0.875 and 1.24, the true value will lie between these bounds four times in ten.

The contours in figure 11.28 can be smoothed by taking these facts into consideration and by assuming that the true spectrum is basically a smoothly varying function. The resulting smoothed spectrum is shown in figure 11.29. An attempt to indicate the very steep forward face has been made. In order to obtain this smoothed version it was only necessary to go outside the 40 percent bounds about 10 times in the area where the estimates were greater than 0.0050.

Analytic representation of the directional spectrum

The curves shown in figure 11.22 and the data tabulated in Table 11.6 provide a way to find an analytic representation for the directional spectrum of the sea. The results of the frequency analysis show that the theoretical Neumann spectrum as a function of frequency fits the data as summed around semicircles quite well.

The spectrum as a function of frequency and direction can therefore be written as equation (11.16).

$$(11.16) \quad [A(\mu, \theta)]^2 = \frac{\pi c e^{-2g^2/\mu^2 v^2}}{2} \cdot [f(\mu, \theta)]$$

where $c = 3.05 \times 10^4$ and all values are in c. g. s. units.

The function, $f(\mu, \theta)$ should have the property that it is zero over half the plane, that

$$(11.17) \quad \int_{-\pi/2}^{\pi/2} f(\mu, \theta) d\theta = 1$$

and that $f(\mu, \theta) \geq 0$.

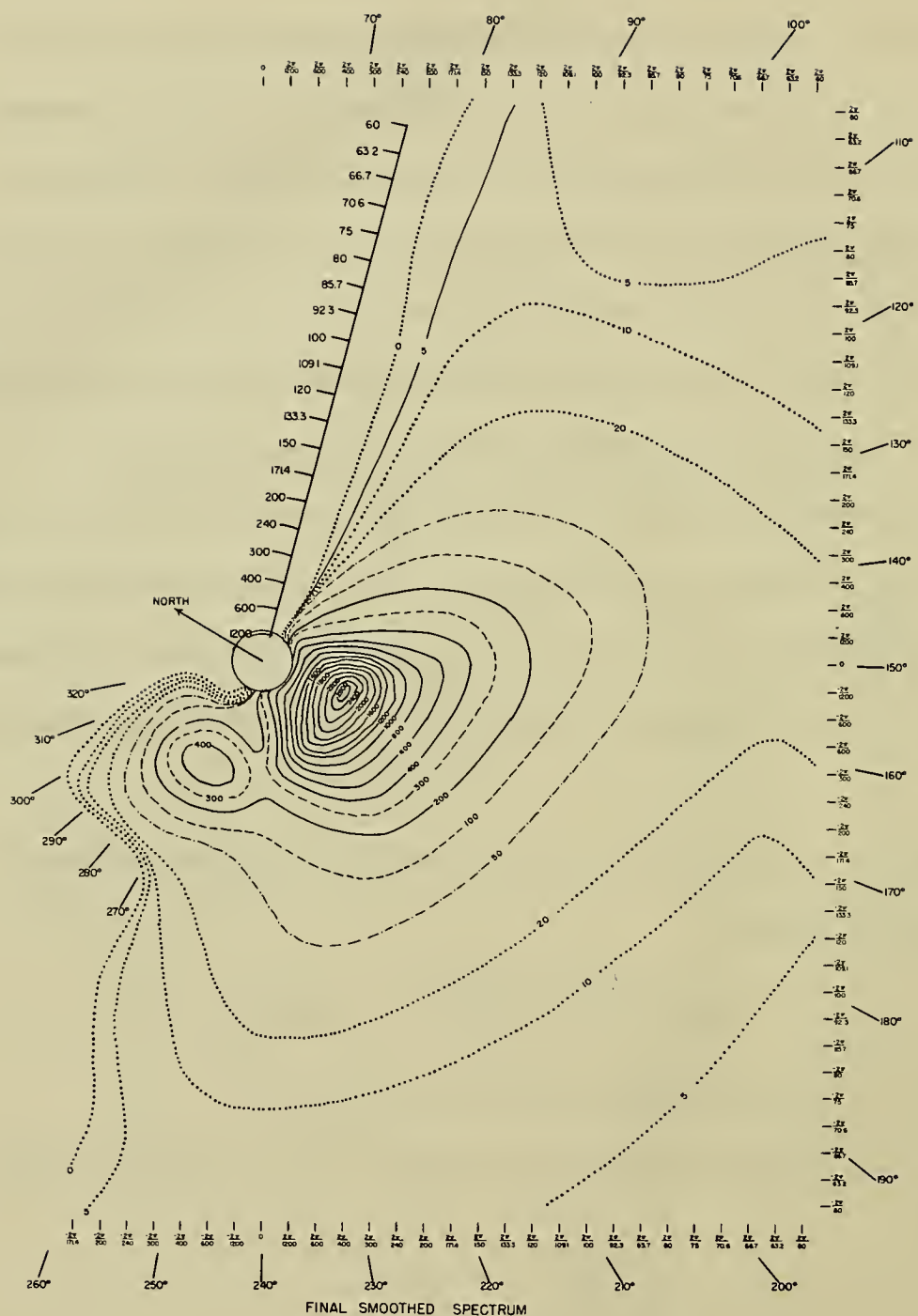


Fig. 11.29

Such a function is given by

$$(11.18) \quad f(\mu, \theta) = \frac{1}{\pi} \left[1 + \sum_{n=1}^N a_n(\mu) \cos 2n\theta + b_n(\mu) \sin 2n\theta \right]$$

for $\theta_m(\mu) - \pi < \theta < \theta_m(\mu)$, and zero otherwise if a_n and b_n can be so chosen that $f(\mu, \theta) \geq 0$ and if $\theta_m(\mu)$ is the angle in the first quadrant where $f(\mu, \theta)$ is a minimum as a function of μ .

If the values of the entries in Table 11.6 are divided by the sum for each column, k , and called $F(k, \theta)$, then

$$(11.19) \quad \sum_{\theta} F(k, \theta) = 1$$

and

$$(11.20) \quad f \left(\frac{2\pi k}{96}, \frac{(m + \frac{1}{2})\pi}{36} \right) \cdot \frac{\pi}{36} \cong F \left(k, \frac{(m + \frac{1}{2})\pi}{36} \right)$$

If the Fourier series given by equation (11.18) is truncated at some particular N as indicated, the effect is to smooth out some of the sampling variation in the data under the assumption that the spectrum is not too complex a function. Since there are only 36 points to fit for a given k , for N large enough a perfect fit within the resolution of the data could be obtained.

The coefficients, $a_n(\mu)$ and $b_n(\mu)$, in equation (11.18) can be computed for a given $\mu_k = 2\pi k/96$, by equations (11.21) and (11.22).

$$(11.21) \quad a_n(k) = 2 \sum_{m=-18}^{+17} F \left(k, \frac{(m + \frac{1}{2})\pi}{36} \right) \cdot \cos \left(\frac{2n(m + \frac{1}{2})\pi}{36} \right)$$

$$(11.22) \quad b_n(k) = 2 \sum_{m=-18}^{+17} F \left(k, \frac{(m + \frac{1}{2})\pi}{36} \right) \cdot \sin \left(\frac{2n(m + \frac{1}{2})\pi}{36} \right)$$

A measure of the variation in $F(k, \theta)$ is given by

$$(11.23) \quad M_T = \frac{36}{k} \sum_{\theta} [F(k, \theta)]^2$$

and since

$$(11.24) \quad M_N = \int_{-\pi/2}^{\pi/2} [f(\mu, \theta)]^2 d\theta = \frac{1}{\pi} \left[1 + \frac{1}{2} \sum_{n=1}^N [(a_n(k))^2 + (b_n(k))^2] \right]$$

the closeness of the fit for a given N is given by

$$(11.25) \quad R_N = M_N / M_T$$

If R_N is one, the fit is perfect for the available data.

Equation (11.18) can also be put in the form of equation (11.26).

$$(11.26) \quad f(\mu, \theta) = \frac{1}{\pi} \left[1 + \sum_{n=1}^N c_n(\mu) \cos(2n(\theta - \gamma_n)) \right]$$

for $\theta_m(\mu) - \pi < \theta < \theta_m(\mu)$, where

$$(11.27) \quad c_n(\mu) = [a_n^2(\mu) + b_n^2(\mu)]^{1/2}$$

and

$$(11.28) \quad \gamma_n(\mu) = \frac{1}{2n} \tan^{-1} \frac{b_n(\mu)}{a_n(\mu)}$$

The values of c_n , γ_n , and R_n for n equal to 1, 2, 3, 4, and 5 were computed by means of the IBM 650 for each k in Table 11.6. The results are given in Table 11.11. The values of c_n and γ_n are plotted as a function of k in figure 11.30.

The values of c_1 and γ_1 show a fairly smooth variation with k as do also the values of c_2 and γ_2 . The values of c_3 , c_4 , and c_5 are low and somewhat erratic, and the values of γ_3 , γ_4 , γ_5 are highly variable

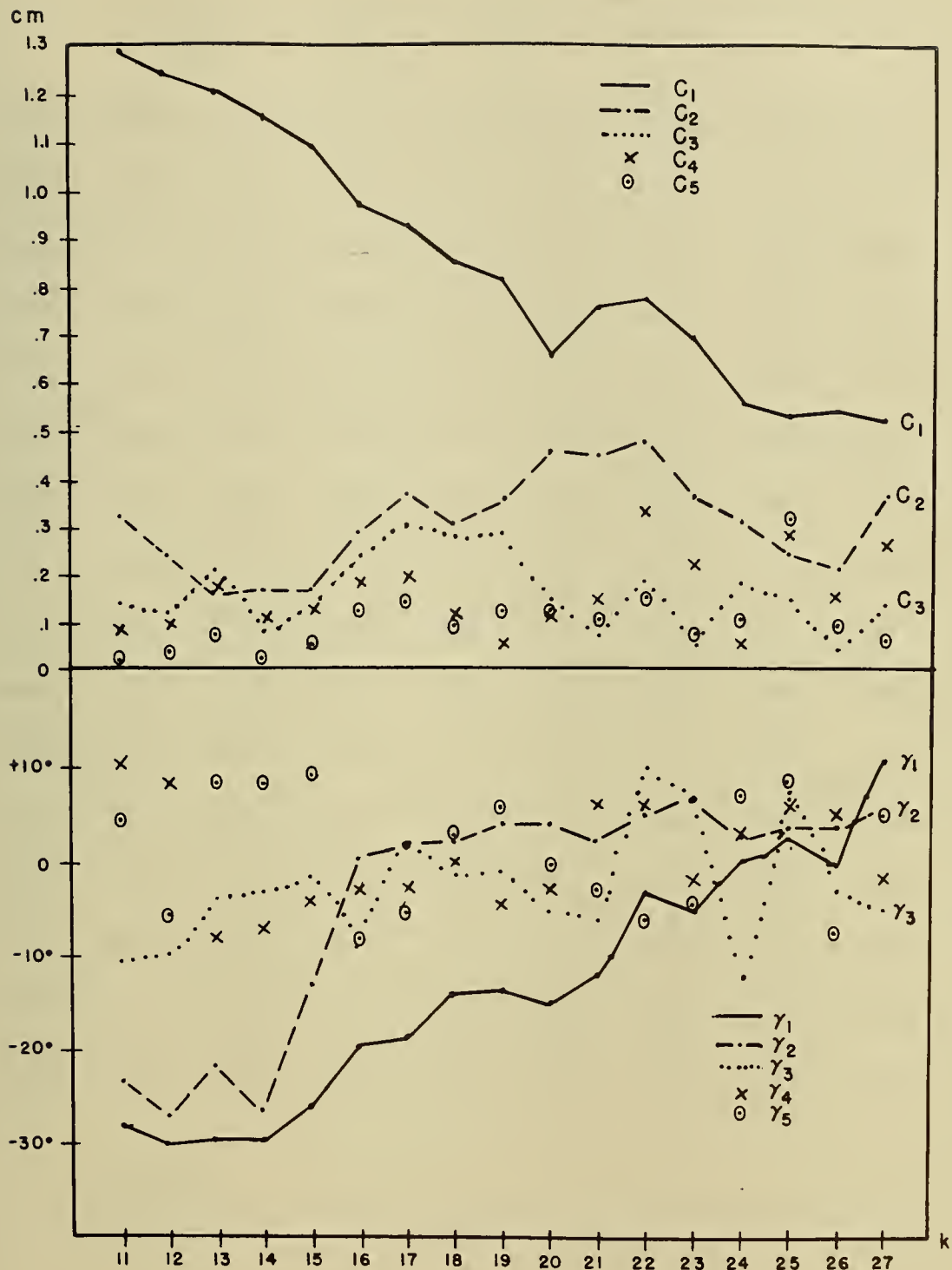


Figure II.30 C_n AND γ_n AS A FUNCTION OF k

Table 11.11. Fourier coefficients, phases and goodness of fit
for the analysis of the angular variation.

k	11	12	13	14	15	16	17	18	19
C ₁	1.29	1.24	1.21	1.16	1.10	0.97	0.93	0.85	0.82
γ ₁	-28.3°	-30.2°	-29.8°	-29.7°	-25.7°	-19.6°	-18.6°	-14.2°	-13.7°
R ₁	.951	.969	.963	.983	.975	.934	.911	.934	.917
C ₂	0.32	0.24	0.16	0.17	0.17	0.29	0.37	0.31	0.36
γ ₂	-23.4°	-27.2°	-21.5°	-26.6°	-13.0°	+0.3°	+1.8°	+2.1°	+4.3°
R ₂	.978	.985	.970	.991	.985	.960	.954	.967	.963
C ₃	0.14	0.12	0.21	0.08	0.13	0.24	0.26	0.23	0.24
γ ₃	-10.9°	-10.0°	-4.0°	-3.2°	-1.7°	-8.3°	2.1°	-1.6°	-1.3°
R ₃	.983	.988	.982	.993	.990	.979	.976	.985	.982
C ₄	0.09	0.10	0.17	0.11	0.13	0.19	0.20	0.12	0.06
γ ₄	+10.1°	+8.3°	-8.0°	-7.1°	-4.3°	-3.1°	-2.8°	-0.1°	-4.7°
R ₄	.985	.991	.991	.997	.995	.990	.988	.990	.984
C ₅	0.02	0.02	0.08	0.03	0.06	0.13	0.15	0.10	0.13
γ ₅	+4.4°	-5.7°	+8.6°	+8.8°	+9.0°	-7.7°	-5.4°	2.5°	5.7°
R ₅	.985	.992	.993	.997	.996	.995	.995	.993	.989

(Cont.)

Table 11.11 (Cont.)

	20	21	22	23	24	25	26	27
C ₁	0.66	0.76	0.78	0.70	0.56	0.54	0.55	0.53
γ ₁	+14.9°	-11.8°	+3.3°	+5.3°	0.2°	+2.2°	-0.6°	+10.4°
R ₁	.974	.885	.847	.910	.879	.859	.906	.854
C ₂	0.45	0.45	0.48	0.37	0.32	0.25	0.22	0.37
γ ₂	+3.8°	2.1°	4.9°	6.5°	2.3°	3.5°	3.5°	5.5°
R ₂	.949	.955	.928	.961	.918	.882	.925	.905
C ₃	0.15	0.08	0.19	0.05	0.19	0.15	0.05	0.14
γ ₃	-5.5°	-6.1°	+9.8°	6.3°	-12.3°	7.5°	+3.4°	-4.9°
R ₃	.956	.957	.940	.962	.932	.891	.926	.912
C ₄	0.12	0.15	0.34	0.23	0.06	0.29	0.16	0.27
γ ₄	+2.6°	+6.1°	+6.3°	+1.7°	+3.1°	+6.0°	4.9°	-1.8°
R ₄	.962	.964	.978	.980	.933	.923	.936	.938
C ₅	0.13	0.11	0.16	0.08	0.11	0.32	0.10	0.07
γ ₅	-0.4°	-3.0°	-5.9°	+4.5°	7.1°	8.0°	-7.5°	+5.1°
R ₅	.967	.969	.986	.982	.937	.962	.940	.940

especially when one notes the way in which γ_n is defined.

The values of R_1 range from 0.983 to 0.847 and the average value is 0.918. Thus over 90 percent of the angular variation on the average is explained by the values of c_1 and γ_1 . The values of R_2 range from 0.991 to 0.882 and the average value is 0.955. Over 95 percent of the angular variation is explained, on the average, by the values of c_1 , γ_1 , c_2 and γ_2 . The erratic behavior of the other coefficients is explained as an attempt to fit the sampling variation of the data.

The graphs of c_1 , γ_1 , c_2 , and γ_2 do not vary as a function of k very rapidly. It would not be difficult to express them as somewhat smoothed functions of k (and hence μ) over the range of k from 11 to 27. The result would then be given by equations (11.29), (11.30), (11.31) and (11.32).

$$(11.29) \quad c_1 = c_1^*(\mu)$$

$$(11.30) \quad \gamma_1 = \gamma_1^*(\mu)$$

$$(11.31) \quad c_2 = c_2^*(\mu)$$

$$(11.32) \quad \gamma_2 = \gamma_2^*(\mu)$$

The directional spectrum could then be defined analytically as a function of frequency and direction by equation (11.33) in which precautions would have to be taken to insure that the square bracket on the right was always positive.

$$(11.33) \quad [A(\mu, \theta)]^2 = \frac{\pi}{2} \frac{c e^{-2g^2/\mu^2 v^2}}{\mu^6} \cdot \frac{1}{\pi} [1 + c_1^*(\mu) \cos(2(\theta - \gamma_1^*(\mu))) + c_2^*(\mu) \cos(4(\theta - \gamma_2^*(\mu)))]$$

Also $f(\mu, \theta)$ would have a minimum in the first quadrant as a function of θ .

for a fixed μ . Let this minimum be $\theta_m^*(\mu)$. Then (11.33) would be defined as

above for

$$\theta_m^*(\mu) - \pi < \theta < \theta_m^*(\mu)$$

and by zero otherwise.

The analytic expression determined as outlined above could then be transformed to Cartesian coordinates in the α, β plane as described in Part 8. If the function $[A(\alpha, \beta)]^2$ so obtained were integrated over a square of the area of one of the squares in the $U(r, s)$ plane the resulting number would then be quite close to the computed values of $U(r, s)$ and it would certainly agree within possible sampling variations with the computed number. However, such an analytic expression would still reflect certain features of the observed data and the wind field which generated the waves which would be difficult to generalize to other cases. In what follows this point will be discussed in more detail and a simpler analytical expression derived for wave forecasting purposes.

Properties of the directional spectrum

By means of the data tabulated and graphed so far, in particular by means of Tables 11.6, 11.10, and 11.11 and by means of figures 11.22, 11.26, 11.27, and 11.29, certain properties of the sea generated by the local winds in the area where the data were obtained can be summarized.

These properties are (1) that the integral over direction of the directional spectrum agrees remarkably well as a function of frequency with the theoretical spectrum derived by Neumann for an 18.7 knot wind, (2) that the angular spectrum is concentrated over narrower angular range for long waves

(low frequencies) and spread out over a wider range for short waves (high frequencies) and (3) that the integrated spectrum continues as predicted into higher frequencies as determined by the wave pole data. The properties should be expected to be the same for other spectra obtained for other conditions at other times.

There are other properties of the particular spectrum studied which are in part probably due to sampling variation and in part due to the particular local wind field which generated the waves. The values of γ_1 show that the peak in the angular variation of the spectrum shifts from what corresponds to 180° in figure 11.29 to 140° as the frequency increases from $2\pi(11)/96$ to $2\pi(27)/96$. Also a secondary peak at frequencies corresponding to $2\pi(16)/96$, $2\pi(17)/96$, $2\pi(18)/96$, and perhaps even for higher frequencies, is indicated in figure 11.22, and by the high values of c_2 and the values of γ_2 in figure 11.30. This secondary peak causes the graphs in figure 11.22 to have the property that they are not even functions about some central value of the direction. The change in γ_1 can be explained partly by sampling variation and partly by the fact that the local wind direction was reported to be from 330° and the winds further to the north were from 360° . Possibly the winds to the north were the ones which generated the longer waves. The skewness of the curves for the angular variation may or may not be real in the sense that it would still show up in a spectrum with a larger number of degrees of freedom. However, it should also be noted that there is a wind shear present over the area of wave generation with the property that the

wind speed increases from east to west across the area under study. A possible effect of the shear would be to produce the skewness in the angular variation as indicated. At some future time it may be possible to extend the concepts of wave theory to permit a representation of the local wave spectrum as a function of wind velocity and wind direction locally and as a function of the change of wind direction up wind and the shear in wind velocity cross wind. To do this would require a greater number of degrees of freedom than this study has obtained, several different spectra for different wind conditions, and a very detailed study of the wind fields.

An idealized directional spectrum

For the present purpose, however, it is desirable to attempt to idealize the results obtained so as to reflect the three results pointed out above and so as to eliminate sampling variation and the effects of changing wind direction and wind shear. It will therefore be assumed that $[A(\mu, \theta)]^2$ is an even function about the local wind direction and that its peak value falls at $\theta = 0$. The values of $c_1(\mu)$ as tabulated above thus determine the amplitude of the $\cos 2\theta$ term and $\gamma_1(\mu)$ is assumed to be zero. (This implies a rotation of -30° for the axes in the figures given above if it is desired to approximate the peak of the spectrum.)

After considerable subjective curve fitting and trying a number of possible functions which did not do as well, it was found that c_1 could be approximated by the following function of frequency and wind speed where the values are in c. g. s. units and v is (18.7×51.5) cm/sec.

$$(11.34) \quad c_1 = 0.50 + 0.82 e^{-(\mu v/g)^4/2}$$

The function $f(\mu, \theta)$ can then be given by

$$(11.35) \quad f(\mu, \theta) = \frac{1}{\pi} [1 + (0.50 + 0.82 e^{-(\mu v/g)^4/2}) \cos 2\theta + c_2 \cos 4\theta]$$

for $-\pi/2 < \theta < \pi/2$.

Since the values of c_1 are greater than one for small μ , $f(\mu, \theta)$ becomes negative for θ near $\pm\pi/2$, and this is not permissible. To avoid this, c_2 must be chosen so as to make $f(\mu, \theta)$ everywhere positive.

Since

$$(11.36) \quad \cos 2\theta = 2(\cos \theta)^2 - 1$$

and since

$$(11.37) \quad \cos 4\theta = 8(\cos \theta)^4 - 8(\cos \theta)^2 + 1$$

equation (11.35) can be rewritten as equation (11.38).

$$(11.38) \quad f(\mu, \theta) = [1 - 0.50 - 0.82 e^{-(\mu v/g)^4/2} + c_2] \\ + [1.00 + 1.64 e^{-(\mu v/g)^4/2} - 8c_2](\cos \theta)^2 + 8c_2(\cos \theta)^4$$

In order to keep the term independent of θ always positive, the smallest possible value of c_2 is given by

$$(11.39) \quad c_2 = 0.32 e^{-(\mu v/g)^4/2}$$

The function, $f(\mu, \theta)$ can then be written in two alternative forms as equations (11.40) and (11.41),

$$(11.40) \quad f(\mu, \theta) = \frac{1}{\pi} [1 + (0.50 + 0.82 e^{-(\mu v/g)^4/4}) \cos 2\theta + (0.32 e^{-(\mu v/g)^4/4}) \cos 4\theta]$$

$$(11.41) \quad f(\mu, \theta) = \frac{1}{\pi} [0.50 (1 - e^{-(\mu v/g)^4/2}) + (1.00 - 0.92 e^{-(\mu v/g)^4/2}) (\cos \theta)^2 + (2.56 e^{-(\mu v/g)^4/2}) (\cos \theta)^4]$$

A value of c_2 greater than 0.33 would make the coefficient of $(\cos \theta)^2$ in (11.41) negative for small μ with the accompanying possibility of negative values for $f(\mu, \theta)$.

The curves for c_1 and c_2 are graphed against the observed values of c_1 and c_2 in figure 11.31. The fit is fairly good for c_1 ; and for c_2 for frequencies corresponding to k equal to 11 through 15, the fit is not too bad. The extension of the curves outside of the region where data are available is quite arbitrary. For the longer waves the value of (11.38) has little total effect on the spectrum because the energy is very low there. For the shorter waves if c_1 became less than 0.50, the effect would be even greater angular spreading. Note that in figure 11.30 γ_1 and γ_2 are close together for k equal to 11 through 14, and that in a sense the value of c_2 used above is only the in-phase part of $\cos 4\theta$ with respect to the original data when k is larger.

A possible functional form for the directional spectrum of a wind generated sea is finally given by equation (11.42) if the wind is uniform in direction and speed over the area of wave generation and if the sea is fully developed.

$$(11.42) \quad [A(\mu, \theta)]^2 = \frac{\pi}{2} \frac{c e^{-2(g/\mu v)^2}}{\mu^6} \cdot \frac{1}{\pi} [1 + (0.50 + 0.82 e^{-(\mu v/g)^4/2}) \cos 2\theta + (0.32 e^{-(\mu v/g)^4/2}) \cos 4\theta]$$

for $-\pi/2 < \theta < \pi/2$, and zero otherwise.

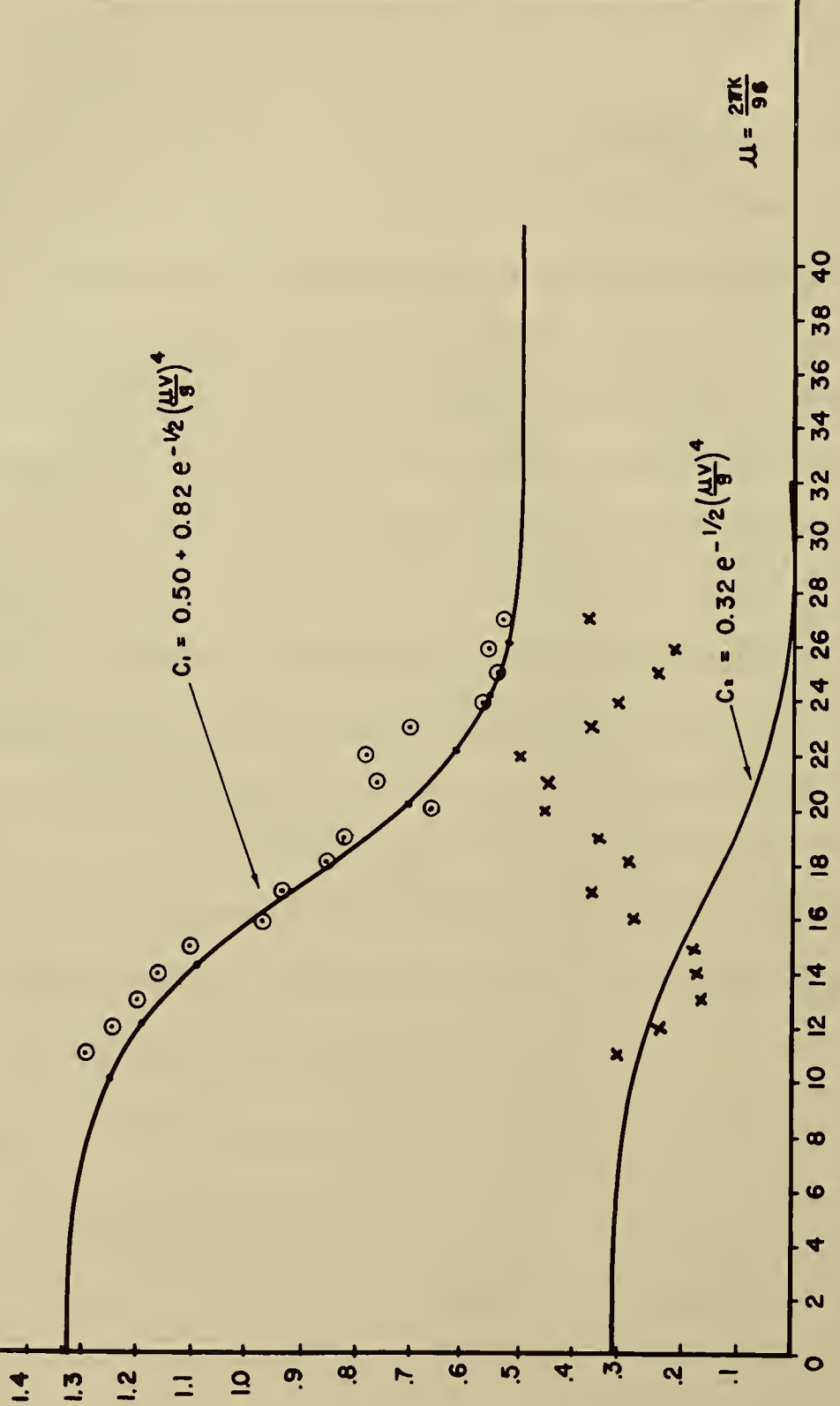


Fig. 11.31 SUBJECTIVELY FITTED COEFFICIENTS, C_1 AND C_2

This idealized directional spectrum still comes fairly close to agreeing with the curves in 11.22. After proper angular rotation, the $(\cos \theta)^4$ term will give good agreement with the curves for low frequencies. Agreement with the higher frequencies is also good. The secondary peak and the skewness at intermediate frequencies is missed.

Caution is recommended in the use of equation (11.42). Within the limitations mentioned above it comes close to describing the sea observed for a wind near 18.7 knots. For higher or lower values of the wind speed, however, it may not work although as a working hypothesis it may lead to useful results. Since only one spectrum was observed the variation in v of $f(\mu, \theta)$ as fitted cannot be tested. One could on the basis of the available data put $v = 18.7$ knots inside the square brackets of equation (11.42) and say that variation in $[A(\mu, \theta)]^2$ as a function of v is caused solely by the occurrence of v in the first term.

However, there are two additional points that can be made in favor of equation (11.42) as written. They are that it would appear to give more realistic swell forecasts than previously used formulas, and that the mean square slope of the sea surface still varies linearly with wind speed as observed by Cox and Munk [1954].

A previously given equation for the directional spectrum of a wind generated sea [Pierson, 1955] is shown in equation (11.43).

$$(11.43) \quad [A(\mu, \theta)]^2 = \frac{c e^{-2(g/\mu v)^2}}{\mu^6} (\cos \theta)^2$$

for $-\pi/2 < \theta < \pi/2$, and zero otherwise.

Equation (11.42) can also be written as equation (11.44).

$$(11.44) \quad [A(\mu, \theta)]^2 = \frac{c e^{-2(g/\mu v)^2}}{\mu^6} \left[0.25(1 - e^{-(\mu v/g)^4/2}) + (0.50 - 0.46 e^{-(\mu v/g)^4/2}) \right. \\ \left. (\cos \theta)^2 + (1.28 e^{-(\mu v/g)^4/2})(\cos \theta)^4 \right]$$

for $-\pi/2 < \theta < \pi/2$, and zero otherwise.

If μ is small, the angular term in (11.44) becomes $0.04(\cos \theta)^2 + 1.28(\cos \theta)^4$ which shows that the spectrum is more peaked at low frequencies than had been assumed in (11.43). Conversely if μ is larger, the angular term in (11.44) becomes $0.25 + 0.50(\cos \theta)^2$ which shows that the spectrum is more evenly spread out at high frequencies than had been assumed previously.

The angular spreading factor used in Pierson, Neumann and James [1955] can be derived from equation (11.43) and it is given by equation (11.45).

$$(11.45) \quad F(\theta) = \frac{1}{2} + \frac{\theta}{\pi} + \frac{\sin 2\theta}{2\pi} \quad \text{for } -\pi/2 < \theta < \pi/2.$$

The angular spreading factor from equation (11.42) can be written as equation (11.46).

$$(11.46) \quad F(\mu, \theta) = \frac{1}{2} + \frac{\theta}{\pi} + \frac{(0.50 + 0.82 e^{-(\mu v/g)^4/2}) \sin 2\theta}{2\pi} + \frac{0.32 e^{-(\mu v/g)^4/2} \sin 4\theta}{4\pi}$$

for $-\pi/2 < \theta < \pi/2$.

The curves for $f(\theta)$ as given by (11.45) and for $F(\mu, \theta)$ with $\mu = 0$ and $\mu = \infty$ as given by (11.46) are given in figure 11.32. Equation (11.43) is seen to be a compromise between the two extremes indicated by equation (11.42).

The new results, if correct, indicate that long period swell will be higher on a line through the center of the generating area parallel to the wind direction than it would be using the methods of Pierson, Neumann and James [1955] and that the short period waves which follow later would be lower. Stated another way, the long period components of the spectrum are more concentrated in

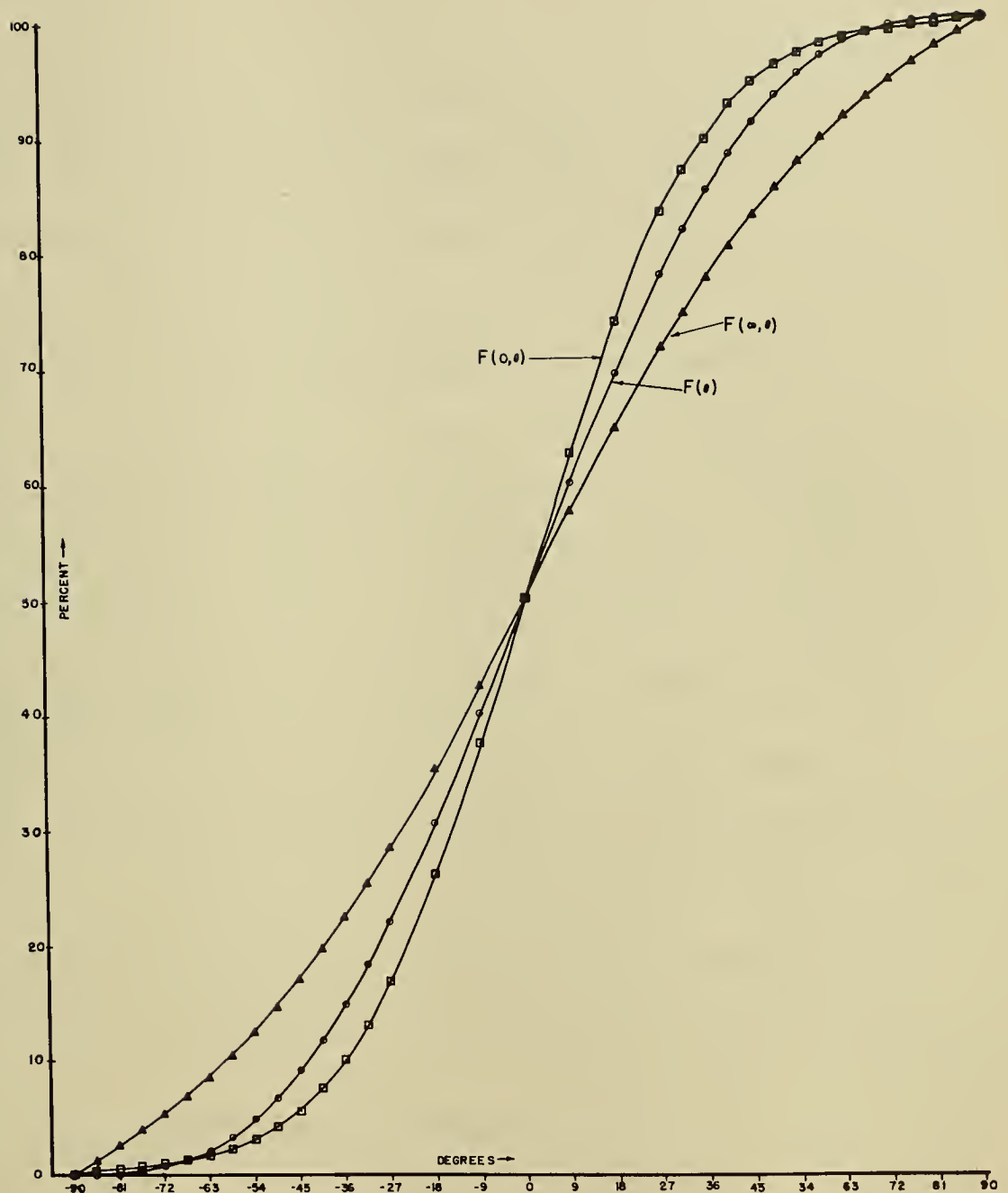


Fig. 11.32 ANGULAR SPREADING FACTOR FOR $F(0,\theta)$, $F(\theta)$ and $F(\pm\theta)$

the direction of the wind and hence in general they should be observed at a greater distance than the short period components which spread angularly over a wide area outside of the generating area. These results are thus another reason, apart from possible effects of viscosity, why swell has a higher period than the waves in the area of generation and why short period swell is seldom observed.

It should be noted that $\mu v/g$ is just another way to write v/c where c is the phase velocity of the spectral component, and it will not be too difficult to write a brief modification of Chapter 3 of H. O. Pub. 603 which will employ a family of angular spreading diagrams as a function of v/c and permit better swell forecasts.

Cox and Munk [1954] have found that the variance of the slope of the sea surface increases linearly with the wind velocity and that the theoretical spectrum of Neumann [1954] correctly predicts the total slope variance of the gravity wave part of the spectrum.

The upwind slope variance is given by equation (11.47) and the crosswind slope variance is given by equation (11.48). (See Pierson, [1955].)

$$(11.47) \quad \sigma_x^2 = \int_0^\infty \int_{-\pi/2}^{\pi/2} [A(\mu, \theta)]^2 \frac{\mu^4}{g^2} (\cos \theta)^2 d\theta d\mu$$

$$(11.48) \quad \sigma_y^2 = \int_0^\infty \int_{-\pi/2}^{\pi/2} [A(\mu, \theta)]^2 \frac{\mu^4}{g^2} (\sin \theta)^2 d\theta d\mu$$

When equation (11.42) is substituted into equation (11.47) the result can be simplified to the form of equation (11.49) where v is in meters/sec.

$$(11.49) \quad \sigma_x^2 = 1.59 \times 10^{-3} v [0.50 + 0.125 + \frac{0.205}{2} \frac{1}{2\pi} \int_0^\infty e^{-a^2/2 - 8/a^4} da]$$

The contribution of the integral to equation (11.49) is quite small and the value of σ_x^2 can be given by equation (11.50) where v is in meters per second.

$$(11.50) \quad \sigma_x^2 = 0.99 \cdot 10^{-3} v$$

Similarly σ_y^2 can be found to be equal to

$$(11.51) \quad \sigma_y^2 = 0.60 \cdot 10^{-3} v$$

These values of the upwind and crosswind slope contributions are in better agreement with the observations than those which result from equation (11.43) although Cox and Munk found σ_x^2 and σ_y^2 to be nearly equal. Perhaps the discrepancy can be explained by the nature of the site at which they obtained their observations.*

If the ratio, $\mu v/g$, used in deriving equation (11.42) had been of the form $\mu v_o/g$ where v_o is a constant equal to the wind observed at the time of the observation, then the integral over a would be a function of v such that the exponent would be $(-a^2/2 - 8/(v a)^4)$. For a surface wind of 15 m/sec there would be a tendency toward a greater contribution to σ_x^2 than observed by Cox and Munk, and similarly a smaller contribution to σ_y^2 .

Barber [1954] has studied the angular variation of waves with a period near two seconds in Waitemata Harbour, Auckland. He found an angular variation somewhat like $[\cos \theta]^4$. However, his results cannot be compared with these results as he writes that "the wind was about 15 knots and 2 sec waves

* See also the end of this chapter.

were dominant; but because the fetch in the wind direction was much greater than elsewhere, it is not expected that the [results] will apply to open water."

Aliasing in the directional spectrum

As shown in figure 11.26 the computed wave pole spectrum at high frequencies is a little high compared to the theoretical Neumann spectrum. The computed energy at frequencies greater than a value corresponding to a k of 27.5 is 0.57 (ft)^2 . Some of this energy is aliased in the directional spectrum back into longer wavelengths. The amount aliased is certainly less than 0.57 because part of the above value is probably white noise and part is correctly located in the corners of the rectangular area of the directional spectrum analysis. Only about 0.37 (ft)^2 lies above k equal to 31 and hence some part of 0.20 (ft)^2 is correctly located. Thus as a very crude estimate something of the order of 0.25 (ft)^2 is actually aliased over the directional spectrum. When spread out over a wide frequency and angular range, this aliased energy is undetectable because of the sampling variation in the higher unaliased values.

Correction to the covariance surface

The covariance surface given in figure 11.15 still has errors due to white noise and column noise in it. The correction for white noise is to subtract $0.56 (\text{mm}^2 \times 100)$ (that is, 0.54×1.032) from $\mu(0,0)$ and 0.191 from the central column (0.186×1.032). The result is the estimated covariance surface of the sea plus the swell as shown in figure 11.33. The major effects are to reduce the peak at the center, and hence increase the correlation of the edges with

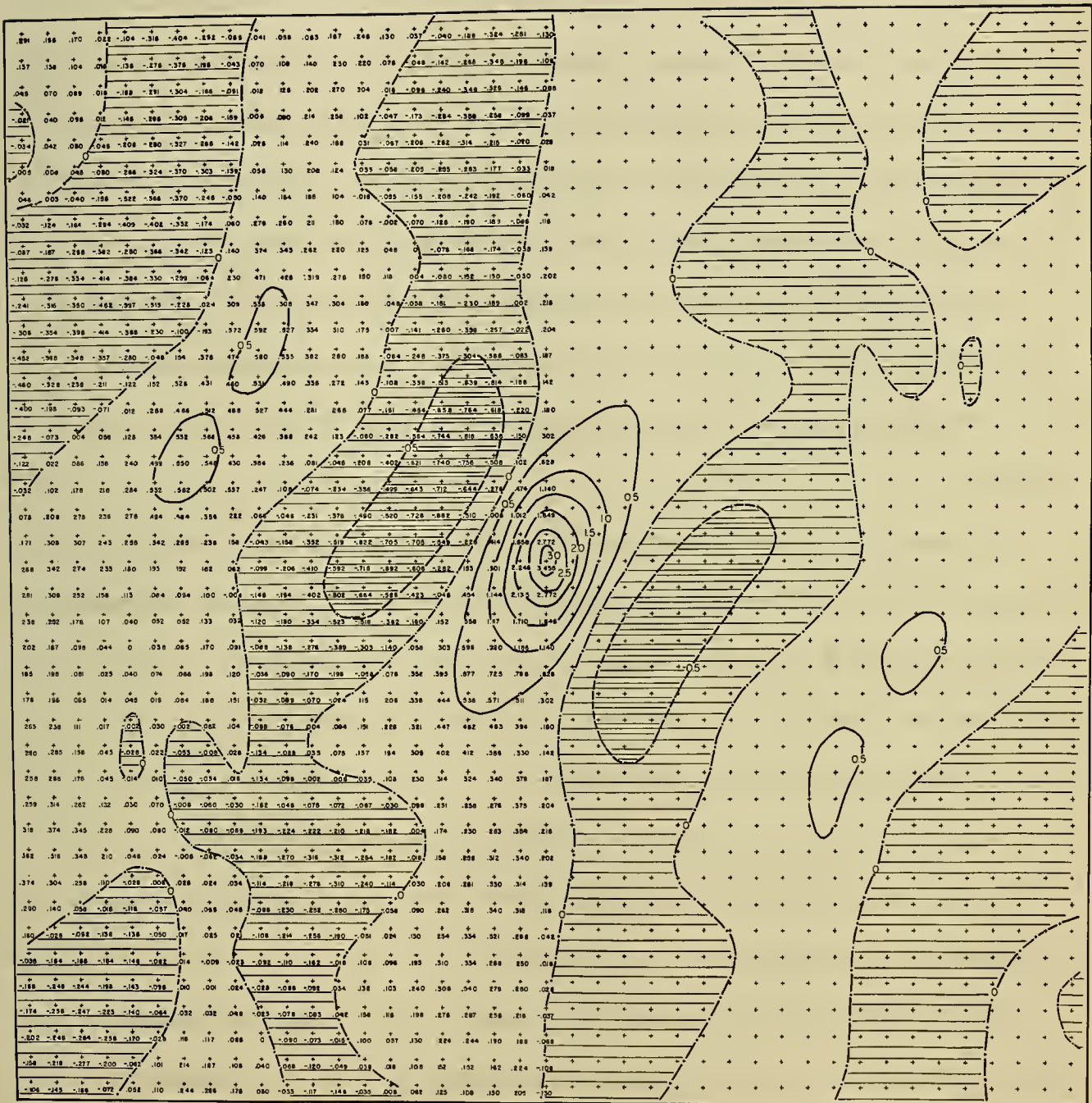


FIGURE II 33 CORRECTED COVARIANCE SURFACE

the center, and to push the zero contour more realistically to the left along the -q axis.

It would not be too difficult to remove the effect of the swell from the covariance surface and to obtain an estimated covariance surface for the sea. However, as Tukey and Hamming [1949] have pointed out the covariance estimates are subject to even more erratic sampling variation than the smoothed spectral estimates and this sampling variation is not well understood.

For example, Tukey [1951] has shown covariance functions computed from portions of the same time series. They were markedly different and yet the spectra computed from the different covariance functions were very similar.

For many types of problems in which knowledge of the covariance function is needed, it has been found that reinverting the smoothed spectral estimates will yield a more reliable covariance surface. Also for simpler problems the simplified spectrum given above which is symmetrical about $\theta = 0$ would give a more tractable covariance surface.

Alternate procedures for determining directional spectra

A number of alternate procedures for determining directional properties of waves have been proposed and attempted.

The methods used by Barber [1954], essentially directional antenna arrays, are by far the simplest and most economical if fixed positions for the wave poles can be maintained. The effects of refraction and perhaps bottom friction and percolation, however, make it difficult to generalize to open sea conditions and study the full range of components in the spectra.

Another way is to take wave records from a moving ship by means of the shipborne wave recorder as described by Cartwright [1956]. The ship is run on courses corresponding to an n sided polygon and the shift in frequency of the spectral components is studied. With enough degrees of freedom per spectral estimate, it should be possible (in principle) to resolve the spectral estimates into a directional spectrum by the inversion of some simultaneous linear equations in an appropriate number of unknowns somewhat along the lines of the method described by Pierson [1952]. However, if the response of the instrument to the waves is different for different headings due to the presence of the ship and if the records are too short so that sampling variation from record to record is pronounced, then the difficulties to be encountered will be even greater than those encountered in this report. Although some of the data reduction might be eliminated by analogue methods, the procedure would have essentially the same degree of complexity as the one used in this report.

The latest proposed procedure for determining directional spectra is given by Longuet-Higgins [1957]. The records from an airborne altimeter capable of measuring $\eta(x,y)$ and $\partial\eta(x,y)/\partial t$ are assumed at the starting point, and then by computing various moments from the data as determined by such quantities as the average distance between successive zeros at various headings and the velocity distribution of zeros, the moments of the spectrum are obtained. Then by an inversion technique the spectrum is deduced.

Pierson [1952] proposed the use of an airborne altimeter to determine the directional spectrum. The method of analysis involved the study of the

spectra obtained at different headings and the solution of a set of simultaneously linear equations.

From the results of this present study, it can be stated that the method proposed by Longuet-Higgins [1957] is not likely to be successful, especially with respect to a sea. Since the data are taken at different times at different headings, each record has a different sampling variation for each spectral estimate. The various moments thus have wide sampling variation.

Moreover, eighth moments are required to give any sort of definition to the spectrum. For the true sea surface the eighth moment is entirely determined by the capillary waves on the water. Some sort of filtering action would be needed in the recording instruments to maintain pure gravity wave conditions otherwise a problem in resolution would arise due to the extreme range of wavelengths covered. The effect of such filters would have to be incorporated in the theory.

Even with the capillary waves filtered out there would be high frequency error noise of some sort or another present in the data. In computing an eighth moment, this noise would blow up beyond all recognition and completely obviate the value of the estimated moment.

In contrast the methods used in this study effectively suppress high frequencies whether real or due to errors in the data. Also various sources of error which will undoubtedly be present in any method of recording waves were isolated and removed.

The very valuable results of Longuet-Higgins [1957] on the statistical

properties of a random moving surface can most efficiently be applied by using the moments computed from the corrected spectrum obtained in this study and allowing for the effects of the white noise and column errors.

Winds

The winds as observed by the R. V. Atlantis were measured by means of a three cup anemometer and a wind vane. The three cup anemometer and the vane were mounted at the end of the main boom above the upper laboratory of the Atlantis at a height of 15 to 18 ft above sea level. The dial of the anemometer was read visually to get the wind speeds. The winds as observed might have been a little high compared to undisturbed measurements over open water due to the presence of the ship.

The theory of the Neumann spectrum is based on observations of the wind at a height of about 25 feet above the sea level. If a logarithmic wind profile is used with a roughness coefficient of 0.75 cm (Neumann [1948]), and if 15 feet is used for the anemometer height of the Atlantis, the 18.7 knot wind becomes a 20 knot wind at 25 feet. It becomes a 19.5 knot wind if 18 feet is used.

The theoretical spectra for 19 and 20 knots are also shown in figure 11.26. On consideration of the confidence bands of the composite spectrum, especially near the peak where there are only 22 degrees of freedom, the variability of the winds during the time when the 18.7 knot average was obtained, and the compensating effects of the presence of the ship and the cor-

rection to a greater height, it is only possible to conclude that the agreement is satisfactory within the range of possible variation of wind speed and true spectral values, and that there is certainly no justification for changing the constant in the Neumann spectrum.

Added notes on the results of Farmer

Farmer [1956] has made further measurements of wave slopes on the windward side of Bermuda. He therefore had an unlimited fetch of open water over which the sea was generated in contrast to the results of Cox and Munk [1954] in which some islands may have interfered with the fetch as pointed out by Darbyshire [1956].

Farmer [1956] found essentially the same total slope variance as Cox and Munk [1954]. The ratios of upwind downwind to total slope variance found by Farmer were 0.57, 0.60, and 0.77, and these compare quite favorably to the theoretical value of 0.625 given by equation (11.49).

References to Parts 10 and 11

- Barber, N. F., [1954]: Finding the direction of travel of sea waves. Nature, v. 174, p. 1048.
- Cartwright, D. E., [1956]: On determining the directions of waves from a ship at sea. Proc. Royal Soc., A, 234, 382-387.
- Cox, C., and W. H. Munk [1954]: Statistics of the sea surface derived from sun glitter. Jour. of Marine Research, 13(2), pp. 198-227.
- Darbyshire, J., [1955]: An investigation of storm waves in the North Atlantic Ocean. Proc. Royal Soc., A, v. 230, pp. 560-569.
- Darbyshire, J., [1956]: An investigation into the generation of waves when the fetch of the wind is less than 100 miles. Q. J. R. M. S., v. 82, Oct. 1956, pp. 461-468.

Farmer, H. G. [1956]: Some recent observations of sea surface elevation and slope. Woods Hole Oceanographic Institution, Ref. No. 56-37, (unpublished manuscript).

Longuet-Higgins, M. S. [1957]; The statistical analysis of a random moving surface. Phil. Trans. Roy. Soc., Ser. A, no. 966, v. 249, pp. 321-387.

Neumann, G., [1948]: Über den Tangentialdruck des Windes und die Rauhigkeit der Meeresoberfläche. Zeit. Meteorol., H 7/8, 193-203.

Neumann, G., [1954]: Zur Charakteristik des Seeganges. Archiv. f. Meteorol. Geophysik und Bioklimat., ser. A, v. 7, pp. 352-377.

Neumann, G., and W. J. Pierson, [1957a]: A comparison of various theoretical wave spectra. To appear in "Proceedings of a Symposium on Ship Motions in Irregular Seas." Ned. Scheepsbouwkundig Proefstation, Haagsteeg 2, Wageningen, Netherlands.

Neumann, G. and W. J. Pierson, [1957b]: A detailed comparison of various theoretical wave spectra and wave forecasting methods. (In preparation, to be submitted to Deut. Hydrogr. Zeits.)

Pierson, W. J., [1952]: A unified mathematical theory for the analysis, propagation and refraction of storm generated ocean surface waves. Parts I and II. Research Division, College of Engineering, New York University, Department of Meteorology and Oceanography. Prepared for the Beach Erosion Board, Department of the Army, and the Office of Naval Research.

Pierson, W. J., [1954]: An electronic wave spectrum analyzer and its use in engineering problems. Tech. Memo. No. 56, Beach Erosion Board, Washington, D. C.

Pierson, W. J., [1955]: Wind Generated Gravity Waves. In Advances in Geophysics, v. 2, Academic Press, Inc., Publishers, New York, N. Y.

Pierson, W. J., G. Neumann, and R. W. James, [1955]: Practical methods of observing and forecasting ocean waves by means of wave spectra and statistics. H. O. Pub. 603.

Press, H., and J. W. Tukey, [1956]: Power spectral methods of analysis and application in airplane dynamics. Flight Test Manual, Vol. IV, Instrumentation NATO Advisory Group for Aeronautical Research and Development, edited by E. J. Durbin. Part IVc, pp. ivc-1 to ivc-41.

Roll, H. U., and G. Fischer, [1956]: Eine kritische Bemerkung zum Neumann-Spektrum des Seeganges. Deut. Hydrogr. Zeits., Band 9, Heft 1.

Tucker, M. J., [1956a]: Comparison of wave spectra as measured by the N. I. O. shipborne wave recorder installed in the R. V. Atlantis and the Woods Hole Oceanographic Institution wave pole. N. I. O. Internal Report No. A6.

Tucker, M. J., [1956b]: A shipborne wave recorder. Trans. of the Institution of Naval Architecture, v. 98, pp. 236-250.

Tukey, J. W., [1949]: The sampling theory of power spectrum estimates. Symposium on Applications of Autocorrelation Analysis to Physical Problems. Woods Hole, Mass., June 13-14 (Office of Naval Research, Washington, D. C.).

Tukey, J. W., [1951]: Measuring noise color. Bell Telephone Laboratories in Murray Hill, N. J. Prepared for distribution at a meeting of the Metropolitan Section Institute of Radio Engineers, 7 Nov. 1951.

Acknowledgments

The help of Mr. Raymond Stevens, Mr. Rudolph Hollman, and Mr. Roy E. Peterson in the preparation of this part of the work is greatly appreciated.

PART 12

RECOMMENDATIONS AND CONCLUSIONS

Conclusions

The directional spectrum of a wind generated sea has been determined from stereo data after correcting the data for differential shrinkage, column noise, white noise and the presence of a swell. This spectrum shows a single peak and the contributions from different wavelengths cover a wide range of wavelengths and directions. When transformed to a frequency spectrum, with directional effects eliminated, the results are remarkably close to the theoretical spectrum derived by Neumann. The longer waves in the spectrum are concentrated over a narrower range of angles about the wind direction than the shorter waves.

The actual spectrum reflects some effects of sampling variation, wind shear, and changing wind direction upwind which are difficult to isolate because of the nature of the wind data and the sampling variation. When these are removed by simplifying assumptions, it is possible to obtain an analytic representation for the spectrum which appears consistent with known properties of swell and sea surface slopes.

The analytic representation which has been obtained rests upon somewhat shaky foundations as far as angular effects are concerned. However, for forecasting it would appear advisable to incorporate these results into the forecasting method without awaiting further verification. Certainly the results on which such a revision would be based are on firmer theoretical ground

than the results on which the original material was based.

The spectrum computed from the wave pole data does not agree with the spectrum computed from the stereo data nor with the corresponding theoretical Neumann spectrum. Variability in the spectrum due to wind variation of the order of one knot would explain the discrepancy. However, a more likely reason for the discrepancy appears to be in the calibration of the wave pole.

The numerical results which have been obtained provide valuable data on a wind generated sea for a fairly low wind speed. It will be particularly useful in studying the topography of the sea surface and in problems connected with seaplanes and small vessels.

Recommendations

The use of stereo photographs to determine the directional spectrum of a sea has proved feasible. Due to attrition, an originally desired 50 degrees of freedom per spectral estimate was reduced to only 19. The computations were lengthy and difficult, but nevertheless results of considerable value were obtained.

It is difficult to generalize the results obtained to higher wind speeds, and one determination of a directional spectrum is not enough to provide comprehensive details on fully generated seas for a range of wind speeds.

It is therefore recommended that an experiment similar to the one described in this report be repeated for a fully developed sea at at least one higher wind speed. A wind of 24 knots, a fetch of 130 NM and a duration of

14 hours should not be too difficult to find. For these conditions the significant wave height would be nearly double and the E value would be nearly four times those observed for the 18.7 knot wind according to the results of Neumann.

If such distorting effects as differential shrinkage and column noise could be eliminated by proper choice of film and preliminary studies of their causes it would then be possible to allow a four-fold increase in the white noise variance without seriously affecting the results. This would permit the planes to fly higher, thus covering a larger area in one stereo pair and providing better resolution and more degrees of freedom. An appendix written by Simeon Braunstein, the Research Division photographer at New York University, follows these recommendations and conclusions. In it is given a discussion of the stability of different types of film bases and of film processing methods which should eliminate the effects of differential shrinkage.

In such an experiment more careful attention should be paid to the wind field, and winds should be recorded at least every hour for as long a time as possible prior to the observations. A decrease of wind speed in the wind field should be avoided. The winds, if possible, should be measured at several heights.

Moreover, now that a fairly good method of analysis for the results has been developed, it should be possible to program additional operations on the spectrum to carry out in just a few minutes all the computations made in Part 11.

As mentioned in Part 11, a calibration study of the wave pole is recommended, but for a new stereo study, it is recommended that the design of the wave pole be altered along the lines suggested by H. G. Farmer.

At or near the same time that the stereo and wave pole data are taken, it might be advisable to take records with an airborne altimeter as developed at the U. S. Navy Hydrographic Office and with shipborne wave recorders installed on several different types of vessels. The airborne altimeter could be flown at a number of different headings and the ships could be operated both hove to in head seas and on polygonal patterns as described by Cartwright. This would require an advance forecast of a stationary state for at least four hours, but this should not be too difficult to achieve.

The wave pole data at the present time appear to be the only data capable of reproducing the higher frequencies correctly, and such data would still be needed. With stereo data, wave pole data, airborne altimeter data, and shipborne recorder data it will be possible to make exhaustive cross checks of the calibrations and responses of all the instruments and to study the relative utility of each.

With such exhaustive measurements of the sea state, additional data of interest to naval architects and electrical engineers could also be obtained at the same time. This would permit their theories and calculations to be based on a firm foundation consisting of adequate knowledge of the state of the sea at the time of their observations.

APPENDIX
The Dimensional Stability of Photographic Films

Abstract

The dimensional stability of several photographic film bases to relative humidity, temperature, processing, handling, and storage is discussed. Permanent and temporary size changes are outlined. Recommendations for the choice, processing, and storage of film intended for photogrammetric use are made.

Sources of errors in stereo-photogrammetry

In addition to optical factors, platform stability, camera tilt, etc., the inherent dimensional instability of flexible photographic film bases may contribute to error in measurements made from aerial stereo photographs. In order to minimize error due to the last cause, care must be taken in the choice of film, storage before and after exposure, processing, and handling.

Dimensional changes in photographic films may be classified under two headings: temporary and permanent. There are two factors involved in temporary changes: temperature and relative humidity.

Temperature effects

The thermal coefficient of expansion of most common film bases (1944) is approximately 5×10^{-5} inches per inch per degree F, or about 0.05 percent per 10°F . Table I shows the effect of temperature, as well as relative humidity and processing, on several film bases (Fordyce, Calhoun, and Moyer, 1955). The expansion is generally 10 to 40 percent greater in the widthwise than in the lengthwise direction. This is the result of the partial orientation of the molecules in the base in the machine direction. It is evidently easier, under these conditions, to increase the distance between them, either by thermal agitation, or by the introduction of moisture, in a direction perpendicular to this alignment.

Humidity effects

The humidity coefficient of linear expansion of common films varies from a low of 1.0×10^{-5} for DuPont "Cronar" to about 10×10^{-5} inches per inch per 1 percent relative humidity change, for standard cellulose acetate. This effect is essentially linear between 20 and 70 percent relative humidity, and somewhat greater below 20 percent and above 70 percent. Photographic films exchange moisture with the air continually. The moisture content of a film is determined almost solely by the relative humidity of the air with which it is in equilibrium.

Table I. Average Processing Shrinkage, Humidity Expansion and Thermal Expansion of Current Eastman Motion Picture Films.

Film	Base	Processing shrinkage, %		Humidity expand- ion per 10% R.H., %		Thermal expand- ion per 10 F, (Range 0-100 F)	
		Length	Width	(Tray development)	20% -70% R.H.)	Length	Width
Black-and-White Negative and Eastman Color Negative	Triacetate	.06	.07	.07	.08	.03	.035
Black-and-White Positive and Sound Recording	Triacetate	.05	.05	.05	.06	.03	.035
Eastman Color Print	Triacetate	.07	.08	.06	.07	.03	.035
Kodachrome Films (16mm)	Acetate propionate	.09	.10	.08	.10	.035	.04

Cronar

A new polyester film support, "Cronar", is now being produced by the Photo Products Division of E. I. Du Pont de Nemours and Company. At present, it is being coated only with the slow, high contrast "photolith" emulsion. Reference to Tables II and III, and Figures 1 and 2, will indicate that "Cronar" shows considerable improvement in dimensional stability over other flexible film supports, in regard to temperature, relative humidity, and processing. There is reason to hope that when "Cronar" is available in larger quantities, it will be coated with an aerial emulsion, in addition to the litho emulsion now available.

Permanent changes

There are three principal causes of permanent dimensional changes in film supports. The first, and most important, is the gradual loss of volatile chemicals (plasticizer and solvents). Film base is cured for about five hours, which eliminates about 96 percent of the volatile chemicals. The subsequent loss of the remaining 4 percent causes shrinkage and related troubles. Shrinkage from this cause is accelerated by heat and moisture, and reduced by preventing free access to air. As with temporary changes in dimension, shrinkage is greater in the widthwise direction.

The compressive force of the emulsion upon the base results in a certain amount of plastic flow or permanent shrinkage. Dimensional changes from this cause are increased by heat, because of increased film plasticity at high temperatures. Moisture also increases base plasticity but inhibits the contraction of the base, and the latter has the greater effect. Thus, an increase in relative humidity, at constant temperature greatly decreases this type of shrinkage. Plastic flow of the base may also be the result of stretching in handling and processing -- resulting in extension lengthwise. Such changes are increased by heat, moisture, amount of tension applied, and the duration of the tension.

TABLE II

Base Type	Humidity Coefficient (length change in inches/inch of length/1% RH change)	Size change example of a 30" litho negative with a 20% increase in RH, using the mid-point of the Humidity-Coefficient Range
.0042" "CRONAR" based PHOTOLITH	1.0 to 2.0×10^{-5}	+ .009" (1.5×10^{-5})
.0058" Standard cellulose acetate based PHOTOLITH	8.0 to 10.0×10^{-5}	+ .054" (9.0×10^{-5})
.0058" Litho sensitized high acetyl cellulose acetate base	5.0 to 7.0×10^{-5}	+ .036" (6.0×10^{-5})
.0055" Litho sensitized polystyrene base	1.0 to 2.0×10^{-5}	+ .009" (1.5×10^{-5})
.0120" Litho sensitized vinyl base	1.0 to 2.0×10^{-5}	+ .009" (1.5×10^{-5})

(Coefficient x film length in inches x % RH change = film size change in inches.)

TABLE III

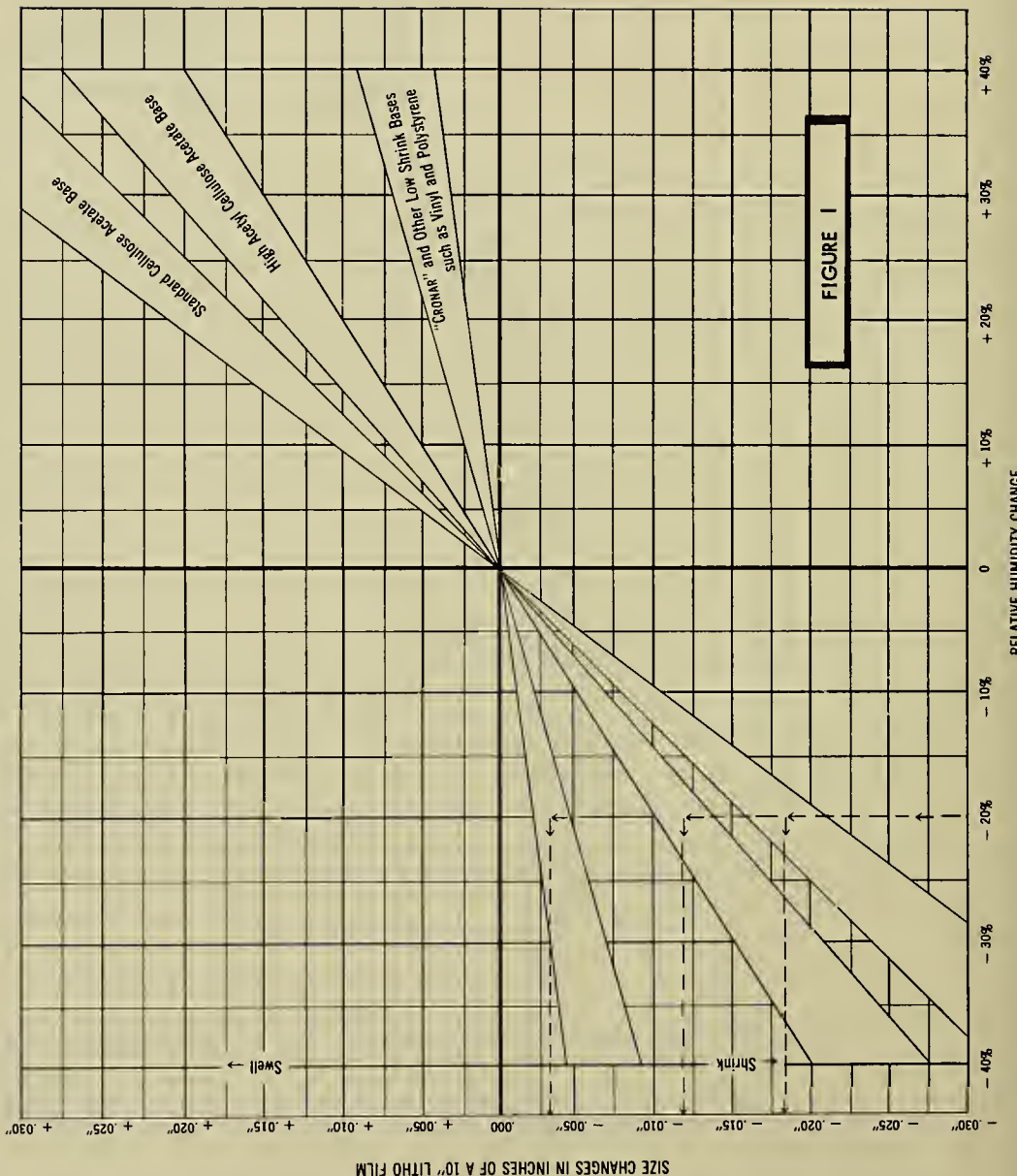
Effect of Temperature Changes on Film Size	Unsensitized Base	Temperature Coefficient (in./in./°F.)	Size change example of a 30" litho negative with a 20° rise in T
"CRONAR" base	2.0×10^{-5}	+ .012"	
Standard cellulose acetate base	3.4×10^{-5}	+ .020"	
High acetyl cellulose acetate base	2.3×10^{-5}	+ .014"	
Vinyl base	3.8×10^{-5}	+ .023"	
Polystyrene base	3.5×10^{-5}	+ .021"	
Glass	0.5×10^{-5}	+ .003"	
Aluminum	1.4×10^{-5}	+ .008"	

(Coefficient x film length in inches x temperature in °F = film size change in inches.)

INSTRUCTIONS

To use this chart in estimating film size changes, establish the relative humidity change that will be encountered (say a 20% RH drop) and locate the corresponding point on the base line (-20%). Now read vertically to the center of the stability bracket that corresponds to the film type in use and then read horizontally from this intersection to the left hand (size change) scale which indicates directly the size change of a 10" negative. In this example, a 10" high acetyl cellulose acetate base film would shrink about .012", a standard cellulose acetate film would shrink .003", and "Cronar" based films would shrink .003". Size change of larger negatives can be quickly calculated from this 10" information.

Values for cellulose base products may vary appreciably as the extremes of low, and high humidity are approached, since their humidity coefficients are not linear functions. However, this chart will serve as a convenient guide in estimating average dimensional performance over a wide range of conditions.



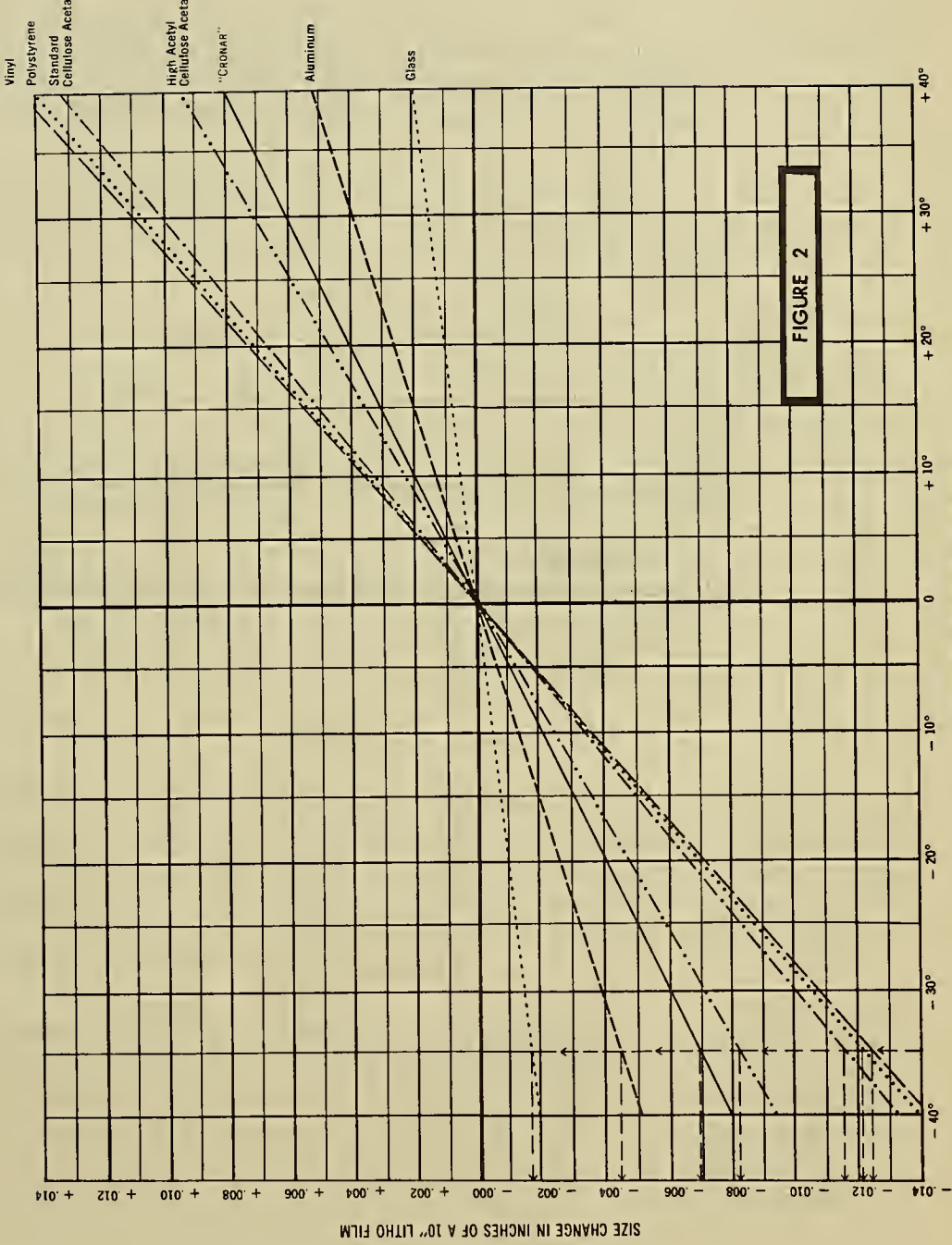
INSTRUCTIONS

The chart below can be used to estimate or visualize the relationship between temperature changes and negative size change.

To use this chart, establish the expected temperature change in degrees Fahrenheit (say a 35° F drop) and locate the corresponding point on the base line (-35°). Now read vertically to the line that corresponds to the base in use, and read horizontally from the desired intersection to the left hand (size change) scale which directly indicates the size change of a

10" negative. In this example, the following approximate shrinkage is indicated for a 10" critical length measurement.

Glass.....	.002"
Aluminum.....	.005"
"Cronar".....	.007"
High acetyl cellulose acetate008"
Standard cellulose acetate012"
Polystyrene012"
Vinyl013"



The third cause of permanent dimensional change is release of strain, or recovery from deformation. If film base is stretched during manufacture under conditions which do not permit reorientation of the molecules, deformation, or creep, occurs, resulting in lengthwise extension and widthwise contraction. Rapid cooling retards recovery of the deformation (primary creep) due to "freezing in of strain". This strain may be released at some time during the life of the film, with consequent lengthwise shrinkage, and widthwise expansion. Where such a strain exists, the rate of recovery is increased by both heat and moisture.

Table IV shows the effect of temperature on the rate of shrinkage of an earlier film base, EK 16 mm safety reversal. Shrinkage was measured in the lengthwise direction, on processed film strips exposed freely to air at the indicated temperatures, and 20 percent relative humidity.

TABLE IV

TIME (months)	% Shrinkage		
	70° F	90° F	120° F
0	0	0	0
1	0.18	0.36	0.76
2	0.30	0.50	1.00
3	0.37	0.52	1.02
4	0.39	0.60	1.06
5	0.40	0.62	1.08
6	0.41	0.63	1.20

Processing shrinkage

Films swell during development, and shrink again during drying. Most films undergo a small permanent shrinkage during processing. However, if the film is not brought to equilibrium with air at the same relative humidity after development as it was before, the permanent processing may be completely masked by the temporary expansion or contraction due to change in relative humidity.

Table V shows the effect of processing on several film bases. Values are given for materials conditioned 4 hours before and after processing at 20 percent relative humidity, 50 percent relative humidity, and 70 percent relative humidity, all at 70°F.

Effect of Processing on Litho Film Size

Representative sensitized films were measured before and after processing to determine processing stability. Values are given

for materials conditioned 4 hours before and after processing at 20% RH, 50% RH and 70% RH, all at 70°F.

TABLE V

	AVERAGE SIZE CHANGES IN %			
	Relative Humidities Before and After Processing	20% RH	50% RH	70% RH
.0042" "CRONAR" base		<.01%	<.01%	<.01%
.0058" Standard cellulose acetate base		-.05%	<.01%	+.01%
.0058" High acetyl cellulose acetate base		+.01%	<.01%	-.02%
.0120" Vinyl base		+.01%	-.01%	-.04%
.0055" Polystyrene base		<.01%	<.01%	<.01%

(All films were developed 2½ min. in Du Pont 7-D Developer, rinsed 20 sec. in clear water, fixed 3 min. in Du Pont 20-F Fixer and washed 10 min., dried below 100°F. and reconditioned at the indicated RH of 70°F.).

As indicated in Table IV, photographic film shrinks during storage. This shrinkage is accelerated by high temperatures and by free contact with air. Table VI illustrates shrinkage of EK nitrate MP film (no longer used) in the lengthwise direction for various periods, under three storage conditions, all at 70°F and 50-65 percent relative humidity. Fig. 3 shows the shrinkage rate of the newer triacetate base.

Du Pont literature states that "Cronar" polyester photographic film base is chemically inert, and contains no plasticizer or solvents to be lost gradually as it ages. Normal storage studies, it is added, have given no indication of base change or deterioration, and forty day accelerated storage tests at 100°C have caused no significant change in processed film properties. Hence, it is expected that this base will remain substantially unchanged over long periods of time.

TABLE VI. Shrinkage of EK Nitrate MP Film.

	% Shrinkage 10 weeks	% Shrinkage 20 weeks	% Shrinkage 30 weeks	% Shrinkage 40 weeks
Rolls in taped cans	0.08	0.12	0.12	0.14
Rolls in untaped cans	0.20	0.25	0.28	0.30
Strips open to air	0.34	0.45	0.46	0.50

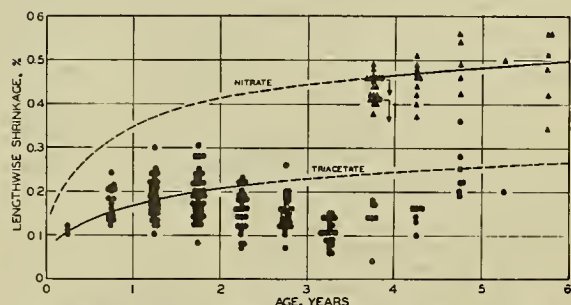


Fig. 3. Shrinkage vs. age for triacetate and nitrate prints scrapped after normal theater use. Measurements made at 70 F and 50% R.H.

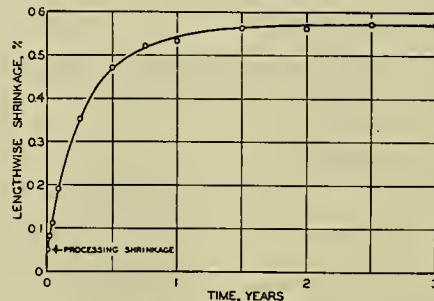


Fig. 4. Average rate of shrinkage of processed triacetate 35mm motion-picture positive film at 90 F and 90% R.H. Controlled tests on strips freely exposed to circulating air; all measurements made after reconditioning at 70 F and 50% R.H.

Kodak aerial films are now coated on two bases. Kodak Aerographic films, (Type 1A) are made on low shrink topographic base, suitable for use in accurate mapping work. Regular Safety Aero base is used for Kodak Ektachrome Aero film, and Recon film. The latter has somewhat higher shrinkage characteristics than the Type 1A. A comparison of dimensional changes in the two bases is shown in Table VII.

Since 1941, Type 1A (topographic) film base has been made from cellulose acetate butyrate. Between 1938 and 1941, it was made from cellulose acetate propionate. Both these bases have substantially lower humidity expansion coefficients than cellulose acetate, used prior to 1938.

APPROXIMATE SHRINKAGE CHARACTERISTICS OF KODAK MATERIALS
USED IN AERIAL PHOTOGRAPHY (Safety Base)

	Kodak Aero-graphic Film (Topographic) Military Type 1A	Reconnaissance-base Film Kodak Aerial Reconnaissance Film and Kodak Ektachrome Aero Film (Non-Topographic) Military Type 1B
All Tests Made on Film in the Form of Flat Strips		
Direction of Test*	L. 8.5	W. 9.0
Humidity Coefficient of Linear Expansion per 1% R.H. $\times 10^5$	D. 0.5	D. 5.5
Thermal Coefficient of Linear Expansion per Degree F $\times 10^5$	L. 4.2	W. 4.4
Processing Shrinkage, %	D. .05	D. .06
Accelerated Aging Shrinkage, % (7 days at 120F - 20% R. H.)	L. .13	W. .14
Long-Time Aging Shrinkage, % (1 year at 78F - 60% R.H.)	L. .13	W. .12

The Aging Shrinkage includes processing shrinkage in case of photographic materials. The Accelerated Aging Test is the same as that required by Military Specification:
"Film, Photographic, Aerial, Black-and-White," MIL-F-26010 (USAF), dated 2 May 1956.

*L = Length

W = Width

D = Difference

TABLE VII

Shrinkage of photographic film is extremely complex. Several different processes are going on at once, and each is affected in a different manner by heat and moisture, and other factors. It is not always easy to predict how a given film will react when subjected to unknown conditions of storage and handling.

Recommendations

Film choice.

The film which shows the least amount of processing and storage change should be used. This, at present, is the Type A, cellulose acetate butyrate base. When it becomes available for aerial film, Du Pont "Cronar" should show some improvement over other bases.

The two rolls intended for stereophotography should be chosen from the same emulsion lot.

Making the photographs

Dimensional errors in aerial negatives caused by humidity or thermal expansion may be reduced by printing (or measuring the negatives) in an air conditioned laboratory, preferably at about 70°F, and 50 percent relative humidity, and by thermostating the cameras at the same temperature. Ideally, the negative should be in equilibrium with air of the same temperature and relative humidity at the time of printing or measurement as at the instant of exposure. Film is in equilibrium with air at approximately 55-60 percent relative humidity when packed in air-tight (taped) cans, and will change very little in the camera if exposures are made in rapid succession; however, temperature changes inside the camera cannot be prevented except by some method of automatically controlled heating. Completely air-conditioned cameras, which provide both temperature and relative humidity control, have been used quite successfully, in the recent past. Dimensional errors have been reduced considerably by this method, as well as markings by static electricity.

Processing

Film should be processed at normal temperatures -- 68-70°F. It should be subjected to as little tension as possible, especially while wet, and should be dried at a relative humidity of about 50 percent, and temperature not in excess of 85°F.

Handling

Film should be handled gently, and, insofar as possible, both rolls intended for stereo photography should receive identical treatment.

Storage

Since access to air increases shrinkage--"Cronar" possibly excepted--film should be stored in sealed cans before and after use and processing. Heat also speeds shrinkage; therefore film should be stored in a cool place. Both rolls of a stereo pair must be stored under identical conditions, both before and after processing.

REFERENCES

1. Calhoun, J. M., 1948: The physical properties and Dimensional behavior of motion picture films. Journal of the Society of Motion Picture Engineers, October.
2. Fordyce, Calhoun, and Moyer, 1955: Shrinkage behavior of motion-picture film. Journal of the Society of Motion Picture and Television Engineers, February.
3. Eastman Kodak Company, 1956: Kodak Materials for Aerial Photography.
4. E. I. Du Pont de Nemours and Co.: "Technical Data on Experimental "Cronar" Polyester Film Base Sensitized with Du Pont Photolith Emulsion."

Distribution List for Project SWOP

1

Department of Defense

1 Assistant Secretary of Defense
Research and Development
Attn: Committee on General Sciences
Pentagon Building
Washington 25, D.C.

Navy

Navy

5 Office of Naval Research Geophysics Branch (Code 416) Washington 25, D.C.	1 Chief, Bureau of Ships Navy Department Washington 25, D.C. Attn: Code 312
	1 320
	1 531
	1 814
	1 845

1 Air Branch, Attn: Flodil

U.S. Navy Hydrographic Off.
Washington 25, D.C.

1 Amphibious Branch,
Attn: Maj. Crownover

10 Division of Oceanography
5 Photogrammetry Division

Chief of Naval Research
Washington 25, D.C.

Chief, Bureau of Aeronautics
Navy Department
Washington 25, D.C.

1 Armament Branch (Code 463)

1 AX-3

1 Undersea Warfare Branch
(Code 466)

1 Attn: Mr. Winik

1 Commanding Officer

Chief of Naval Operations
Navy Department
Washington 25, D.C.

Office of Naval Research
346 Broadway
New York 13, N.Y.

1 Attn: Op-533D Navy Aerology

1 Commanding Officer

1 Chief, Bureau of Yards and
Docks
Navy Department
Washington 25, D.C.

Office of Naval Research
495 Summer Street
Boston 10, Mass.

3 Director

Navy Electronics Laboratory
San Diego 52, Calif.
Attn: 2230

1 Commanding Officer

Office of Naval Research
The John Crerar Library Bldg.
86 E. Randolph Street
Chicago 1, Illinois

1 Commander

Naval Ordnance Laboratory
White Oak
Silver Spring 19, Maryland

1 Commanding Officer

Office of Naval Research
1030 East Green Street
Pasadena 1, Calif.

5 Commanding Officer

U.S. Navy Mine Countermeasure
Station
Panama City, Florida

7 Commanding Officer

Office of Naval Research Br. Office
Navy #100, Fleet Post Office
New York, N.Y.

1 Commanding Officer

U.S. Navy Underwater Sound
Laboratory
New London, Conn.

6 Director, Naval Research Lab.

Attn: Technical Services
Information Officer
Washington 25, D.C.
Attn: Mr. Brodzinski

Distribution ListNavy

- 1 Project Arowa
U.S. Naval Air Station
Building R-48
Norfolk, Virginia
- 1 Superintendent
U.S. Naval Academy
Annapolis, Maryland
- 2 Department of Aerology
U.S. Naval Post Graduate School
Monterey, Calif.
- 20 David Taylor Model Basin
Washington 7, D.C.

Air Force

- 1 Commanding General
Research and Development Div.
Department of the Air Force
Washington 25, D.C.
- 1 Chief, Air Weather Service
Department of the Air Force
Washington 25, D.C.
- 1 Commanding Officer
Cambridge Field Station
230 Albany Street
Cambridge 30, Mass.
Attn: CRHSL

Army

- 1 Commanding General
Research and Development Div.
Department of the Army
Washington 25, D.C.
- 1 Chief, Armed Forces
Special Weapons Project
P.O. Box 2610
Washington , D.C.
- 20 U.S. Army Beach Erosion Board
5201 Little Falls Road, N.W.
Washington 16, D.C.
- 1 U.S. Waterways Experiment Sta.
Vicksburg, Miss.

Other U.S. Government Agencies

- 1 Office of Technical Services
Department of Commerce
Washington 25, D.C.
- 25 Armed Services Technical Information Center
Documents Service Center
Knott Building
Dayton 2, Ohio
- 1 National Research Council
2102 Constitution Avenue
Washington 25, D.C.
Attn: Comm. on Undersea Warfare
- 1 Commandant (DAO)
U.S. Coast Guard
Washington 25, D.C.
- 1 Director
U.S. Coast and Geodetic Survey
Department of Commerce
Washington 25, D.C.
- 2 Chief, U.S. Weather Bureau
2400 M Street N.W.
Washington 25, D.C.
Attn: Dr. H. Wexler
- 30 Director
Woods Hole Oceanographic Inst.
Woods Hole, Mass.
- 1 Project Officer
Laboratory of Oceanography
Woods Hole, Mass.
- 1 Director
Narragansett Marine Laboratory
Kingston, Rhode Island
- 1 Bingham Oceanographic Labs.
Yale University
New Haven, Conn.
- 75 Department of Meteor. and Ocean.
New York University
New York 13, N.Y.
- 1 Director
Lamont Geological Observatory
Torrey Cliff
Palisades, N.Y.

Research Labs.Distribution List

- 1 Hudson Laboratories
Columbia University
145 Palisades Street
Dobbs Ferry, New York
- 1 Dr. F.B. Berger
General Precision Laboratory
Pleasantville, New York
- 1 Dr. L. Goldmuntz
Technical Research Group
56 W. 45th St.
New York 36, N.Y.
- 2 Director
Chesapeake Bay Institute
Johns Hopkins University
Baltimore 18, Maryland
- 1 Dr. C.I. Beard
Applied Physics Laboratory
Johns Hopkins University
8621 Georgia Avenue
Silver Spring, Maryland
- 1 Mr. Henry D. Simmons, Chief
Estuaries Section
Waterways Experiment Station
Corps of Engineers
Vicksburg, Mississippi
- 1 Director
Marine Laboratory
University of Miami
Coral Gables, Florida
- 1 Head, Dept. of Oceanography
Texas A and M College
College Station, Texas
- 5 Director
Scripps Institution of Oceanography
La Jolla, Calif.
- 1 Allan Hancock Foundation
University Park
Los Angeles 7, Calif.
- 1 Department of Engineering
University of California
Berkeley, Calif.
- 1 Dr. Wayne V. Burt
Oregon State College
Corvallis, Oregon
- 1 Head, Dept. of Oceanography
University of Washington
Seattle 5, Washington
- 1 Director
Arctic Research Laboratory
Box 1070
Fairbanks, Alaska
- 1 Geophysical Institute of Univ.
of Alaska
College, Alaska
- 20 Society of Naval Architects
and Marine Engineers
74 Trinity Place
New York, N.Y.
- 1 Mr. Richard Timme
National Marine Consultants, Inc.
Administration Building
Santa Barbara Airport
Goleta, Calif.
- 1 Prof. M.S. Uberoi
Dept. Aeronautical Engineering
University of Michigan
Ann Arbor, Michigan
- 1 General Dynamics Corp.
Convair Division
3165 Pacific Highway
San Diego 12, Calif.
Attn: Mr. H. Brooke
- 1 The Glenn L. Martin Co.
Baltimore 3, Maryland
Attn: Mr. J. Pearson
- 1 Grumman Aircraft Engineering Co
Bethpage, L.I. New York
- 1 EDO Corporation
College Point, N.Y.
Attn: Mr. S. Fonn

Distribution List

The Glenn L. Martin Co.
Baltimore 3, Maryland

1 Attn: Mr. J. Pearson
1 Dr. C. E. Carver, Jr.

1 Grumman Aircraft Engineering Co.
Bethpage, L.I., New York

1 Edo Corporation
College Point, N.Y.

Attn: Mr. S. Fenn

1 Dynamic Developments Corp.
St. Marks Lane
Islip, L.I., New York

Attn: Mr. W. Carl

1 Mr. Joseph Chadwick
Sperry Marine Division
Garden City, L.I., N. Y.

